An examination of multiple SynGAP isoforms in mammalian central neurons

Aoife Christina McMahon (*BSc, MRes*)

A thesis submitted for the degree of Doctor of Philosophy at the University of Edinburgh

August 2010

One Gene, One Protein.

When nothing abnormal is detected, it is difficult to draw any conclusions. As Lewis Wolpert commented on the supposed absence of a phenotype: «I say, have you taken your mice to the opera? Can they still tell Wagner from Mozart?»

Wolpert L, Ghysen A, Garcia-Bellido A. Debatable issues. Int J Dev Biol (1998) 42:511–9

Declaration

This work was carried out in the School of Biomedical Sciences at the University of Edinburgh. I hereby certify that this thesis and its composition are entirely my own work, with the exception of the following:

1) Screening of the plasmid cDNA library, until the stage of the initial identification of positive bacterial colonies, was performed by Rachel Seville and Mark Barnett

2) Some PCR reactions and TA cloning (SynGAP B and C fragments for the construction of clones (p72), and some of the UTR clones(p67)) were carried out by an undergraduate student, Aleks Domanski, under my supervision.

No part of the work contained in this thesis has been submitted for any other degree or professional qualification.

Signed …… Date ……..

Abstract

The ability of neurons to dynamically regulate their response to changing inputs is essential for the correct development and function of a nervous system capable of learning and memory. The post synaptic compartment of excitatory synapses contains a dense proteinaceous complex of molecules that link excitatory glutamatergic neurotransmission to downstream signalling pathways that ultimately result in modification of the synapse. One of the most abundant of such postsynaptic signalling molecules, synaptic GTPase activation protein, SynGAP, represents a key signalling link between the activation of the NMDA sensitive glutamate receptor to outcomes such as the structural rearrangement of synaptic sites and altered synaptic content of AMPA type glutamate receptors, molecular processes that underly learning and memory.

The primary finding of this thesis is that different isoforms of SynGAP, which varies at it N terminus through alternative transcription start sites and at its C terminus through alternative splicing, can differentially affect the function of the synapse. Using primary murine neuronal cultures we show that despite being crucial for the survival of the mouse the absence of SynGAP does not effect mean dendritic spine morphology and density or miniature excitiatory post synaptic currents under a range of experimental conditions (days in vitro 10 – 14, with and without serum, high and low cell plating density). In order to examine the effects of different SynGAP isoforms we cloned two full length transcripts (SynGAP A-alpha-2 and SynGAP E-alpha-1) which were used to construct a range of isoforms. Whole cell patch clamping of SynGAP transfected neurons revealed that the post synaptic expression of SynGAPs which terminate as an alpha-1 isoform can lead to the elimination of mEPSCs, while isoforms that terminate as an alpha-2 isoform can lead to synaptic strengthening. The magnitude of the effect in both cases is determined by the identity of the N terminus of the protein; SynGAP A-alpha-1 has the largest synaptic weakening effect and SynGAP B-and C alpha-2 strenghten the synapse. The changes in miniature electrophysiological properties are not mirrored by changes in dendritic spine morphology, whole cell AMPA/NMDA currents, or synaptic responsiveness to stimulation suggesting an undefined novel mechanism of action. SynGAPs A, B and C appear to be under the control of different promoters which are differentially regulated by development and synaptic activity, thus the differential function of SynGAP N and C terminal combinations could play a part in the activity dependent regulation of synaptic strength.

Contents

List of Figures

Abbreviations

Explanations of abbreviations are not always given in the text, for example. the names of some proteins.

AMPA	α-amino-3-hydroxy-5-methyl-4-isoxazole propionic acid
4-AP	4-Aminopyridine
aa	amino acid
APV	d-2-amino-5-phosphonopentanoate
AraC	cytosine β-D-arabino-furanoside hydrochloride
Bic	Bicuculline
bp	base pair
BSA	bovine serum albumin
BTK	Bruton's tyrosine kinase
C2	calcium/lipid-binding domain
CaMKII	calcium/calmodulin-dependent protein kinase II
CAPRI	calcium-promoted Ras inactivator
CNQX	6-cyano-7-nitroquinoxaline-2,3-dione
DM	Dissociation medium
DMEM	Dulbecco's Modified Eagle Medium
DSCAMs	Drosophila melanogaster gene Down syndrome cell adhesion molecules
EM	electron micrsocopy
EPSC	excitatory post synaptic current
EPSP	excitatory post synaptic potential
ERK/MAPK	extracellular regulated kinase/mitogen activated protein kinase
FBS	foetal bovine serum
GAP	GTPase activating protein
GAPIPB4B	GAP - Ins(l,3,4,5)P4-binding protein
GEF	guanine exchange factor
GRP1	general receptor for phosphoinositides-1
GTP/GDP	tri-or di-phosphate guanosine nucleotide
JNK	c-Jun amino-terminal kinase
LTD	long term depression
LTP	long term potentiation
MAGUKS	membrane-associated guanylate kinase homologs
MEK	MAPK/ERK kinase
NF1	neurofibromatosis type I
NMD	nonsense mediated decay
NMDA	N-methyl-d-aspartate
ORF	open reading frame
PDZ	post synaptic density protein (PSD95), Drosophila disc large tumor suppressor (DlgA), and zonula occludens-1 protein (zo1)
PDZ-GEF	PDZ-guanine nucleotide exchange factor

Pen/Strep	penicillin/streptomycin
PGC1	peroxisome proliferator-activated receptor-coactivator 1
PH	pleckstrin homology domain
PI3K	phosphoinositide 3-kinase
PIP2	phosphatidylinositol(4,5)-bisphosphate
PIP3	phosphatidylinositol(3,4,5)-triphosphate
PKB	protein kinase B (also known as AKT)
Pleckstrin	platelet and leukocyte C kinase substrate protein
PSD	post synaptic density
PSD95	post synaptic density protein
Ptx	Picrotoxin
RabD	Dictyostelium Rab14-related GTPase
RASAL	Ras-GTPase-activating-like protein
RasGAP	Ras GTPase activating protein
RasGRF	Ras-specific guanine nucleotide-releasing factor 2
RE	restriction enzyme
REM	Ras exchange motif
RNA-PET	RNA paired end tag
RNApol II	RNA polymerase II
RT	room temperature
RUST	regulated unproductive splicing and translation
SAP 102	Synapse-associated protein 102
SAP-97	synapse-associated protein-97
SNAP-25	synaptosomal protein 25 kDa
Sos	son of sevenless
SynGAP	Synaptic GTPase activating protein
TARP	transmembrane AMPAR regulatory protein
TM	transfection medium
Ttx	Tetrodotoxin citrate
VGCC	voltage gated calcium channel

1 Chapter One: Introduction

1.1 Background

To survive living organisms must be able to sense and respond to their surroundings. For this to occur, their constituent cells in turn must be able to sense and respond to stimuli. Cells have evolved a range of mechanisms by which extracellular cues can be sensed and messages transmitted to within the cell. The stimulus sensing receptor is rarely directly coupled to a response mechanism but the cascade of signalling it initiates can change the characteristics of the cell; the structure, the intracellular milieu, or the extracellular receptors, so that in future the cell may respond differently to the same stimulus. The focus of this thesis is on one protein, *Syn*aptic *G*TPase *a*ctivating *p*rotein (SynGAP), a key regulator of highly conserved signalling pathways used in cells from slime mould to human (2008).

Cells of the brain, like all other cells, sense and respond to their environment. However these cells have additional levels of specialisation that allow them to form a vast communicating network that can co-ordinate the body, remember its experiences and learn from them. To this end brain cells co-opt and modify the basic signalling mechanisms with which all cells are equipped. SynGAP is one such protein that is expressed exclusively in neurons (Chen *et al.*, 1998; Kim *et al.*, 1998). It is present at the sites of contact between neurons, the synapses, where it appears to form a key link between the activation of post-synaptic receptors by molecules released from the presynaptic neurons (specifically the excitatory neurotransmitter glutamate) and downstream signalling pathways (Krapivinsky *et al.*, 2004; Vazquez *et al.*, 2004; Rumbaugh *et al.*, 2006). When SynGAP mediated regulation is compromised the effect on synaptic function is profound; deficits in cognitive processes are observed in both humans and animals (Komiyama *et al.*, 2002; Hamdan *et al.*, 2009; Muhia *et al.*, ; Pinto *et al.*) .

Mechanistically SynGAP is a multi-functional GTPase activating protein that enhances the inactivation of the small G proteins Ras and Rap, proteins that mediate a wide variety of cellular responses (Kim *et al.*, 1998; Pena *et al.*, 2008). In neurons these pathways regulate the synaptic content of neurotransmitter receptors and the physical structure of the synaptic site, thus determining how the neuron

responds to synaptic input (Pak *et al.*, 2001; Zhu *et al.*, 2002; Goldin & Segal, 2003; Alonso *et al.*, 2004).

The collection of components required to carry out the intricate processes involved in generating and maintaining a living, breathing and thinking organism is staggeringly complex. Early estimates stated that about 100,000 genes would be required to make up a mammal; however, the actual number is less than one-quarter of that, barely four times the number of genes in budding yeast. (Nilsen & Graveley). It is now clear that the additional information is in large part provided by alternative splicing, the process by which multiple different functional messenger RNAs, and therefore proteins, can be synthesized from a single gene. SynGAP is an excellent example of this phenomenon; it is encoded by one gene but a multitude of protein isoforms exist. The main functional domain, the GAP domain is invariant between isoforms, but the protein can vary in amino acid sequence at both its amino (N) and carboxy (C) termini. Intriguingly SynGAP variants are differentially regulated in response to synaptic activity and in development, suggesting that they may have different roles to play in different circumstances.

The relevance of SynGAP to the function of neurons is the main interest of this thesis. I am particularly interested in the molecular complexity of SynGAP; specifically how, if at all, various isoforms differentially alter the outcomes of SynGAP regulated processes? In order to investigate this, the morphological and electrophysiological consequences of manipulated SynGAP regulated signalling are examined.

1.1.1 Organisation of this thesis

This chapter gives an overview of the background literature relevant to SynGAP and outlines observations on which the hypothesis of this thesis is based.

Chapter Two describes the experimental and analytical methods used in this thesis.

Chapters Three, Four and Five are the main results chapters. They each provide an introduction and a motivation for the work, and briefly reiterate previous work done on SynGAP in the area with which they are concerned. The results are presented and discussed.

Chapter Three is concerned with the molecular complexity of the SynGAP gene, transcript and protein. It describes the cloning and construction of various SynGAP variants that are used in morphological and functional assays in the remainder of the thesis. During the cloning process a number of novel SynGAP transcripts were discovered and these are described.

Chapter Four comprises an analysis of the effect of the removal of all SynGAP isoforms and the overexpression of specific SynGAP isoforms on the morphology of the sites of excitatory synapses, the dendritic spines.

The key finding of this thesis appears in Chapter Five, which deals with the electrophysiological effect of the removal of all SynGAP isoforms and the overexpression of specific SynGAPs. A striking differential effect among SynGAP isoforms is described.

Chapter Six presents some final thoughts on all the data taken together and suggests future directions and experiments in the study of SynGAP.

1.1.2 Small G protein related deficits in synaptic function

SynGAP is a regulator of two key signalling molecules of the Ras family of small G proteins, Ras and Rap. The Ras family, classically associated with cell proliferation, has been co-opted in terminally differentiated non-dividing neurons to serve in activity dependent regulation of neuronal development and function, that is synaptic plasticity, as well as the regulation of neuronal survival (Sweatt, 2001).

Accumulating reports have associated genetic mutations of various molecules involved in Ras and Rap signalling with several mental disorders causing learning disability, further underscoring the essential role of Ras and Rap signalling in both the physiology and the pathology of human learning and memory (Pinto *et al.*, 2010; Stornetta & Zhu). Similarly the targeted mutation of small G protein regulators in model organisms commonly leads to a host of synaptic plasticity and learning deficits.

SynGAP at the synapse

SynGAP is ideally placed in the post synaptic compartment to regulate the signalling pathways that occur there. Neurotransmission by the main excitatory neurotransmitter in the brain, glutamate, is mediated by NMDA, AMPA and kainate type glutamate receptors. SynGAP is thought to link signalling through the NMDA receptor to downstream pathways, including the ERK/MAPK and p38 MAPK signalling pathways, which in turn regulate the synaptic content of AMPA receptors.

SynGAP has been localised to the post synaptic signalling complex of excitatory synapses, the post synaptic density (PSD), by a range of techniques; immunocytochemistry, PSD purification, electron microscopy and co-immunoprecipitation with synaptic proteins (Chen *et al.*, 1998; Barnett *et al.*, 2006; Moon *et al.*, 2008). A number of studies using semi-quantitative mass spectrometry approaches have highlighted that SynGAP is remarkable in its synaptic abundance. It is by far the most abundant G protein related protein in the PSD fraction (Peng et al., 2004). Cheng et al. (2006) have found that it is as abundant as its binding partner the scaffolding protein PSD-95, which together with the Ca^{2+} regulated kinase CaMKII, represent the three most prevalent proteins of the core synaptic components at the PSD.

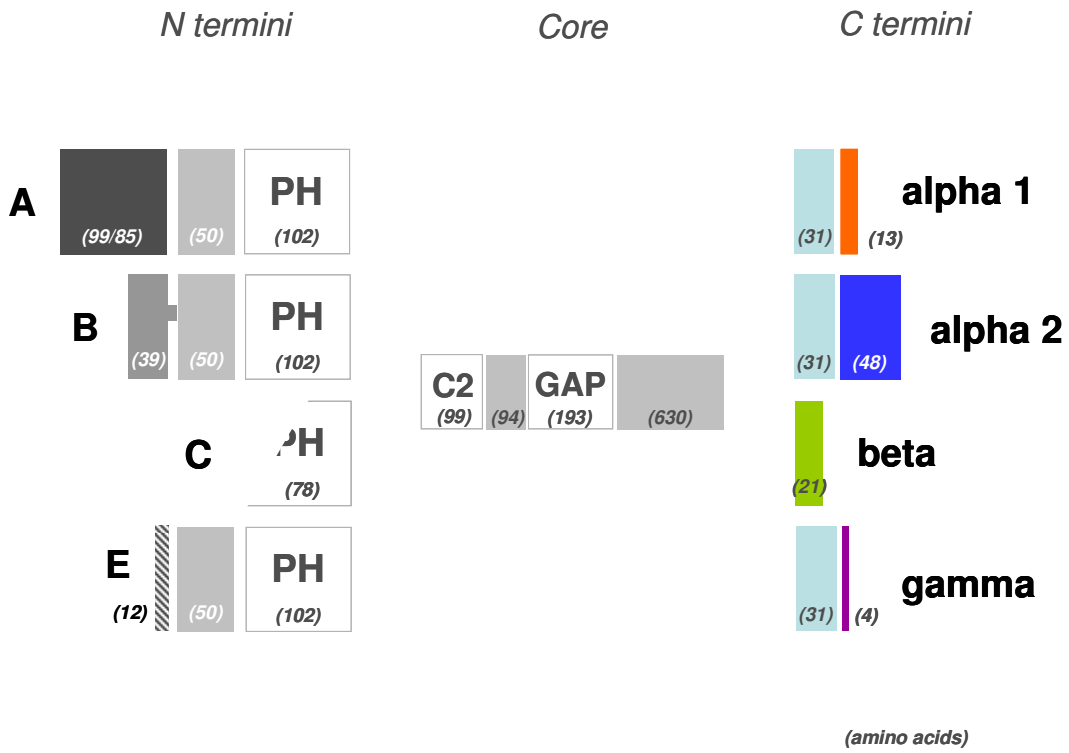

Figure 1. 1 The protein domain structure of SynGAP isoforms.

The central portion of SynGAP is composed of a PH domain, a C2 domain and a GAP domain. Different N-terminal peptides arise from different transcription start sites. SynGAPs A, B and E have unique amino acid sequences and SynGAP C is a truncated form that lacks part of the PH domain. C-terminal peptide tail variation arises from alternative mRNA splicing. Peptide lengths in amino acids are given in parentheses. Diagram is not to scale.

1.1.3 SynGAP in Behaviour

The phenotypic outcomes of alteration in SynGAP expression give an indication of its importance in normal synaptic function.

Human Behaviour

De novo truncating mutations in *SYNGAP* have been identified in three girls with non-syndromic forms of moderate to severe mental retardation (Hamdan et al., 2009). These patients exhibit severe language impairment but do not exhibit autistic behaviours; they all have normal non-verbal social interactions. Two patients have epilepsy which is controlled by the AMPA type glutamate receptor inhibitors

topiramate or valproate, suggesting that AMPA receptor trafficking may be defective. Very recently reductions in *SYNGAP* copy number have also been found in patients with autism (Pinto *et al.*).

Animal Behaviour

Null mice appear be normal upon birth but fail to thrive and die from postnatal day 2 to 7. Heterozygotes are viable, grow normally and are fertile. Behavioural experiments were performed on these animals, who express half the amount of SynGAP protein as wild type animals. The reduction in SynGAP has resulted in multiple behavioural traits suggestive of aberrant cognitive and non-cognitive processes.

SynGAP $^{+/-}$ animals exhibit subtle spatial learning deficits in the Morris water maze, severe working and reference memory deficits in the radial arm maze task, and a deficiency in an elevated T-maze. In contrast, object recognition memory performance is not impaired in *SynGAP* $^{+/-}$ mice (Komiyama *et al.*, 2002; Muhia *et al.*).

In the non-cognitive domain, *SynGAP* $^{+/-}$ mice are hyperactive in the open field and appear less anxious in the elevated plus maze test (Muhia et al.). Additionally, they exhibit enhanced startle reactivity as well as lack of social memory and a propensity toward social isolation. Deficits in cued fear conditioning and working memory indicate abnormal function of circuits that control emotion and choice (Guo et al., 2009). *SynGAP* $^{+/-}$ animals display increased vigor in the execution of learned operant behaviour without compromising its temporal control, it is thought this may be associated with the hyperactivity (Muhia et al., 2009).

1.1.4 SynGAP in Development

Abnormal adult function may be due to defective development and as such it is often difficult to disentangle acute from chronic effects. Early in development SynGAP is expressed in the developing neural tube, somites and heart, and by embryonic day (E) 10.5, in the limb buds. By E14.5 it is expressed in cortex, basal ganglia and thalamus, first becoming visible in the hippocampus and hypothalamus at E16.5.

Expression levels are highest in the second postnatal week and subsequently decline in most areas except the hippocampus (Porter et al., 2005). This peak in expression coincides with a period of profligate synaptogenesis and developmental plasticity, again indicating a role for SynGAP in these processes. In adult animals SynGAP is present in hippocampus, cortex, olfactory bulbs, striatum, cerebellum and the amygdala (Porter *et al.*, 2005; Barnett *et al.*, 2006; Moon *et al.*, 2008).

SynGAP is essential for the postnatal anatomical development of whisker-related patterns in the developing somatosensory pathways in mouse forebrain. Normally cortical neuronal cell bodies would segregate postnatally into cell dense structures called barrels, with thalamocortical axons occupying the cell sparse region in a process that is regulated by glutamate neurotransmission (Woolsey & Van der Loos, 1970; Erzurumlu & Kind, 2001). Cortical neuronal cell bodies fail to segregate in *SynGAP* $^{-/-}$ brains, and segregation is impaired in *SynGAP* $^{+/-}$ brains, reinforcing the notion that SynGAP represents a link between glutamatergic neurotransmission and cellular outcomes (Barnett et al., 2006).

1.1.5 Synaptic plasticity

SynGAP clearly has a role to play in regulating the development and cognitive function of the brain. What cellular mechanisms underlie this role? Examination of the functional properties of individual neurons and brain regions gives some indication as to what processes are involved. In *SynGAP* $^{+/-}$ mutant mice, the induction of LTP in the hippocampal CA1 region is strongly impaired in the absence of any detectable alteration in basal synaptic transmission or NMDA receptor-mediated synaptic currents (Komiyama *et al.*, 2002; Kim *et al.*, 2003). This indicates that basal synaptic activity of AMPA receptors is normal but that their recruitment upon appropriate stimulation is defective.

Synaptic plasticity itself is not explicitly studied in this thesis but the effect of SynGAP on the processes that underlie it; synaptic delivery of AMPA receptors and the structural maturation of synaptic sites are examined. It is unlikely that the mechanisms that govern these processes in different circumstances are completely different but that the basic machinery is modified depending on requirement. A broader definition of synaptic plasticity includes the changes that accompany developmental synaptic maturation, these are also examined.

Interest in synaptic plasticity stems from the belief that this process underlies crucial aspects of adaptive cognitive function, such as learning and memory, and is the key mechanism by which neurons acquire their complex function and specificity during development (Bliss & Collingridge, 1993; Malenka & Nicoll, 1999). Long-term synaptic plasticity, the sustained synaptic modification after periods of repetitive synaptic activity, was first discovered in the rabbit hippocampus (Bliss & Lomo, 1973) and has since been described in many species and in many other brain areas. Much effort has gone into understanding different forms of synaptic plasticity, with the cellular, molecular, and signalling mechanisms best illustrated for NMDA-sensitive glutamate receptor dependent forms of synaptic plasticity (Kerchner & Nicoll, 2008). The opening of the NMDA receptor and the influx of Ca^{2+} ions through its pore are two essential cellular events that trigger synaptic plasticity. A common mechanism for the expression of synaptic plasticity is mediated by the altered synaptic presence of another class of glutamate receptor, the AMPA receptor.

AMPA receptors allow the influx of positive sodium ions into the cells in response to glutamate binding, this short lived depolarisation of the transmembrane potential is called an excitatory post synaptic potential (EPSP). Changes in the synaptic content of AMPA receptors cause different magnitude depolarisations in response to the same stimulus. Ultimately when the depolarisations cross a threshold, a different pattern of action potential firing can result. Thus the tuning of synaptic strength results in changes to the input to output relationship of a given neuron. Central to the challenge of understanding synaptic plasticity is the problem of how the initiating signals (NMDA receptor activation) are communicated to induce the expression mechanism (altered AMPA receptor trafficking) (Kandel, 2000).

Physiological and behavioural studies have indicated that Ras family signalling is involved in long term potentiation (LTP), memory formation and synaptic development (Brambilla *et al.*, 1997; Silva *et al.*, 1997; Atkins *et al.*, 1998; Schafe *et al.*, 2000; Giese *et al.*, 2001). Ras activation in these processes requires Ca^{2+} influx, thus Ras family activity and its downstream signalling cascades serve as key biochemical cascades linking activation of NMDA receptors and calcium influx with phosphorylation and trafficking of AMPA receptors during synaptic plasticity.

Although classical activation of Ras family, via receptor tyrosine kinases and adaptor proteins, does occur in neurons in response to neurotrophins, Ras family activation in response to membrane depolarisation or glutamatergic signalling represents a non-classical pathway. Precisely how Ca^{2+} entry leads to Ras activity is a question not yet resolved. Implicated are the Ras regulatory proteins, the GAPs and GEFs, particularly those that are directly or indirectly regulated by Ca^{2+} (Walker et al., 2003). SynGAP represents an excellent candidate to fulfil this role.

Expressions of plasticity: AMPA receptors and dendritic spines

There are multiple mechanisms for the expression of NMDA receptor mediated synaptic plasticity and development including altered presynaptic release, modulation of AMPA receptor function by phosphorylation and altered AMPA receptor trafficking. The functional outcome of altered synaptic content of AMPA receptors is associated with structural plasticity, whereby functional maturation of synapses is accompanied by structural maturation of the synaptic sites. The second and third chapters of this thesis deal specifically with these two phenomena in relation to the role of SynGAP.

1.1.6 SynGAP regulates AMPA receptor trafficking

As mentioned, data from LTP experiments in *SynGAP* $^{+/-}$ mutant mice indicates that basal synaptic activity of AMPA receptors is normal but that their recruitment upon appropriate stimulation is defective. No presynaptic deficits have been found. Long term depression (LTD), when induced by paired pulses at a low frequency (PP-1 Hz), is unaffected by the reduction in SynGAP expression (Kim et al., 2003). However, LTD induction by the bath application of NMDA, which normally induces AMPA receptor internalization, is impaired in *SynGAP*$^{+/-}$ hippocampal slices.(Ehlers, 2000; Carlisle *et al*., 2008).

Synaptic AMPA receptor content can also be examined by looking at small AMPA mediated excitatory currents that occur spontaneously in the absence of action potential mediated neurotransmitter release. Due to the quantal nature of neurotransmitter release in these circumstances the amplitude of these miniature excitatory post synaptic currents (mEPSCs) is correlated with the number, or the

synaptic strength, of AMPA receptors at the synapse. The frequency of mEPSCs can give us information on the number of synapses; interpretations of AMPA mEPSCs will be discussed further in the introduction to Chapter Five.

AMPA mEPSCs in cultured *SynGAP* $^{-/-}$ neurons are increased in frequency compared to control however there are conflicting reports regarding mEPSC amplitude. Vazquez and co-workers (2004) see an increase in mEPSC amplitude, but Rumbaugh et al. (2006) see no change. The immunocytochemical appearance of AMPA receptor puncta are thought to indicate the presence of synapses. These puncta are increased in size and density when mEPSC amplitude and frequency are increased (Vazquez et al., 2004). However where an increase in frequency, but not amplitude was observed the associated immunocytochemisty indicated an increase in puncta size, but not density, potentially indicating a conversion of silent to non-silent synapses (Rumbaugh et al., 2006). Despite inconsistencies, these data indicate that in these culture systems, SynGAP is negatively regulating the insertion of AMPA receptors.

Additional evidence for this view comes from the overexpression of a GFP fusion protein of SynGAP that results in a depression of mEPSCs and a significant reduction in synaptic AMPA receptor surface expression. Crucially, this effect is dependent on an intact C-terminal tail of the particular isoform used, SynGAP alpha-1, highlighting the importance of this domain for SynGAP function. Unfortunately other isoforms were not tested (Rumbaugh et al., 2006).

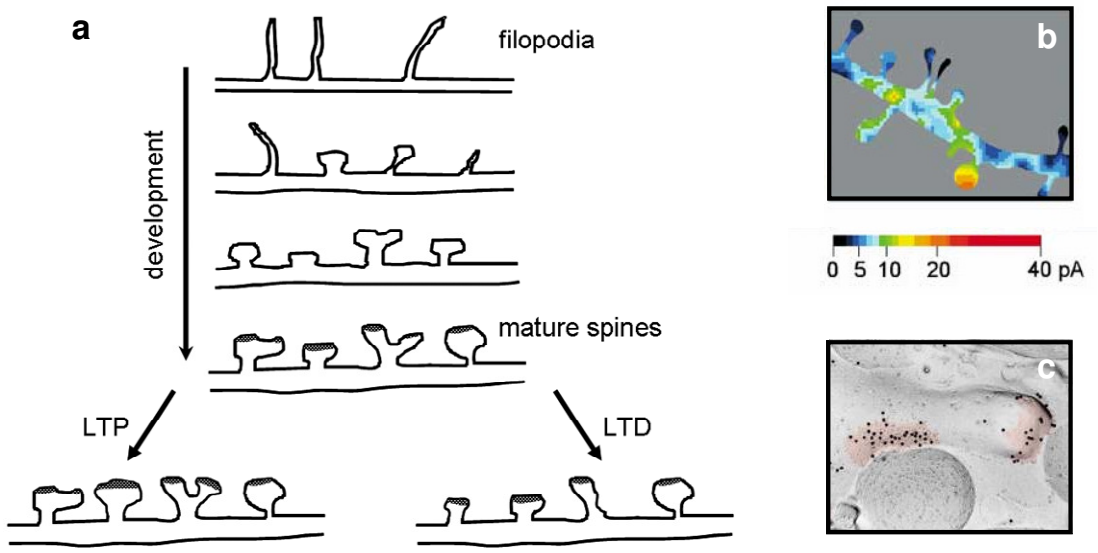

Figure 1. 2 Dendritic spines are the sites of excitatory synapses

a) A schematic representation of the morphological changes of dendritic spines during development and after LTP and LTD. Taken from (Sala et al., 2008). b) A map of glutamate sensitivity of a stretch of dendrite. Amplitudes of glutamate-induced currents are represented by the pseudo-color code shown at the bottom of this panel. From Matsuzaki et al. (2001). c) AMPA receptor distribution at synapses (colored in red) in the molecular layer of the cerebellum shown by SDS-digested freeze-fracture replica labeling. Dark immunogold particles indicate AMPA receptors (GluR1-4). Adapted from Matsuzaki et al. (2007).

1.1.7 SynGAP regulates dendritic spine morphology

Dendritic spines are small actin enriched protrusions that extend from the dendritic shaft and form the physical location of many excitatory synapses. Dendritic spine morphology is thought to be intimately linked to the function of synapses. Changes in spine morphology are associated with synaptic plasticity; the strength of a synapse is correlated with the size of the spine head, which is, in turn, correlated with the size of the postsynaptic density and the content of AMPA receptors (Harris & Stevens, 1988; Yuste & Bonhoeffer, 2001; Newpher & Ehlers, 2009) (Figure 1. 2). The mechanisms by which these pathways are regulated then must be coordinated. Several studies have shown that synaptic stimulation alters the spine cytoskeleton

(Lin et al., 2005), and that altering the actin dynamics interferes with synaptic plasticity (Fukazawa *et al.*, 2003; Rabenstein *et al.*, 2005). Actin dynamics are influenced by NMDA receptor mediated Ca^{2+} influx that regulates the activity of Rho family and Rac small G proteins, which in turn regulate the enzymatic reactions that control actin polymerisation (Kennedy et al., 2005). Spine size is also influenced by the additional membrane and proteins that are inserted there by trafficking endosomes (Park *et al.*, 2006).

As one would predict of manipulations that cause changes in synaptic AMPA receptor content altering SynGAP expression also results in changes to dendritic spine morphology. Vazquez et al. (2004) see a premature development of dendritic spines that accompanies the observed increase in mEPSC amplitude in *SynGAP* $^{-/-}$ neurons. The dendritic spine phenotype is rescued by the reintroduction of SynGAP with an intact, but not a mutated, C-terminal alpha-1 tail again hightlighting the importance of this region in mediating signalling. No other SynGAP isoforms were examined. Enlarged dendritic spines are also seen in adult *SynGAP* $^{+/-}$ hippocampus indicating that exaggerated spine development is not merely a developmental precociousness (Carlisle *et al.*, 2008). Deficits were also found in elements of actin regulatory signalling pathways and the authors suggest that these effects are mediated through altered Ras signalling effecting Rac activity

The above evidence indicates that two key aspects of synaptic function, synaptic AMPA receptor insertion and structural synaptic maturation, are negatively regulated by SynGAP (Figure 1. 3).

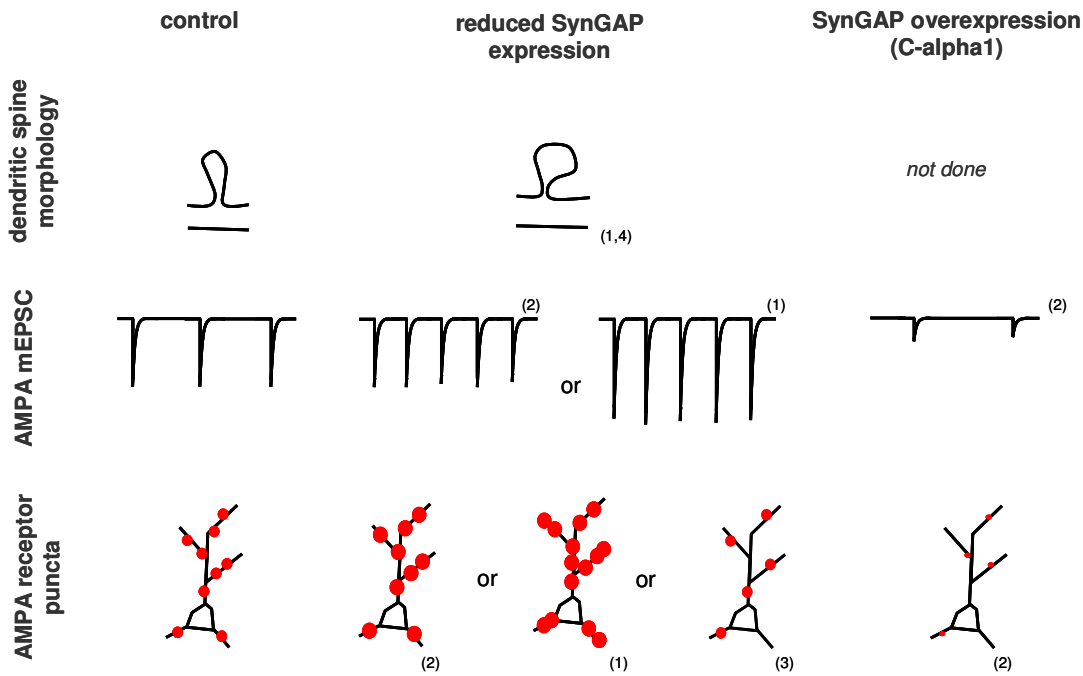

Figure 1. 3 The effects of altering SynGAP expression

Schematic summary of the effects of altered SynGAP expression on dendritic spine morphology (top panel), AMPA mEPSC amplitude and frequency (middle panel) and AMPA receptor puncta size and density (red dots, bottom panel). Data is drawn from (Vazquez et al., 2004)[1] using homozygous knock out cultured hippocampal neurons, (Rumbaugh et al., 2006)[2] homozygous knock out and overexpression in cultured forebrain neurons, (Krapivinsky *et al.*, 2004)[3] siRNA knock down of alpha-1, alpha-2 and gamma in cultured rat neurons, (Carlisle et al., 2008)[4] heterozygous knock out in adult hippocampus.

1.1.8 How does SynGAP regulate neuronal function?

For SynGAP to mediate its negative regulatory role on synaptic maturation it must have a functional GAP domain (Vazquez *et al.*, 2004; Rumbaugh *et al.*, 2006). This implicates the dampening of activity of SynGAP targets in the constraint of synaptic maturation. What is the molecular function of SynGAP and how does it lead to the cellular outcomes described above?

The main functional domain of SynGAP is the GAP domain, which can stimulate the GTPase activity of the small G proteins Ras and Rap. The activity of small G proteins is dependent on their ability to cycle between tri-or di-phosphate guanosine nucleotide (GDP/GTP) binding states. In the active GTP bound state G proteins are capable of recognising and activating downstream effector proteins (Kandel, 2000). GAP domains enhance the inactivation of small G proteins by promoting their intrinsic GTPase activity. A large body of work implicates a wide range of small G proteins, also known as the Ras superfamily, as critical regulators in a diverse range of biological processes (summarised in Appendix Table 2.1). The Ras branch of the Ras superfamily includes the small GTPases Ras and Rap. Although it was initially assumed that the Ras proteins share essentially identical functions it now seems that the are functionally distinct (Reuther & Der, 2000). Interestingly, there is evidence that the two pathways can operate antagonistically. Data regarding the general cellular roles of Ras and Rap is summarised in Appendix Table 1.2).

Ras and Rap in synaptic plasticity

It has been proposed that in neuronal cells, Ras, Rap1 and Rap2, are differentially stimulated by different forms of synaptic activity via activation of NMDA receptors and influx of calcium to independently control three activity-dependent AMPA receptor trafficking events[1]. (Figure 1. 4) (Thomas & Huganir, 2004; Tada & Sheng, 2006; Gu & Stornetta, 2007; Stornetta & Zhu). This model entails the synaptic

[1] Tetrameric AMPA receptors can be classified into two groups based on their composition of subunits encoded by four genes (GluR 1-4). One group consists of subunits with long cytoplasmic tails (GluR1, GluR2L and GluR4), the other group consists of subunits with short cytoplasmic tails (GluR2, GluR3 and GluR4c). Malinow R & Malenka RC. (2002). AMPA receptor trafficking and synaptic plasticity. *Annual review of neuroscience* **25,** 103-126..

insertion of AMPA receptors being regulated by Ras while the synaptic removal of AMPA receptors is mediated by Rap signalling.

1) *Synaptic potentiation – Ras/ERK / Ras/PI3K – synaptic AMPA receptor insertion*

LTP-inducing stimuli activate the Ras/MEK/ERK and Ras/PI3K/protein kinase B (PKB/AKT) signalling pathways, which phosphorylate AMPA receptors with long cytoplasmic-termini and drive these receptors into synapses (Zhu *et al.*, 2002; McCormack *et al.*, 2006).

The link between NMDA receptor activation and Ras activation may be calcium/calmodulin-dependent protein kinase II (CaMKII) which is activated by Ca^{2+} prior to Ras activation. Many studies have demonstrated a key role for CaMKII in synaptic plasticity and learning (Lisman et al., 2002). Crucially, Ras activity is required for CaMKII to drive the insertion of AMPARs into synapses (Zhu et al., 2002). This is consistent with the suggestion that CaMKII regulates Ras signalling via molecules that activate Ras (RasGEFs) and/or RasGAPs, such as SynGAP (Kim et al., 2003; Rumbaugh et al., 2006)

2) *Synaptic depression –Rap/p38 MAPK – synaptic AMPA receptor removal*

LTD-inducing stimuli (e.g., low frequency synaptic inputs) activate Rap1, which activates p38MAPK and leads to synaptic removal of the AMPA receptors with short cytoplasmic-termini (GluR2/3) (Zhu *et al.*, 2002; McCormack *et al.*, 2006). Activation of p38 MAPK signalling has been shown to mediate impairments in LTP (Butler *et al.*, 2004; Hsieh *et al.*, 2006) and overexpression of Rap1 or Rap2 causes a decrease in miniature AMPA mediated currents (Fu et al., 2007). The substrates for p38 MAPK that mediate these effects in response activation of NMDA receptors remain to be identified. Among the many molecules signalling downstream of p38 MAPK are transcription factors, protein kinases and the small GTPase Rab5, which is essential for early endocytosis (Shi & Gaestel, 2002). An attractive hypothesis is that activation of p38 MAPK may accelerate glutamate receptor endocytosis by stimulating the formation of the guanyl nucleotide dissociation inhibitor-Rab5 complex (Huang et al., 2004). Another potential mechanism involves the

phosphorylation of GluR2 to disrupt its interaction with glutamate receptor-interacting protein/AMPA-binding protein (GRIP/ABP) and reduces the recycling of GluR2/3 AMPA receptors and thus depresses synaptic transmission (Matsuda et al., 2000; Chung et al., 2003).

Furthermore, the identification of two RapGAPs that are enriched in PSDs indicates that Rap signalling is probably important at synapses (Pak *et al.*, 2001; Roy *et al.*, 2002). Overexpression of one of these RapGAPs (spine-associated RapGAP, SPAR), which should inhibit Rap and consequently p38 MAPK signalling, leads to increased size of dendritic spines thought to be associated with increased synaptic AMPA receptors (Pak *et al.*, 2001). This again indicates that Rap1 is involved with AMPA receptor removal from the synapse.

3) *Synaptic depotentiation – Rap2/JNK – AMPA receptor removal*

Rap2 can control synaptic removal of AMPA receptors with long cytoplasmic-termini during depotentiation. In response to depotentiation-inducing stimuli (e.g. low frequency synaptic inputs after LTP) Rap2 appears to stimulate JNK activity (Zhu *et al.*, 2005; Kielland *et al.*, 2009). Although less work has been done elucidating Rap2's role in neurons there is reason to believe that it may be significant. Proteomic analysis of the NMDA receptor complex has shown that Rap2 associates more closely with it than Rap1 (Husi et al., 2000) and SPAR stimulates Rap2 GTPase activity more efficiently than it does Rap1 GTPase activity (Pak *et al.*, 2001).

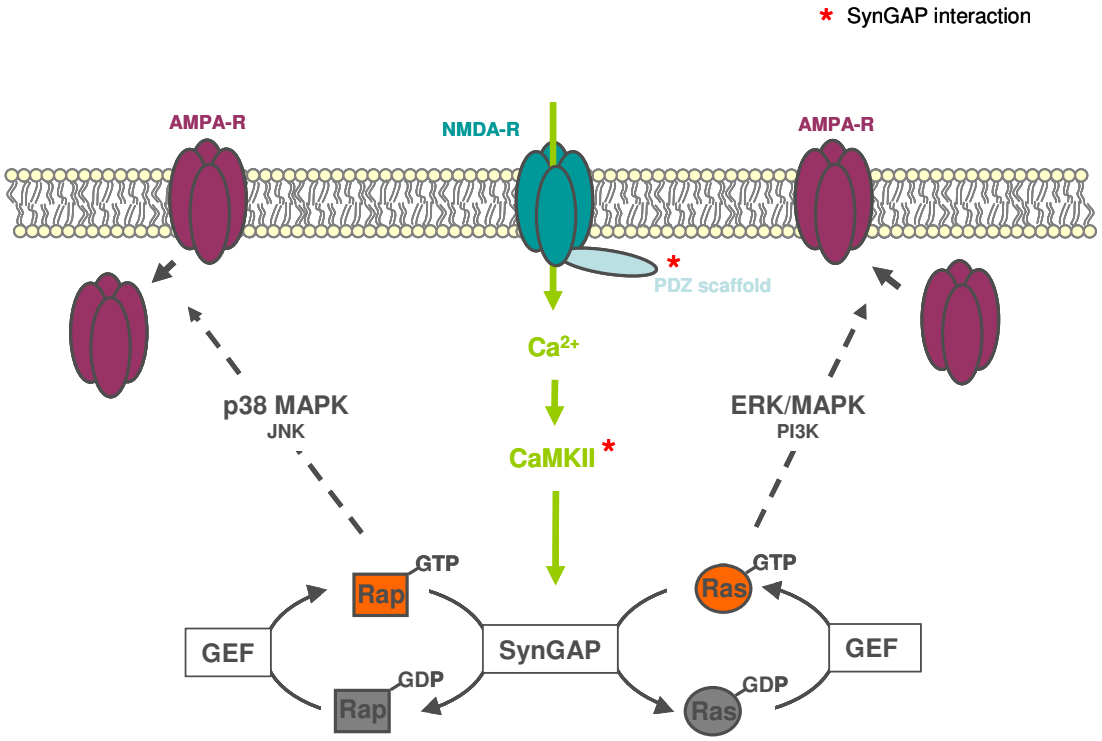

Figure 1. 4 A schematic diagram of the components of the post synaptic compartment implicated in SynGAP mediated signalling events

A red asterisk indicates proteins which have been shown to interact with SynGAP, specifically SynGAP alpha-1 has been shown to interact with a number of PDZ domain containing scaffolding proteins; PSD-95 (Kim *et al.*, 1998; Li *et al.*, 2001) , SAP-102, (Kim *et al.*, 1998; Yoshii & Constantine-Paton, 2007), MUPP1 (Krapivinsky *et al.*, 2004) and MAGI-SSCAM (Noboru Komiyama, personal communication). SynGAP beta has been shown to interact with CAMKII (Li *et al.*, 2001)..

This simple model, whereby Ras signals to potentiation and Rap signals to depression is unlikely to be the whole story (Figure 1. 4). Although the evidence for the above outlined roles for Ras signalling are quite strong, the precise roles of Rap1 and Rap2 have yet to be determined. Far less work has been performed on the later two molecules, and a lot of the key findings reported by Zhu and co-workers (points 2 and 3 above) have yet to be replicated in different labs. However, distinctive effects of constitutively active Rap1 and Rap2 on the morphology of

growth cones and dendritic spines support the idea that these two GTPases have different functions in neurons (Richter et al., 2007).

Behaviourally, ERK signalling is required for certain forms of spatial memory and fear-dependent learning but the roles of p38 MAPK have yet to be determined. Additionally, other studies have provided compelling evidence that, in certain neuronal cell types, Rap signalling can control the activation of ERK owing to its ability to activate the 'Ras' effector B-Raf isoform (York *et al.*, 1998; Grewal *et al.*, 2000). B-Raf is the Raf isoform that is expressed in neuronal processes and so the isoform likely involved in synaptic signalling. One study has suggested that Rap1 can signal through B-Raf to ERK in normal circumstances (Morozov *et al.*, 2003) but this may have been an artefact of overexpression.

Although Ras and Rap in strictly opposing roles is an oversimplification they clearly do have distinct roles. The question then arises; how can SynGAP regulate both of them?

Is there evidence for SynGAP regulating both Ras and Rap, and their downstream effector pathways (ERK and p38 MAPK)?

Named as a RasGAP by similarity to other RasGAPs, initial experiments on SynGAP showed that it does indeed regulate the Ras/ERK/MAPK pathway *in vivo* and *in vitro*[2] ERK activation is up-regulated in neurons from *SynGAP* knockout mice, whereas p38 MAPK function is depressed (Chen *et al.*, 1998; Kim *et al.*, 1998; Komiyama *et al.*, 2002; Rumbaugh *et al.*, 2006). Furthermore, overexpression of SynGAP alpha-1 decreased ERK activity and potentiated p38 MAPK signalling (Rumbaugh et al., 2006).

[2] Basal levels of ERK activation were elevated in cultured SynGAP $^{-/-}$ neurons and could not be increased by stimulation (Rumbaugh et al., 2006). Similar experiments on hippocampal slices from SynGAP $^{+/-}$ mice also reveals increased basal ERK activation. However NMDA stimulation of these neurons, perhaps reflecting a gene dosage effect, did induce a robust increase in ERK activation (Komiyama et al., 2002). These experiments indicate that SynGAP is a negative regulator of Ras, however Rap and p38 MAPK were not examined by these investigators.

Carlisle et al. (2008) demonstrate a transient increase in the phosphorylation SynGAP in response to NMDA receptor activation which decreases to below baseline levels if the stimulation is maintained. These authors see an increase in active Ras that follows the same transient increase and decrease timescale, they postulate that SynGAP acts to limit the time over which Ras is active. The knock down of SynGAP has resulted in sustained, rather than transient, ERK activation, supporting the notion that SynGAP acts to shut down stimulation induced Ras activity (Kim *et al.*, 2005).

However, other studies reveal opposing effects; knockdown of SynGAP by Krapivinsky (2004). resulted in a marked increase in p38MAPK activity without affecting ERK activity. In response to NMDA receptor activation SynGAP was seen to be dephosphorylated, increasing its activity as measured by a deactivation of the p38 MAPK pathway (Krapivinsky *et al.*, 2004)[3].

This discrepancy is apparent in conflicting results regarding the effect of the reduction of SynGAP expression on AMPA receptor trafficking (Figure 1. 3). In different studies surface AMPA receptor puncta are 1) increased in size and density, 2) size but not density and 3) decreased in size and density (Krapivinsky *et al.*, 2004; Vazquez *et al.*, 2004; Rumbaugh *et al.*, 2006).

Thus it appears that SynGAP can regulate both ERK and p38 MAPK pathways *in vivo.* How can the ability of SynGAP to regulate two potentially opposing pathways be reconciled? What governs its capacity to do so?

[3] There are many possible sources of discrepancies between these data sets. It is likely that these pathways are subject to fine temporal control and as such different time courses make it difficult to compare results. The stimulation of NMDA was achieved in one case by bath application of NMDA (Carlisle et al., 2008), and in the other of glutamate and bicuculine (Krapivinsky et al., 2004) however in both cases effects were abolished by the NMDA open channel blocker MK-801). In a separate set of experiments, in which SynGAP was not under study, an NMDA receptor mediated transient increase in activation of p38 MAPK was dependent on the concentration of stimulating NMDA, adding an additional level of complexity (Waxman and Lynch, 2005). Discrepancies also may arise from examination of total phosphoryation (Krapivinsky et al., 2004) or the phosphorylation of specific sites (Carlisle et al., 2008). It would be illuminating to know the time course of activation of SynGAP phosphorylation, Ras/Rap activity and p38/ERK MAPK activation under the same experimental conditions.

1.1.9 SynGAP as a bifunctional GAP

Small G proteins are regulated by two main classes of protein; those that activate G proteins by stimulating the dissociation of GDP to be replaced by the more abundant GTP, the guanine exchange factors (GEFs); and those that stimulate the inactivation of G proteins by catalysing their intrinsic GTPase activity, the GTPase activating proteins (GAPs).

The first identified GAP for the Ras superfamily was a RasGAP (p120 GAP) (Adari et al., 1988). It was expected that when a GAP was discovered for Rap it would be very similar to RasGAPS. However RasGAPs and RapGAPs are structurally unrelated (Rubinfeld et al., 1991). Reflecting this difference, the mechanism by which Ras and Rap1 GAPs enhance the GTPase activity of their respective GTPases is distinct. (The catalytic mechanism of Rap2 has not been studied directly, but it is thought have slower intrinsic and stimulated GTPase activity than Rap1 (Ohba et al., 2000). For RasGAPs a catalytic arginine residue, the arginine finger, is supplied by the GAP molecule into the active site of Ras, increasing the reaction rate by >1,000-fold (Scheffzek et al., 1997). Instead, Rap1 GAPs provide a catalytic asparagine, the asparagine thumb, to stimulate GTP hydrolysis. (Daumke *et al.*, 2004; Scrima *et al.*, 2008).

A bifunctional GAP is one that can catalyse the GTPase activity of two classes of G protein, in this case Ras and Rap. Apart from SynGAP the remaining bifunctional Ras/RapGAPs that have been identified are all members of the GAP1 family (CAPRI, RASAL, GAP^{IP4BP})[4] (Kupzig et al., 2006). Work on the catalytic mechanism of one of these molecules, GAP^{IP4BP} revealed an unusual mechanism, the arginine-finger of the GAP domain is crucial for both activities of the bifunctional GAP, despite the fact the coordinating active site residue used in Ras is not present in Rap1 (Kupzig et al., 2006). Additionally Pena *et al* showed that the arginine finger residue is important for efficient RapGAP catalysis of SynGAP (Arg/R486 in Figure 3. 2). Thus, the catalytic RapGTPase mechanism of the bifunctional GAPs is closer to RasGTPase activity than canonical RapGAP activity.

[4] The fourth member of the GAP1 family , $GAP1^{m}$, displays only Ras GAP activity.

What then determines if bifunctional GAP domains work as Ras or RapGAPs? Crucially it appears that regions outwith the GAP domain are essential for multifunctionality. By sequence homology SynGAP is closer to a RasGAP than a RapGAP and, when examined in isolation the GAP domain functions as a RasGAP, but not a RapGAP (Chen *et al.*, 1998; Kim *et al.*, 1998; Pena *et al.*, 2008). However, if GTPase function is assayed when the GAP domain is linked to its C2 domain the intrinsic catalysis of Rap is stimulated by approximately 1×10^4 fold (Pena et al., 2008). Moreover, when compared side by side full length SynGAP stimulated Rap GTPase activity much more potently than Ras GTPase activity (2-fold maximum stimulation of Ras GTPase compared to a 10-fold stimulation of Rap GTPase). The authors suggest that the possible contact of the mobile C2 domain with Rap and/or the GAP domain would promote catalysis, for example by making accessible a catalytic residue of GAP or Rap.

SynGAP is not alone among bifunctional GAPs in its requirement for additional domains to allow multifunctionality. Kupzig et al. (2006) and Sot et al. have demonstrated that bifunctional members of the GAP1 family also require domains outside the GAP domain, such as C2 and/or PH/BtK for their RapGAP activities. The authors support a similar model to that proposed for SynGAP, that conformational changes in the N-terminal C2 and C-terminal PH domains induce a shift in G protein specificity by the altered positioning of catalytic residues. (C2 and PH domains are also present in SynGAP and are discussed in more detail later, p44)

An especially interesting example of the regulatory capacity of extra GAP domain domains in GAP regulation comes from bifunctional GAPs RASAL and CAPRI. In response to Ca^{2+} oscillations RASAL associates and dissociates from the membrane but CAPRI, due to its membrane interacting PH domain, once translocated is refractory to further changes in Ca^{2+} concentration. Intriguingly, RASAL and CAPRI only operate as RasGAPs when associated with the plasma membrane. Thus CAPRI seems to low-pass filter the Ca^{2+} signal, converting different intensities of stimulation into different durations of Ras activity. In contrast, RASAL preserves the Ca^{2+} frequency information suggesting sophisticated modes of Ca^{2+}-regulated Ras deactivation (Walker *et al.*, 2004; Liu *et al.*, 2005). It is unknown how the RapGAP function of these molecules is regulated.

More generally GAPs are regulated by either protein-protein or protein-lipid interactions, binding of second messengers, and/or posttranslational modifications (Bernards & Settleman, 2004). Regions outwith the GAP domains may provide sites for these interactions.

1.1.10 A key observation; differential regulation of *Syngap* variants in development and in response to synaptic activity

The above data indicate that we should look outside the GAP domain in order to understand the normal physiological function of SynGAP. As mentioned the *SynGAP* gene gives rise to a number of alternative mRNA transcripts which encode different isoforms (Figure 1. 1). All isoforms have the same central regions, including the GAP domain. However there are a number of N-terminal isoforms (A,B,C,E) that arise from alternative transcription start sites and a number of C-terminal isoforms (alpha-1, alpha-2, beta, gamma) that are caused by alternative splicing.

A key observation that forms the impetus for much of the work in this thesis was made in our laboratory by Mark Barnett. These data suggests that the 5' alternative transcripts are differentially regulated in response to synaptic activity and in development (Figure 1. 5). Stimulation of synaptic activity in cultured neurons induces the downregulation of *SynGAP A* transcript but the upregulation of *SynGAPs B* and *C* [5]. Despite these changes total *SynGAP* and *SynGAP E* mRNA levels are unchanged. In the developing mouse cortex, total *SynGAP* mRNA levels increase steadily from birth and peak at post natal day 14 (p14). *SynGAP A* and *SynGAP B* mRNA transcript follows this profile but *SynGAP C* is almost undetectable at the earliest ages and is dramatically upregulated at p14.

Although we do not know if protein expression levels are correlated with mRNA expression (specific antibodies against the different N-termini do not exist)

[5] Mouse cortical cultures (DIV 10 – 12) were stimulated with bicuculine (50 µM) and 4 amino-pyridiine (250 µM) for 4 hours. *SynGAP B* and *SynGAP C* were upregulated (1.69 +/- 0.07 and 2.5 +/- 0.15 times compared to control levels), SynGAP A was downregulated to 0.7 +/- 0.1 times compared to control levels (One way ANOVA, Post hoc Tukey t-test, $p<0.01$ for all).

translation of the different mRNA profiles would lead to different complements of SynGAP proteins. SynGAPs A, B and E each have unique amino acid sequences as well as a common region to the N terminus of the PH domain. SynGAP C is a truncated protein and lacks a complete PH domain (amino acid lengths are given in Figure 1. 1).

mRNA levels	Total *Syngap*	*Syngap* A	*Syngap* B	*Syngap* C	*Syngap* E
Response to synaptic activity	no change	**repressed**	**induced**	**induced**	no change
Developmental expression	peak at p14	peak at p14	peak at p14	dramatic upregulation at p14	peak at p14

Figure 1. 5 *SynGAP* 5' variants are differentially regulated in development and in response to synaptic activity

Given the recently established role of the SynGAP N-terminal C2 domain in determining GTPase specificity and the potentially antagonistic effects of Ras and Rap signalling, the differential regulation of 5' variants led us to hypothesise that they may have a role in regulating GTPase activity. Crucially, most of the isoforms have been found in the post synaptic density by mass spectrometry suggesting that they may have some functional role to play (Seth Grant, personal communication) (alpha-1, beta (Peng et al., 2004)). The exceptions to this are SynGAP B, E and SynGAP C, which does not have any unique amino acid sequence and cannot be identified .

We do not know if C-terminal isoform expression is regulated or correlated with N-termini, but it is known that the C-terminus is important for determining SynGAP's interactions with other proteins. Altered protein protein interactions may provide a mechanism for the regulation of SynGAP by differentially positioning it with respect to regulators and effectors, as well as the direct allosteric effect of the interaction. The N-terminal isoforms have not been studied, in the literature they appear only when first described, and so it is not known if they mediate any interactions. When considering what molecules SynGAP isoforms may interact with and how they may be regulated one must also consider the putative interaction domains that are

common to all isoforms. These common regions may complement or override potential functionalities of the isoform specific regions.

In the remainder of this chapter I will outline the different SynGAP protein isoforms (Figure 1. 4) and how they arise from mRNA variants (Figure 1. 6) before describing what is known about SynGAP interactions and potential interactions[6].

1.1.11 SynGAP isoforms and how they arise

Alternative transcription start sites and splicing will be discussed generally in the introduction to Chapter Three, which is concerned with the molecular complexity of SynGAP transcription and translation. An overview of the exonic structure of the SynGAP gene and how different transcripts arise is given in Figure 1. 6.

overleaf

Figure 1. 6 A schematic diagram of the exonic structure of the *SynGAP* gene.

The exonic structure of the SynGAP gene is shown in full in the upper panel. Transcribed DNA is illustrated by boxes (unshaded indicates untranslated DNA, shaded and coloured indicates translated DNA), intronic DNA is illustrated by a horizontal line. Isoform specific untranslated region (UTR) is indicated by a lower case letter within the box. Where divergence occurs at the same locus the different possible outcomes are shown above and below the midline. Alternatively present sequence is highlighted with dashed lines. The bottom panel shows the exons that contribute to each individual isoform, only isoform specific UTR is shown. Isoform specific protein sequence is shown with different colours/shading.

[6] This description of the SynGAP gene, mRNA and protein is based on published reports (Chen et al., 1998; Kim et al., 1998 ; Li et al., 2001), and sequences deposited in online databases (NCBI/GenBank). It includes, but is not a comprehensive description of, data from our laboratory by Mark Barnett and Patrick Stoney on the transcription start sites of 5' variants using primer extension and 5' rapid amplification of complementary ends (RACE).

Figure 1.5 A schematic diagram of the exonic structure of the *SynGAP* gene

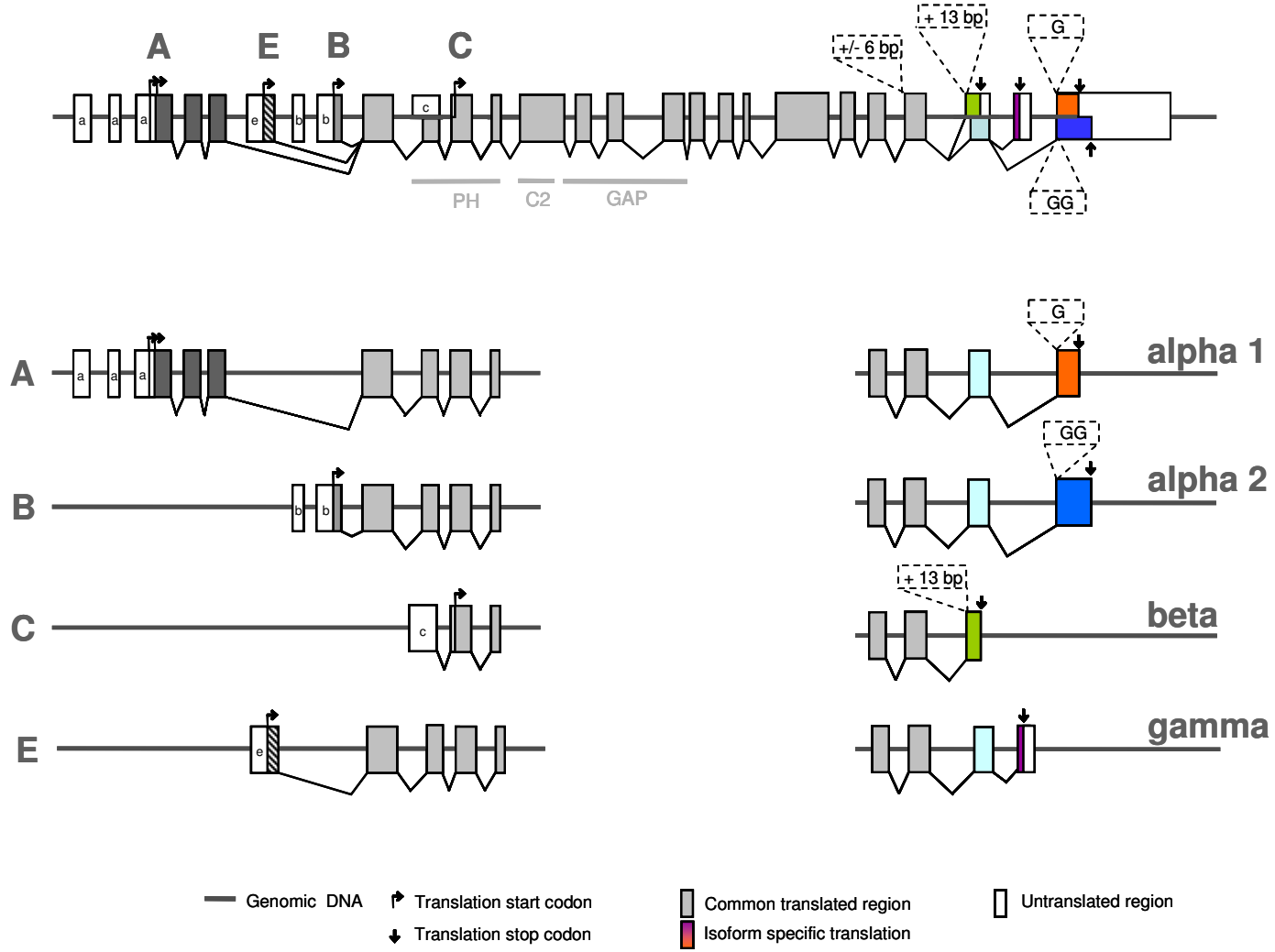

5' region / N-termini

Of the four alternative N-termini SynGAPs A, B and E have unique coding regions, while SynGAP C does not. All are associated with unique regions of 5' untranslated region (5' UTR). The longest N terminus is SynGAP A. This form arises from the most 5' transcription start site and has the longest unique region of 5' UTR (Figure 1. 6). There are at least two potential initiation codons which are 15 amino acids apart, it is unclear which of these is used as the primary initiation codon. SynGAP E is not published and is not present in an online sequence database, however it has been cloned multiple times in our laboratory (Mark Barnett, personal communication). It consists of one unique exon and encodes the shortest unique N terminus (12 amino acids). SynGAP B is encoded by a number of unique exons. Exons of SynGAPs A, B and E splice into a common exon (exon 'ABE'). The next exon codes for the N-terminal portion of the PH domain and is also present in the 5' UTR of the transcript for *SynGAP C*, in which case it is extended upstream to include a region of specific *SynGAP C* 5' UTR. SynGAP C translation does not begin until the next exon resulting in a truncated protein.

3' region / C-termini

There are four major SynGAP C-termini, SynGAP alpha-1, alpha-2, beta and gamma that arise through alternative splicing events. Alternative splicing proceeds in a number of ways (Figure 1. 6) including the inclusion or exclusion of an entire exon from the final transcript. Splicing of this type gives rise to SynGAP gamma which occurs when a short exon is included in the transcript; this exon encodes four unique amino acids before termination. However the majority of alternative splicing at the 3' end of *SynGAP* occurs through the use of alternative splice site selection. SynGAP beta is caused by the inclusion of 13 base pairs (bp) at the 5' end of an exon present in all *SynGAP* transcripts. The 13 bp causes a frameshift and the inclusion of 21 unique amino acids before termination. The inclusion of an additional guanine residue at the next exon-exon boundary determines the translation of SynGAP alpha-2. If only one guanine is present at that position SynGAP alpha-1 is translated. I refer to this as the G insert position.

Other variation occurs that does not cause a frameshift or have major effects on the coding sequence. An alternative choice of splice junction (upstream of the region described above) leads to the inclusion or exclusion of an in-frame 6 bp which codes for valine and lysine (VK). An additional 3 bases (TGG) may also be present at the G insert position, thus the possibilities at this position are G / GG / GGTGG.

Given four N-termini and four C-termini there are 16 possible combinations but additional complexity is added by absence or presence of amino acids such as the in-frame VK insert and possible alternative translation start sites of SynGAP A.

Syngap alpha-1 and *alpha-2* transcripts differ by only one base pair so their differential detection by RT-PCR or in situ hybridisation, although technically possible, is challenging in reality. Confoundingly, the interpretation of G insert status for alpha-1/alpha-2 coding outcomes is only possible if the 13 bp beta insert and gamma exons are also known not to be present. The detection of *SynGAP beta* and *gamma* would be more feasible given their longer and more 5' specific exons. Antibodies against SynGAP alpha-1 and beta exist, and an antibody against SynGAP alpha-2 has very recently become available. An experiment examining differential regulation of the protein isoforms is now possible.

1.1.12 The protein-protein interactions of SynGAP C-terminal isoforms

Some interacting proteins have been established for SynGAPs alpha-1, alpha-2 and beta. There is no published indication of what, if any, proteins interact with the N-terminal isoforms or SynGAP gamma.

SynGAP alpha-1 interacts with PDZ domain containing proteins

Two labs independently cloned SynGAP alpha-1 in 1998 in a manner that gave an early indication of its functional role. Chen et al. (1998) isolated SynGAP

fragments from a library screen using probe sequence derived from tryptic digests of purified post synaptic densities (PSDs), indicating that SynGAP is highly enriched in the PSD. Kim et al. (1998) identified SynGAP alpha-1 in a yeast two hybrid screen using a PDZ domain of synapse associated protein 102 (SAP102) as bait. Since then many studies have shown that SynGAP alpha-1 can interact with a number of molecules that contain the synaptically prominent protein-protein interaction motif the PDZ domain, specifically PSD-95, SAP102 and MUPP1.

PDZ domains are protein-interaction domains that are often found in multi-domain scaffolding proteins. At the synapse a class of PDZ domain containing scaffolding proteins, known as MAGUKS, assemble large molecular complexes (Kim & Sheng, 2004). PDZ domains bind to, amongst many other targets, the intracellular tails of the NMDA receptor and potassium channels and mediate the recruitment of a host of PDZ binding proteins to the PSD (Irie et al., 1997). Although NMDA receptors bind directly to PSD-95 family members, AMPA recepotors indirectly associate with PSD-95 through auxiliary transmembrane AMPAR regulatory proteins (TARPs) (Nicoll et al., 2006).
Scaffolds can be multimerised through disulfide linkages and as such act to cluster receptors and channels. PDZ scaffolds also bind to the cytoplasmic domain of the neuronal cell adhesion molecules, such as neuroligins, implying a role in the coordination of the pre and post synaptic compartments (Hirao et al., 1998).

The binding of SynGAP-alpha-1 to the PDZ domain is mediated mainly by its last four amino acids, QTRV, which constitute a canonical PDZ binding domain (T/SXV). This sequence is essential for SynGAP's interaction with PSD-95 (all three PDZ domains) and SAP102 (Chen *et al.*, 1998; Kim *et al.*, 1998; Li *et al.*, 2001; Krapivinsky *et al.*, 2004). The interaction of SynGAP-alpha-1 and MUPP1 seems to be less specific than that of SynGAP-alpha-1 and PSD-95. Krapivinksy et al. (2004) needed to use a blocking peptide fragment consisting of the final 111 SynGAP amino acids to disrupt the SynGAP/MUPP1 interaction. Approximately half the sequence of this peptide is present in all SynGAP isoforms, suggesting that MUPP1 may also interact with other isoforms of SynGAP.

SynGAP and PSD-95 are present in roughly similar molar quantities at the PSD, so one would predict that PSD-95 is SynGAP's major binding partner in stoichiometric terms (Cheng et al., 2006). Nevertheless, it has become clear that the interaction of SynGAP with PSD-95 is not necessary for SynGAP to reach the synapse (Barnett et al., 2006), possibly due to SynGAP binding to CaMKII or other PDZ domain containing scaffolds. The spatial and temporal expression patterns of the two genes are overlapping but distinct, and the phenotypes of the ablation of expression are quite different (Migaud *et al.*, 1998; Porter *et al.*, 2005; Barnett *et al.*, 2006). Disruption of the MUPP1 interaction also does not prevent SynGAP reaching the synapse (Krapivinsky *et al.*, 2004).

The other PDZ scaffolding protein that has been demonstrated for SynGAP alpha-1 is SAP-102. Yoshii and Constantine-Paton (2007) co-immunoprecipitated SynGAP alpha-1 with SAP102 but not PSD-95 (p14 mouse visual cortex). The LTP and learning deficits caused by SAP102 knock out closely phenocopy those of *SynGAP* $^{+/-}$ mice (reduced induction of LTP and specific spatial memory deficits that can be overcome with additional training) (Komiyama *et al.*, 2002; Cuthbert *et al.*, 2007).

It has been established that NMDA receptor activation can have differential effects on AMPA receptor trafficking, depending on the subunit composition of the NMDA receptor. This phenomenon is illustrated by the inhibition of NR2B-containing receptors which blocks the induction of LTD but not LTP in CA1 synapses, whereas specific antagonists of NR2A-NMDARs prevent the induction of LTP without affecting LTD (Liu et al., 2004; Massey et al., 2004). Related evidence indicates that a major signalling function of NR2B-NMDARs, particularly in mature neurons, is to dampen the magnitude and limit the duration of ERK activation (Kim *et al.*, 2005). In this system, SynGAP was preferentially associated with the NR2B, but not 2A, subunit suggesting that the differential effects of the subunit activation are mediated, at least in part, via SynGAP. The authors suggest the association of SynGAP to NR2B is mediated by the preferential binding of SAP102 to NR2B (rather than NR2A). However, the co-immunoprecipitation evidence on which this claim is based indicates only a very mild preference of SAP102 for NR2B (PSD-95 for NR2A) (Sans et al., 2000). A far more likely candidate is CaMKII which in these same

experiments also co-immunoprecipitates almost exclusively with NR2B. It is worth remembering that there are many scaffolding proteins and functional redundancy is likely to be rife.

SynGAP alpha-2 interacts with Unc51.1

SynGAP alpha-2 has been identified as a binding partner for the serine/threonine kinase Unc51.1 by a yeast two hybrid screen (Tomoda et al., 2004). Unc51.1, otherwise known as ULK1, is involved in the regulation of autophagy and in neurite extension in cerebellar granule neurons (Tomoda *et al.*, 1999). SynGAP alpha-2 bound to Unc51.1 baits 'with slightly higher affinity' than alpha-1. The authors state, but do not show, that a GFP fusion of the SynGAP alpha-2 tail was localised to extending axons, while GFP-SynGAP alpha-1 tail was restricted to the cell soma of cerebellar granule cells. For these reasons only alpha-2 was carried forward in their further experiments which show that SynGAP and Unc51.1 cooperate in inducing granule cell neurite outgrowth. Unc51.1 is also expressed in the adult rat hippocampus and cortex (Okazaki et al., 2000).

SynGAP beta interacts with CaMKII

SynGAP beta does not co-immunopreciptate with PSD-95 but despite this is more restricted to the PSD fraction than SynGAP-alpha-1 (Chen *et al.*, 1998; Li *et al.*, 2001). This synaptic restriction may be mediated by the ability of SynGAP beta to bind to Ca^{2+}/calmodulin-dependent protein kinase II (CaMKII), a highly abundant synaptic protein.

CaMKII has long been known as one of, if not the most abundant protein at the postsynaptic density (Kennedy *et al.*, 1983; Cheng *et al.*, 2006). It is activated when it binds calmodulin in the presence of Ca^{2+} and, once autophosphorylated, remains active in the absence of Ca^{2+} (autonomous form). CaMKII-mediated

phosphorylation of PSD components is likely to underlie changes in synaptic strength (Lisman et al., 2002).

Regulation of SynGAP by CaMKII

How SynGAP is regulated by NMDA receptor mediated events remains a contentious issue. It is clear is that SynGAP can be phosphorylated at many sites and this phosphorylation is dependent on CaMKII (Song *et al.*, 2003; Krapivinsky *et al.*, 2004; Oh *et al.*, 2004; Song *et al.*, 2004; Carlisle *et al.*, 2008). Despite preferentially binding SynGAP beta all the CaMKII phosphorylation sites identified are within regions common to all SynGAPs (Jaffe et al., 2004; Oh et al., 2004). The precise effect of phosphorylation is not firmly established as interpretation of the data is confounded by inconsistency in which of the many phosphorylation sites are examined.

Phosphorylation of SynGAP enhances its *in vitro* RasGAP activity (Oh et al., 2004). In quiescent neurons SynGAP is phosphorylated at a basal level that is dependent on NMDA receptor and CaMKII activity. The phosphorylation and downstream signalling effects of SynGAP in response to stimulation of NMDA receptors seems to be finely temporally tuned (Krapivinsky *et al.*, 2004; Carlisle *et al.*, 2008). Some residues in SynGAP are preferentially phosphorylated by the form of CaMKII that is autonomously active even after a Ca^{2+} transient has passed (Dosemeci & Jaffe). Interestingly, Ca^{2+} entry through voltage gated calcium channels in response to depolarisation is not sufficient to induce changes in SynGAP phosphorylation, again highlighting the importance of the NMDA receptor mediated Ca^{2+} entry (Krapivinsky *et al.*, 2004).

1.1.13 The common protein domains of SynGAP

The domain structure of SynGAP is similar to other GAPs which, like GEFs, are usually multi domain proteins and have domains such as PH, C2, SH3 and SH2 eg p120RasGAP, CAPRI. RASAL (Bernards, 2003; Pamonsinlapatham et al., 2009). The role of the SynGAP C2 domain in determining GTPase specificity has been discussed in Section 1.1.9 but there are other ways in which extra GAP domains

could affect SynGAP function. Often these domains are lipid or protein interacting indicating that they serve as localisation signals or scaffolds in the formation of protein complexes. It is thought that these domains play an important part in the regulation of GAPs and GEFs (Bos et al., 2007). Therefore, it is worth mentioning the other domains of SynGAP as these have a bearing on its functional properties and potentially its regulation.

The N-terminal domains found in SynGAP, the pleckstrin homology domain (PH) and the calcium/lipid-binding domain (C2) domain, often interact with the plasma membrane but this has never been examined in the case of SynGAP.

PH domain

Pleckstrin homology (PH) domains, one of the most abundant domain classes in the human genome, are structurally conserved functional domains that can undergo both protein/protein and protein/lipid interactions (Lemmon, 2004). PH domains can mediate inter- and intra-molecular binding events to regulate enzyme activity. The number and variety of host proteins with PH motifs are staggering (over 100 at last count). Despite minimal sequence homology, the three-dimensional structures are remarkably conserved and are best known to bind phosphatidylinositol lipids within biological membranes (Rebecchi & Scarlata, 1998; Lemmon, 2008).

PH domains are well known effectors of the lipid second messengers PIP_3 and PIP_2, which can be generated transiently upon activation of cell surface receptors (Cantley, 2002). A small subclass of PH domains, including those from Bruton's tyrosine kinase (BTK), general receptor for phosphoinositides-1 (GRP1) and protein kinase B (PKB; also known as AKT), recognize one or both of these second messengers with remarkable specificity and affinity. These PH domains represent classic examples of signal-regulated membrane-targeting modules. In each case, the isolated PH domain (as a GFP fusion protein) is predominantly cytosolic in unstimulated cells, but undergoes a dramatic transient relocalisation to the plasma membrane upon signal-dependent generation of the second messengers by PI3K (Varnai & Balla, 2006).

However, PH domains that are known to strongly and specifically bind to phosphoinositides represent only a small minority of a large and poorly understood class of domains (10% of the approximately 235 PH domains in the human proteome) (Lemmon, 2008).

SynGAP C lacks a portion of the PH domain, suggesting a mechanism by which it may be differentially regulated or localised compared to other isoforms with intact PH domains. In some cases two halves of PH domains from two separate proteins can come together to form a single functional PH domain, presenting a potential mechanism for SynGAP C specific interactions (Lemmon, 2005).

C2 domain

C2 domains are most well known as Ca^{2+} dependent membrane binding domains, which serve as Ca^{2+} effectors for divergent Ca^{2+}-mediated cellular processes. The C2 domain represents the second most abundant lipid binding domain behind the PH domain (Cho & Stahelin, 2006). A number of non-mutually exclusive mechanisms have been proposed for the Ca^{2+} mediated membrane binding of C2 domains that may involve membrane penetration or surface interaction (Grobler *et al.*, 1996; Shao *et al.*, 1997; Davletov *et al.*, 1998; Verdaguer *et al.*, 1999). The insertion of C2 domains into the plasma membrane can cause the membrane to bend, a process which is involved in the fusion of synaptic vesicles with the plasma membrane (Martens et al., 2007). This has led to the implication of the C2 domains as the main functional modules of the fusion machinery proteins, synaptotagmin-1 and Doc2b, in Ca^{2+} dependent fusion event (McMahon et al.).

Based on the diversity of Ca^{2+} responsiveness, it has been suggested that C2 domains may serve as differential calcium sensors in the cell. Many C2 domains, including C2 domains of conventional PKCs and cPLA2, have been shown to translocate to cell membranes in linear response to cellular Ca^{2+} oscillations (Evans *et al.*, 2001; Evans *et al.*, 2006). If the membrane association of a protein is dominated by its Ca^{2+}-responsive C2 domain(s) the host protein can also linearly respond to the Ca^{2+} oscillation. The bifunctional GAP, RASAL (previously mentioned on p33) which has two C2 domains, operates as a linear decoder of Ca^{2+} signals,

associating to and dissociating from the membrane as the cellular Ca^{2+} concentration fluctuates (Walker et al., 2004). However, other protein moieties come into play in determining the duration of membrane residence. CAPRI, a structural and functional homolog of RASAL, displays a long-lasting Ca^{2+} triggered translocation that is refractory to cytosolic Ca^{2+} oscillations due to the interaction of its PH domain with the membrane. Thus an interaction initiated by the Ca^{2+} responsiveness of the C2 domain is maintained by the PH domain (Liu et al., 2005).

It is important to stress, however, that not all C2 domains are capable of Ca^{2+}-dependent membrane binding. Indeed, a significant subgroup of C2 domains do not bind Ca^{2+} at all, and several are now known to proteinaceous bind targets (Cho & Stahelin, 2006).

Other regions of interest

There is region rich in proline residues (aa 785-815, Figure 3. 2) and as such may be a target for SH3 binding. The SH3 domain is a prototypical protein protein interaction domain commonly found in a wide range of signalling molecules (Mayer, 2001). The protein annotation of SynGAP in the UniProt database highlights this region as a potential SH3 binding domain but other bioinformatics tools do not indicate this region as such (NCBI Conserved Domains Search, SMART database).

A stretch of 10 histidine residues are located towards the C terminus of SynGAP (aa 958 – 968, Figure 3. 2). As far as I am aware there no definite function has been established for such a sequence. Stretches of histidine residues do occur, and are conserved, in a diverse range of proteins eg. voltage gated Ca^{2+} channel, Zic3/4, Ubiquitin carboxyl-terminal hydrolase (BLASTP). Imidazole side chains of histidine are known to be important for coordination with metal ions and functionally relevant metal and haem binding has been demonstrated in proteins with histidine rich regions, however these regions rarely have such long consecutive repeats. (Jones *et al.*, 2005; Arvanitis *et al.*, 2007).

1.2 Hypothesis

To summarise, SynGAP is a protein that can regulate many, and potentially antagonistic, arms of crucial signalling pathways in neurons. Its synaptic localisation combined with the various phenotypes associated with its manipulation suggests that it regulates synaptic strength in a dynamic manner. Evidence suggests that regions outwith SynGAP's central core are involved in determining which pathway it can regulate. The existence of various N- and C-termini, which we have seen to be differentially regulated in response to synaptic activity and mediate SynGAPs interaction with key molecules at the synapse, is suggestive of a mode of regulation of function. The central hypothesis of this thesis is that different isoforms of SynGAP have different functions. We posit that the different N- and C-termini of SynGAP have a role in determining its function, be it by altering its catalytic specificity, rate, localisation or partner proteins. All these specific mechanisms will not be examined directly rather the hypothesis will be addressed by examining the functional outcomes of manipulated SynGAP expression in neurons. Two aspects of neuronal function, which have been shown to be affected by SynGAP regulated processes, namely neuronal morphology and electrophysiology are studied. The effect of removing all SynGAP protein, to assess the dominant function of the molecule, and the effect of the expression of individual isoforms is examined

The question of the biochemical effect of SynGAP isoforms on its target molecules, Ras and Rap, is not examined here but should remain to the fore in considering the data presented.

2 Chapter Two: Methods

The methods used in this thesis are presented here, first methods that are common to most of the work, such as primary tissue culture and genotyping. Methods specific to each chapter are shown under the heading of the chapter in which they are used.

2.1 Detailed Index of Methods

2.2 Common Methods

2.2.1 Tissue culture

Primary neuronal tissue culture

Neurons are grown on 15 mm glass coverslips in 24 well plates for up to 14 days in a humidified incubator at 37 ^{o}C, 5% CO_2. Coverslips are washed in absolute ethanol before sterilisation by baking. Coverslips are coated with Poly D-Lysine (13 µg/ml, 70 – 150 kDa, Sigma, P0899) and Laminin from Engelbreth-Holm-Swarm murine sarcoma basement membrane (5 µg/ml, Sigma, L2020) in PBS using 400 µl/well. While coating coverslips are placed in the incubator for at least 3 hours or overnight. Coverslips are washed at least twice in sterile double distilled water prior to the commencement of dissections and are left to dry in the flow hood while dissections are performed

Neuronal cultures are established from mouse embryos of timed matings at embryonic day 17.5 (E17.5). The mother is killed by cervical dislocation, the abdominal area is sprayed with ethanol as are all the previously baked dissection tools. The birth canal is removed by caesarean section, individual embryos are removed and immediately decapitated. A piece of tail is taken for DNA for genotyping if a transgenic culture is being performed.

Dissection

The heads are placed on ice in pre-chilled dissociation medium. Brains are removed under a dissecting microscope; the skin is torn along the midline and peeled off the head. The head is kept steady against the platform by piercing through the nose with curved forceps. Using straight forceps the skull is cut along the midline from the cerebellum at the rear to between the eyes, and snipped around the base of both hemispheres. The skull caps are pulled back from the midline to reveal the brain. The brain is scooped out of the skull base, from the cerebellum, with a spatula and placed in ice cold dissociation medium (DM). All brains are removed before hippocampal or cortical dissections are begun. For

SynGAP cultures care is taken to remove the olfactory bulbs with the brain; if the nasal skull cuts are rostral enough and care is taken peeling back the skull the olfactory bulbs should lift out attached to the brain. These are used for lacZ staining to aid genotyping (Table 2. 1). The transgenic locus contains the lacZ gene which codes for beta-galactosidase. Conversion of the beta-galactosidase substrate X gal (5-bromo-4-chloro-3-indolyl- beta-D-galactopyranoside) to a blue colour indicates the presence of the transgene.

LacZ stain	
	Concentration
$MgCl^2$	2 mM
NP-40/IGEPAL	0.02%
NaDeoxychorate	0.01%
potassium ferric cyanide	5 mM
potassium ferro cyanide	5 mM
X-Gal	1 mg/ml
made up in PBS	

Table 2. 1 LacZ stain

Brains are transferred individually to 35 mm Petri dish containing fresh ice-cold DM for further dissection. If required olfactory bulbs are snipped off and replaced in DM on ice. Removal of the olfactory bulb aids with the removal of the meninges which are peeled off, taking care not to gouge the cortices. Each hemisphere is teased away from the thalamus by gently snipping at the connecting tissue. The hippocampi are removed using the tip of the forceps to cut along the entorhinal axis with small pinching motions. If cortices are required striatal tissue is snipped off using curved forceps. The cortex is trimmed of the most ventral part,corresponding to the archecortex, leaving the neocortex. The cerebellum is removed from the thalamus, and reserved for DNA extraction in the case of a transgenic culture. Tissue is transferred to DM on ice.

Dissociation

Prior to beginning brain dissection 25 – 30 U/ml fresh papain suspension (Worthington, Lakewood, NJ, USA supplied through Lorne Laboratories, Reading, UK) are added to DM supplemented with L-cysteine (approx 0.5 mg/ml, DM+C) and dissolved at 37 ^{o}C. The dissolved enzyme is filter sterilised immediately before the tissue is added. The tissue is incubated for 15 minutes in a 37 ^{o}C oven and is agitated very gently every five minutes. After this time the tissue is washed of enzyme by serial dilution. The tissue is transferred using a lightly fire polished pipette, a 2ml pipetteman pipette is necessary for the volume of tissue produced in pooled cortical cultures. Four washes are prepared for each piece of tissue in a transgenic culture. The tissue is transferred gently into each wash and let settle, no additional manipulation is made, before transferring to the next wash. The first two washes are DM, the second two are growth medium. The final wash is the medium in which the tissue is triturated. Tissue is triturated for approximately one minute using first a lightly fire polished, wide bore, glass pipette, then for an additional minute using a pipette fire polished to achieve a narrower bore. After this time there should be no very large visible lumps of tissue remaining. The cell suspension is let to settle for one or two minutes before gently removing the supernatant. This step is excluded for individual hippocampal cultures to maximise the cell yield.

Cell counting

50 µl cell suspension is combined with an equal volume Trypan Blue vital exclusion dye (Sigma, T8154) and cells which exclude the blue dye are counted in a haemocytometer and the cell count calculated. Cells are plated at a final density of 200 cells/mm^2 (low density) or 1500 cells/mm^2 high density. For 24 well plates cells are plated in 500 µl.

Maintenance

All the growth medium is aspirated on DIV1 and immediately and gently replaced with prewarmed growth medium (1ml). Additional growth medium (1ml) is added on DIV 4. Neurons are fed again at DIV 7 and 10 by removing half the volume (1ml) and replacing with fresh growth medium. In every instance the time neurons are out of the incubator is kept to an absolute minimum.

If FBS is included in the growth medium on DIV 4 cytosine β-D-arabino-furanoside hydrochloride (AraC, Sigma, C6645) is added to a final concentration of 4.6 µM. AraC blocks DNA replication and is used to stop glia from dividing. AraC is maintained at this concentration with all subsequent medium changes.

Solutions

Dissociaton medium (DM) (1X); Hank's Balanced Salt Solution, without Ca^{2+}/Mg^{2+} (Invitrogen, 14175053) supplemented with 10 mM $MgCl_2$, 1 mM kynurenic acid, 10 mM HEPES. This is made as a 10X stock solution (DM-S) which is heated to dissolve kynurenic acid, filter sterilised and stored at -20 ^{o}C in 50 ml aliquots. Upon reconstitution as a 1X solution DM is further supplemented with 0.1 % phenol red (Sigma, 0.5% in DPBS, P0290) and 50 U/ml penicillin,50 µg/ml streptomycin (Sigma, 100X; 10,000U/ml penicillin / 10mg/ml streptomycin, P0781).

Growth medium; Neurobasal A medium (Invitrogen, 10888-022) supplemented with 1X B-27 (Invitrogen, 175504-044), 0.25% GlutaMAX (Invitrogen, 35050061), Pen/Strep (as DM) and potentially 1 % foetal bovine serum (FBS, Invitrogen, 17504-157). See text regarding FBS.

Dissection tools; Surgical scissors, Iris scissors, Curved Dumont #7 forceps, Dumont #5 forceps (×2), Spatula (5 mm width), Pasteur pipettes (x3

Maintenance of HEK293 cells

HEK 293 cells are maintained in Dulbecco's Modified Eagle Medium (DMEM, Invitrogen, 41965-039) supplemented with 10 % foetal bovine serum (FBS), 1mM sodium pyruvate and 50 U/ml penicillin/streptomycin (Pen/Strep) in uncoated flasks. Cells are passaged when they reach confluence by detachment by brief (approximately 1 minute) trypsinisation (0,05% Trypsin-EDTA in growth medium, Invitrogen). Sloughed off cells are diluted with additional growth medium before centrifuging (800 rpm, 2 minutes). The cell pellet is resuspended in growth medium and split 1:10. Half the volume of growth medium is replaced every 4 days. For transfections cells are grown on poly-D lysine coated plates/coverslips in the same

manner as for neurons except; laminin is omitted and plates are coated for a minimum of 30 minutes. Cells are transfected when at approximately 80 % confluence.

Transfection of cells

Transfection of neurons

Neurons are transfected using a proprietry liposome based transfection product, Lipofectamine 2000 (Invitrogen). Transfection is performed from DIV 8 at the earliest to DIV 13 at the latest. Neurons are always used 16 to 36 hrs after the transfection complexes are added to the cells. The following amounts are for one well of a 24 well plate. On the morning of transfection the normal growth medium is removed and replaced with 0.5 ml pre warmed transfection medium (TM). The cells are returned to the incubator for at least 3 hours. 200 µl of conditioned TM is removed from the well. Lipofectamine 2000 (1 µl) is diluted in 33 µl conditioned TM and left at room temperature in the flow hood for 5 minutes while the DNA is being diluted. 0.3 µg total DNA (0.1 µg eGFP and 0.2 µg SynGAP or empty vector) is diluted in 33 µl conditioned TM. All the diluted Lipofectamine 2000 is then pipetted gently into the diluted DNA. The mixture is gently pipetted up and down 3 – 4 times and left in the flow hood at room temperature for 20 minutes. All of the DNA/Lipofectamine mixture is then added dropped gently into the original well which is swirled gently to ensure even distribution. The cells are incubated for at least 3.5 hours before all the transfection medium is removed and replaced with fresh growth medium.

Solutions

Transfection medium (TM); 'Salt, glucose, glycine' solution (SGG) supplemented with 10 % Minimum Essential Medium (MEM) with Earle's salts, without L-glutamine (Invitrogen, 21090-022) and 1.5 % Insulin-transferrin-sodium selenite media supplement (ITS, Sigma, I1884, vial reconstituted in 50ml). 1.5 % ITS is equivalent to 0.6 µg/ml each of insulin from bovine pancreas, human transferrin and sodium selenite.

Salt, glucose, glycine (SGG); 114 mM NaCl, 32.7 mM $NaHCO_3$, 5.3 mM KCl, 1mM $MgCl_2$, 2mM $CaCl_2$, 10 mM HEPES, 1 mM glycine, 20 mM glucose, 0.5 mM sodium pyruvate, 0.1 % phenol red (Sigma, 0.5% in DPBS, P0290).

Transfection of cell lines

Hek cells are transfected in a similar manner to neurons except that the DNA and Lipofectamine 2000 are diluted in OptimMEM (Invitrogen) supplemented with glucose. The complexes are added directly to the cells which are left in HEK cell growth medium. The complexes are not removed.

2.2.2 The SynGAP mouse model and genotyping

The SynGAP knockout mouse

The SynGAP knockout mouse used in this thesis was generated by Komiyama et al. (2002). Briefly targeting constructs were electroporated into 129 E14TG2a embryonic stem (ES) cells. An internal ribosomal entry site upstream of a beta-galactosidase reporter gene was introduced to monitor the cellular expression pattern. A coding sequence for hemagglutinin (HA) epitope tag was inserted in frame at an XhoI site in the C2 domain at the 3' end of the 5' homology arm and followed by stop codons and internal ribosomal entry site (IRES)-lacZ-polyA - MC1neo-polyA cassette. The resultant vector deletes exons encoding the C2 and part of the GAP domain. Chimeric mice were produced by injecting targeted ES cells into C57BL/6 blastocysts, and heterozygous mutants were generated from these animals. These were bred initially onto an MF1 genetic background and obtained from the Sanger Centre. In our laboratory the knock out allele was partially backcrossed onto a C57/B6/J/ola/HSD.

Genotyping

DNA for genotyping is extracted from ear notches taken from mice at weaning or, for cultures, from tail clips or cerebellar portions from embryonic mice. The extractions are performed using the Wizard DNA extraction kit (Promega) according to

manufacturers instructions. Genotyping using a standard NaCl/Tris/SDS/EDTA extraction is not consistently successful. PCR reactions were carried out using 1U HotStart Taq Polymerase (Promega), 0.3 mM dNTPs, 1X HotStart PCR buffer, 0.6 µM primers and 1 µl of DNA from the extraction described above (generally 20 - 80 ng). Thermocycling conditions are listed in Table 2. 3. A common reverse primer, Syn12R; 5' – CAT ACA AGA ATT GCT GCA TAG AAC – 3', is used in conjunction with either a forward primer complementary to the wild type sequence, Syn11<, 5' – TTC ATG GAG CGG GAA CAC CTC ATA T – 3', or a forward primer complementary to the transgenic cassette, FCass1A, 5' - CTT CCT CGT GCT TTA CGG TAT C – 3'. The PCR product of the wild type reaction is approximately 2.5 kb and the product of the transgenic reaction is approximately 1 kb.

During the later stages of this work the wild type reaction began to consistently fail. It became necessary to perform this reaction using a different Taq polymerase, namely Expand Long Template System (Roche, 11681842001). Component concentrations were the same as for Hotstar Taq polymerase reactions. Thermocycling condiditons were the same as Table 2. 2 except dNTPs, primers and DNA were combined and heated to 95 °C for 15 minutes prior to the addition of Expand Polymerase and PCR buffer (manufacturer supplied).

Table 2. 2 SynGAP genotyping thermocycling conditions

SynGAP genotyping thermocycling conditions		
Step	Temperature (°C)	Duration
1	95	30 s
2	94	10 s
3	56	30 s
4	68	3 m
5	go to Step 2 x 10	-
6	94	10 s
7	56	30 s
8	68	3 m + 20 s/cycle
9	go to Step 6 x 20	-
10	68	7 m
11	4	hold

2.3 Methods of Chapter Three: Molecular Biology and Biochemistry

2.3.1 Molecular biology

PCR

PCR reactions were carried out using 1U HotStart Taq Polymerase (Promega), 0.2 mM dNTPs, 1X HotStart PCR buffer,1 µM primers and varying concentrations template DNA; typically 1 µl of cDNA from the syntheses described below (~200 ng). For the full length amplification of SynGAP from plasmid template; 2.6 U Expand High Fidelity Taq (Roch), 1X Expand PCR buffer, 0.2 mM dNTP, 300 nM primers, 0.1 – 250 ng DNA template were used. Thermocycling conditions are listed in Table 2. 3.

Table 2. 3 PCR Thermocycling conditions

Thermocycling conditions for full length PCR of SynGAP from plasmid template using Expand High Fidelity Taq

Step	Temperature (°C)	Duration
1	94	2 m
2	94	15 s
3	60	30 s
4	72	3 m
5	go to Step 2 x 10	-
6	94	15 s
7	60	30 s
8	72	3 m + 5s/cycle
9	go to Step 6 x 18	-
10	72	7 m
11	4	hold

Generic thermocycling conditions

Step	Temperature (°C)	Duration
1	96	3 m
2	96	30 s
3	55*	30 s
4	72	1 m
5	go to Step 2 x 32	-
6	72	5 m
7	4	hold

The annealing temperature is calculated based on the melting temperatures of the primer pair minus 5 °C

Cloning and subcloning

Cloning was performed in three ways; the screening of a cDNA library, (described later p65), T/A cloning and restriction enzyme mediated digestion and ligation. All

restriction enzyme mediated cloning performed in this thesis was technically subcloning as they always involved the transfer of a piece of DNA from one vector to another.

T/A cloning

PCR derived products, even if they involved the addition of specific restriction enzyme cleavage sites, were all TA cloned initially. This allowed the confirmation of mutation free sequence before the subcloning of the product to the final vector. T/A cloning relies on the ability of Taq polymerase to add an overhanging A base onto the end 3' ends of all products. All PCR products of the approximate correct length, as assessed and extracted from an electrophoresed agarose gel are ligated into a linearised vector with complementary T overhangs. The linearised vector used is pGEMTeasy (Promega) which allows selection of plasmids with inserts by blue/white selection. If no PCR product is inserted and the plasmid religates beta galactosidase is expressed and the resultant transformed colonies are blue when grown in the presence of beta-gal substrate X-gal. If PCR product ligates to the plasmid the lacZ gene is interrupted and the resultant transformed colonies are white. White colonies are selected for isolation of plasmid DNA.

PCR products were purified for cloning by cutting out the band on an agarose gel. DNA was extracted using QIAquick gel extraction protocol (Qiagen) according to manufacturers instructions except the DNA was eluted in 30 µl rather than the 50 µl specified. Gels were stained with SyberSafe DNA gel stain (Invitrogen) and visualised using a blue light Dark Reader transilluminator (Clare Chemical research). Using blue light avoids the mutagenic effects of ultra-violet radiation and is no less sensitive.

A-tailing

As TA cloning relies on a 3' A overhang added non specifically by Taq polymerase the efficiency of cloning can be increased by enzymatically adding A tails in a separate step. The step is necessary when proof reading Taq mixtures, such as HighFidelity or Herculase are used; these include enzymes that have 3' – 5' proofreading activity and as such often remove the overhanging A nucleotides. The

maximum amount of DNA is used (4 µl from a gel extraction elution), with 1 U Taq polymerase (not hotstart), 0.2mM ATP, 1X PCR buffer in 10 µl ddH_20 and heated at 70 ^oC for 20 minutes. Ligations are performed as normal (p60).

Restriction enzyme digest

Restriction enzyme (RE) digests are performed either as a diagnostic test, eg to confirm the presence of an insert, or for subcloning. Typically 10 units of RE (1 µl) was used on 10 µg DNA (approximately 2 µl of a miniprepped sample) in a final volume of 10 µl using the appropriate buffer, follow be incubation for an hour at the recommended temperature (usually 37 ^oC). For double digests with compatible buffers, to avoid the final glycerol concentration exceeding 5%, 0.5 µl of each enzyme (which are stored in 50% glycerol) was used. Double digests with incompatible buffers were performed sequentially. Buffers and enzymes were supplied by Promega and New England Biosciences (NEB). Guidelines on buffer compatibility were from NEB.

Ligations

Reactions are performed in a 10 µl volume using 1 µl T4 DNA polymerase (Promega) 1 µl pGemTeasy linearised vector (Promega). The amount of DNA template used was between 1 – 4 µl, calculated using the equations in the pGemTeasy manual (http://www.promega.com/tbs/tm042/tm042.pdf) for optimisation of Vector insert ratio; this depends on the length the of the DNA template. Slow ligations were performed in 1x ligation buffer overnight at 4 ^oC using 10x ligation buffer, T4 DNA polymerase (Promega) or for 4 hours at RT using 2x Rapid ligation buffer, T4 DNA polymerase (Promega).

Transformation of bacterial cells

Bacterial cells used for transformation of plasmids were the chemically competent JM109 E.coli strain (Promega). Cells stored at -70 ^oC were thawed on ice, 50 µl cells were used per transformation. 1.5 µl of the above ligations were added and gently mixed before incubating the cells on ice for 30 minutes. Cells were heat shocked fro 45 seconds in a heat bath at 45 ^oC and then were immediately replaced on ice for 2 minutes before addition of 1 ml LB or SOC. Cells were allowed to

recover for 90 minutes at 37 °C before they were plated on prewarmed LB agar plates containing appropriate selection antibiotic of the transformed plasmid (ampicillin, 100 µg/ml; kanamycin, 30 µg/ml). If TA cloning / blue white selection was being performed the plates were spread with 100 µl of 100 mM IPTG and 20 µl of 50 mg/ml X-Gal. For additional details see the Promega Technical manual for pGEM-T Easy vector systems, TM042. Plates were incubated inverted overnight at 37 °C.

RNA isolation

Tissue harvesting for RNA work was performed observing the usual precautions for RNA work; all dissection tools were baked at 300°C for four hours or more, RNAse free plastics were used, tissue was snap frozen on dry ice and stored at -80°C prior to use. RNA was isolated using the RNeasy Mini Kit from Qiagen according to manufacturer's instructions except for the homogenisation step; Buffer RLT was added to tissue according to weight (600 µl for 20-30 mg, 350 µl for < 20 mg tissue), the tissue was pulled through a 23G hypodermic needle, spun for 3 min 10,000rpm in a bench top centrifuge and the supernatant treated according to the manufacturer's protocol.

Glycerol bacterial stocks

Glycerol stocks of E.coli harbouring clones were created to allow easy generation of large quantities of plasmid DNA without the need for retransformation. LB (5 ml) was innocuated from a single colony of a clonally pure streak plate and grown overnight, shaking at 37 °C. The culture was spun and the pellet resuspended in 2.5 ml 4.4% v/v glycerol, 1M K_2HPO_4, 1M KH_2PO_4, $MgSO_4$. The volume is split and frozen at -70 °C in two aliquots. When streaking from glycerol stocks tubes were removed, transferred on ice, scrapped streaked and returned immediately to -70 °C.

Preparation of plasmid DNA

Plasmid DNA was isolated by mini-prep and maxi-prep depending on the quantity and quality of DNA required. Mini-preps were used for cloning procedures; 4ml LB was inoculated from single colonies and grown overnight, shaking at 37 °C. Maxi

prep was used for the preparation of high quality endo-toxin free DNA for transfection of cells; 250ml LB was inoculated. Mini preps were performed using QIAprep spin miniprep Kit (Qiagen) per manufacturers instructions. Typical yields were ~300 ng/µl (50 µl volume). Maxi preps were performed using an endotoxin free kit, Endofree Plasmid Maxi kit as per manufacturers instructions except the last two steps centrifuge steps which were; precipitating by centrifugation in a endotoxin free 50 ml plastic Falcon tube for 1 hour at 10,000g at 4 °C, and post washing of the DNA pellet centrifuging for 30 min at 10,000g at 4 °C. Typical yields were ~2000ng / µl eluted in 250 µl. Maxiprepped DNA was diluted to 1000 ng/ µl with sddH_20. DNA and RNA concentrations were determined using a Nanodrop spectrophotometer (Nanodrop Technologies).

cDNA synthesis

cDNA was reverse transcribed from RNA with Moloney Murine Leukemia Virus (MMLV) reverse transcriptase (Promega, 9PIM170) primed with random hexamers (Promega, C118a). Briefly, 0.5-1 µg RNA (typically 1 µl from the above isolation) was diluted with 19.95 µl RNAse free water and heated to 75°C for 5 minutes. After cooling on ice 8.05 µl of the following mix was added, 0.5 µg random hexamers / µg RNA, 3mM $MgCl_2$, 500 µM dNTPs. RNAse inhibitor, 1 U / µl in standard PCR buffer. After incubation at 42 °C form 5 minutes 2ul MMLV reverse transcriptase was added, then incubated for a further hour at 42 °C. Reactions were terminated by heating to 96 °C for 5 minutes. cDNA samples were stored at -20 °C.

For attempts at full length PCR of SynGAP cDNA was synthesised with the SuperScript III First Strand Synthesis SuperMix from Invitrogen(18080-400) according to manufacturer's instructions.

Annotation of SynGAP domains

The annotations of protein domains in schematics and alignments (Figure 1. 1, Figure 1. 6, Figure 3. 2) is based on the coordinates given in the UniProtKB/Swiss-Prot record for human SynGAP (accession number Q96PV0, human-1 Figure 3. 2). Thus the numbering begins from the most upstream initiator methionine in SynGAP A. The domains are defined as PH (150 – 251, 102 aa), C2 (249 – 347, 99 aa),

GAP (443 – 635, 193 aa) and potential SH3 binding (785 – 815, 31 aa). These coordinates are identical in the rat sequence (UniProtKB/Swiss-Prot Q9QUH6).

A note on primers

All primers listed here include the names given to primers upon ordering. This is to facilitate the reuse of these primers should it be required. Additionally I have included the position of the primers on a genomic reference sequence, a mouse bacterial artificial chromosome (BAC clone RP24-335I14, accession number AC144621.3). This mouse BAC is a 207 kb fragment of mouse chromosome 17 which includes the SynGAP locus. Primers were designed to be between 17 and 25 bp long, of approximately 50% GC content with maximum difference of 5^{o}C between the melting temperatures of pairs (calculated based on 4^{o}C per G/C and 2^{o}C per A/T).

Bioinformatics tools

mRNA to genomic DNA alignment program; Spidey
(http://www.ncbi.nlm.nih.gov/spidey/)

Chromatogram viewer; 4Peaks
Protein domain homology searching:

* NCBI conserved domains
  (http://www.ncbi.nlm.nih.gov/Structure/cdd/cdd.shtml)
* Simple Modular Architecture Research Tool (SMART)
  (http://smart.embl-heidelberg.de)

Cloning and construction of SynGAP variants

Cloning of SynGAP

PCR (unsuccessful)

Full length PCR was attempted with a range of primers pairs (not listed here).

cDNA template was generated using SuperScript™ II reverse transcriptase for first-strand synthesis to generate full-length and high-yield cDNA which should allow reverse transcription of long polyadenlyated transcripts. Expand Long Template System (Roche, 11681842001) which is modified to favour the amplification of long template, and Herculase Taq (Stratagene) which is modified for the amplification of long or GC-rich DNA templates were used. No full length SynGAPs were cloned.

Phage library screen (unsuccessful)

The choice of phage library was limited as many available libraries are made using Xho digestion which cleaves SynGAP multiple times. The mouse brain large insert cDNA library (in lambda TiplEx phagemid, Clontech, 634235) was chosen as it is not digested with Xho and is size selected for enrichment of large inserts. The library was amplified and lawns of E.coli bacterial cells exposed to phage. Plaques were lifted and probed with radioactive probes against SynGAPs pan, A and B. No positive hits resulted. PCR screening of the library indicated that no SynGAP sequences were present. Additional PCR screening indicated that other abundant molecules were also absent from the library (Arg3.1, PSD 95).

Plasmid library screen

The cDNA plasmid library used was from Invitrogen (10655025, in pCMV-sport6) and was derived from young adult C57/Bl6 mouse brain.

PCR screen of plasmid library (unsuccessful)

Repeated rounds of PCR screening, division and dilution was performed on an aliquot of the plasmid library. Only aliquots positive for SynGAP were further divided for subsequent screening. No SynGAP clones were isolated from bacterial cells transformed with plasmid library aliquots tested positive by PCR for SynGAP.

GeneTrapper cDNA Positive Selection System on plasmid library (unsuccessful)

GeneTrapper cDNA Positive Selection System (10356020 , Invitrogen) is a method for the isolation of specific cDNA sequences from cDNA libraries. The GeneTrapper System should capture the clone of interest by solution hybridization of a biotinylated gene-specific oligonucleotide to single-stranded plasmid DNA (prepared

from a total cDNA library *in vitro*) and selection with paramagnetic beads. No SynGAP clones were isolated in this manner.

Colony hybridisation of plasmid library (successful)

Large numbers of E.coli were exposed to relatively low numbers of plasmid such that each colony transfected contained only one plasmid clone. The colonies were then lysed on nitrocellulose, their DNA denatured *in situ* and fixed on the filter. The nitrocellulose filters bearing the denatured DNA were then hybridised with a radioactively labelled SynGAP DNA probe. Colonies carrying the sequence of the probe were then identified by the location of the dark spot on the autoradiograph. The colonies were picked and streaked out to isolate individual colonies. Colony PCR was performed and positive colonies were re-streaked, this process was repeated until a pure clonal population (all colonies on a given plate were positive for SynGAP) was achieved. The probes used were for a common region of SynGAP (pansg_for and rev) and SynGAP A (sgApro_for and rev) (Table 2. 4, A)

A

Primers used to generate DNA probes		
Primer name	Primer sequence 5'-3'	Position on BAC
pansg_f	CGA AGT GCT GAC CAT GAC	183683
pansg_r	CGGCTGTTGTCCTTGTTG	187538
sgApro_f	CTA TGC ACC GAA CCC AAT AC	175199
sgApro_r	ACA GAG ACG GTG CGT CTC AG	177258

B

Primers used for the construction of a range of SynGAP variants			
Primer name	RE site added	Primer sequence 5'-3', RE site	Position on BAC
ACSG31_r	EcoRV *	GTG TCC AGG TTG GAT ATC TC	190565
ACSGB1_f	Age1	TTA CCG GT C TGC TGA CTG ACT GCC TAT C	182847
ACSGC1_f	Age1	TTA CCG GTC TCT TCT CCA TGT TCT TC	183485
SGA1_H3B2_f	HindIII BglII	GTAT AAGCTT AGATCT CAT CCC CGC GAT GTC CTA TG	172038
SGB1_H3B2_f	HindIII BglII	GTGT AAGCTT AGATCT C TGC TGA CTG ACT GCC TAT C	182844
SGC1_H3B2_f	HindIII BglII	GTAT AAGCTT AGATCT C TCT TCT CCA TGT TCT TCC	183484
FLSyn_E1_r	EcoR1	GTAT GAATTC CT AGT GGT CTG CGG TGT TCC	201176

* this EcoRV site is endogenous

Table 2. 4 Primers used for the cloning and construction of *SynGAP* variants

Construction of SynGAP variants

SynGAP A-alpha-1 construction

SynGAP A-alpha-1 was constructed by digestion of the two library pulled clones, A-alpha-2 and E-alpha-1, with Age1 and Sph1. This digest resulted in the release of 5' regions (2.7 kb for A and 2.5 kb for E) and the 3' regions on the plasmid backbone (7.3 kb for alpha-2 and 6.1 kb for alpha-1). Digest products were gel electrophoresed, extracted and purified. The 5' A fragment was ligated to the backbone containing the 3' alpha-1 region, and vice versa. The resulting plasmids were transformed, grown up, purified. Correct ligations were confirmed by restriction enzyme digest (EcoR1 and Bbs1) and then sequenced across the junctions (forward primer, Sp6, reverse primer; SphJuncRev, 5'-TGATGGGAGGAAGGTGGAC -3'). Identity of the 3' region was confirmed by sequencing encompassing the VK and G insert positions (PreVK_for; 5' ATTCCCAGACTCCATCCACG 3'). The SynGAP A-alpha-1 clone was found to be intact, however no successful ligations occurred for the SynGAP E-alpha-2 clone.

Generation of SynGAPs B/C - alpha-1/alpha-2

SynGAP B and C 5' regions for the construction of full length B and C alpha-1 and alpha-2 plasmids were cloned by PCR. cDNA template for the amplification of SynGAP B and C fragments was reverse transcribed from RNA from p14 mouse cortex. B (ACSGB1_for, ACSG31_rev) and C (ACSGC1_for, ACSG31_rev) PCR fragments were TA cloned into pGemTeasy and sequenced to confirm identity. An Age1 RE site was added to the 5' end of B and C, an endogenous EcoRV site was used at the 3' end. Primer sequences are given in Table 2. 4, B.

SynGAPs B and C-alpha-1 and alpha-2 were then created by the digestion of the 5' B and C fragments (in pGemTeasy) and SynGAPs A alpha-1 and alpha-2 (in pCMV sport 6) by Age1 and EcoRV. Digested fragments were gel extracted, purified and ligated in the appropriate combinations.

The resulting plasmids were transformed into E.coli, grown up and purified. Correct ligations were confirmed by restriction enzyme digest (Age1, EcoRV, HindIII; three fragments, <2, ~2.5 and 3/4 kb) and then sequenced across the junctions (primers; Sp6, XM_1698, XM-3695).

Full length PCR of SynGAP from pCMVsport6

Due to a lack of appropriate restriction enzyme cleavage sites in order to remove the 3' UTR the entire coding region was amplified by PCR and TA cloned into pGemTeasy. Full length SynGAPs were amplified from the pCMVsport6 vector by PCR using HYPUR gel purified oligo primers (MWG, Germany) and Expand High Fidelity Taq (Roche, 11732641001). The HYPUR® technique is based on PAGE and removes most truncated failure sequences and achieves purity levels of 90% and above. These primers were used as they increase the chances of producing amplified DNA with the full primer sequence which is essential for the addition of the restriction enzyme cleavage sites. The forward primers were specific for SynGAP A (SGA1_H3B2_f), B (SGB1_H3B2_f) and C (SGC1_H3B2_f) and included additional restriction enzyme cleavage sites to facilitate the subcloning of SynGAPs into the CMV backbone (-eGFP-C1) plasmid (BglII) and or the inducible expression vector pcDNA4/TO (HindIII). A common reverse primer (FLSyn_E1_r) located at the most downstream stop codon (alpha-2, position 201176 on BAC, ac144621) included the addition of an EcoR1 site also for this purpose. Primer sequences are given in Table 2. 4.

PCR products were ligated into pGEMTeasy and fully sequenced to confirm that no mutations were introduced during the PCR. These constructs were then digested with BglII and EcoR1 to release full length SynGAPs which were ligated into a CMV backbone which had been similarly digested. The CMV backbone used was from the eGFP-C1 vector (Clontech, accession number U55763) from which the eGFP gene had been removedby digestion with Age1 and BspE1 and religation. The resultant constructs were again sequenced across the vector junctions and isoform specifiying regions for confirmation of construction (Figure 2. 1).

Sequencing primers		
Primer name	Primer sequence 5'-3'	Position on BAC
XM_721_f *	AACAGCCGCCGAGTAGATAACG	187537
XM_1224_f *	TGTGACCAACCATTACCG	188040
XM_1698_f *	AGAGGACATTGCTGACAGGCTG	190226
XM_2232_f *	GATGCGGGACCTCAATAG	191055
XM_2752_f *	TCCAGAACCCTCTCTTCC	192430
XM_3263_f *	AGCAGAGCCTCAGCAAAG	192958
XM_3610_f	AGGTTGCTGTCCCAGGAAG	195459
XM_3695_f *	AGCAGCAGGTGGAGAAGGAC	195544
XM_955_f	AAGCGGAAGAAGGACAAG	187771
MBAC201859_f	ACACCTGATCTGCTCTTGG	201859
MBAC_202023_f	TACCCTGACATGCAGCCAG	202023
MBAC_202560_f	TGTGAAATTTTATCCCATGC	202560
MBAC_202488_f	CCTTCGGTCTAACCCTCTAC	202488
MBAC_187767_rev	TGTCCTTCTTCCGCTTTTTG	187767
MBAC_188410_rev	CCAATGGCATCCTTGAGGTA	188410
202447_for	CCAGACTCCAGACTCGATCTT	202447
201719_for *	GCTCAGCACGCACAAACTC	201719
202020_rev	GGGATGGGACTGTACGTCG	202020
SphJunc_rev	TGATGGGAGGAAGGTGGAC	2861
202611.1_REV	GGAGGGAGGAGGTTCAAGG	202611
PreVK_for	ATTCCCAGACTCCATCCACG	193466
419Afrag *	ACAACCCAAACTTGACCG	183631
419Afrag_r	CGGTCAAGTTTGGGTTGT	183631
Aa_973_rev	GGTACAGATGCAGCCGAA	187739
Aa_178_rev	GGGTGTATCTCATCCTCA	183631
Sp6 *	GATTTAGGTGACACTATAG	vector
T7 *	GTAATACGACTCACTATAGGGC	vector

* Primers highlighted with an asterisks should be sufficient to seqeunce through the gene. MBAC 201719_for is within the long UTR

Table 2. 5 Sequencing primers

DNA sequencing and sequence confirmation

Plasmid DNA was sequenced by primer extension (MWG, Germany or Cogenics/Lark, Essex, UK). Sequencing reads were typically between 300 – 800 bp long. Chromatograms were examined to ensure good quality sequence and sequences were clipped to remove poor quality and primer / vector sequence. Sequences were aligned against the mouse genomic sequence to confirm exon exon boundaries (Spidey mRNA to genomic DNA alignment program, default

settings). The mouse bacterial artificial clone RP24-335I14 (accession number AC144621.3) was used as the reference. Sequencing primers are listed in Table 2. 5.

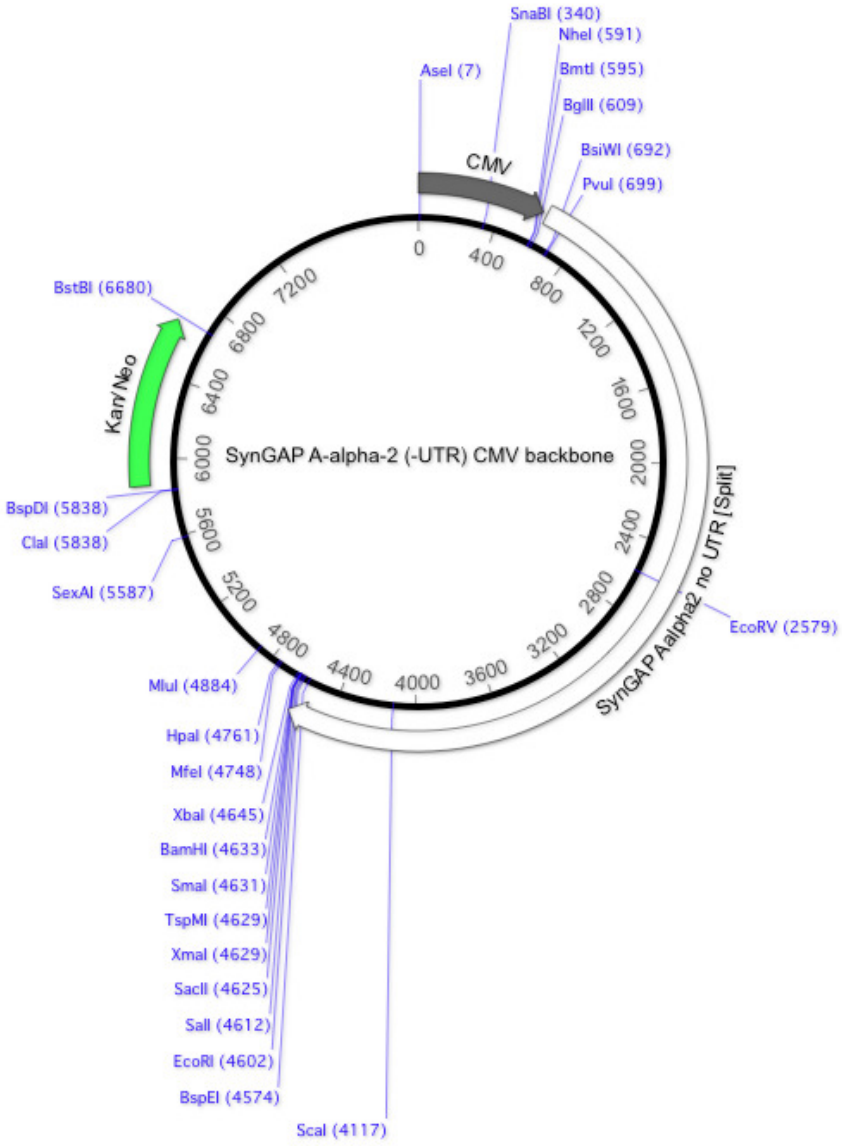

Figure 2. 1 Example plasmid map of a SynGAP expression vector

A plasmid map of full length *SynGAP A-alpha-2,* without UTR, in the expression vector. The expression vector is the backbone of pEGFP-C1 from which eGFP has been removed. No additional unique restriction enzyme cleavage sites are present in any of the other isoforms constructed.

UTR experiment

cDNA was synthesised from RNA derived from p14 mouse cortex. PCR was performed using a range of different primer pairs. Many primer pairs were used in order to optimise chances of the amplification of longer products; the 3' region of SynGAP is repeat rich which makes the design of primers challenging. Forward primers were positioned upstream of the isoform specifying alternative inserts and reverse primers were positioned within the alternatively spliced UTR exon. A number of reverse primers were designed to lie immediately upstream of the polyadenylation but only one of these, 3UTR_5.0_r, resulted in successful amplification (Figure 2. 2).

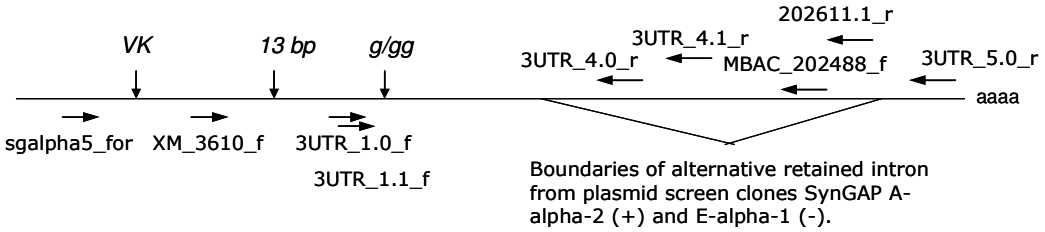

Figure 2. 2 Locations of primers for establishing a link between C-terminal coding sequence and 3' UTR.

A schematic diagram of the 3' end of SynGAP with positions of primers shown with respect to alternatively present sequence. The diagram is not to scale.

Primers for establishing a link between C terminal coding sequence and 3' UTR		
Primer name	Primer sequence 5'-3'	Position on BAC
3UTR_1.0_f	GATGCTGGTGGAGGAGGAGC	197435
3UTR_1.1_f	CGCTGCCTGAGCCCAAGAAG	197487
3UTR_4.0_r	TGAGGCAGAGGACAGGGATAGC	201471
3UTR_4.1_r	CATAACAAGGGGGGGCAGG	201638
3UTR_5.0_r	GTGGGAGAAAAGGGGGGG	202938
sgalpha5_f	AAGAGTACAAGCTCAAGGAG	193627
XM_3610_f	AGGTTGCTGTCCCAGGAAG	195459
MBAC_202488_f	CCTTCGGTCTAACCCTCTAC	202488
202611.1_r	GGAGGGAGGAGGTTCAAGG	202611

Table 2. 6 Primers for establishing a link between C-terminal coding sequence and 3' UTR

2.3.2 Biochemistry

Western blotting

Sodium dodecyl sulphate polyacrylamide gel electrophoresis (SDS-PAGE) was performed on samples prepared by boiling in Laemmli buffer containing 5% beta-mercaptoethanol (Sigma-Aldrich). Equal amounts of protein (10 µg) were loaded per well of a mini-gel apparatus (Bio-Rad). Protein concentrations were established by Bradford assay. Adherent cell samples were harvested by scraping in lysis buffer (200 µl/ well of a 24 well plate). p14 mouse cortices tissue were homogenised in 500 µl/pair hemispheres. 7 % resolving gels were made using resolving gel buffer (1.5M Trisbase, 0.4% SDS, pH 8.9) supplemented with acrylamide/bis-acrylamide, tetramethylethylenediamine (TEMED) and fresh 10% ammonium persulphate (APS). Water saturated butan-1-ol was layered on top to prevent access of oxygen. Stacking gels were made to 4% using stacking gel buffer (0.5 M Trisbase, 0.4% SDS, pH 6.8) also supplemented with the above components. Gels were run at constant current (15-20 mA/gel) in buffer containing Tris, glycine and SDS. Proteins were then electroblotted onto nitrocellulose membrane (Bio-Rad) at constant current, either 50 mA/tank overnight, or 200 mA/tank for 2 hours, in buffer containing Tris, glycine and methanol. Molecular weight markers (Kaleidoscope prestained markers, Bio-Rad) were run on all gels. Protein transfer onto the nitrocellulose membrane was confirmed by the presence of prestained markers and by staining with 1% (w/v) amido black.

Blots were then probed with primary antibodies against the proteins of interest overnight or approximately 5 hours at room temperature. Blots were washed repeatedly in tris based saline (TBS) with 0.2% Triton X-100 before adding Alexa Fluor conjugated secondary antibodies for incubation for 1 hour at room temperature. Blots were again washed and dried before imaging with the LiCor Odyssey infrared imaging system (Li-COR Biosciences UK Ltd, Cambridge, UK). The use of fluorescently labelled secondary antibodies allows the detection of multiple antigens on the same membrane. Antibodies were diluted in DMEM (Invitrogen,), 0.2% TX-100, 5% fetal calf serum. Primary antibodies used were

panSynGAP (1:8000, Cambridge Biosciences, PA1-046), SynGAP alpha-1 (1:2000, Upstate, 06-900), SynGAP beta (1:4000, a gift from the laboratory of (Li et al., 2001)), GFP (1:5000, NeuroMAb), beta actin (1:10,000, AbCam). Secondary antibodies were all used at 1:1000, goat anti rabbit 800, goat anti mouse 680 (Invitrogen).

Cell markers for subcellular localisation

The fusion protein markers used to examine subcellular localisation in HEK cells were encoded by the following plasmids. Golgi apparatus; pECFP-Golgi (Clontech, 6908-1) which encodes a fusion protein of enhanced cyan fluorescent protein (eCFP) and a sequence encoding the a region of human beta 1,4-galactosyltransferase (GT-1) that contains the membrane anchoring signal peptide that targets the fusion protein to the trans-medial region of the Golgi apparatus. Endosome; pEYFP-Endo (Clontech, 6936-1) which encodes a fusion protein of enhanced yellow fluorescent protein (eYFP) and human RhoB GTPase which targets to the vesicles of the endocytic pathway. Endoplasmic reticulum; dsRed2-ER (Clontech, 632409) which encodes a fusion protein of *Discosoma sp*. Red fluorescent protein-2, the ER targeting sequence of calreticulin and the sequence encoding the ER retrieval sequence, KDEL. Autophagosome; LC3-GFP (Addgene incorporated, plasmid 11546, Jackson et al., (2005)) consists of a eGFP fusion protein with the microtubule-associated protein 1 light chain 3 (LC3) which is associated with the autophagosomal membrane after processing. F-actin was stained with phalloidin conjugated to Alexa Fluor 633 (Invitrogen, A22284). Phalloidin was prepared according to manufacturers instructions and applied for 20 minutes to permeabilised cells (5 minutes with 0.1% Triton x-100 in PBS) at the concentration of 5 µl methanolic stock solution in 200 µl PBS for each coverslip.

Volume rendering was performed on a Nyquist sampled undeconvolved image stack using the ImageJ plugin 3D viewer.

2.4 Methods of Chapter Four: Imaging and Analysis

Cultured cell density assessment

In order to assess the cell density and cell viability in mature cultures coverslips were fixed in the normal way and stained with the nuclear stain Topro3 (1:1000, Invitrogen) in PBS for a minimum of 10 minutes. To calculate total nuclei density (nuclei / mm^2) mounted coverslips were examined using a x20 objective with a graticule. All nuclei, irrespective of morphology, were counted from at least 4 randomly selected fields of view per coverslip. 2-3 coverslips were counted per embryo. To calculate the level of cell death a x40 objective with a graticule was used to count healthy appearing nuclei. The greater level of magnification was required to assess the morphology of the nuclei. Nuclei were counted as healthy if they were round or oval, not fragmented or condensed.

Imaging neurons for protrusion analysis

GFP expressing pyramidal type neurons were imaged by laser scanning confocal microscopy on a Axiovert from Zeiss. Confocal stacks composed of 30-60 images with a Z section interval of 0.13 µm were taken using a x 63 oil immersion objective (NA 1.4) with 3.1 zoom. The dendritic section was placed diagonally across the field of view to maximise the imaged length. Under these conditions the diagonal straight line is 66 µm, therefore the dendrite section lengths imaged range from 45-70 µm. Apical and basal dendrites from 50 - 200 µm from the cell body were imaged. Crossing dendrites were avoided to facilitate analysis. Neurons that exhibited signs of stress, including dendritic beading and blebbing, were not imaged. At least 3-4 dendritic segments per neuron, from 3-4 neurons per embryo, where applicable, are imaged and analysed. The stacks were deconvolved using the Huygens Essential deconvolution software.

Protrusion morphology analysis

A maximum intensity projection of each deconvolved stack was manually analysed using the ImageJ plugin NeuronJ (Meijering et al., 2004) (Figure 2. 3). All protrusions up to a certain length (8 µm) were measured. I do not refer to the protrusions as spines because long filopodia are also included under this criterion. I cannot discount the possibility that some of the longer protrusions may be short neurites. The length of each protrusion was measured from the point of attachment to the dendritic shaft to the furthest tip. The widest point of protrusion tip was measured as the protrusion width. The length of the dendritic segment was measured in order to calculate the protrusion density. Bifurcating protrusions were analysed as two protrusions. Three to four dendritic segments of 45-70 µm in length were analysed for each neuron.

NeuronJ is an ImageJ plugin designed to facilitate the tracing and quantification of elongated structures in two-dimensional images in particular neurites in fluorescence microscopy images. It is not designed specifically for measuring dendritic protrusions or spines. NeuronJ allows the user to define the starting point of a tracing. Then by moving the cursor toward the end of the neurite NeuronJ applies a search algorithm to find the optimal path towards that point. The path is displayed in realtime as the cursor is moved. If the presented path deviates from what is considered by the user to be the true path the tracing can be fixed by a mouse click. The algorithm will begin searching again from that manually fixed point.

For the protrusion analysis in this thesis a section of dendrite is traced along its length using the default parameters of NeuronJ. To trace the protrusions I alter certain search parameters to optimise for tracing small thin tracts (Snap window size: 1x1, default = 9x9, Path search window size: 100 x 100, default = 900 x 900). Each projection is then traced from its point of attachment to the shaft to its tip. Each protrusions' width is then traced at the widest point of its tip. Bifurcating protrusions are traced and counted as two protrusions. Protrusions up to 8 µm are included in the analysis. Protrusion density is calculated by dividing the dendrite length by the protrusion number (protrusions / µm).

Due to limitations of the ‘GFP fill’ approach and confocal microscopy, measurements are not necessarily accurate in an absolute quantitative sense, but are valid for comparing relative dimensions between groups of neurons.

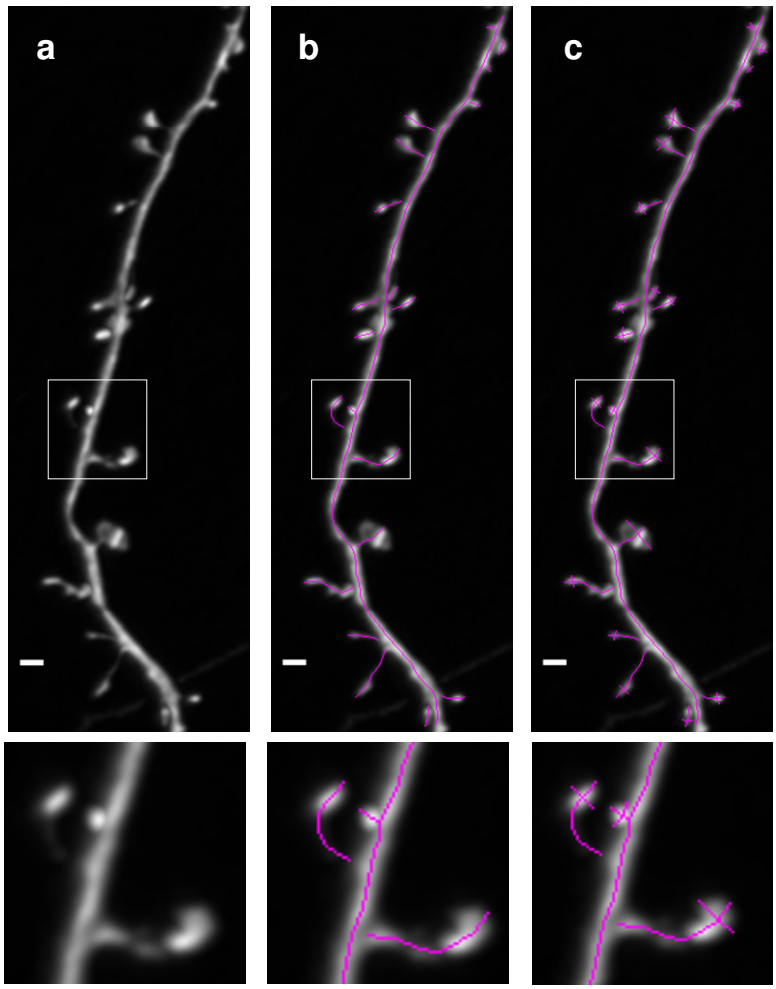

Figure 2. 3 Dendritic protrusion morphology and density are analysed by manual tracing

A section of dendrite from a GFP filled hippocampal pyramidal type neuron at DIV 14 is shown to illustrate the method of analysis. The dendrite is traced along its length, then each projection is traced from the point of attachment to the shaft to its tip (b). Each protrusions' width is then traced at the widest point of its tip (c). The measurements for the section of dendrite shown are as follows: protrusion density (0.62 protrusions/µm), mean protrusion length (1.13 µm) and width (0.58 µm). The area in the box is shown expanded below. Scale bar is 1 µm.

Immunocytochemistry

Cells were fixed with room temperature freshly thawed 4 % paraformaldehyde in PB. Growth medium was aspirated and fix was added directly to the wells without prior washing. After 10 minutes at RT fix was aspirated and cells washed at least 3 times with PBS. If not used immediately cells were stored in PBS at 4 ^{o}C for a maximum of a few days. For experiments on HEK cells permeablising (0.2 % Triton X-1000, quenching (50 mM NH_4Cl) and blocking (0.3 % bovine serum albumin, BSA) were performed in one step (30 minutes, RT), best results in neurons were obtained when these steps were performed separately (10, 10 and 10 minutes, interspersed with PBS washes, RT). Cells were then washed x 3 in PBS before incubation with primary antibody in PBS/0.3 % BSA for one hour (pan SynGAP (1:1000, Cambridge Biosciences, PA1-046). Cells were washed again (x 3, PBS) then incubated with Alexa fluorescently conjugated secondary antibodies (Invitrogen) in PBS/0.3% BSA for 30 minutes. For antibody incubation coverslips were upturned onto a 100 µl drop of antibody solution on a sheet of Parafilm (Pechiney Plastic Packaging Company, Chicago, IL). Nuclei were counterstained with DAPI/Hoescht (Invitrogen) which was added to a final 10 minute PBS incubation at 1:1000. Coverslips were dipped in PBS then water before mounting in Mowiol mounting medium and stored at 4 ºC protected from light.

Protein expression quantification by relative fluorescence levels

The level of expression of overexpressed SynGAP isoforms was quantified in SynGAP $^{-/-}$ neurons by quantitative fluorescence microscopy. Neurons were co-transfected with SynGAP and eGFP in the normal way. SynGAP isoforms were detected with the pan SynGAP antibody and dendritic sections were imaged by laser scanning confocal microscopy. All immunocytochemistry was performed in one batch. The same laser power and microscope settings were used for all neurons and it was ensured that no pixels were saturated. Fluorescence levels were quantified in ImageJ. Briefly, the integrated density (mean grey value multiplied by area) for the whole area of the image was taken. From this the integrated density of the background (calculated by multiplying the mean grey value from sample regions

of the background by the whole area of the image) was subtracted to yield a value of the corrected integrated density. The corrected integrated density of SynGAP antibody fluorescence was divided by the corrected integrated density of eGFP fluorescence to yield relative fluorescence level value.

Note on statistics

The two-sample Kolmogorov-Smirnov test (KS-test) and Mann-Whitney test (MW-test) are two of the useful and general alternative nonparametric methods of two-sample t-test. They can be used to test whether two samples come from the same distribution. The two-sample Kolmogorov-Smirnov test uses the maximal distance between cumulative frequency distributions of these two samples as the statistic. However, the Mann-Whitney test takes the difference between mean ranks of these two samples as the statistic, is closer to examining the median. For spine protrusion analysis; all data on which a KS test was performed was also analysed by the Mann-Whitney test and the same results were found.

2.5 Methods of Chapter Five: Electrophysiology

Basic Electrophysiology methods

Recordings were made on the day *in vitro* (DIV) indicated. Neurons were kept in a 37°C incubator prior to transfer to the recording rig in room temperature extracellular recording solution (Table 2. 3). Neurons were continually perfused with room temperature extracellular recording solution, except during recordings performed on high amplifier gain, i.e. mEPSC recordings, to minimise perfusion artefacts. Each coverslip was used for a maximum of 45 minutes or for three usable cells. Wild type coverslips were alternated with SynGAP $^{-/-}$ coverslips to minimise effects of, for example, variation in internal and extracellular recording solution batch or aliquot, or systematic variation in access resistance due to drift in the diameter of patch electrode pulled by the electrode puller. Thick walled (0.86 mm internal diameter, 1.5 mm OD) glass capillaries with internal filaments were pulled to the desired resistance (4-9 mOhm) using a Sutter p95 electrode puller. Data are sampled directly from the low-pass filtered (5 kHz) output of the patch amplifiers using LabVIEW 8.2 (National Instruments Inc.). The sampling rate is fixed at 10 kHz with a resolution of 16 bits per sample. Data acquisition and analysis software were written in LabVIEW 8.2 by Timothy O'Leary (O'Leary *et al.*, ; O'Leary, 2008). Recordings are analysed off-line.

Concentrations of drugs used are given in Table 2. 8.

Table 2. 7 Solutions used for electrophysiological recordings

Internal Recording Solution		
	Concentration (mM)	
	Standard	Cesium based
K-gluconate	130	-
KCl	10	-
Cs-gluconate	-	130
CsCl	-	10
HEPES	10	10
EGTA	0.1	0.1
Glucose	10	10
Na phosphocreatine	10	10
Mg ATP	4	4
Mg GTP	0.5	0.5

The pH is adjusted to 7.3 using KOH (4M); osmolarity is 290-300 mOsm.

External Recording Solution	
	Concentration (mM)
$CaCl_2$	2.5
$MgCl_2$	1.3
Glucose	10
NaCl	150
KCl	3
HEPES	10
Glycine	0.05

The pH is adjusted to 7.3 using NaOH (4M); osmolarity is 310-320 mOsm. Divalent cations are added fresh before each.

Drugs	
	Concentration
TTX *(Tetrodotoxin citrate)*	500 nM
PTX *(Picrotoxin)*	50 µM
CNQX *(6-cyano-7-nitroquinoxaline-2,3-dione)*	5 µM
APV *(d-2-amino-5-phosphonopentanoate)*	50 µM
NMDA *(N-methyl-D-aspartic acid)*	100 µM
AMPA *(a-amino-3-hydroxyl-5-methyl-4-isoxazole-propionate)*	50 µM
Bic *(Bicuculline)*	50 µM
4-AP *(4-Aminopyridine)*	250 µM
Glycine	50 µM

Table 2. 8 Drug concentrations used in electrophysiological experiments (unless otherwise stated)

AMPA mEPSCs

AMPA mEPSCs were isolated electrophysiologically by blocking neurotransmitter receptors other than AMPA receptors and preventing action potential driven neurotransmitter release. The cell's transmembrane potential was voltage clamped at -70mV. At -70mV the voltage sensitive NMDA receptor is blocked. The extracellular recording solution was supplemented with tetrodotoxin (TTX) picrotoxin (Ptx) and magnesium chloride (Mg_2Cl, 1.3 mM). TTX binds to the pore of voltage gated, fast action sodium channels and prevents action potentials, thus blocking action potential driven neurotransmitter release. Ptx was used to block GABAergic events. Magnesium is used to ensure the NMDA receptor's voltage gated magnesium block is available. Access resistance was monitored between recordings and recordings were abandoned if the access resistance was unstable or above 28MΩ. Recordings with fluctuations in the baseline or a large amount of noise (greater than 4 pA RMS) are excluded.

mEPSC analysis

Typically, at least three two minute recordings were made from each cell, depending on mEPSC frequency. At least 300 events were analysed per cell. mEPSC amplitudes, risetimes and decay time contants were averaged to yield a mean per

cell. The mEPSC frequency was calculated by averaging the inter event intervals (ms), then obtaining the reciprocal value (Hz). The mean mEPSC amplitude (pA) and frequency (Hz) from each neuron was then averaged to give a value for the entire population.

Figure 2. 4 shows the method of analysing an mEPSC. mEPSCs are detected by setting an amplitude threshold relative to a baseline which is perturbed only by events with a characteristic duration greater than 2 ms, a value that is comparable to the rise-time of mEPSCs. An event amplitude threshold is set at 5 pA above this baseline, which is twice the typical RMS noise that is measured in these recordings. The process for analysing individual events is as follows. Event amplitudes are calculated relative to a 15 ms baseline preceding the event, risetimes are calculated as the time taken for the event to reach 90% of its maximum value after exceeding 10% of its maximum, and decay time-constants are estimated by fitting a single exponential curve to the decaying phase of the event. Each of these parameters is fitted automatically and adjusted by hand if the initial fit is unsatisfactory. Events that are separated by an interval of less than 15 ms are excluded from the analysis; this imposes a cut-off on the maximum event frequency and inter-event-interval (IEI). Fluctuations in the current which are isolated as events but do not resemble mEPSCs are excluded from the analysis.
To calculate mean values, the individual fitted traces are aligned to the time of the half-maximal value during the rising phase.

NMDA mEPSCs are recorded in the presence of CNQX, Ptx and Ttx.

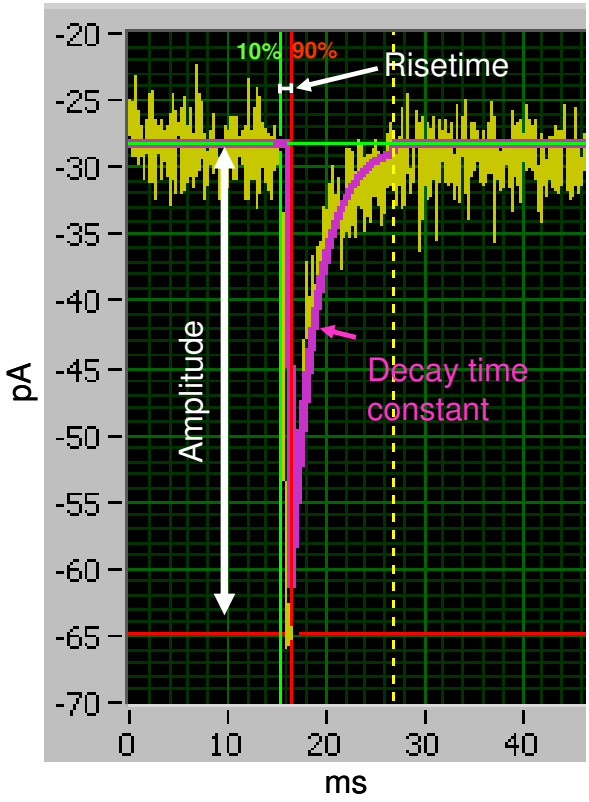

Figure 2. 4 mEPSC measurement

mEPSC event amplitudes, 10-90% rise-time and exponential decay time-constants are calculated automatically but are monitored and can be hand-fitted if necessary.

Whole Cell Currents

Cells are voltage clamped at -70mV. The external recording solution for eliciting AMPA currents includes AMPA at the saturating concentration of 50 µM, $MgCl_2$ and the NMDA receptor antagonist APV (Table 2. 8). This AMPA cocktail is bath applied until the inward current reaches a plateau, then washed out until the baseline holding current is restored before a repeat application is performed to ensure a stable response. The extracellular recording solution containing Mg^{2+} is then replaced with Mg^{2+} free recording solution to remove the NMDA receptor's Mg^{2+} block and permit its activation. NMDA is then bath applied until the inward current

reaches a plateau, then washed out until the baseline holding current is restored before a repeat application is performed to ensure a stable response. The NMDA receptor co-agonist Glycine is also included, as is the AMPA receptor antagonist CNQX. All solutions contain TTX to prevent action potential mediated influx of current, and Ptx to block GABAergic receptors.

Whole cell currents are quantified by averaging the trace values in an area of the stable plateau phase of the current. Coverslips were used for a maximum of two sets of agonist application to avoid desensitisation of AMPA and NMDA receptors.

Capacitance measurements

Cell capacitance was measured in two ways. Whole cell capacitance neutralisation was performed using the amplifier. The series resistance and whole cell capacitance were altered together to achieve neutralisation of the capacitance transient (N. B. Standen, 1987). The value of the capacitance was then read from the whole cell capacitance dial. However a neuron is not single electrical compartment and doesn't behave like a single capacitor in parallel with a resistor so neutralistion is always an approximation. A more accurate way to measure the capacitance is to measure the charge transferred following a voltage step of a known size and this is implemented with the software. Similar values were obtained, however the later method was used as it is believed to be more accurate.

Measurement of neuronal soma upper surface area

Single fluorescent images of fixed GFP transfected cells were captured with a x40 lens. All pixels were within the dynamic range. Soma were outlined using the 'region of interest' tool in ImageJ. The resulting area measurements equates to an approximate 2D measurement of the area of the upper surface of the 3D cell bodies.

Transfection of neurons for electrophysiology

Neurons were transfected in the same manner as for morphological analysis (Chapter Two Methods). Quantities of Lipofectamine 2000 and DNA were modified

to optimise conditions for electrophysiological recording. See Appendix One for the optimisation of transfection protocol for electrophysiological recordings and the confirmation of cotransfection resulting in coexpression. The optimised transfection conditions were ; 0.3 µg DNA/ 1ul Lipofectamine 2000 per well of a 24 well plate. 0.1 µg eGFP was used with 0.2 µg of a SynGAP construct or an empty vector. Recordings were made from 16 to 36hrs from the time the complexes were added to the cells.

Classification of 'silent' cells

Neurons were included for classification as silent or non silent cells if they met following criteria. Recordings with low noise (<3.5 RMS) and low holding current (<-150pA). A minimum recording length of 2 minutes where no mEPSCs were apparent was required for a cell to be classified as silent.

No minimum recording length was necessary to designate a cell has non silent, the appearance of obvious mEPSCs was sufficient. Cells with high RMS noise but with mEPSCs obvious above the noise were not included in this analysis.

Spontaneous and stimulated activity

Neurons were voltage clamped at -70mV, all recordings were performed in the presence of Mg^{2+}. Spontaneous activity was recorded for at least 5 min before the bath application of bicucculine and 4-AP (Bic/4-AP). Bic/4AP was perfused on for 30s while stimulated activity was recorded continuously for 5 min, Bic/4AP was perfused on again after 3 min for 30s. CNQX was used to block AMPA receptors.

Statistics

All statistical analyses were performed in GraphPad Prism 5. T-tests are students unpaired t-test unless otherwise specified. Bar graphs display the mean +/- standard error of the mean (SEM) and a line on scatter plots also shows the mean.

The D'Agostino-Pearson test is used to test for normality. The D'Agostino-Pearson normality test performed by Prism is the 'omnibus K2'. It first computes the skewness and kurtosis to quantify how far from Gaussian the distribution is in terms of asymmetry and shape. It then calculates how far each of these values differs from the value expected with a Gaussian distribution, and computes a single P value from the sum of these discrepancies. The distribution of the mEPSC frequencies within conditions is not normal (D'Agostino and Pearson normality test, $p<0.05$ for all groups except SynGAP A-alpha-1 (Figure 5. 15, Figure 5. 16) thus the data should not be analysed by one way ANOVA. However the non-parametric version of one way ANOVA, the Kruskal Willis test, assumes that the shapes of the distributions are identical which is not the case. I have presented the results both using one way ANOVA and transformed the data to normalise the distributions.

Chi square (population) and Chi square test for expected vs observed values were performed on the online calculator at graphpad.com. Dunnett's post hoc test compares all groups to the control group. Bonferroni planned comparison test compares all groups to the control group, but is not corrected for multiple comparisons.

2.6 Methods of Appendix 1

Calculation of co-transfection efficiency

Co-transfection efficiency was calculated to determine if transfection with two separate plasmids resulted in the same neurons expressing both plasmid products. Two plasmids encoding fluorophores (eGFP-N1 and mCherry-N1) were used to allow visual assessment of co-transfection. 7 ratios of eGFP to mCherry (from 0.25 – 4) were used to optimise co-transfection rates. 3 coverslips per condition were transfected and all fluorescent cells in 5-8 fields of view per coverslip were noted as being red, green or both using a x 40 objective. The filter cube used for visualisation of mCherry fluorescence filters between 515-560 nm. These wavelengths are submaximal for the excitation mCherry (excitation, 587nm, emission, 610nm).

Calculation of transfection efficiency

Transfection efficiency was calculated by counting all eGFP expressing neurons and DAPI stained healthy appearing nuclei using a x 20 objective with graticule. 3 coverslips were counted per conditions and 5-8 fields of view were counted per coverslip.

3 Chapter Three: Molecular Biology

3.1 Introduction

This chapter is concerned with the structure of the SynGAP gene, as well as its transcription and translation. As described in the main introduction SynGAP is a complex gene, with N-terminal variation arising from multiple transcription start sites and C-terminal variation arising from alternative splicing. I will give a brief introduction to the mechanisms that give rise to such complexity, and how they may be regulated, before more specifically addressing the work performed in this chapter.

More than half of human genes (at least 53%) have alternative promoters (Kimura et al., 2006). To initiate and modulate transcription, factors interact with chromatin and DNA sequence features in regulatory regions surrounding the transcription start site of a gene. In this region, factors of the transcription machinery interact directly with DNA sequence motifs to ensure the proper recruitment of RNA polymerase II and transcription of the pre-mRNA.

From the moment a gene is transcribed, it undergoes a series of post-transcriptional regulatory modifications in the nucleus and cytoplasm until its final deployment as a functional protein. Initially, a message is subjected to extensive structural regulation through alternative splicing, which is capable of greatly expanding the protein repertoire by generating, in some cases, thousands of functionally distinct isoforms from

a single gene locus. Then the mature mRNA is packaging into neuronal transport granules and potentially recognised by RNA-binding proteins and/or microRNAs which are capable of restricting protein synthesis to selective locations and under specific input conditions. The tight regulation of spatial and temporal deployment is well adapted to the extreme morphological requirements of the neuron. The expression profiles of splice isoforms are modified during development and to response to changes in neuronal activity (Ule *et al.*, 2005; Li *et al.*, 2007).

Insights into the importance of splicing in the development of the complexity of an organism comes from comparative genomics. Among unicellular eukaryotes, alternative splicing seems to be relatively rare: only three genes of the budding yeast Saccharomyces cerevisiae are reported to be alternatively spliced; alternative splicing is observed also in a more distant fission yeast Schizosaccharomyces pombe and in the malaria parasite Plasmodium falciparum. The estimated fraction of alternatively spliced Arabidopsis genes ranges from 10– 20% and remains consistently lower than that of animal genes (Artamonova & Gelfand, 2007).

Surprisingly, splicing events are often less conserved than the total level of conservation between two species. About one quarter of human alternatively spliced transcripts are not present in the orthologous mouse gene products, and about half of alternatively spliced genes have species-specific isoforms (Nurtdinov et al., 2003).

3.1.1 Types of pre-mRNA alternative splicing

There are various types of alternative splicing categorised depending on the nature of the alternative sequence. Entire exons may be present or absent, an alternative splice site may be chosen at the beginning or end of an existing exon, or an intronic sequence may be retained in the mature mRNA. Alternative promoters that initiate transcription at different exons which are spliced onto common exons is also included as a splicing mechanism. These types of splicing are illustrated in Figure 3.1. In all cases the alternative regions may be in-frame or out of frame. In-frame regions lead to the inclusion or exclusion of amino acids without changing the sequence of the remainder of the protein. Out of frame alternative sequence leads

to a frameshift in the open reading frame (ORF) which completely changes all subsequent protein sequence.

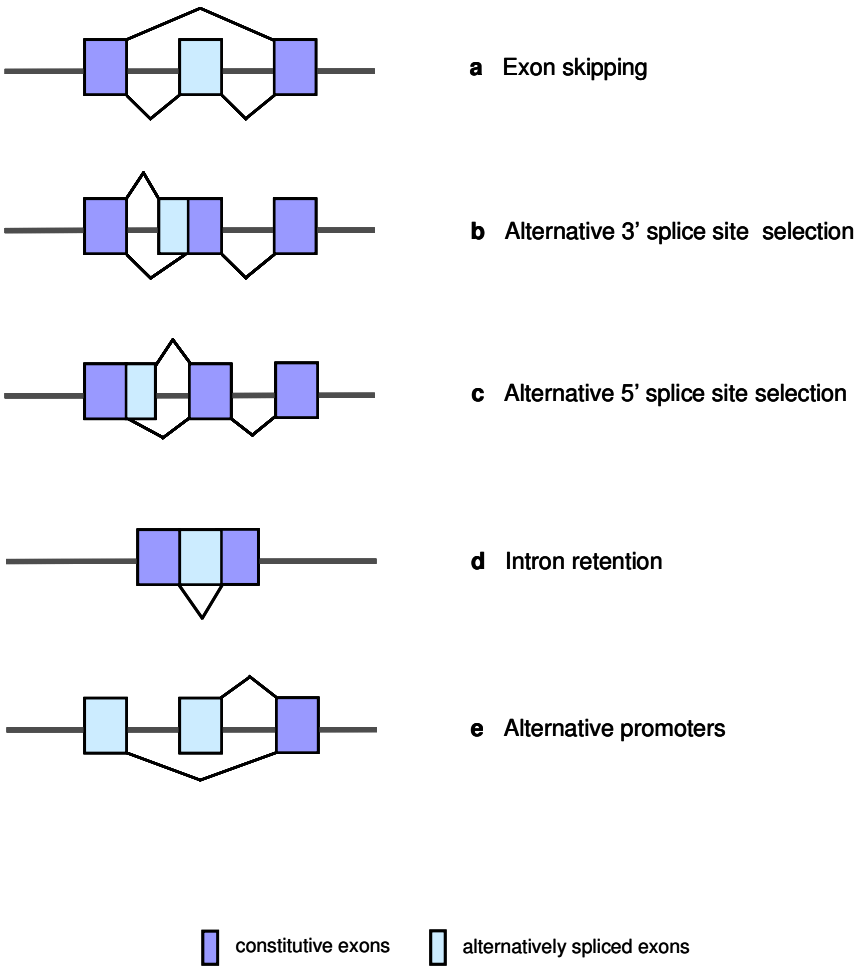

Figure 3.1 Types of alternative splicing

Exon skipping (a), the inclusion or exclusion of a 'cassette' exon, represents the most common type of alternative splicing (Sultan et al., 2008). Exon skipping accounts for 40% of alternative splicing events in higher eukaryotes. Through the use of alternative 3' (b) or 5' (c) splice sites exons can be extended or shortened in length (19% and 8% of splicing events, respectively). The excision of an intron can be suppressed, to leave the intronic sequence in the mature mRNA (d, < 5% of splicing events). Transcriptional initiation at different promoters generates alternative 5'-terminal exons that can be joined to a common 3' exon downstream (e). Similarly, alternative 3' exons, with alternative polyadenylation sites, can be joined to a common upstream exon (not shown). Sometimes paired cassette exons show mutually exclusive splicing, where one exon or the other is included, but not both (not shown). Introns are represented by the horizontal line and lines exon connecting represent splicing options.

3.1.2 Regulated alternative splicing

Splicing is carried out by the spliceosome, a massive structure in which five small nuclear ribonucleoprotein particles (snRNPs) and a large number of auxiliary proteins cooperate to accurately recognize the splice sites and catalyse the splicing reaction. The decision as to which exon is removed and which exon is included involves RNA sequence elements and protein regulators. Splicing decisions can be profoundly influenced by the strength of the individual 5' and 3' splice sites and by auxiliary RNA sequences that tune splice site strength via enhancement or silencing mechanisms. Protein regulators are a combination of tissue and developmental stage specific and ubiquitously expressed RNA binding factors which influence splicesome assembly (Black, 2003). Additionally, there has been accumulating evidence showing that RNA transcription can be coupled to splicing regulation (Batsche *et al.*, 2006; Moldon *et al.*, 2008; Chen & Manley, 2009). The coupling of promoter related machinery with splicing machinery is of particular interest in the study of SynGAP because it may determine the linkage between N and C-termini.

3.1.3 Regulated alternative promoter usage

Many different promoter expression and splicing patterns are induced during neuronal development, presumably as a result of changes in the expression of splicing regulators and transcription factors. Use of alternative promoters enables diversification of transcriptional regulation within a single locus and thereby plays a significant role in the control of gene expression in various cell lineages, tissue types and developmental stages.

It appears that the transcription of alternative SynGAP N termini are under the control of distinct promoters as they are differentially regulated in development and in an activity dependent manner (Figure 1. 5).

It is well established that new gene transcription is necessary for the long term storage of memory (Bailey et al., 1996). The first wave of gene transcription to occur after stimulation is called immediate early gene transcription. It is mediated by the host of transcription factors and accessory proteins that are the ultimate

effectors of such signalling pathways as ERK/MAPK, eg CREB (Abraham et al., 1993). Further changes in gene transcription are mediated by the immediate early gene products and it is likely that SynGAP falls into this category as the changes in SynGAP mRNA levels are only apparent after 4 hours, but not 1 hour, of stimulation (Mark Barnett, personal communication).

To the best of our knowledge SynGAP is the only example of synaptic activity dependent differential regulation of alternative promoter usage within a gene [7]

3.1.4 Neuronal regulation of alternative splicing

Alternative splicing is especially common in the nervous system and as such it is expected that many more regulatory elements and proteins are involved compared to other tissue types (Li et al., 2007). Several *trans*-acting splicing regulators that direct neuron-specific splicing have been identified, including Nova-1/2, Hu proteins and Fox-1/2 (Ule et al., 2005; Underwood et al., 2005; Zhu et al., 2006). There are numerous examples of changes in alternative splicing of ion channels, receptors and synaptic signalling proteins at different development stages and in adaptive changes associated with neuronal excitability and synaptic efficacy (Lipscombe, 2005; Wu *et al.*, 2010).

Particularly relevant examples that demonstrate how different splice forms can have different activities include the SynGAP-related RasGAP neurofibromatosis type I (NF1) which when spliced to exclude exon 23a shows 10 times greater ability to down-regulate Ras signalling than the isoform that includes exon 23a (Barron *et al.*,

[7] The synaptic scaffolding protein Homer is referenced in the literature as being an example of activity dependent alternative promoter usage. However, the activity dependent regulation of Homer actually appears to be alternative splicing rather than alternative promoter or TSS. Xiao B, Tu JC & Worley PF. (2000). Homer: a link between neural activity and glutamate receptor function. *Curr Opin Neurobiol* **10,** 370-374.
, Tappe A & Kuner R. (2006). Regulation of motor performance and striatal function by synaptic scaffolding proteins of the Homer1 family. *Proc Natl Acad Sci U S A* **103,** 774-779..Brakeman PR, Lanahan AA, O'Brien R, Roche K, Barnes CA, Huganir RL & Worley PF. (1997). Homer: a protein that selectively binds metabotropic glutamate receptors. *Nature* **386,** 284-288.

2010). The N-terminally extended splice variant of Rap1 GAPII, contains a motif which mediates its interaction with heterotrimeric G proteins and results in the activation of its GAP activity (Mochizuki *et al.*, 1999). Finally, in postsynaptic membranes a splice variant of the synapse-associated protein-97 (SAP-97) recruits AMPA receptors to and enlarges cortical spines. Overexpression of an alternative form that lacks a single exon has no effect. SAP-97 splicing therefore represents a mechanism to up and downregulate the efficacy of glutamatergic synapses (Waites et al., 2009)

The regulation of splicing by cell excitation.

Some splicing events can be controlled dynamically in mature excitable cells. Splicing switches are common in ion channels, neurotransmitter receptors and proteins that are involved in calcium signalling or the control of membrane physiology. Many of these splicing events are themselves altered by cell excitation or by treatments that stimulate calcium signalling pathways. Exons in calcium-ATPase, SNAP25, NMDAR1, the large-conductance, calcium- and voltage-gated potassium channels (BK channels) and other transcripts are repressed by shifting cells into high-potassium media. In many cases, inhibiting L-type calcium channels blocks this repression, indicating that a calcium signalling pathway is required, but other pathways can also be involved (Lipscombe, 2005)

The case of activity induced changes in the NMDA receptor subunit NR1 splicing is particularly noteworthy. Neuronal activity promotes the choice of splice site that leads to one C-terminal tail (C2), while blockade of activity leads to the translation of a different tail (C2') that accelerates the transport of the receptor to the plasma membrane (Zukin & Bennett, 1995; Mu *et al.*, 2003). Indeed some sequence motifs essential for depolarisation and CaMKIV-dependent splicing of NR1 have been identified (An & Grabowski, 2007; Lee *et al.*, 2007).

Neuronal activity has also been shown to promote alternative mRNA processing (alternative polyadenylation) specifically of the immediate early gene targets of the transcription factor MEF2, leading to the production of truncated mRNAs that may have different functions than their full length counterparts (Flavell *et al.*, 2008).

It would be illuminating to know if 3' alternative splicing of SynGAP, like its 5' alternative promoter usage, is also subject to activity dependent regulation.

3.1.5 Aims of this chapter

The main objective of this thesis is to determine if these N and C-terminal variants of SynGAP have any influence on its function. The experiments performed in this chapter were primarily geared toward equipping ourselves with the tools required to perform the assays of the remainder of the thesis. In order to perform these morphological and functional experiments physical clones of *SynGAP* were needed. Here, I will describe the cloning and construction of the *SynGAP* variants that are used throughout this thesis. During the process of cloning a number of novel transcripts were found that add further complexity to the transcriptional, and possibly, translational profile of SynGAP. The cloning experiments which led to the discovery of new transcripts were not an attempt at a comprehensive characterisation of SynGAP transcriptional variation and as such are not exhaustive. In instances where the discovery of a new variant had implications for the planned functional assays additional investigations were performed.

Additionally, as I have outlined in the main introduction, SynGAP contains a number of domains that may mediate localisation independent of synapse specific mechanisms. In order to investigate if SynGAP displayed any recognisable pattern of subcellular localisation that could be attributed to these domains or give an indication of a possible function of the N and C-termini I examined localisation in a non-neuronal cell line.

3.2 Results

3.2.1 Overview of Results

The SynGAP protein, and all its isoforms, are highly conserved between human, rat and mouse. Multiple isoforms of SynGAP are expressed endogenously.

Two full length SynGAP cDNA clones were isolated from a plasmid library screen; these were *SynGAP E-alpha-1* and *SynGAP A-alpha-2*. The full length *SynGAP E-alpha-1* clone has a shorter 3' UTR than the *SynGAP A-alpha-2* clone, which is extended due to a retained intron. The two clones share the same polyadenylation signal.

Further cloning of the 3' end of *SynGAP* revealed that there is no absolute correlation between length of 3' UTR and the isoform coding status of an mRNA transcript.

A *SynGAP B* clone with a novel 4 bp insertion that is predicted to result in premature truncation of translation was isolated.

Full length open reading frames (ORFs) of SynGAP *A-alpha-1, B-alpha-1, C-alpha-1* and *A-alpha-2, B-alpha-2, C-alpha-2* were constructed and expressed successfully, at the predicted molecular weights in a heterologous cell line, HEK293.

In HEK 293 cells overexpressed SynGAP was apparent as hollow spheroid bodies of varying size and unknown provenance. Spheroid bodies were also sometimes present in the soma of neurons overexpressing SynGAP.

3.2.2 *SynGAP* is conserved among species

Multiple alignment of *SynGAP* sequences between species indicated that it is highly conserved among species (Figure 3. 2). Between human and the rodents, rat and

mouse, there is 99% homology on the protein level and 92% homology on the gene level (see NCBI HomoloGene 84739 for additional comparisons). There are no amino acid substitutions between rodents and human in the PH, C2, GAP or proline rich domains. The alternatively spliced protein regions are also present unchanged in the rodents and human. (The sequences shown in Figure 3. 2 are the isoforms present in the curated protein database UniProt which is not an exhaustive list for each species.)

The association between N and C-termini shown here is not indicative of true linkage as most sequences have been compiled from overlapping clones. The exceptions to this are the two clones isolated in this thesis, *SynGAP E-alpha-1* and *A-alpha-2*. The other rodent full length *SynGAP* clone described, *SynGAP C-alpha-1*, was isolated by Kim et al. (1998) but the GenBank sequence has since been replace by a sequence coding for *SynGAP C-alpha-2* and this is the sequence that appears here. Full length *SynGAP A-alpha-1* has been found in the human (accession number AK307888.1). Bioinformatic analysis of the unique peptide regions reveals no predicted conserved domains or motif sequences apart from the PDZ binding domain at very C terminus of SynGAP alpha-1 (NCBI conserved domains, SMART).

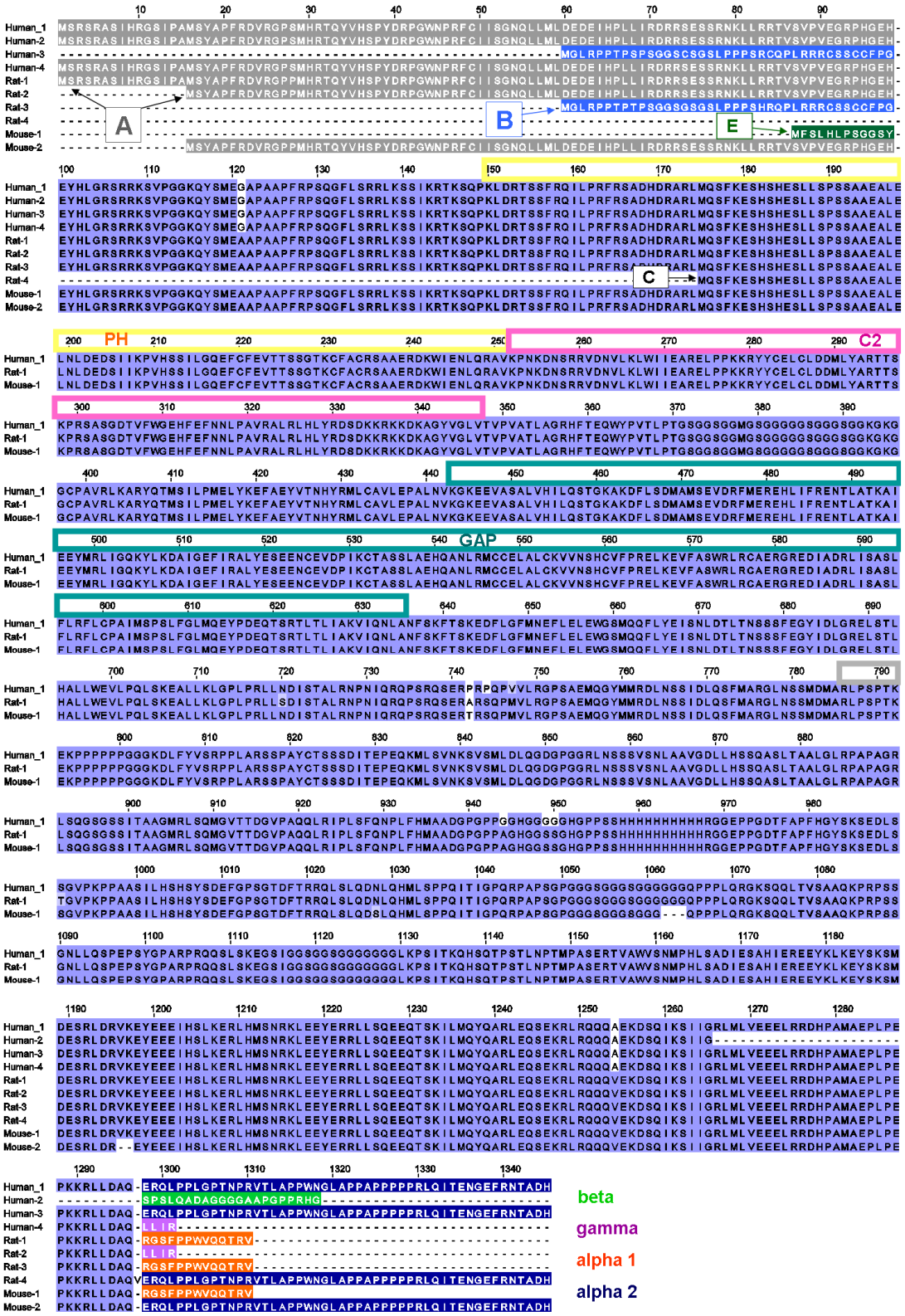

Figure 3. 2 A multiple alignment of SynGAP protein isoforms from human, rat and mouse

Figure 3.2 A multiple alignment of SynGAP protein isoforms from human, rat and mouse

All SynGAP protein sequences present in the UniProt database are aligned against the protein translation of the two clones, *SynGAP E-alpha-1* (Mouse 1) and *SynGAP A-alpha-2* (Mouse 2) pulled from the library. The alignment at the N and C-termini has been manipulated for clarity and coloured according to isoform. The N-termini are; A (grey), B (blue), E (green) and C (no colour, a truncation) and the C-termini are; alpha-1 (orange), alpha-2 (dark blue), beta (light green) and gamma (purple). Only one sequence per species is shown in the central common section. Full homology is indicated by the solid blue colouring, differences are indicated by light blue (> 60 % homology) and white (< 40 % homology). Protein domains are highlighted in the scale bar above the sequence. Homology scoring is based on the Blossum62 substitution matrix. The accesion numbers are Q96PV0 (human) and Q9QUH6 (rat).

3.2.3 Endogenous SynGAP expression

Western blot analysis of endogenous SynGAP reveals a triplet band around 130 kDa indicating that indeed multiple SynGAP isoforms are expressed (Figure 3. 3). The lower two bands, but not the upper band, of the triplet also appear when the blot is probed with antibodies specific to SynGAP alpha-1 and beta. Mass spectrometry data indicates that SynGAPs A, B, alpha-1, alpha-2, and beta can all be found in the PSD (Komiyama, N, personal communication). SynGAP C cannot be specifically detected as it is a truncated protein with no unique sequence.

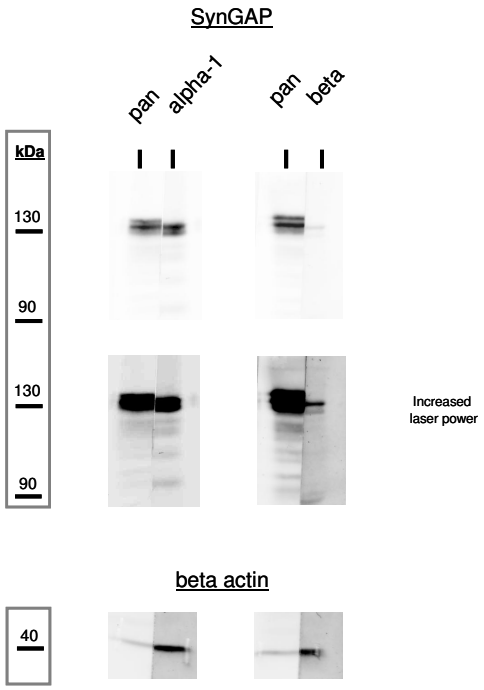

Figure 3. 3 Western blot of endogenous SynGAP probed with antibodies against SynGAP alpha-1, beta and a common region (pan).

Mouse cortex homogenate was stained with antibodies against a region common to all isoforms (pan SynGAP), SynGAP alpha-1 and SynGAP beta. Protein bearing nitrocellulose lanes were cut in half and each half incubated with pan SynGAP and the C-terminal specific antibody. The middle panel shows the same blot imaged using a higher intensity laser setting to effectively increase the exposure and allow the discrimination of the lower band in SynGAP beta. Blots were also probed with anti beta actin to confirm that the two halves of each lane were aligned correctly.

3.2.4 Cloning SynGAP

In order to study the function of different SynGAP isoforms the coding sequences needed to be cloned. A range of different approaches were tried in order to isolate full length *SynGAP* clones. These included;

- Full length PCR of SynGAP from cDNA derived from tissue failed repeatedly despite multiple attempts using a variety of primer pairs and locations. The

optimisation of the thermocycling conditions, quality of cDNA template and specialised Taq polymerases similarly failed to produce positive results.

- A lambda zap phage library (mouse brain large insert cDNA library, Clontech) was screened for SynGAP with negative results and later found to entirely lack SynGAP sequence.
- A cDNA plasmid library was screened by conventional PCR and a magnet bound probe system (GeneTrapper, Invitrogen), both of these approaches were unsuccessful. However the plasmid library was positive for SynGAP sequences and was successfully screened by the colony hybridisation technique.

3.2.5 The isolation of two full length SynGAP clones

Two full length SynGAP clones were isolated from the plasmid library colony hybridisation screen. Briefly, this involved probing a library of plasmids that contained cDNA fragments from a mouse brain. Large numbers of E.coli were exposed to relatively low numbers of plasmid such that each colony transfected contained only one plasmid clone. Plates of bacterial colonies were then screened with a radioactive DNA probe derived from a portion of SynGAP which is present in all isoforms (pan SynGAP) and a SynGAP A specific region. Two bacterial regions that were positive for SynGAP signal were isolated further by sequential plating and single colony PCR until a pure clonal population was derived. Sequencing of the clones revealed them to be *SynGAP E-alpha-1* (pan SynGAP probe) and *SynGAP A-alpha-2* (SynGAP A probe) (Figure 3. 4).

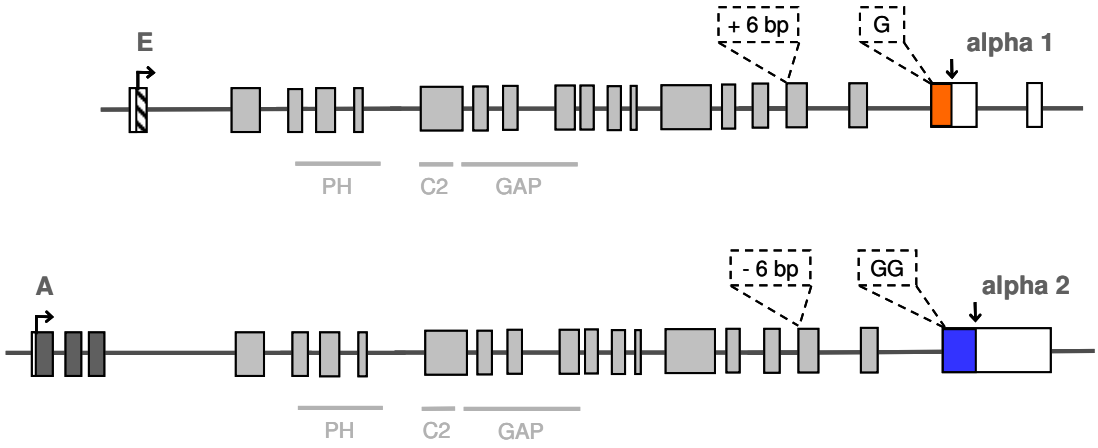

Figure 3. 4 A schematic diagram of the exonic structure of two clones, *SynGAP A-alpha-2* and *SynGAP E-alpha-1* isolated from a plasmid library screen.

The exonic structure of two clones, *SynGAP E-alpha-1* (upper) and *SynGAP A-alpha-2* (lower) is illustrated by boxes, intronic DNA is illustrated by a horizontal line. Translation initiation codons (right angle arrows) and termination codons (straight arrows) are shown. Shaded boxes indicate translated sequence, unshaded boxes indicate untranslated regions. C-terminal alternatively present sequence is highlighted (dashed line). For reference protein domains are indicated by light grey lines. Diagram is not to scale

SynGAP E-alpha-1 (Figure 3.1, upper) consisted of 4171 nucleotides with a coding sequence of 3657 nucleotides. *SynGAP E* is an undescribed N-terminal isoform which contains 12 unique amino acids before splicing into the exon common to SynGAPs A and B. Although *SynGAP E* is not present in the literature or online databases the unique E fragment has been cloned previously in our laboratory (personal communication, Mark Barnett). The C terminus of this clone contains only one G at the G insert position, therefore is translated as *SynGAP alpha-1*. The clone is also positive for the 6 bp insert (valine lysine coding). Translation of this clone would give rise to a protein of 1219 amino acids with a predicted molecular weigh of 134 kDa.

SynGAP A-alpha-2 (Figure 3. 4, lower) consisted of 5921 nucleotides, with a coding sequence of 3969 nucleotides. This clone a longer 'A' N terminus (downstream Met,

beginning MSYAP) and has two Gs at the G insert position therefore is translated as *SynGAP alpha-2*. This clone does not contain the VK insert. Translation of this clone would give rise to a protein of 1323 amino acids with a predicted molecular weigh of 146 kDa.

The two clones differed in length of the 3' untranslated region (UTR). The UTR of *SynGAP A-alpha-2* was 1761 bp long from its stop codon to the polyadenylation signal and was an uninterrupted continuation of the same exon. The clone was polyadenylated 16 bp after a canonical polyadenylation signal (aataaa). *SynGAP E-alpha-1* had a shorter 3'UTR (454 bp after the alpha-1 stop codon, 350 bp after the alpha-2 stop codon) but shared the same final 116 bases, including the polyadenylation signal, with *SynGAP A-alpha-2*. Therefore there was alternatively spliced 3' UTR exon of 1414 bp that was present in the *A-alpha-2* clone but absent in the E-alpha-1 clone. The same long UTR, with the same polyadenylation signal is present in human *SYNGAP* (accession number of compiled sequence NM_006772). The splice junctions of the short UTR do not fit the normal consensus splice sequence of 3' end of intron:GU, 5' of intron; AG, instead the sequence is 3' end of intron, AG, 5' of intron; AC.

3.2.6 Association between UTR and isoform

SynGAP alpha-1 and *alpha-2* mRNA transcripts differ by only one bp which hampers differential detection. If the long UTR were always associated with *SynGAP alpha-2* transcripts and the short UTR with *SynGAP alpha-1* transcripts the probing for these regions would facilitate differential detection. Additionally, an isoform coding/UTR linkage would inform the choice of clones to use for the functional studies. UTRs often contain regulatory sequences that determine the stability, localisation and translation of an mRNA transcript (Wilkie et al., 2003). If there was a clear association between ORF and UTR it would be appropriate to use a clone with the endogenous UTR for expression. However, if no linkage was apparent the consistent use of clones with different UTRs to express different isoforms could introduce experimental artefacts.

In order to establish if there was an association between UTR and isoform coding additional regions of the 3' end of *SynGAP* were cloned by PCR amplification of cDNA. In this group of clones there is no absolute association between the length of the UTR and the isoform coding status of a transcript (Figure 3. 5). The presence of one or two guanines (at position 324, Figure 3. 5) determines the translation of alpha-1 or alpha-2 however both cases appear in clones that have long and short UTRs.

Transcripts containing the *SynGAP beta* specifying 13 bp insert were also cloned. Each of these three clones had a long UTR but we cannot conclude that *SynGAP beta* transcripts with short UTRs do not exist.

A short 3' UTR identical to that of the original full length *SynGAP E-alpha-1* (ie the same exon-exon boundaries) was not found again. Instead a number of different shorter UTRs were present (190 – 320 bp shorter than that of *SynGAP E-alpha-1*). Three of these clones code for SynGAP alpha-1 and have a 5' splice junction that is upstream of the *SynGAP alpha-2* stop codon. If this very short UTR (134 or 137 bp from the alpha-1 stop codon) were present in an *alpha-2* clone it would lead to the translation of a truncated protein with a few unique amino acids, but there is no evidence to suggest that such a transcript does exist. An additional two short UTR transcripts (alpha-2 coding) were found, both of the 5' splice junctions are downstream of the stop codon. There was also variation in the position of the 3' splice junction of the short UTRs (-19 to +10 bp from the 3' splice site of *SynGAP E-alpha-1*)(Rogozin et al., 2005). The splice junctions of these UTRs also do not fit the consensus splice junction sequence.

In summary, there is no association between SynGAP alpha-1/alpha-2 coding status and the length of the 3' UTR.

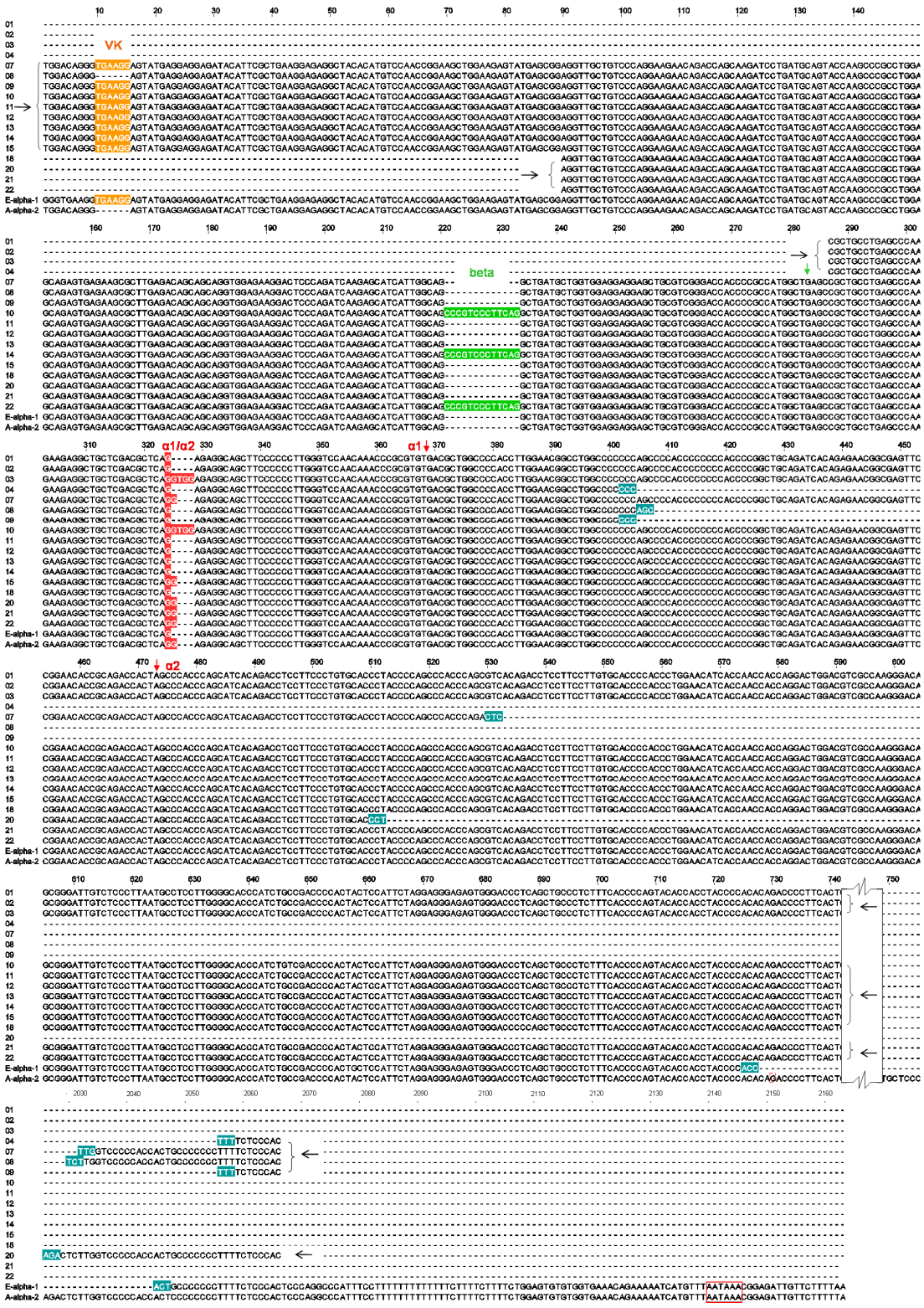

Figure 3. 5 An alignment of the 3' end of S*ynGAP* cDNA transcripts

Legend overleaf

Figure 3.5 An alignment of the 3' end of *SynGAP* cDNA transcripts
A multiple alignment of the 3' end of *SynGAP* including clones derived by PCR from cDNA (clones 1-22) and the two clones isolated from the library screen, *SynGAP A-alpha-2* and *SynGAP E-alpha-1* (bottom two lines). Highlighted are alternatively present inserts, the 6 bp VK insert (orange, TGA AGG), the 13 bp beta insert (green, CCC GTC CCT TCA G) and the alpha-1/alpha-2 determinant (red, G/GG/GGTG). Stop codons for beta, alpha-1 and alpha-2 are shown by coloured arrows. Splice junctions in the UTR are indicated by teal highlighting. The sequence is abridged for brevity (boxed region 740 – 2020 is omitted). Horizontal arrows indicate primer positions. The polyadenylation signal (aataaa) is boxed in red.

3.2.7 Construction of a range of SynGAP variants

A range of SynGAP variants were constructed from the two clones described above. Initially *SynGAP A-alpha-1* was constructed by cutting the N terminus from the *SynGAP E-alpha-1* clone and replacing it with the N terminus that had been cut from the *SynGAP A-alpha-2* clone. Despite multiple attempts *SynGAP E* failed to ligate to the *alpha-2* 3' region. Coding sequence for the N-termini was not isolated from the library*, SynGAPs B* and *C*, was cloned by PCR from cDNA derived from mouse brain. By PCR restriction enzyme cleavage sites were added to these *SynGAP B* and *C* fragments which facilitated their replacement of *SynGAP A* in full length *SynGAP alpha-1* and *alpha-2* constructs.

As I found that there was no strict association between C-terminal isoform coding and the length of 3' UTR I felt it was necessary to remove the different length UTRs from *SynGAP alpha-1* and *alpha-2* in order to avoid any potential confounding effects, for example, on expression level. Due to a lack of suitable restriction enzyme cleavage sites within the UTR the coding regions of all 6 clones were amplified by PCR. Restriction enzyme cleavage sites were added to the primers to facilitate the subcloning of the genes into a different expression vector, also under the control of the CMV promoter. Subcloning into the eGFP-C1 vector, to create SynGAP fusion proteins, was done in parallel with subcloning into the same vector from which GFP had been removed (henceforth the CMV backbone). Despite apparently successful confirmation digests and sequencing, the eGFP fusion

proteins did not express SynGAP protein (data not shown). Untagged SynGAP proteins did express correctly (Figure 3. 8).

3.2.8 SynGAP B-shift

During the cloning of *SynGAP B* fragments a novel form of *SynGAP* was found (Figure 3. 6). This B isoform is identical to the normal B coding region except for the addition of 4 base pairs at the 3' end of the second B specific exon. These four base pairs lead to a frameshift in the open reading frame which terminates in a premature stop codon. This 92 amino acid fragment would include 53 novel residues not present in canonical SynGAPs We termed this putative truncated fragment SynGAP B-shift. Two clones encoding *SynGAP B-shift* were found from two separate experiments. We do not know if this fragment is expressed as there are no antibodies against any region within the peptide. However, the entire length of the coding region for *SynGAP B-shift* is 5' of the insertion site of the deletion cassette in the knock out animal used in this thesis. It is conceivable therefore that *SynGAP B-shift* may be expressed in the *SynGAP* $^{-/-}$ mouse. *SynGAP B-shift* (B with the 4bp insertion with the alpha-1 3' end) was subcloned in the same manner as the other full length clones described above.

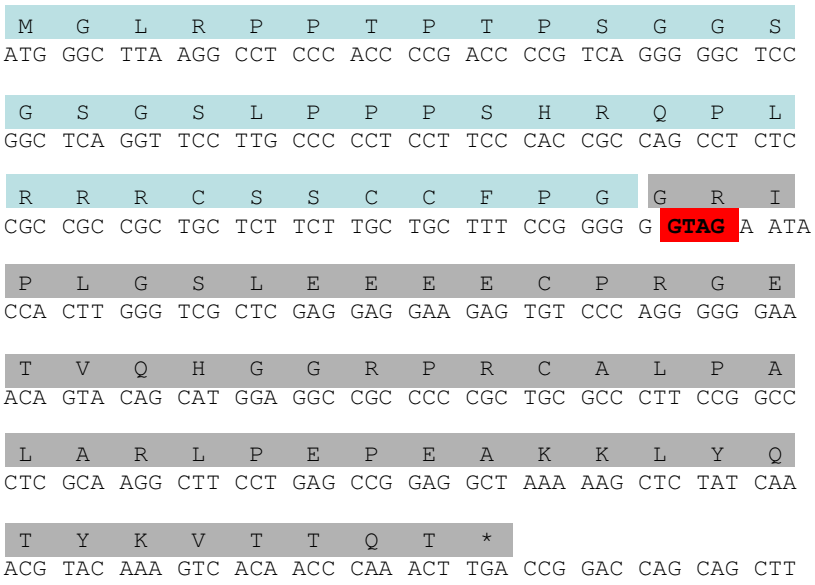

Figure 3. 6 Truncation of SynGAP B by a 4bp insertion

The nucleotide sequence, from the initiation codon, of SynGAP B with a novel 4bp insertion (highlighted in red). The canonical SynGAP B amino acid sequence is highlighted in blue until the frameshift which results in non-canonical SynGAP B sequence (highlighted in grey). Termination codon is indicated by *. This truncated peptide has been termed SynGAP B-shift.

3.2.9 An updated view of the exonic structure of the *SynGAP* gene

An updated view of the exonic structure of the *SynGAP* gene including the data presented here is given in Figure 3. 7. The alternatively spliced 3' UTR region is indicated. The position of the 4bp insertion which could give rise to *SynGAP B-shift* is also shown. An additional isoform that contains the first A specific exon but lacks next two A specific exons, including the A translation start codon, is shown as *SynGAP F*. *SynGAP F* was found by PCR during attempts to clone full length *SynGAP*. This isoform contains an open reading frame that begins at the next methionine downstream from the second (canonical) A start codon and would be

translated as slightly truncated version of this protein (7 amino acids shorter than the SynGAP A clone pulled from the library screen).

Figure 3. 7 An updated schematic diagram of the exonic structure of the SynGAP gene.

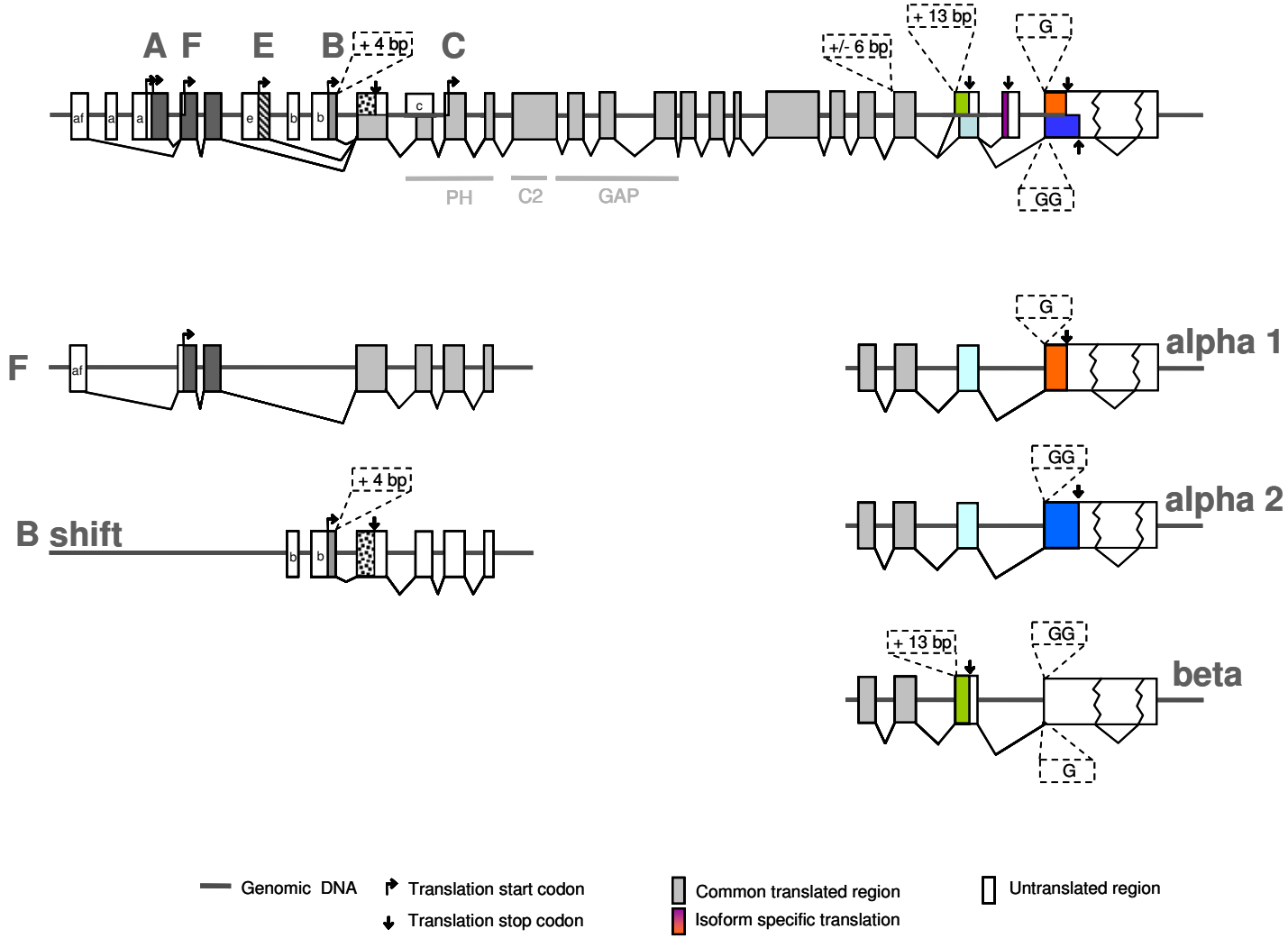

Figure 3. 7 An updated schematic diagram of the exonic structure of the SynGAP gene.

The full exonic structure of the SynGAP gene is given in the upper panel with new variants of SynGAP transcript in the lower panel. This figure complements Fig x in the introductions which includes all previously described SynGAP variants. 3' regions are included to illustrate alternative UTR splicing. Exons are illustrated by boxes (shaded indicates translated regions, unshaded indicates untranslated regions) and intronic DNA is illustrated by a horizontal line. Isoform specific UTR is indicated by a lower case letter within the box. Alternatively present sequence is highlighted with dashed lines. Where divergence occurs at the same locus the different possible outcomes are shown above and below the midline. Diagram is not to scale.

3.2.10 Confirmation of expression of SynGAP isoforms in transfected cells

In order to confirm that the constructed SynGAP isoforms had been built correctly and were capable of being expressed I transfected cells of a heterologous line (HEK 293) with equal amounts of *SynGAP* plasmid DNA. Enhanced green fluorescent protein (eGFP) was used as a cotransfection marker. Cell lysates were analysed by western blot using an antibody against the central domain of SynGAP that recognises all canonical isoforms (pan SynGAP) (Figure 3. 8). HEK 293 cells do not express endogenous SynGAP protein as was confirmed by the lack of signal from cells expressing eGFP only. All isoforms yielded strong signal at the approximate predicted molecular weight (~135 kDa, expected molecular weights are given in the figure legend). Differences between the weights of the isoforms were also evident; SynGAP alpha-2 isoforms were consistently heavier than the alpha-1 isoforms of the same N-terminal. N-terminal differences were also apparent, SynGAP A appeared slightly heavier than B while both were considerable heavier than C. This indicated that all isoforms were expressed as expected. SynGAP B-shift was also transfected and was not recognised by the antibody as expected.

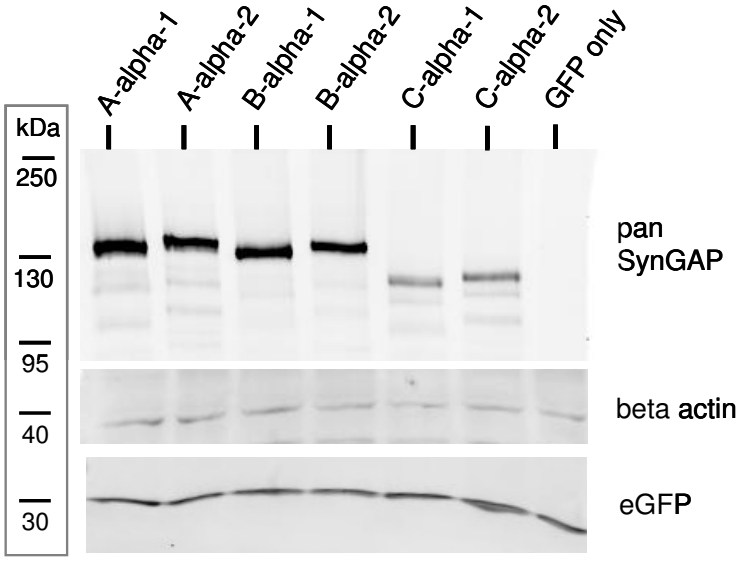

Figure 3. 8 Transfected SynGAP isoforms are expressed at the expected molecular weights in HEK 293 cells

A western blot of HEK 293 cells transfected with eGFP and various SynGAP isoforms probed with an antibody that recognises all forms of SynGAP (pan SynGAP), beta actin and eGFP. The expected molecular weights are; SynGAP A-alpha-1, 142 kDa, 1309 aa; SynGAP A-alpha-2, 146 kDa, 1323 aa; SynGAP B-alpha-1, 137 kDa, 1248 aa; SynGAP B-alpha-2, 141 kDa, 1282 aa; SynGAP C-alpha-1, 125 kDa, 1136 aa; SynGAP C-alpha-2, 129 kDa, 1170.

Expression levels of the isoforms, relative to beta actin and eGFP, were also calculated by fluorescence densitometry. No statistically significant differences were found by one way ANOVA, data not shown (n = 3). The appearance of bands at lower molecular weights is likely to be due to SynGAP degradation products rather than non-specific binding of the antibody (no bands appear when GFP only is expressed) or cryptic start sites (no bands appear when SynGAP B-shift is expressed).

Overexpressed SynGAP forms spheroid bodies

In neurons SynGAP is localised mainly at the synapse where its interaction with a number of PSD proteins is thought to be mediated by its C terminus. In order to examine the localisation determination of the protein domains of SynGAP, excluding its interaction with the PSD, I transfected cells of a non-neuronal line (HEK 293) with SynGAP. HEK 293 cells do not express endogenous SynGAP or synaptic proteins (data not shown) thus the localisation of SynGAP in this context may be determined by protein/membrane interactions not specific to neurons. Surprisingly SynGAP forms cytoplasmic spheroid bodies when overexpressed in HEK 293 cells
Figure 3. 9, d - f). These bodies are remarkably sphere like and occur in different sizes throughout a given cell. They appear to consist of a membrane vesicle the inside of which is hollow. These bodies can also be seen as round or ring like deformations on the surface of cells when viewed by differential interference microscopy (DiC) (Figure 3.9, g-i). Spheroid bodies can also occur in the soma, but not the dendrites, of neurons when SynGAP is overexpressed (Figure 3.9, a-c). They are not apparent in GFP only expressing cells (not shown).

In order to determine what the spheroid bodies were I coexpressed SynGAP with a number of subcellular markers. The spheroid bodies did not express markers of the endoplasmic reticulum, golgi apparatus or lysosome (Figure 3. 10, a-f). A marker of the stress related proteolytic organelle, the autophagosome, was expressed throughout the cytoplasm, as would be expected for an unstressed cell. There was some indication that this marker was slightly enriched within spheroid bodies but this was not clear (Figure 3. 10, g,h). SynGAP can regulate turnover of the actin cytoskeleton in neurons and another synaptic GAP, SPAR, has been shown to reorganise the actin cytoskeleton in heterologous cells (Pak *et al.*, 2001; Carlisle *et al.*, 2008). However the expression of SynGAP did not have any obvious effect on F-actin filaments and the spheroid bodies did not appear to recruit F-actin (Figure 3. 10, I,j).

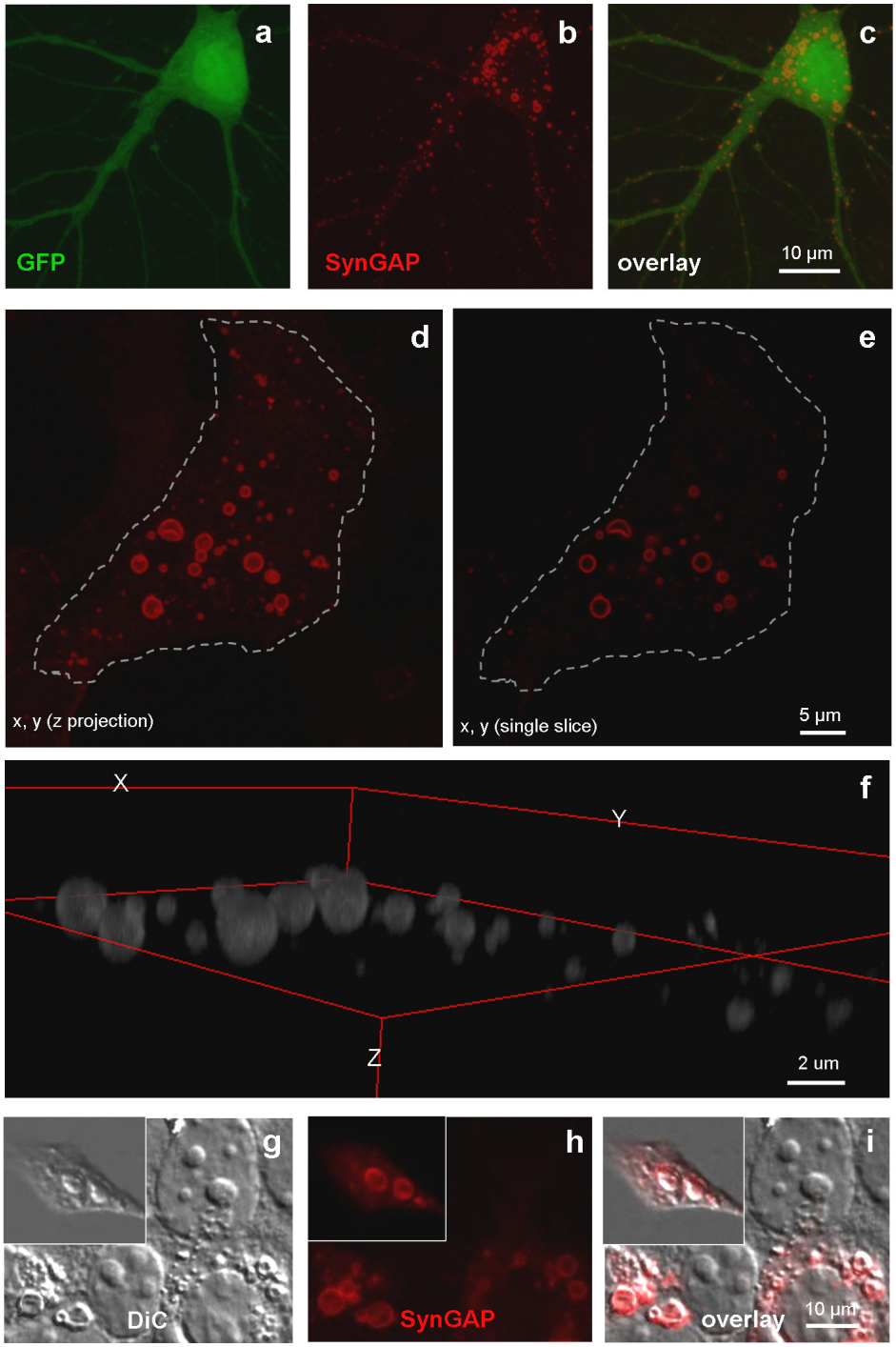

Figure 3. 9 SynGAP forms spheroid bodies when overexpressed in cells

When SynGAP is overexpressed in cells (SynGAP -/- neurons, a-c, and HEK 293, d-i) and detected by immunocytochemistry it appears as spheroid bodies in the somatic cytosol. D,e and f show the spheroid bodies of one HEK cell, outlined by a dotted line in the z projection (d) and a single optical slice (e) and volume rendered in (f). Differential interference microscopy (DiC) allows the visualisation of the features on the surface of cells where the spheroid bodies can also be seen (g-i, inset is another example). Scale bars as shown.

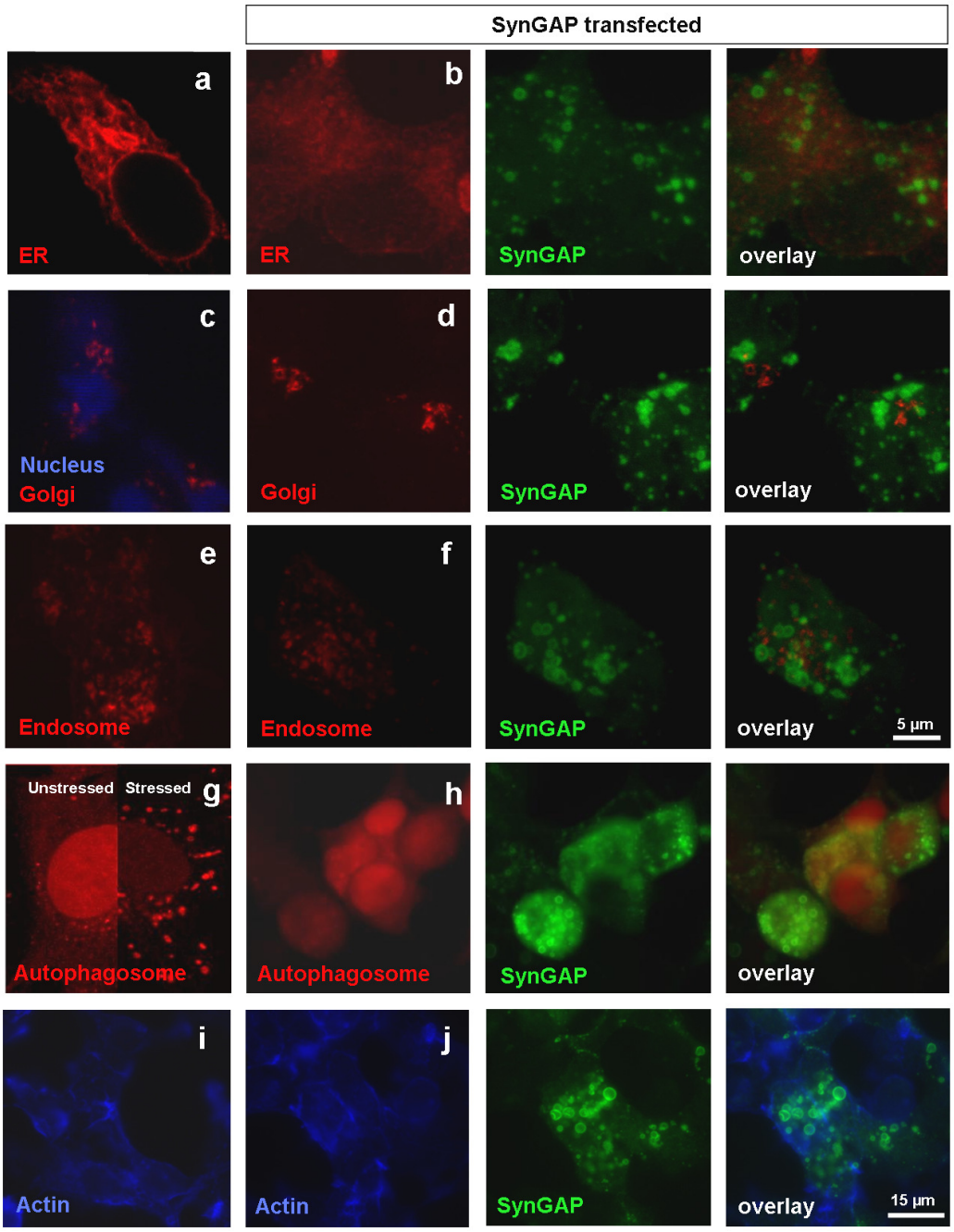

Figure 3. 10 SynGAP spheroid bodies do not colocalise with markers of endoplasmic reticulum, Golgi apparatus, endosome, autophagosome or F-actin.

An example of the localisation of each marker in the absence of SynGAP is shown in the left most panel (a, c, e, g, i). Cells coexpressing SynGAP and markers for endoplasmic reticulum (b, ER), Golgi apparatus (d), endosome (f), autophagosome (h) and actin (j) are shown on the right. The nucleus (DAPI) is also shown with the Golgi apparatus in (c) to highlight its perinuclear localisation. The scale bar for a - g is 5 µm and for h - j is 15 µm. Panel g is from the lab of J. Lippincott-Scwartz.

3.3 Discussion

The initial aim of the work of this chapter was to clone and construct *SynGAP* variants for expression. This was accomplished and during this process novel *SynGAP* transcripts were found and an unexpected pattern of localisation was encountered when SynGAP was expressed in a heterologous cell line.

The identification of an alternatively spliced transcript does not prove that it is functionally relevant. Besides its abundance relative to other products from the gene, one indication of the functional significance of an mRNA variant is evolutionary conservation. Many important splicing changes are highly conserved across mammals or vertebrate species. The presence of all the previously described isoforms[8] in human and the mouse and rat indicates that they may have some functional role (Figure 3. 2). The presence of a transcript also does not guarantee its translation or stability however the finding of all the unique peptide sequences at the synapse confirms their existence in protein form.

Is SynGAP unusual in its complexity?

There are many reports of extraordinarily complex alternative splicing; the classic spectacular example used to illustrate this are the DSCAMs (*Drosophila melanogaster* gene *Down syndrome cell adhesion molecules*), which can generate 38,016 distinct mRNA isoforms, a number far in excess of the total number of genes (~14,500) in the organism (Schmucker et al., 2000). DSCAMs are thought to provide the molecular basis of axonal pathfinding self-avoidance and the innervation of non overlapping synaptic fields (Hattori et al., 2008). The *KCNMA1* pre-mRNA contains multiple alternative 5' splice sites, alternative 3' splice sites and sequence corresponding to cassette exons. Together, these allow more than 500 mRNA isoforms to be synthesized from a single pre-mRNA (Nilsen & Graveley) A less terrifying, and more familiar, example of complexity comes in the form of Kalirin, a brain specific Rho GEF that has at least 3 alternative promoters and 3 alternatively spliced 3' termini. It is known that all possible exonal combination of mRNA are present (McPherson et al., 2002, 2004).

[8] N-terminal isoforms SynGAP A, B and C and C-terminal isoforms alpha-1, alpha-2, beta and gamma.

Consensus estimates of alternative splicing frequency in the human genome have rapidly expanded from an estimate of 5% of genes in the mid-1990s. Now, new high-throughput sequencing technology has revealed that > 90% of human genes undergo alternative splicing — a much higher percentage than anticipated (Wang *et al.*, 2008). As elucidation of alternative splicing events continues apace perhaps it will become apparent that the level of complexity of SynGAP is, rather than being unusual, the norm.

cis connectivity of exons (or which N-terminus with which C-terminus ?)

The cloning of two full length cDNA clones in this thesis brings to four the number of known linkages between SynGAP N- and C-termini. To reiterate, these are *SynGAP A-alpha-2* and *E-alpha-1* (this thesis, mouse), *C-alpha-1* (Kim *et al.*, 1998) and *A-alpha-1* (accession number AK307888.1, human).

Questions arise that are not addressed experimentally in this thesis but inform the interpretation of the data that is presented here. Is there specificity in the linkage of N- and C-termini, or like Kalirin, can all N-termini be coupled to all C-termini? How can we determine what N-termini are linked to what C-termini? How might such associations be mediated? Does the linkage between N- and C-termini matter? I will discuss these questions in reverse order.

Does the linkage between N and C-termini matter? Presumably it does. The differential regulation of 5' variants combined with the proven functional relevance of the C-termini indicates that the different ends of the protein do have roles to play.
The appearance of three discrete bands on a Western blot when endogenous SynGAP is probed by a common antibody suggests there are certain isoforms that are predominantly expressed. However, it is impossible to predict which isoforms these bands correspond because the molecular weights of the different potential isoforms are too close to be resolved. Additionally, SynGAP can be extensively phosphorylated (Dosemeci & Jaffe, ; Oh *et al.*, 2004) and may be subject to other forms of postranslation modification which would alter its molecular weight.

How might such linkage be mediated? As mentioned in the introduction there has been accumulating evidence showing that RNA transcription can be coupled to splicing regulation (Batsche *et al.*, 2006; Moldon *et al.*, 2008; Chen & Manley, 2009), references 18-22 in Chen). Two models have been proposed to explain this coupling.

For transcription to initiate at a particular site on genomic DNA a host of transcription factors and accessory proteins need to mediate the recruitment of RNA polymerase II. The first model is known as the recruitment model, in which the transcription machinery, RNA polymerase II (RNApol II) and the transcription factors, interact either directly or indirectly with splicing factors and alter the efficacy of splicing. For example PGC1, a transcription co-activator that is recruited to target genes by specific transcription factors, can modulate alternative splicing by interacting with other splicing factors and the elongating form of RNAPol II (Monsalve et al., 2000) Importantly, the ability of PGC-1 to function in RNA processing appears to require its prior entry into a transcriptional initiation complex.

The second, kinetic model posits that the regulation of alternative splicing depends not only on the interaction of splicing protein factors with splicing regulatory elements in the pre-mRNA, but also on the rate and pausing of transcriptional elongation (Chen & Manley, 2009). In this model the rate of elongation influences the time window within which the splicing machinery has to assemble. In support of this model a slowly elongating RNAPol II was found to greatly enhance the inclusion of an alternate exon with weak splice sites (de la Mata et al., 2003). The rate of elongation can itself be determined in part by the rate of initiation which is influenced by the strength of the promoter thus linking 5' initiation events to more downstream splicing choices (Epshtein & Nudler, 2003).

Therefore it could be possible that alternative promoters could lead to different splicing patterns (Kornblihtt, 2005). Interestingly some authors have observed that genes with alternative promoters tend to demonstrate more alternative splicing compared to genes with a single promoter, and genes with more alternative promoters tend to have more alternative splicing variants. Furthermore transcripts from different alternative promoters tend to splice differently (Xin et al., 2008). An association between the use of different transcription start sites with the inclusion of specific cassette exons has also been established bioinformatically (Chern et al.,

2008). It is possible that internal splicing variants are the consequence of important changes in pre-mRNA secondary structure resulting from different first exon sequences. Whether such mechanisms could have an effect over considerable distances is unclear (in the case of *SynGAP* up to 6 kb in the mature mRNA). Furthermore, most of the evidence regarding the link between transcription and splicing regards cassette exons. It remains to be seen what happens with alternative splice site choice, especially of only a few base pairs difference as is the case with *SynGAP*, *in vivo*.

How then can we determine which N-termini are linked to which C-termini?
Exhaustive screening and cloning from full length cDNA libraries would inform us of exon combinations that do exist. However, partly due to potential PCR bias, such a technique is not quantitative and we could not make any conclusions regarding abundance. More importantly we could not conclude that because a certain combination was not cloned that it does not exist. Furthermore, the disadvantages of costliness and time intensiveness should not be overlooked if quantitatively reliable data is not a potential outcome.

High throughput second generation sequencing has massively increased our knowledge of the complexity of the transcriptome, but due to the short nature of the sequencing reads produced cannot inform us of the long range connectivity between exons (Sultan et al., 2008). Sequencing reads of second generation sequencing are generally very short (35-100 bp) where conventional Sanger di-deoxy sequencing reads give a maximum of about 800bp. Clearly reads of this length are no use in determining linkage of sequences separated by thousands of bases.

The new technology of paired end reads, which produces short reads from both ends of a long fragment of DNA, could potentially provide the type of information we require. Currently the focus in the development of this technology is on genome sequencing, specifically in determining long-range positional information, de novo assembly and structural variations such as chromosomal rearrangements and copy number variations. RNA paired end tag (RNA-PET) libraries have been constructed from full length cDNA libraries; these consist of the first few bases of a transcript linked to the last few bases. This technology is ideal for demarcating the first exon (transcription start site) in combination with the last (polyadenylation site), however it

cannot yield sequence from the interior of the transcript that we require (Fullwood et al., 2009).

A less direct strategy would be to attempt to assess if the regulation, in response to synaptic activity and in development, of specific 3' ends mirrors that of the 5' ends. If this was the case we could infer connectivity, but this would not be conclusive evidence. Difficulties again arise regarding the difficulty of detection of 1 and 2 bp changes, even 13 bp is challenging. Lately a SynGAP alpha-2 antibody has become available so the proteins levels of SynGAPs alpha-1, alpha-2 and beta could be correlated with the transcript levels of SynGAPs A, B, C and E. Again, this is not ideal as transcript levels do not necessarily correlate with protein expression.

Immunoprecipitation using isoform specific antibodies followed by mass spectrometric analysis would allow the identification of linkage between isoforms with unique peptide sequence (i.e. not SynGAP C). Clearly, the generation of antibodies specific to all the unique peptide sequences would be enormously useful.

The choice of isoforms for further study

As we do not know if there is specificity in the linkage of N and C-termini the choice of isoforms for use in the functional experiments of this thesis was determined by a number of factors. The previously demonstrated importance of the C-terminal alpha-1 tail guaranteed its inclusion and the differential regulation of *SynGAPs A, B* and *C* merited further study. SynGAP alpha-2 was used as a C-terminal tail whose synaptic function had not been studied, and which we isolated form the library screen. SynGAP E was not carried forwards for functional study as it does not exhibit differential regulation in development and in response to synaptic regulation. Additionally the number of isoforms needed to be limited for practical time considerations. The remaining isoforms may be studied in future.

UTR

The discovery of two alternately spliced sections of 3' UTR in the initial library screen derived clones posed some questions and offered some hope of a potential isoform specific probe (Figure 3. 4).

UTR, especially 3' UTR, is heavily involved in mediating the trafficking, stability and translation of mRNAs. This can be mediated by non mutually exclusive *cis* regulatory elements, that is sequence determined structural features like secondary structure, and *trans* acting elements in the form of proteins or miRNAs that bind to those regions (Wilkie et al., 2003). Thus, alternative UTRs could provide a mechanism of differential regulation of different isoforms. Isoform specific regulation could only be the case if there was an absolute linkage between ORF and UTR. This question was partially addressed experimentally and it appears that there is not a definite correlation between isoform coding and the length of 3' UTR (Figure 3. 5). The purpose in further analysing the 3' end was not to comprehensively screen for all possible UTRs but rather to resolve a specific question that had bearing on the future expression of SynGAP. The experiment performed was not exhaustive and merely tells us some of the combinations of alternative splicing. Additionally the data set has to be biased, due to the choice of certain primer pairs, as well as PCR and cloning bias. The use of an oligo-dT reverse primer would go some way to rectifying the primer induced bias.

The finding of a range of different splice sites within the 3' UTR is puzzling but, given the extensive variability of 3' end of *SynGAP*, not entirely unexpected. The splice junctions do not observe the consensus splice site recognition sequences, particularly the especially conserved AG dinucleotide at the 3' splice site (GT/AG) (Ast, 2004; Rogozin et al., 2005). These type of alternatively spliced non conventional transcripts at the 3' end of SynGAP have been cloned previously in our lab (Mark Barnett, Patrick Stoney, personal communication). The presence of non-conventional splicing junctions in the *SynGAP E-alpha-1* clone isolated from the library screen indicates that these types of clones are not necessarily an artefact somehow introduced by PCR. There are reports in the literature of non-conventional alternative splicing. The unfolded protein response mediates the non spliceosomal splicing of a limited number of genes (Ma & Hendershot, 2001) and there is a second spliceosome that mediates a different type of non-conventional splicing of a rare class of introns more common in metazoan (Patel & Steitz, 2003). However the SynGAP transcripts do not contain the consensus sequences or splice junctions described for either of this two mechanisms. This aspect of the *SynGAP* transcriptional profile is potentially intriguing, but currently mysterious.

SynGAP B-shift

The isolation of a number of clones with a novel 4 bp insertion at the start/end of a *SynGAP B* specific exon adds to SynGAP's repertoire of alternative splice site selection variants. This one, if translated, would give rise to a truncated peptide. It is possible that a truncated SynGAP peptide could have some functional role. While we have no evidence translation occurs, a concern that the transcript could be present in the *SynGAP* $^{-/-}$ mouse used in this thesis prompted the further study of what we term SynGAP B-shift. This experiment is described in Chapter Four.

Another possibility is that *SynGAP B-shift* transcript may be degraded in a regulatory mechanism known as nonsense mediated decay (NMD). NMD is a recently discovered surveillance mechanism against transcripts that contain exon–exon junctions downstream of a termination codon (Lejeune & Maquat, 2005). NMD is thought to have evolved to select mRNAs with an intact reading frame from a pool of splice combinations generated by the splicing machinery. Indeed, a large-scale computational study demonstrated that as much as one-third of mRNA transcripts may be subject to NMD. Combined with the 'noisy splicing' view, which supposes that splicing is inherently noisy and spurious transcripts are common, it is suggested that RUST (regulated unproductive splicing and translation) is one of the major regulatory mechanisms for establishing the right level of gene expression (Green et al., 2003)(Lewis et al., 2003; Zhang et al., 2009). If this view is correct SynGAP B-shift could be one of many transcripts destined for degradation.

Spheroid bodies

The appearance of spherical bodies enriched in SynGAP in transfected HEK cells is surprising (

Figure 3. 9). Morphologically the bodies do not appear to be like any normal cellular organelle. This is supported by patterns of expression patterns of a number of organellar markers (Figure 3. 10). Clearly these bodies are an artefact of overexpression as they are not present in wild type neurons probed with an antibody against SynGAP, however they may tell us something about localisation or recruitment.

The first point to take from this localisation is that the PH and C2 domains were not sufficient to mediated translocation to the plasma membrane. It is possible that the protein might translocate if the cells were stimulated to release intracellular stores of Ca, as in the case of CAPRI and RASAL (Liu et al., 2005). SynGAP also had no effect on the actin cytoskeleton of the cells despite a previously demonstrated role in the neuronal regulation of the actin depolymerising protein cofilin (Carlisle et al., 2008). One could postulate that other synaptic proteins are required to mediate this activity, or that, again stimulation is required.

The spheroid bodies appear to be hollow membranous vesicles, perhaps implicating the potentially membrane interacting PH and C2 domains (although these normally associate with plasma membranes). Incubation with FM dyes would allow the assessment of whether or not these inclusions arise from the plasma membrane (Cochilla *et al*., 1999). The C2 domain has been demonstrated to have a role in membrane bending (see main introduction, p46). Membrane bending proteins usually bend membranes to a specific geometry and it is unlikely that the large variety in vesicle seen here would be caused.

Fairly equal distribution of bodies throughout the soma and the apparent health of associated nuclei suggests that they are not fragmenting Golgi apparatus (
Figure 3. 9, d-f,). The Golgi marker used, which does not co-localise with the spheroid bodies, is for the trans-medial Golgi and thus will not be expressed in all Golgi compartments (Figure 3. 10, c,d). Therefore, it might be useful to use additional Golgi markers to conclusively exclude the possibility of fragmented Golgi. When stressed mitochondria can swell, or balloon, into more rounded structures than their normal elongated shape (Rintoul et al., 2003). Although the extreme spherical nature of the SynGAP bodies combined with the variability in size, including very large structures, indicates that they are not stressed mitochondria, I cannot exclude this definitively until I co-stain with a mitochondrial marker.

The spheroid bodies are reminiscent of the enlarged endosomes caused by expression of a constitutively active forms of Rab5 and RabD (Roberts *et al*., 2000; Li & Liang, 2001; Harris & Cardelli, 2002). Rab is considered to be a rather local switch that controls specific membrane fusion events during endocytosis (Tall *et al*.,

2001; Ng & Tang, 2008). The enlarged vesicles in these cells are due to excessive early endosomal fusion. The endosomal marker used in Figure 3. 10 (e,f) is RhoB which is restricted to the late, degradative pathway and does not co-localise with early endosomal markers (Wherlock et al., 2004). For this reason we would not expect RhoB to mark these spheroid bodies if they were enlarged early endosomes. A more comprehensive experiment would make use of an expanded range of endosomal markers such as EEA1 or fluorescent-labelled transferrin to saturate the early and recycling endocytic compartments, CD63 for late endosomes and LAMP-1 for late endosomes/lysosomes.

In addition to the multiple studies that indicate an ability of SynGAP to regulate Ras and Rap, one study has demonstrated an *in vitro* Rab5 GAP activity of the isolated GAP domain of SynGAP (Tomoda et al., 2004). If SynGAP is deactivating Rab in these cells the presence of enlarged endosomes is even more surprising. The Rab mutants mentioned above are constitutively active but the presence of SynGAP should mediate the inactivation of Rab5 (inactive mutants of Rab5 do not cause enlarged endosomes).

To continue speculating, it is worth noting that one major pathway for controlling the abundance of synaptic AMPA receptors is local endocytic recycling. Activity-dependent translocation of recycling endosomes (REs) into spines is required to supply a mobilizable pool of AMPA receptors to synapses during long-term synaptic plasticity (Ehlers, 2000; Park *et al.*, 2006). It has been shown that Rab5 activation drives the specific internalization of synaptic AMPA receptors in a clathrin-dependent manner and that this activity is required for NMDA receptor dependent LTD. (Brown *et al.*, 2005). If SynGAP has a role in regulating Rab mediated endosomal trafficking this may be the mechanism by which it exerts its effect on altered AMPA receptor trafficking.

To summarise, SynGAP is a highly conserved protein of high molecular complexity. A number of differenti isoforms are expressed endogenously, as is evident by Western Blot analysis, but the precise identity of the combinations of N and C termini are not known. We have cloned two full length isoforms (SynGAP A-alpha-2 and E-alpha-1) and used these to construct a range of isoforms (A, B, C combined

with alpha-1 and alpha-2) to be used in the assays in the remainder of this thesis. Additionally, we have shown that there are many different lengths of SynGAP 3' UTR exist but that there is no absolute linkage between UTR identity and C terminus coding ability. The potential existence of a truncated SynGAP, SynGAP B shift, was examined and discussed, as was the appearance of anamolous SynGAP enriched spheroid bodies in SynGAP transfected cells.

4 Chapter Four: Morphology

4.1 Introduction

This chapter is concerned with the morphological implications of altering SynGAP expression. SynGAP is found in abundance at excitatory synapses, which are located primarily on small protrusions called dendritic spines. The main objective of this chapter was to first examine the effect of the removal of all SynGAP isoforms on dendritic spine morphology. Second, to determine if spine morphology would be differentially affected by the overexpression of particular isoforms of SynGAP.

Dendritic spine morphology is tightly regulated as it plays a major role in the functional development and plasticity of synapses. Spines are thought to provide biochemical as well as electrical signalling compartmentalisation and are present in many shapes and sizes (Nimchinsky *et al.*, 2004; Noguchi *et al.*, 2005). Broadly spines can be categorised as; mushroom, a protrusion with a clearly defined neck supporting a larger head; stubby, a short protrusion lacking neck/head definition; and thin, a thinner protrusion again lacking neck/head definition (Peters & Kaiserman-Abramof, 1970). Longer thin protrusions are classified as filopodia which are probably the precursors to spines (Vaughn, 1989; Fiala *et al.*, 1998). Greater diversity is conferred by variations in spine head size and shape, from spherical, oval and cup to irregularly shaped heads. Spine necks can be thin or thick, bent or straight, branch or unbranched. Spines are highly dynamic structures which can shift shape over the course of seconds to minutes (Dailey & Smith, 1996; Fischer *et al.*, 1998; Dunaevsky *et al.*, 1999).

The dynamic nature of spines is key to their functional role in plasticity and development (Bonhoeffer & Yuste, 2002; Holtmaat & Svoboda, 2009). The most mobile protrusions are the filopodia which seem to continually extend and retract, before becoming more stable when they partner with a presynaptic terminal to form a synapse. Mushroom spines are the most stable form of protrusion, and although

some are present only transiently, they can persist for months and potentially the lifetime of an animal (Grutzendler *et al.*, 2002; Trachtenberg *et al.*, 2002; Zuo *et al.*, 2005). There is a strong correlation between the strength of a synapse and the spine head size, thought to be due to the high levels of AMPA receptors found in the PSD of larger spines (Matsuzaki *et al.*, 2001; Kasai *et al.*, 2003). LTP and experience dependant plasticity can induce the formation of new spines and the transition of thin spines to mushroom type. The reverse is true for LTD (Nagerl *et al.*, 2004; Okamoto *et al.*, 2004; Hofer *et al.*, 2009). Interestingly the correlation of spine structure with function is not clear cut and can be decorrelated in many cases (Ehrlich & Malinow, 2004; Kopec *et al.*, 2007; Wang *et al.*, 2007). Wang et al. demonstrate several conditions in which spine size is unrelated to trafficking of AMPA receptors and that NMDAR-LTD and spine shrinkage diverge in the downstream signalling events, and can occur independently of each other.

As mentioned, spines are regulated by multiple parallel pathways that seem to converge on two mechanistic cellular processes; the trafficking of post synaptic proteins and the regulation of actin dynamics. Larger spines contain greater amounts of PSD proteins and the insertion of additional plasma membrane with the fusion of trafficking endosomes also contributes to the increase in size (Harris & Stevens, 1988; Park *et al.*, 2006). With an eye to SynGAP it is worth noting that many small G proteins, and their regulators, have been implicated in spine morphology regulation. Rap1, Rap2, Rnd1, Rac, Cdc42 and especially Rho and Ras have all been found to alter spine morphology or density (Pak *et al.*, 2001; Ishikawa *et al.*, 2003; Xie *et al.*, 2005; Xie *et al.*, 2007). Actin polymerisation and depolymerisation plays a major part of the physical mechanism by which spines change shape and can be regulated by the Rho/Rac/Cdc42 family of G proteins (Fischer *et al.*, 1998).

Altered actin regulatory networks have been observed in a *SynGAP* $^{-/-}$ mouse (Carlisle et al., 2008). Vasquez et al. (2004) find an enlargement of spine heads in *SynGAP* $^{-/-}$ hippocampal neurons at day *in vitro* (DIV) 14, cultured in the absence of FBS. They also find an increase in spine density. Hippocampi of adult *SynGAP* $^{+/-}$ animals also have the same prematurely developed spine heads (Carlisle et al., 2008). Rumbaugh et al. (2006) do not directly examine spine morphology, but find an increase in 'synapse cluster size', but not density. The impact of the

overexpression of different SynGAP isoforms on spine morphology has not been assessed. Expression of SynGAP A-alpha-1 in *SynGAP* $^{-/-}$ neurons is sufficient to rescue the enlarged spine head phenotype observed by Vazquez et al. Mutation of the PDZ binding domain removes the ability of SynGAP A-alpha-1 to rescue the spine phenotype while a GAP domain mutant retains the ability to rescue some elements of the phenotype, namely premature synaptic clustering of PSD-95. These findings suggest that SynGAP and its various domains influence spine formation by distinct but overlapping mechanisms. Here I will further this work by describing the *SynGAP* $^{-/-}$ spine phenotype which had not yet been examined in this mouse model, and address for the first time the effects and dendritic localisation of various SynGAP isoforms in wild type neurons.

4.2 Results

Part One:

Morphological analysis of dendritic protrusions of wild type and *SynGAP* $^{-/-}$ neurons.

Part Two:

Morphological analysis of dendritic protrusions of wild type cells overexpressing various SynGAP isoforms.

4.2.1 Overview of Results

Part One: Morphological analysis of dendritic protrusions of wild type and *SynGAP* $^{-/-}$ neurons.

It is possible to maintain viable *SynGAP* $^{-/-}$ neurons in culture and, by transfecting them with enhanced green fluorescence protein (eGFP), visualise their morphology.

In both cortical and hippocampal cultures, mean dendritic protrusion length and width is unchanged in *SynGAP* $^{-/-}$ compared to wild type neurons. Dendritic protrusion density is mostly unchanged, however there is a significant increase in protrusion density in *SynGAP* $^{-/-}$ cortical neurons at DIV 10.

Despite a lack of difference in the means there are changes in the distributions of measurements; there is a shift toward shorter spines in *SynGAP* $^{-/-}$ cortical and hippocampal neurons. This difference is not observed in hippocampal neurons when they are cultured in the absence of FBS.

In the presence of FBS, the distributions of protrusion widths in *SynGAP* $^{-/-}$ cortical neurons, but not hippocamapal neurons, is shifted toward thinner heads (cultured with FBS). When hippocampal neurons are cultured without FBS the distribution is shifted in the other direction, toward thicker heads.

Insights into protrusion development in culture include the observation that, compared to hippocampal neurons, the protrusions of cortical cells are very sparse at DIV 10 but treble in density by DIV14. While the protrusion density of hippocampal cells stays constant over this time period the width of the protrusion heads does increase.

The main effect of the removal of FBS from the culture protocol is a decrease in mean protrusion length.

Part Two: Morphology of neurons overexpressing various SynGAP isoforms.

Overexpression of SynGAP isoforms A-alpha-1, B-alpha-1 or A-alpha-2 in wild type neurons does not affect the mean protrusion length, width or density of dendritic protrusion.

All isoforms have the same effect on the distribution of protrusion lengths; a shift toward shorter protrusions. In contrast, the effect of isoforms on the distribution of protrusion widths diverges; overexpression of SynGAPs A and B-alpha-1 cause a decrease in prevalence of the thinnest and the widest heads while SynGAP A-alpha-2 has no effect.

There is divergence in the dendritic localisation patterns of overexpressed SynGAPs which indicates that localisation is determined by the combination of N and C-termini.

4.2.2 Part One: Morphological analysis of dendritic protrusions of wild type and *SynGAP* $^{-/-}$ neurons.

Viable neurons can be maintained in culture

The experimental system of this thesis is dissociated neuronal culture. The hippocampus or cortex is dissected from 17.5 day old embryos (E17.5) derived from timed matings. The tissue is enzymatically treated and mechanically dissociated. Viable neurons are counted in a haemocytometer and plated at high density (1500 cells/mm^2) or low density (200 cells/mm^2). See Methods (p51) for additional details. Upon plating very few cell bodies had short appendages but most neurons had grown visible neurites the day after plating. One week after plating a network of neurons was easily recognisable. A glial layer was visible through breaks in the network when the neurons were cultured in the presence of foetal bovine serum (FBS).

4.2.3 Neuronal morphology can be visualised by filling cells with green fluorescent protein

Neurons were transfected with enhanced green fluorescent protein (eGFP) using a proprietary liposome based system (Lipofectamine 2000, Invitrogen). For the purposes of morphological analysis neurons were transfected at DIV 9 or DIV13, then fixed with paraformaldehyde on the subsequent day. 16 hours after transfection was sufficient time to allow the development of bright, fully filled green fluorescent neurons. The first signs of green appeared from as little as 4 hours after transfection. The transfection rate was approximately 1-2% (see Appendix 1). A wide range of neuronal morphologies were visible in both hippocampal and cortical cultures. Figure 4. 1 (upper panel) shows a typical field of view of a hippocampal culture. A classical pyramidal neuron and some bipolar neurons are indicated. Multipolar neurons were also observed. The cell bodies of untransfected neurons are visible due to autofluorescence. Only neurons of pyramidal type morphology were analysed in order to limit experimental variability. Pyramidal neurons are typified by a pyramid or triangular shaped soma, a prominent main dendrite

resembling the in situ apical dendrite and shorter basal dendrites arising from the cell body, or often the tips of the cell body. Some examples of pyramidal type neurons are shown in Figure 4. 1 (bottom panel).

Dendritic spines are visible on eGFP expressing cultured neurons

Protrusions from dendritic shafts were visible on eGFP expressing cultured neurons from at least DIV 9 (Figure 4. 2). The protrusions ranged in morphology from long filopodia and short thin protrusions to protrusions with a clear thin neck with a thicker head that could be classified as mushroom spines. Short stubby spines were also evident. Bifurcating protrusions of the long thin and mushroom type also occured.

Imaging and analysing dendritic spines

In order to obtain high definition images amenable to analysis confocal microscopy was used to capture sections of dendrites bearing spines. The length and head width of protrusions up to a certain length (8 µm) were measured manually I do not refer to the protrusions as spines because long filopodia are also included under this criterion. I cannot discount the possibility that some of the longer protrusions may be short neurites. Additional details are present in Methods (p75).

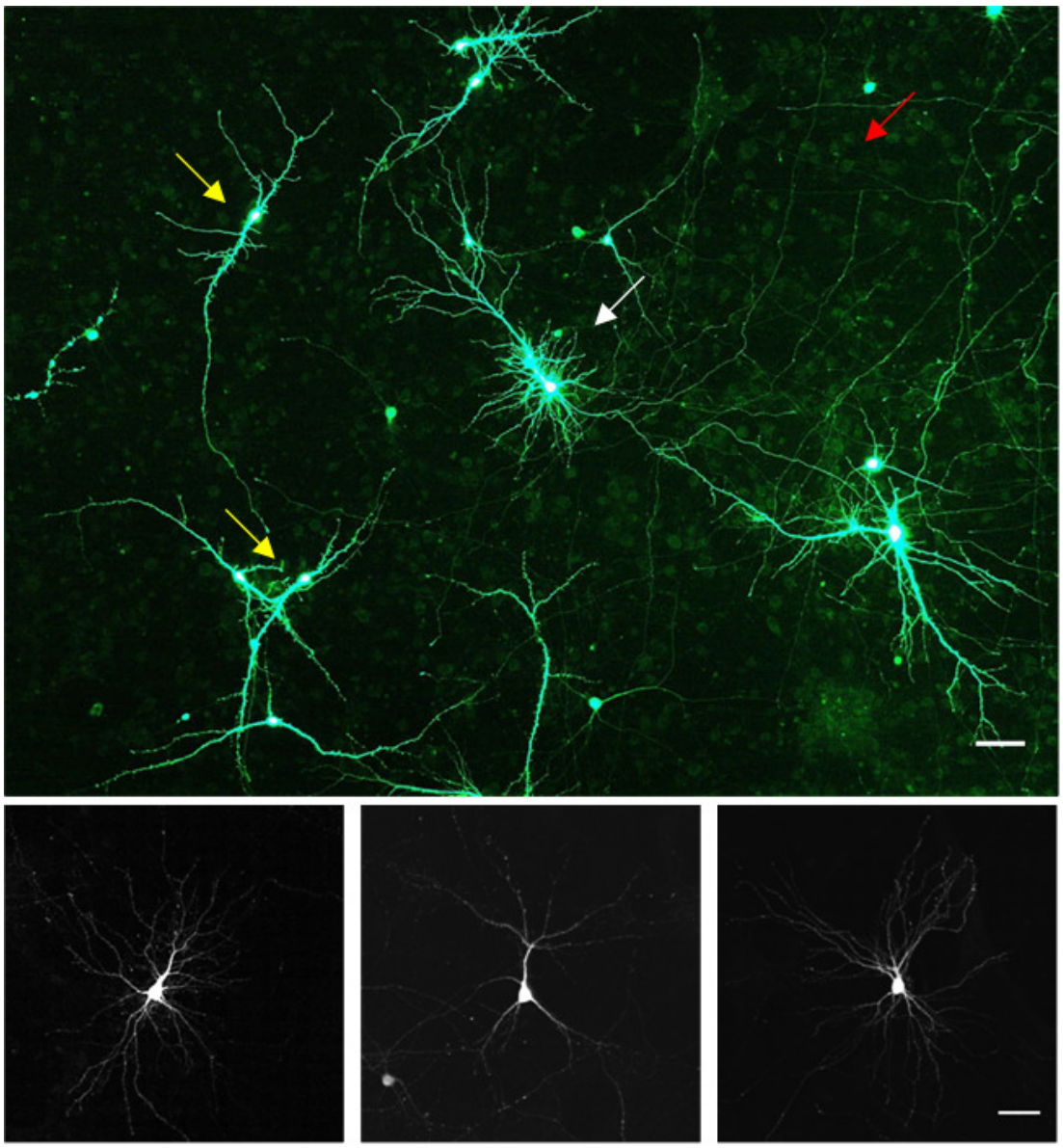

Figure 4. 1 eGFP expressing cultured neurons display different morphologies

Shown is a representative field of view of a DIV 10 hippocampal culture transfected at DIV 9 with eGFP (upper panel). A pyramidal type neuron is indicated by the white arrow. Bipolar neurons are indicated by yellow arrows. The autofluorescing cell bodies of untransfected neurons are visible (Red arrow). In order to capture the dendrites effectively the cell body most be overexposed, the white colour here indicates that this region is outside of the dynamic range of the image. Examples of pyramidal type neurons in a hippocampal culture at DIV 14 are shown in the bottom panel. Scale bars are 50 µm.

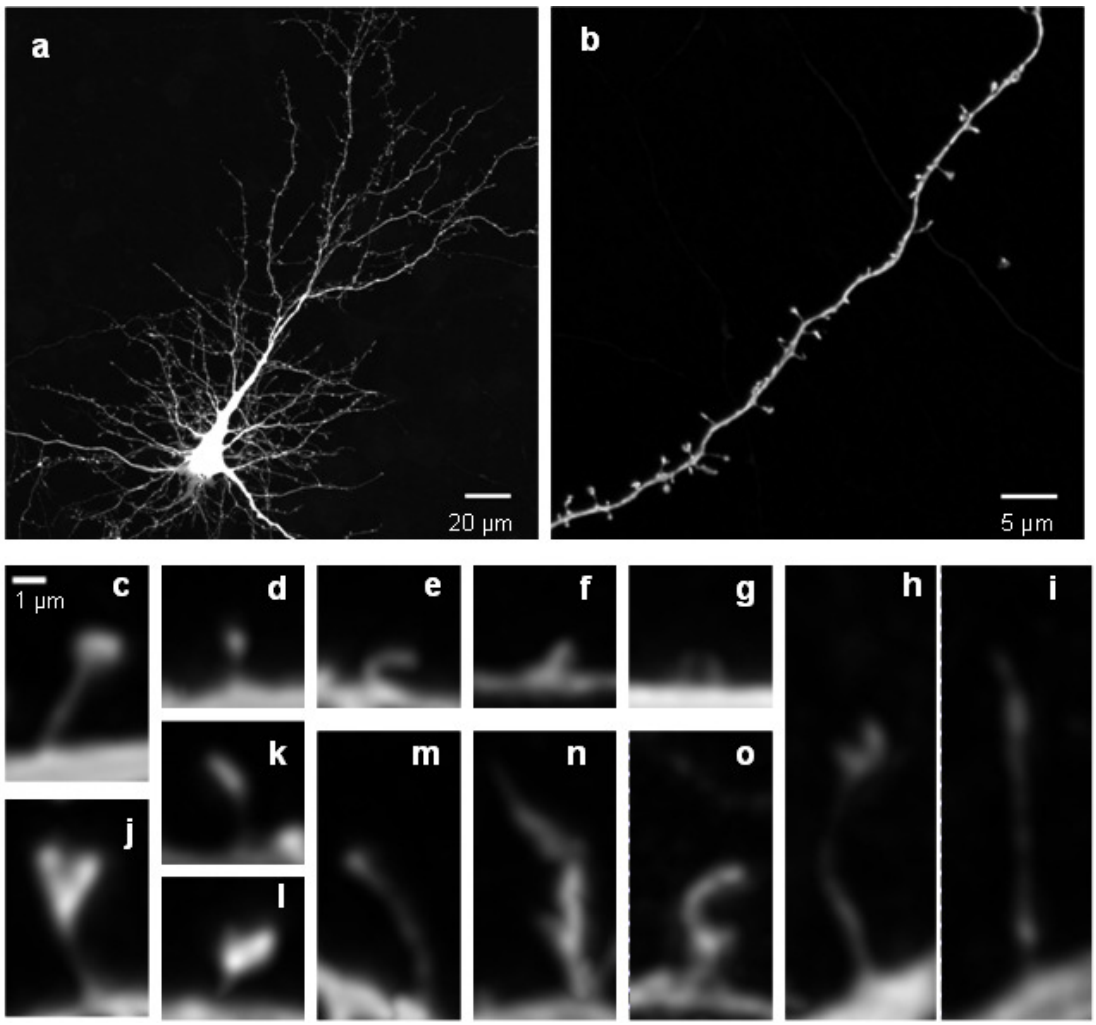

Figure 4. 2 **Dendritic protrusions are visible on GFP filled neurons**

A pyramidal type neuron (a) and a representative stretch of dendrite (b) are shown in the upper panel. Various examples of the type of dendritic protrusions observed on GFP expressing pyramidal type neurons in culture are shown in the bottom panel (c-o). These spines could be classified as mushroom (c, d, k, l), short (e, f, g) long or filopodia (h, I, m–o) and bifurcating (j). The examples shown here are z projections of deconvolved image stacks drawn from hippocampal and cortical cultures. Scale bars are indicated above.

Viable SynGAP $^{-/-}$ neurons can be maintained in culture

SynGAP $^{-/-}$ mice die a few days after birth, P2-7,(Komiyama *et al*., 2002; Kim *et al*., 2003; Vazquez *et al*., 2004) but *SynGAP* $^{-/-}$ neurons can be maintained in culture. *SynGAP* $^{-/-}$ embryos and cultured neurons were grossly morphologically identical to wild type litter mate controls. There was no difference in cell density between mature *SynGAP* $^{-/-}$ and wild type cultures. Equivalent numbers of cells with healthy appearing nuclei were found indicating that there is not a difference in propensity toward cell death (Figure 4. 3).

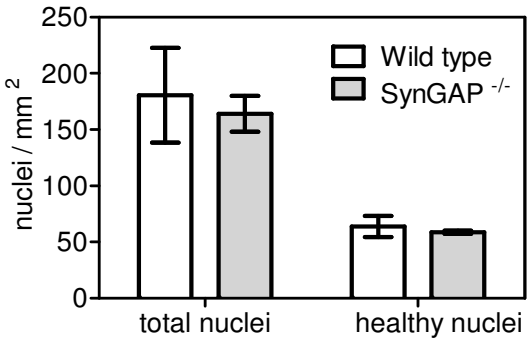

Figure 4. 3 Cell density and survival in *SynGAP* $^{-/-}$ and wild type cultures

There is no difference in total nuclei density in wild type and *SynGAP* $^{-/-}$ low density hippocampal cultures at DIV 10. Nuclei were stained with Topro 3. All nuclei, irrespective of morphology, were counted to yield a total nuclei density. The proportion of healthy appearing nuclei is unchanged in the *SynGAP* $^{-/-}$ cultures. This data indicates a 40% survival rate to DIV 10 at this density. Data are from three wild type and three *SynGAP* $^{-/-}$ embryos from two separate cultures. Data are mean +/- SEM.

4.2.4 Dendritic protrusion morphology in SynGAP $^{-/-}$ neurons

I examined dendritic protrusion morphology and density in *SynGAP* $^{-/-}$ neurons from cortical and hippocampal cultures at different time points. There was no difference in mean dendritic protrusion length, width or density between *SynGAP* $^{-/-}$ cortical or

hippocampal neurons at DIV 10 or 14 (Figure 4. 4 and Figure 4. 5, two way ANOVA, post hoc Bonferonni t-tests). The only trend towards a difference was the apparent increase in protrusion density in cortical *SynGAP* $^{-/-}$ neurons (0.33 +/- 0.03 protrusions/µm) compared to wild type (0.22 +/- 0.03 protrusions/µm) (Figure 4. 4, g). If this data is examined in isolation an individual student's t-test indicates a statistically significant difference, $p = 0.02$.

Nevertheless it appears that cortical and hippocampal protrusions develop differently. In cortical neurons protrusion density increased with development in both wild type type (0.22 +/- 0.03 protrusions/µm at DIV 10 to 0.58 +/- 0.2 protrusions/µm at DIV 14) and *SynGAP* $^{-/-}$ neurons (0.33 +/- 0.03 protrusions/µm at DIV 10 to 0.69 +/- 0.07 protrusions/µm at DIV 14, two way ANOVA, $p<0.001$, post hoc Bonferroni t-test, all $p < 0.001$) (Figure 4. 4, g). On the other hand density was unchanged with time in hippocampal neurons (Figure 4. 5, g) but protrusion width increased as the neurons aged (Figure 4. 5,d). Again this is equally true for wild type (width of 0.31 +/- 0.01 µm at DIV 10 to 0.42 +/- 0.03 µm at DIV 14) and *SynGAP* $^{-/-}$ neurons (width of 0.32 +/- 0.01 µm at DIV 10 to 0.41 +/- 0.01 µm at DIV 14, two way ANOVA, $p<0.0001$, post hoc Bonferroni t-test, all $p<0.001$).

Analysis of the distributions of all the protrusions lengths and widths analysed revealed some significant changes between wild type and knock out. (The D value indicates the maximum difference between the two cumulative frequency histograms (not shown here)). In *SynGAP* $^{-/-}$ cortical neurons there was a slight shift towards shorter, thinner protrusions which is more marked at DIV 10 than DIV 14 (two sample Kolomogorov-Smirnov test, all $p < 0.05$, width; DIV 10 $D = 0.25$, DIV 14 $D = 0.08$, length; DIV 10 $D = 0.22$, DIV 14 $D = 0.11$) (Figure 4. 4, b, c, e, f). The distribution of protrusion widths in *SynGAP* $^{-/-}$ hippocampal neurons was unaffected (Figure 4. 5, e,f) but again the distribution of lengths was shifted slightly toward more shorter protrusions (Figure 4. 5, b,c). Again the magnitude of the difference was greater at the younger age (two sample Kolomogorov-Smirnov test, both $p < 0.05$, DIV 10 $D = 0.14$, DIV 14 $D = 0.07$).

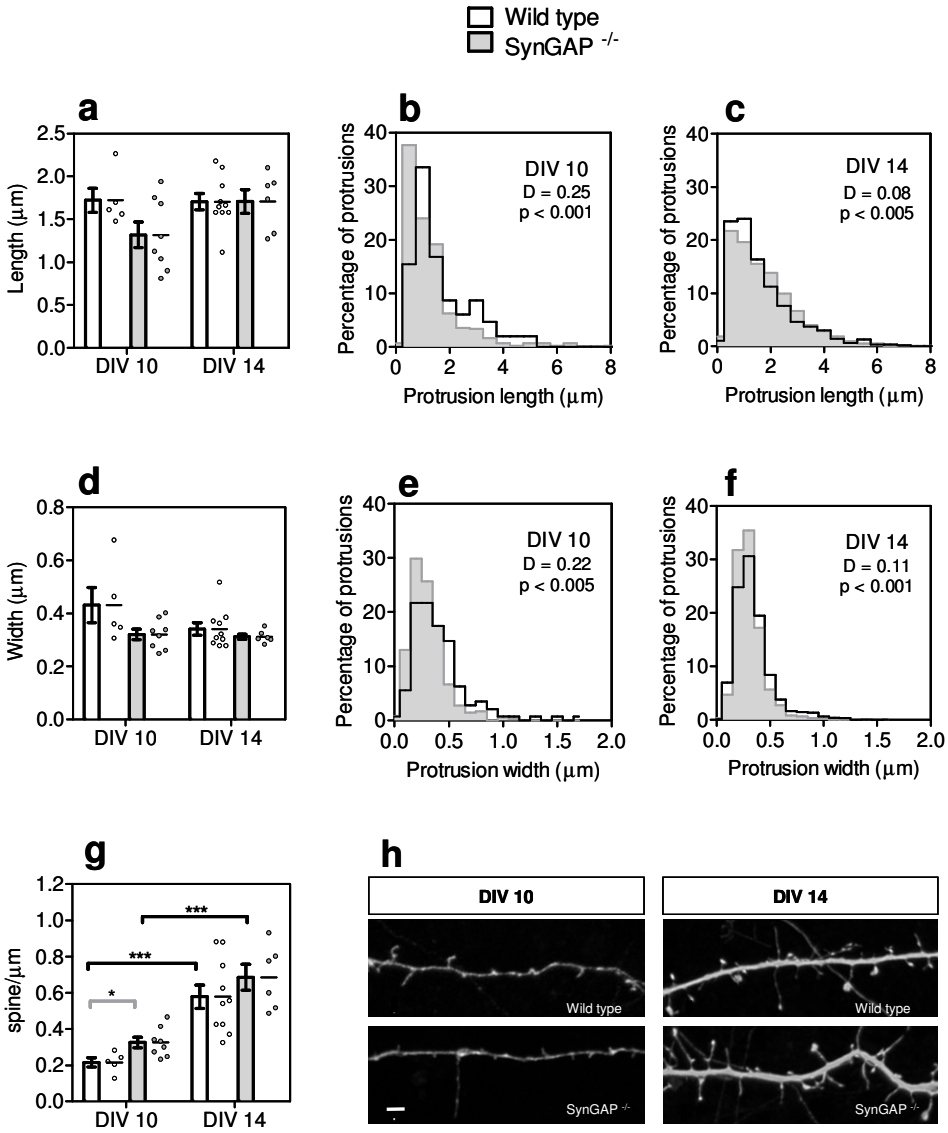

Figure 4. 4 Dendritic protrusions in wild type and *SynGAP* $^{-/-}$ cortical neurons

Mean dendritic protrusion length, width and density from wild type and *SynGAP* $^{-/-}$ cultured cortical cells at DIV 10 and DIV 14 are shown in the left most panels (a, d, g, DIV 10; WT n = 5, *SynGAP* $^{-/-}$ n = 8, DIV14; WT n = 10, *SynGAP* $^{-/-}$ = 6). Data from individual cells are indicated in the scatter plot. Spine density increases with development (g) in the wild type and knock out (two way ANOVA, $p < 0.001$; wild type, DIV 10 = 0.22 +/- 0.06 spines/µm to DIV 14 = 0.58 +/- 0.2 spines/µm, $p < 0.001$***; *SynGAP* $^{-/-}$, DIV 10 = 0.33 +/- 0.08 spines/µm to DIV 14 = 0.69 +/- 0.17 spines/µm, $p < 0.001$***, post hoc Bonferroni t-tests). A student's t-test indicates an increase in spine density in the knock out compared to wild type at DIV 10, ($p = 0.02$*, grey connecting line). Frequency histograms of the lengths (b, c) and widths (e, f) of all dendritic protrusions are shown on the right (DIV 10; WT n = 143, *SynGAP* $^{-/-}$ n = 359, DIV 14; WT n = 1059, *SynGAP* $^{-/-}$ n = 999, two sample Kolomogorov-Smirnov test,

all $p \leq 0.05$). The p and D values of two sample Kolmogorov-Smirnov tests are inlaid in the graphs. Representative sections of dendrite appear in (h). Scale bar is 2 µm. Data are from 5 wild type and 5 *SynGAP* $^{-/-}$ embryos from 2 separate cultures.

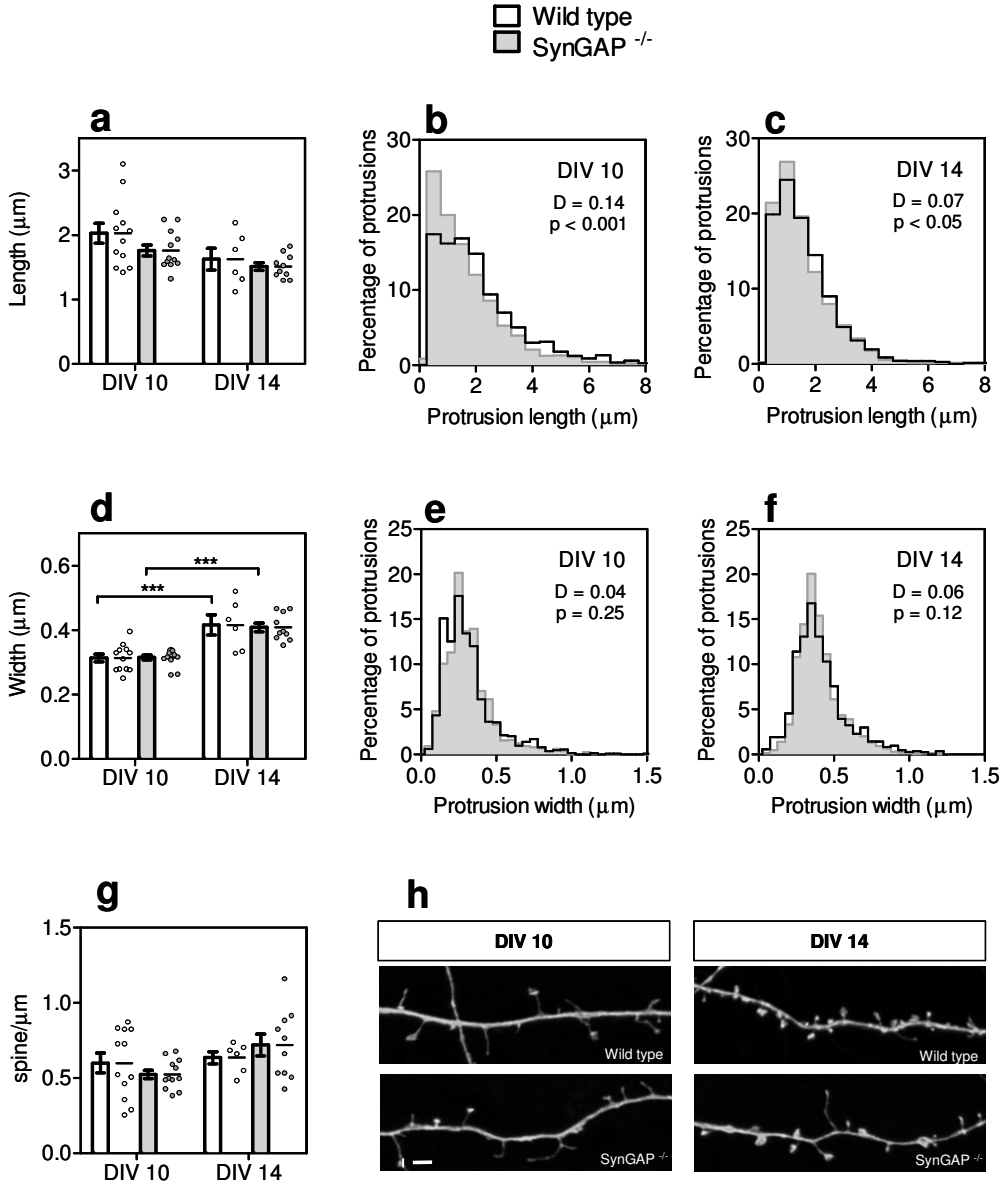

Figure 4. 5 **Dendritic protrusions in wild type and *SynGAP* $^{-/-}$ hippocampal neurons**

Mean dendritic protrusion length, width and density from wild type and *SynGAP* $^{-/-}$ cultured hippocampal cells at DIV 10 and DIV 14 are shown in the left most panels (a, d, g, DIV 10; WT n = 10, *SynGAP* $^{-/-}$ n = 12, DIV14; WT n = 6, *SynGAP* $^{-/-}$ = 10). Data from individual cells is indicated in the scatter plot. Spine width increases with development (d) in wild type and knock out cells (two way ANOVA, $p < 0.001$, wild type, DIV 10 = 0.31 +/- 0.04 µm to DIV 14 = 0.42 +/- 0.07 µm, $p < 0.001$***; *SynGAP* $^{-/-}$, DIV 10 = 0.32 +/- 0.03 µm to DIV 14 = 0.41 +/- 0.04 µm, $p < 0.001$***, post hoc Bonferroni t-tests). Frequency histograms of the lengths (b, c) and widths (e, f) of all dendritic protrusions are shown on the right (DIV 10; WT n = 1125, *SynGAP* $^{-/-}$ n = 1291, DIV 14; WT n = 834, *SynGAP* $^{-/-}$ n = 1351). The p and D values of two

sample Kolmogorov-Smirnov tests are inlaid in the graphs. Representative sections of dendrite appear in (h). Scale bar is 2 µm. Data are from 6 wild type and 6 *SynGAP* $^{-/-}$ embryos from 2 separate cultures.

Previous work that found an increase in dendritic spine width in *SynGAP* $^{-/-}$ neurons was performed on cultures grown in the absence of foetal bovine serum (FBS) (Vazquez et al., 2004). The results I have described up to now are derived from cultures maintained in the presence of FBS. In order to determine if the presence of FBS has an effect on protrusion morphology or density I cultured wild type and *SynGAP* $^{-/-}$ hippocampal neurons without FBS. I found no difference in mean protrusion morphology or density between wild type and knock out with this treatment (Figure 4. 6, a, d, g). However the absence of FBS did effect spine development. Both wild type and *SynGAP* $^{-/-}$ neurons cultured in the absence of FBS had a shorter mean protrusion length compared to equivalent neurons cultured with FBS (two way ANOVA, $p<0.0001$; wild type + FBS, 1.63 +/- 0.17 µm compared to wild type - FBS, 1.09 +/- 0.05 µm, post hoc Bonferroni t-test, $p<0.001$; *SynGAP* $^{-/-}$ + FBS, 1.51 +/- 0.06 µm compared to *SynGAP* $^{-/-}$ - FBS, 1.15 +/- 0.11 µm, post hoc Bonferonni t-test, $p<0.05$) (Figure 4. 6, a). This change was also apparent in the different distributions of protrusion length (two sample Kolomogorov-Smirnov test, both $p < 0.001$, wild type $D = 0.28$, *SynGAP* $^{-/-}$ $D = 0.22$) (Figure 4. 6, b, c).

In the absence of FBS the distribution of wild type widths was unchanged compared to the +FBS condition (Figure 4. 6, e), however the distribution of *SynGAP* $^{-/-}$ widths was slightly different between the two cases (*SynGAP* $^{-/-}$; +/- FBS, widths, $D = 0.14$, $p < 0.001$) (Figure 4. 6, f). The shift of the *SynGAP* $^{-/-}$ distribution was toward slightly wider protrusion heads. This change is borne out when wild type and *SynGAP* $^{-/-}$ width distributions (-FBS) are compared directly (-FBS; wild type v *SynGAP* $^{-/-}$, widths, $D = 0.11$, $p < 0.001$) (Figure 4. 7).

In order to assess if any given sub type of spine was affected by the removal of SynGAP, eg long and thin, or short and thick, I calculated the correlation between protrusion length and width. There is no correlation between protrusion length and width within any of the populations of protrusions analysed (data not shown, Pearson's correlation coefficients). There was no apparent differences in the scatter of the data between wild type and *SynGAP* $^{-/-}$ data.

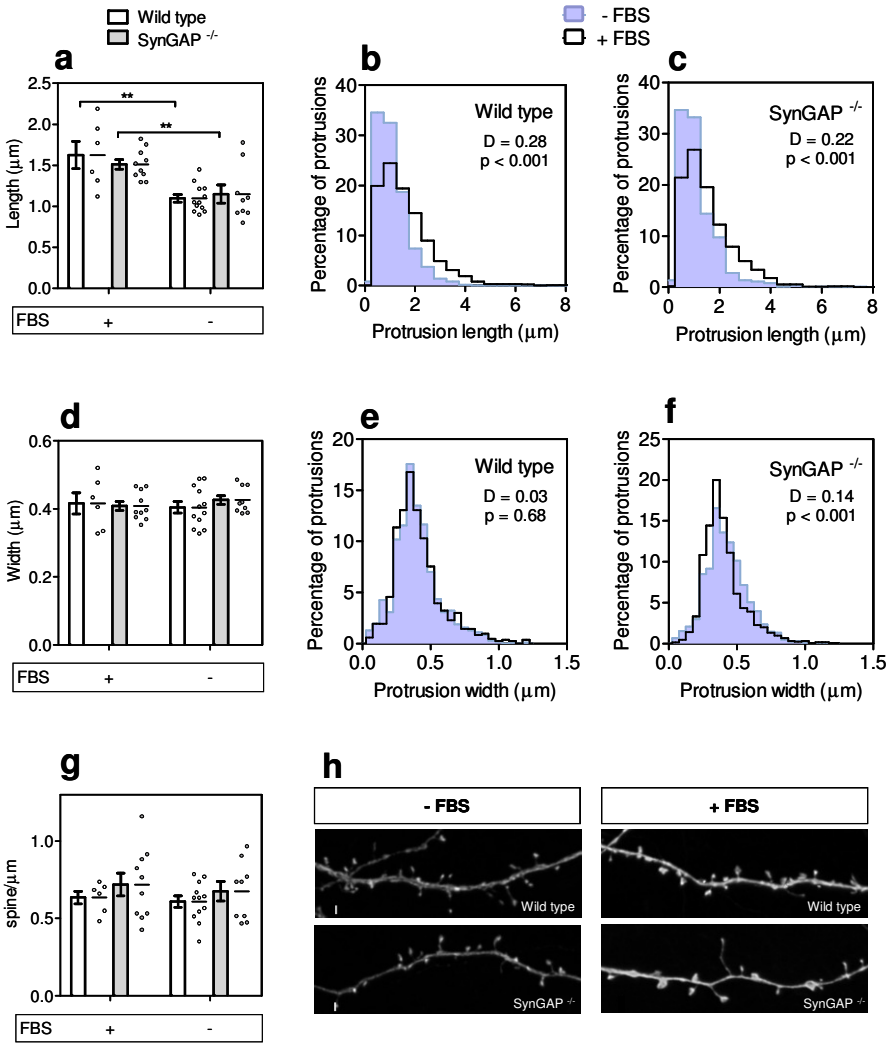

Figure 4. 6 Dendritic protrusions in wild type and *SynGAP* $^{-/-}$ hippocampal neurons cultured in the presence and absence of foetal bovine serum (FBS)

Mean dendritic protrusion length, width and density from wild type and *SynGAP* $^{-/-}$ cultured hippocampal cells at DIV 14 are shown in the left most panels (a, d, g, + FBS; WT n = 6, *SynGAP* $^{-/-}$ n = 10, - FBS; WT n = 12, *SynGAP* $^{-/-}$ = 9). Data from individual cells is indicated in the scatter plot. Protrusion lengths (a) of wild type and knock out neurons is decreased in the absence of FBS cells (two way ANOVA, $p < 0.001$, wild type, + FBS = 1.63 +/- 0.41 µm to –FBS = 1.1 +/- 0.17 µm, $p < 0.001$***; *SynGAP* $^{-/-}$, + FBS = 1.51 +/- 18 µm to –FBS = 1.15 +/- 0.34 µm, $p < 0.001$*, post hoc Bonferroni t-tests). Frequency histograms of the lengths (b, c) and widths (e, f) of all dendritic protrusions are shown on the right (+ FBS; WT n = 834, *SynGAP* $^{-/-}$ n = 1351, - FBS; WT n = 1081, *SynGAP* $^{-/-}$ n = 906). The p and D values of two sample Kolmogorov-Smirnov tests are inlaid in the graphs. Representative sections of

dendrite appear in (h). Scale bar is 2 µm. Data are from 5 wild type and 5 *SynGAP* $^{-/-}$ embryos from 3 separate cultures. Note that the data for the + FBS condition here is the same as shown in figure 4.6.

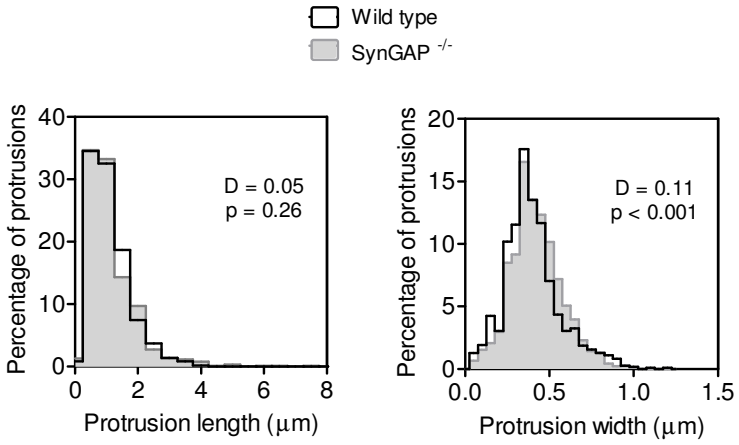

Figure 4. 7 Direct comparison of the distributions of wild type and *SynGAP* $^{-/-}$ dendritic protrusion length and width in neurons cultured in the absence of FBS

Frequency histograms of dendritic protrusions measurements from wild type and *SynGAP* $^{-/-}$ hippocampal neurons at DIV 14. All data was derived from neurons cultured in the absence of FBS (WT n = 1081, *SynGAP* $^{-/-}$ n = 906). The p and D values of two sample Kolmogorov-Smirnov tests are inlaid in the graphs.

4.2.5 Part Two: Morphological analysis of dendritic protrusions of wild type cortical cells overexpressing various SynGAP isoforms.

4.2.6 Dendritic protrusion morphology in wild type neurons overexpressing SynGAP isoforms

A range of SynGAP isoforms, SynGAP A-alpha-1, SynGAP B-alpha-1, SynGAP A-alpha-2 were expressed in wild type cortical cells to assess their effect on the morphology and density of dendritic protrusions. SynGAP was co transfected with GFP to allow the identification of cells expressing SynGAP. See Appendix 1 for the optimisation of the co-transfection protocol and confirmation of co-expression of GFP and SynGAP. None of the isoforms had any effect on protrusion density, mean length or width as compared to GFP only expressing control cells (Figure 4. 8).

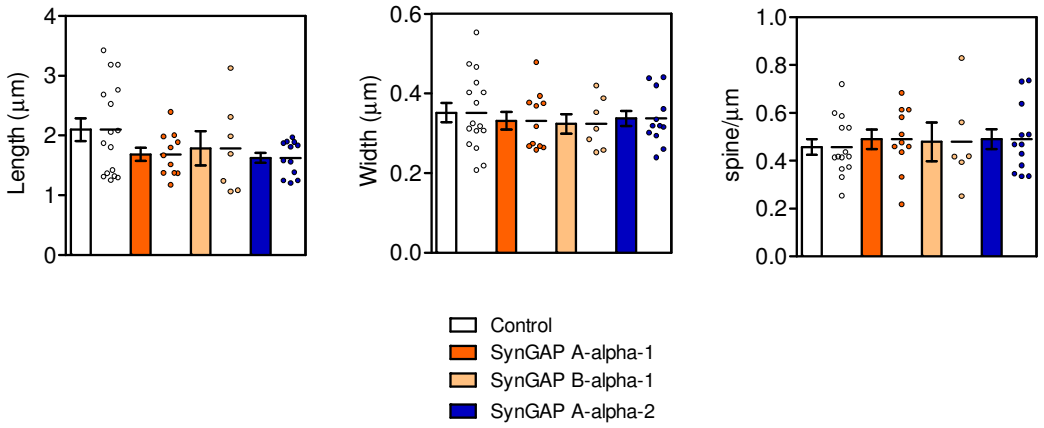

Figure 4. 8 Dendritic protrusions in wild type cortical cells transfected with various SynGAP isoforms.

Dendritic protrusions length, width and density were analysed on neurons transfected with GFP only or GFP and the SynGAP isoform indicated. The population mean is displayed (GFP only, n = 14, SynGAP A-alpha-1, n = 11, SynGAP B-alpha-1, n = 6, SynGAP A-alpha-1, n = 12) as well as each individual cell (the mean is indicated by a horizontal line). Data are from 3 separate cultures.

To examine this data in greater detail frequency histograms are shown in Figure 4. 9 illustrating the distribution of all protrusion lengths and widths in SynGAP expressing cells compared to the control distribution. Comparison of the distributions exposed statistically significant but small differences (small based on the D value which illustrates the maximum distance between cumulative histograms). There was a shift toward shorter spines with overexpression of all the isoforms (two sample Kolomogorov-Smirnov test, all $p < 0.05$). When the distributions were categorised based on the quartile values of the control population this shift was apparent in the expansion of the 'shortest protrusion' category (Figure 4. 9, bottom panel).

Moreover, expression of different isoforms had a differential effect on the distribution of protrusion widths; SynGAP A-alpha-2 (Figure 4. 9, e) had no effect but expression of SynGAPs A and B-alpha-1 both result in an increase in the kurtosis of the distribution (Figure 4. 9, a, c) (two sample Kolomogorov-Smirnov test, both $p < 0.05$, kurtosis values; control = 2.44, SynGAP A-alpha-1 = 3.55 , SynGAP B-alpha-1 = 4.04, SynGAP A-alpha-2 = 2.44). Kurtosis quantifies whether the shape of the data distribution matches the Gaussian distribution. A Gaussian distribution has a kurtosis of 0. A flatter distribution has a negative kurtosis, and a more peaked distribution has a positive kurtosis. These values indicate a shift away from the smallest and largest lengths and an expansion of the medial categories (Figure 4. 9, g).

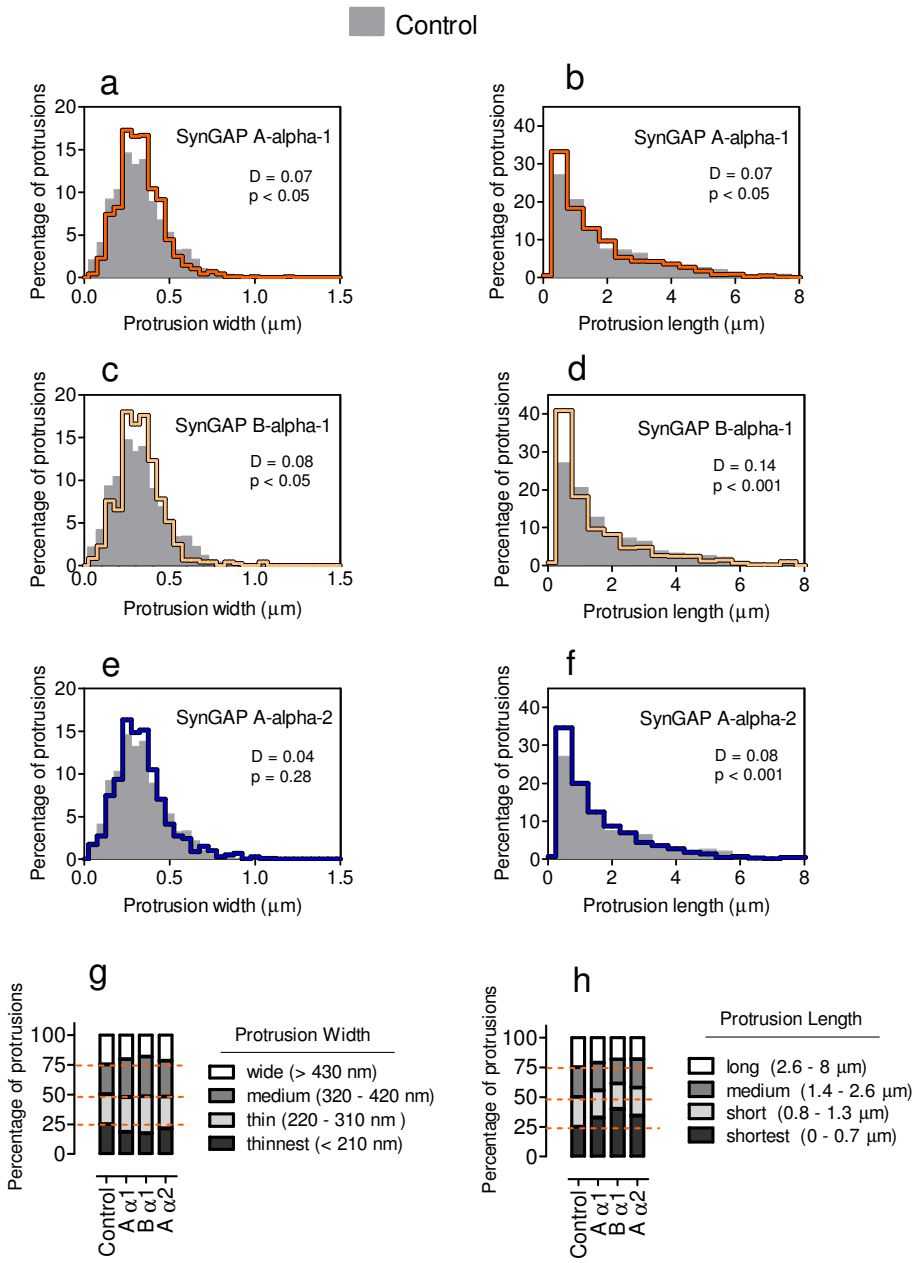

Figure 4. 9 Frequency histograms of dendritic protrusion length and width from wild type cortical neurons transfected with various SynGAP isoforms.

Frequency histograms of the lengths and widths of all dendritic protrusions of cortical neurons transfected with SynGAP isoforms (coloured line) are overlaid on the histogram for GFP only control cells (filled grey area). (control, n = 1019, SynGAP A-alpha-1, n = 875, SynGAP B-alpha-1, n = 489, SynGAP A-alpha-2, n = 990). The p and D values of two sample Kolmogorov-Smirnov tests are inlaid in the graphs. Protrusion widths and lengths are classified into four categories (legend) based on the quartiles of the control populations (illustrated by the broken orange line) (bottom panel). Data are from three separate cultures.

4.2.7 Localisation of overexpressed SynGAP isoforms

It is known that endogenous SynGAP is localised to the post synaptic compartment (Chen *et al.*, 1998; Li *et al.*, 2001; Barnett *et al.*, 2006). We wanted to know if the overexpressed SynGAP molecules were present in dendrites and able to reach the synapse, and if the isoforms were differentially localised. Due to the lack of availability of isoform specific antibodies the isoforms were expressed in *SynGAP* $^{-/-}$ neurons thereby allowing detection with one SynGAP antibody that recognises a central domain common to all isoforms. Examples of dendritic stretches overexpressing SynGAPs A, B and C alpha-1 and alpha-2 are shown in Figure 4. 10. The dendritic localisation of the all isoforms is clearly not identical. It appears that both SynGAP A isoforms (alpha-1 and alpha-2) (Figure 4. 10, a-d) had strong punctate localisation with minimal diffuse signal in the dendritic shaft, this distribution was similar to that of SynGAP B-alpha-1 (Figure 4. 10, e,f). The puncta were localised both in spines and on the dendritic shaft. While puncta were distinguishable in dendrites expressing SynGAP C-alpha-1 there was much more uniform staining along the dendritic shaft and in protrusions (Figure 4. 10, I, j). The almost uniform stain observed upon expression of SynGAPs B and C-alpha-2 was very similar to that of the GFP expression (Figure 4. 10, g, h, k, l).

4.2.8 Expression levels of SynGAP isforms

Overexpressed proteins can mislocalise due to saturation of trafficking mechanisms or binding partners. The same quantities of SynGAP DNA are transfected for each isoform but it is not necessarily the case that all SynGAP isoforms will be expressed equally. Although all isoforms are under a very strong promoter (CMV) it is still possible that their expression level and/or turnover may be differentially regulated. Differential expression levels could be an explanation for differential function or localisation. Overexpressed SynGAP was undetectable by western blotting of lysates of transfected *SynGAP* $^{-/-}$ neurons, presumably due to the extremely low transfection rate. Therefore I quantified the protein expression level of overexpressed SynGAP isoforms by semi-quantitative fluorescence microscopy (Figure 4. 11). The use of one antibody facilitated this approach as the confounding effect of different binding affinities should be minimal. The expression level of SynGAP B-alpha-1 was higher than that of all other isoforms. This is the case for

the expression level relative to eGFP (one way ANOVA, $p < 0.01$, see figure legend for pairwise t-test values) and for absolute fluorescence values (data not shown).

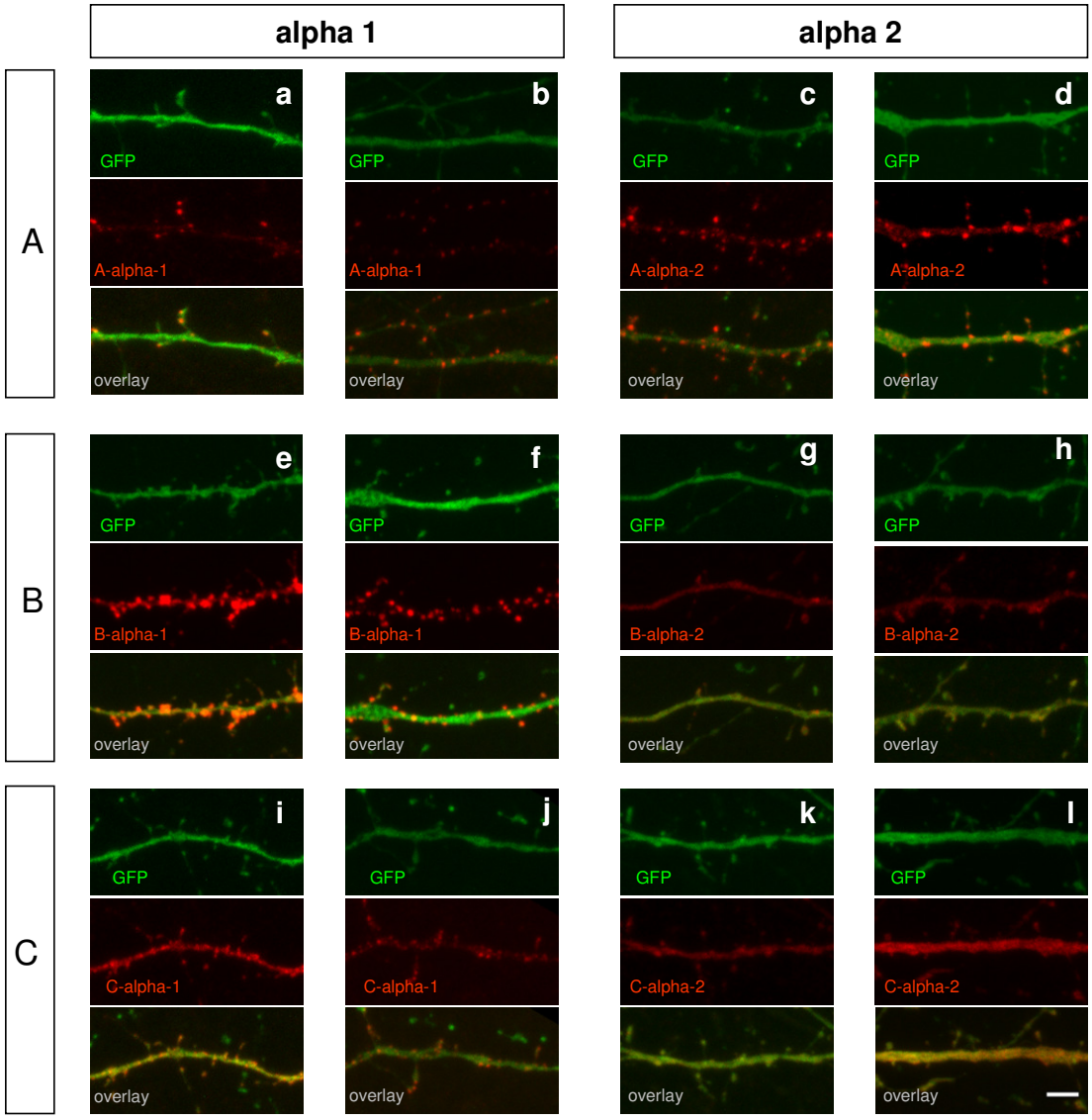

Figure 4. 10 Localisation of various SynGAP isoforms overexpressed in SynGAP $^{-/-}$ neurons

SynGAP $^{-/-}$ neurons transfected with various SynGAP isoforms were probed with an antibody against all SynGAP isoforms. Examples of dendritic sections from two different neurons are shown for each isoform. The GFP filled segment (green) and the antibody probed segment (red) are shown above the overlaid images. These images were acquired by confocal microscopy but are not Nyquist sampled or deconvolved. Scale bar is 2 µm.

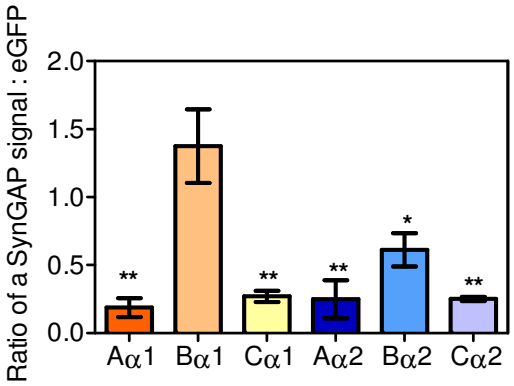

Figure 4. 11 Quantification of the protein expression levels of various SynGAP isoforms expressed in *SynGAP* $^{-/-}$ neurons.

Dendritic protein expression levels of various SynGAP isoforms were quantified by semi-quantitative confocal microscopy. SynGAP isoforms were expressed in *SynGAP* $^{-/-}$ neurons and detected by immunocytochemistry with an antibody against all SynGAP isoforms. The fluorescence signal from SynGAP is expressed as a ratio against GFP fluorescence. One way ANOVA with post-hoc Tukey t-tests indicate statistical significance only between SynGAP B-alpha-1 and the other isoforms. Asterisks above the bars signify statistical significance between the isoform indicated and SynGAP B-alpha-1 (one way ANOVA, $p = 0.02$, pairwise post-hoc Tukey t-tests, $p < 0.05$*, $p < 0.01$**, $p < 0.005$***). Data are from four neurons per isoform from two cultures.

4.3 Discussion

The aim of this chapter was to examine the role of SynGAP in dendritic protrusion development by two methods, removal of all SynGAPs and the overexpression of specific isoforms of SynGAP. The main result of this chapter is the inability to repeat the previously published effect of the ablation of SynGAP expression (Vazquez et al., 2004). Namely, I failed to reproduce the results of enlarged, prematurely developed dendritic spines on pyramidal neurons in *SynGAP* $^{-/-}$ cultures. Despite examining dendritic protrusions at different DIV and in cultures derived from regions with the highest expression level of SynGAP, the hippocampus and cortex, the phenotype was not observed (Kim *et al.*, 1998; Barnett *et al.*, 2006) (Figure 4. 5 and Figure 4. 4). Manipulation of the protocol to closely adhere to the experimental procedure used in the previous publication (removal of FBS) did not alter this finding (Figure 4. 6). However, subtle and varied changes were observed in the distributions of spine morphology among tissue types and ages, indicating that SynGAP's regulatory role may be more nuanced than previously thought.

Is the culture system behaving as expected?

Before discussing the particulars of this data regarding SynGAP the first issue to be addressed is whether the experimental system is behaving as expected. Generally the morphology of the neurons grown were similar to those described by many other groups (Kriegstein & Dichter, 1983; Ishikawa *et al.*, 2003; Vazquez *et al.*, 2004). Neurons which exhibited signs of stress, specifically dendritic blebbing, were excluded from the analysis. Mirroring the *in vivo* development of filopodia and spines the first protrusions of cultured neurons begin to appear around DIV 7 or 8. The densities of protrusion found here are very much in agreement with other preparations. Although protrusion density is generally found to be much lower in culture (slice and dissociated) than in the brain there is remarkable consistency between culture preparations. To illustrate; Pak et al (2001) and Ishikawa et al. (2006) find a density of 0.5 spines/µm in dissociated rat hippocampal neurons cultured with serum and without serum reµspectively. Collin et al. (1997) describe rat hippocampal slice cultures with a density of 0.6 spine/µm. Another culture method, the Banker method, where neurons grow in the presence of, but not in

contact with, a layer of glial feeder cells, again yields a density of 0.5 spine/ µm for hippocampal neurons (Boyer et al., 1998). Other groups find lower spine densities, even in apparently very similar culture conditions; Papa et al. (1995) describe protrusion densities of 0.2 spines/µm in hippocampal culture with serum and Vazquez et al. (2004) show this same density but in cultures without serum. All the protrusion densities described in this thesis were within this range, 0.2 – 0.6 spines/ µm. Protrusion density on cultured cortical neurons also falls within a similar range within this time window (0.2 – 0.8 spines/µm), and again encompasses the data reported here (Hayashi & Shirao, 1999; Penzes *et al.*, 2003).

It is more difficult to determine if protrusion morphology is found to be consistent between labs and preparations as there is often disparity in the method of analysis. The dimensions of spines are often not measured but instead assigned to the classical mushroom, thin, stubby and filopodia categories. The criteria for classification can vary between investigating groups and even between experimenters if it is done manually or semi-manually. Clearly a classification method obscures what is in reality a continuum of spine variety into artificially discrete groupings; at what arbitrary length does a thin spine become a filopodium? This system is convenient and useful in certain cases, it is probably most suited to older cultures and brains where a greater proportion of protrusions are likely to fit into these categories. The relatively immature cultures examined here would be grossly misrepresented by the classification of their protrusions.

Divergence in methodology remains even when dendritic spine head is measured; for example, the finding of enlarged spine heads in *SynGAP* $^{-/-}$ neurons was established by Vazquez et al. by measuring the width of the bounding rectangle, a method which likely underestimates differences as bends in filopodia increase their recorded width. Often protrusion measurements are given in terms of volume or surface area (Harris & Kater, 1994; Xie *et al.*, 2007). Direct measurement of the widest point of a protrusion head taken from a z projection of a stack of confocal images, the method used in this thesis, is also common. Despite differences in method of measurement my data fits within the range of 0.5 – 1.5 µm which is often reported for the mean spine head widths of cultured neurons (Pak *et al.*, 2001; Ishikawa *et al.*, 2003). Additionally the distribution of protrusion lengths that I see is

remarkably similar to that previously described, in slice and dissociated culture, at the same approximate age (Dailey & Smith, 1996; Boyer *et al.*, 1998)

Insights into protrusion development from control cells

Although secondary to the examination of SynGAP loss on protrusion development the data presented in this chapter give insight into the programme of protrusion developmental in hippocampal and cortical cultures, as well as the effect of the presence of FBS.

Compared to hippocampal neurons the protrusions of cortical cells were very sparse at DIV 10 but treble in density by DIV14. While the density of hippocampal cells stayed constant over this time period the width of the protrusion heads did increase (Figure 4. 4 and Figure 4. 5). What is perhaps most surprising was the similarity between neurons cultured with and without FBS (Figure 4. 6 and Figure 4. 7). The only difference being a decrease in protrusion length in the absence of FBS. (Figure 4. 6, a) Given the documented importance of glia in synapse and spine development (discussed later), in addition to direct trophic effects of the serum itself, I would have expected a greater effect. The decrease in protrusion length could be attributed to a loss of trophic factor or a shift away from immaturity indicated by the longest, filopodia like spines.

Subtle changes in the SynGAP $^{-/-}$ distributions of protrusion length and width

It is abundantly clear that a phenotype of greatly exaggerated spine development was not present in these experiments but I did find subtle differences between the wild type and *SynGAP* $^{-/-}$ distributions of protrusion width and length in certain circumstances. In cortical neurons the distribution of protrusion widths was shifted slightly toward thinner spines, a change opposite to that which would be expected given previous work (Figure 4. 4, e, f). Surprisingly the distributions of protrusions lengths are shifted slightly toward shorter protrusions in both hippocampal and cortical neurons (Figure 4. 4, Figure 4. 5, Figure 4. 6, all b, c).

Protrusion length is not such a widely examined metric in the study of spine development, the spine head width is a more reliable measure of spine stability and

maturity. Long protrusions can often be classified as filopodia, which normally do not bear mature synapses, and so can be interpreted as an indicator of immaturity. These early protrusions, characterised by shorter lifetimes and high motility, are thought to transition to mature spines (Dailey & Smith, 1996; Lendvai *et al.*, 2000; Portera-Cailliau *et al.*, 2003). Therefore the shift away from longer protrusions in *SynGAP* $^{-/-}$ neurons could be interpreted as premature maturation, which is consistent with previous work. I have observed 'long' protrusions, up to ~ 4 µm, supporting mature appearing mushroom type heads of ~1 µm in width (eg Figure 4. 2, c) so this interpretation should be made with caution. An additional confound to this interpretation is the finding that in adult hippocampi of *SynGAP* $^{+/-}$ mice spines appear to be elongated, as well as increased in head volume (Carlisle et al., 2008).

The influence of serum on neuronal cultures

The work described above (Figure 4. 4 and Figure 4. 5) was performed on cultures maintained in the presence of FBS and, as mentioned, experiments showing the exaggerated spine development in cultured *SynGAP* $^{-/-}$ neurons were grown in the absence of FBS. Historically serum has been essential for the maintenance of healthy neuronal cultures as it provides a raft of identified and unidentified growth promoting factors (Sasaki et al., 1998). However serum is chemically undefined and varies from batch to batch so introduces several variables that should otherwise be tightly controlled. In recent years much effort has gone into the development of serum free tissue culture systems. A strong impetus for this change is concern regarding safety and contamination when the end product is used in human therapeutics. Serum free medium also provide advantages in the research setting as it provides a more defined, controlled cell culture environment. Serum free neuronal culture is made possible by commercially available supplements (eg. B27) that support long term neuronal survival, but crucially, do not allow glial proliferation. Therefore there is a key difference between neurons cultured in the presence and absence of FBS, namely, the levels of glial cells. When culturing with FBS glial proliferation is terminated after four days (by the addition of a cell cycle inhibitor, cytosine β-D-arabinofuranoside (AraC)) by which time a confluent base layer of glial cells has formed. In the absence of FBS, some glial cells are present but they do not proliferate. We should consider then what effect glial cells might have on synapses and spines.

The influence of glia on synapses and spines

Far from being passive support cells which 'glue' the brain together it has emerged that glia play a major part in regulating the neuronal environment and are crucial for processes such as synaptic plasticity and synaptogenesis (reviewed by (Allen & Barres, 2005). Astrocytes (a class of glial cell) can respond to neurotransmitters and release neuroactive molecules which control synapse formation (Cornell-Bell *et al.*, 1990; Ullian *et al.*, 2004; Christopherson *et al.*, 2005), regulate presynaptic function (Mauch et al., 2001) and modulate the response of the postsynaptic neuron to neurotransmitters (Stellwagen & Malenka, 2006). The notion of the tripartite synapse, composed of presynaptic and postsynaptic neuronal compartments ensheathed by a responsive and active astrocytic projection illustrates the intimate nature of glial involvement in synaptic function (Perea et al., 2009).

It would not be surprising then if the presence or absence of glia could have dramatic effects on protrusion development. Astrocytic processes can have a direct role in the shaping of dendritic spine morphology via ephrin/eph signalling and stable astrocytic contacts are found at stable spines (Murai *et al.*, 2003; Stellwagen & Malenka, 2006). Astrocytically released molecules (TNFalpha and ATP) have been shown to have a direct impact on synaptic AMPA receptor content (Beattie et al., 2002; Gordon et al., 2005). This release seems to be important for the maintenance of synapses and synaptic scaling, and if reduced one could envisage how compensatory regulatory mechanisms might involve SynGAP, leading to dysregulation in the knockout. To look at it another way, with a high complement of glial cells (+FBS) the regulation of synaptic AMPA receptor content or spine shape might be more robust than in the case of a low complement of glial cells (-FBS).

Interestingly I did find a shift towards wider spines in the distribution of *SynGAP* $^{-/-}$ protrusions, agreeing with the results of Vazquez et al., when the neurons are cultured without FBS (Figure 4. 7), indicating that different pathways to spine development might be activated in the presence and absence of serum. However there were no differences in mean protrusion width, length or density (Figure 4. 6, a, d, g).

What do changes in distribution mean?

Despite some indications of a shift away from immaturity in the form of reduced spine lengths the expected phenotype of greatly enlarged spine heads was not found here. When cultured without FBS protrusion widths in *SynGAP* $^{-/-}$ neurons are slightly increased but magnitude is not as great as that described by Vazquez et al.. Indeed, the opposite result, an indication of thinner protrusion heads, is found in *SynGAP* $^{-/-}$ neurons from the cortex. All these differences are statistically significant based on the comparison of the distributions of the entire population of measurements. Do these differences have any functional significance?

It is difficult to know how to interpret such changes. It is possible that the trend toward thinner spines in cortical neurons wouldn't be recapitulated if the experiment was performed in the absence of FBS, and so this result is not directly comparable the finding of a shift toward increased width in hippocampal cell (+FBS). Nevertheless it is perhaps simplistic to expect that a large outright change in spines would occur, even if it has been shown before, given our hypothesis of SynGAP as a multifunctional molecule which regulates opposing pathways. It is very possible that all the changes in distribution observed are real and indicative of elements of SynGAP function that are exposed given the precise set of experimental circumstances. We do not know which isoforms are expressed where. It is unlikely the intracellular milieu of cortical cells is identical to that of hippocampal cells and therefore unlikely that they will be affected in exactly the same way by the removal of all the SynGAP isoforms. Therefore, if we truly accept our hypothesis of SynGAP as a bidirectional switch then the lack of a clear change in either direction becomes a likely outcome. The magnitude of these changes may be too small to be seen in the mean given the number of neurons examined here.

Increased protrusion density in SynGAP $^{-/-}$ cortical neurons at DIV 10

I found an increase in protrusion density in *SynGAP* $^{-/-}$ cortical neurons at DIV 10, but not at DIV 14 (Figure 4. 4) and not in any hippocampal neurons (Figure 4. 5). Potential reasons for discrepancies between my findings and previously published work will be addressed below and the variety in tissue type and age have been mentioned above. Here I will consider two potential mechanisms by which an

increase in protrusion density might occur namely exaggerated stabilisation or impeded stabilisation.

Deletion of SynGAP could lead to an exaggeration of stabilisation whereby more protrusions are stabilised than normal. These 'stabilisation' mechanisms could be further sub-divided into two categories, depending on the mechanism of spine stabilisation. First, structural stabilisation could be the primary event; changes in the actin dynamics lead to the creation of a larger spine, perhaps with more scaffolding molecules, which can accommodate a larger synapse. Second, that the insertion of the functional moieties, in this case AMPA receptors, into the membrane with the concomitant insertion of additional membrane is the primary mechanism of stabilisation. It is most likely that these two mechanisms, both affected by SynGAP, are complementarily and co-ordinately regulated (Rumbaugh *et al.*, 2006; Carlisle *et al.*, 2008). Where an increase in spine density occurs with an increase in spine head size (cultured *SynGAP* $^{-/-}$ and *in vivo SynGAP* $^{+/-}$ neurons) the proposed mechanism is of increased stabilisation, both via AMPA receptor insertion and altered actin dynamics.

Alternatively, if ablation of SynGAP prevents protrusions from being stabilised then perhaps the neuron will put forth additional protrusions in an attempt to compensate for the lack of input; this could give rise to an increase in density of immature, possibly filopodial processes, similar to the phenotype observed in Fragile X syndrome (Cruz-Martin et al.). Because I saw a slight shift toward thinner spine heads this latter mechanism, lack of stabilisation, provides a more parsimonious model for the increase in protrusion density than the former.

Enhanced Ras activity can increase spine number (Goldin & Segal, 2003; Gartner *et al.*, 2005) so this premature increase in density fits with the schema of SynGAP functioning mainly as a RasGAP. Interestingly the Ras induced increase in density does not necessarily involve changes in the profile of large spines. Indeed stimulations that enhance Ras mediated MAPK activity increase the density of protrusions primarily through the addition of new filopodia, rather than the stabilisation of protrusions already present (Wu et al., 2001). Thus, the deletion of

SynGAP could remove the negative regulation of Ras leading to the addition of new thin spines

However, this effect did not penetrate all cases examined here and was not recapitulated in a particular setting in which it was observed before. An increase in spine density has been shown in DIV 14 *SynGAP* $^{-/-}$ hippocampal neurons however by DIV 21 there was no longer a difference between wild type and knock out densities (Vazquez et al., 2004). Therefore we could conclude that SynGAP RasGAP function is not entirely dominant but that it is sensitive to the precise neuronal conditions. Furthermore, SynGAP can act on both Rap1, the overexpression of which can have no effect on spines, and Rap2, which can induce a decrease in spine density (Krapivinsky *et al.*, 2004; Fu *et al.*, 2007). Interestingly both molecules decrease AMPA receptor mediated mEPSC amplitude and frequency (Zhu *et al.*, 2002; Huang *et al.*, 2004). This shows that SynGAP can regulate a pathway in which structure and function may be decorrelated, suggesting that the lack of a structural phenotype is not necessary predictive of the lack of a functional role.

Why is the morphological phenotype in this SynGAP $^{-/-}$ mouse different to the published phenotype?

We must consider what experimental factors might be causing the disparity in phenotype between the work presented here and previously published work. Despite efforts towards aligning the experimental protocols obvious differences remain in the form of the knock out mouse models.

There are three different *SynGAP* $^{-/-}$ mice models in existence. The mouse generated by (Vazquez et al., 2004) which I term the Kennedy mouse, the mouse used in this thesis (Komiyama et al., 2002) which I term the Grant mouse, and the mouse generated by (Kim et al., 2003) which I term the Huganir mouse. The names refer to the principal investigator of the labs which generated the mice.

When we speak about the differences between mouse models there are two main aspects to be considered. Firstly the genetic background strain of the mouse that carries the knock out allele, and secondly the knock out allele itself. In the case of

SynGAP both the background strain and the transgenic allele are different in all three knock out models.

Mouse genetic background

It is clear that phenotypes can differ wildly between inbred strains of mice. There are thousands of inter breed phenotypic differences categorised in the Jackson Laboratories Mouse Phenome Database (http://phenome.jax.org) ranging from disease susceptibility, aging, obesity, neurosensory disorders to behaviour and learning/memory ability. For example, BTBR T+tf/J has a severe defect in corpus collosum development and exhibits extreme behavioral phenotypes. JF1/Ms has congenital eye abnormalities and has remarkably high percent body fat; and B6.Cg-Ay/J exhibits severe obesity-related phenotypes (Grubb et al., 2009). Even substrains develop differences; a range of different fear responses are observed between the C57BL6/J and C57BL/6N substrains (Stiedl et al., 1999).

Unfortunately there is variety in the background on which *SynGAP* $^{-/-}$ alleles are maintained. The Kennedy and Huganir mice were maintained on C57Bl6 (Kim et al., 2003; Vazquez et al., 2004) but lately have been crossed with an unspecified 129 substrain or 129 sv/ev respectively due to breeding problems on the pure background (Carlisle et al., 2008; Guo et al., 2009). Original experiments on the Grant mouse were performed when it was on an F2 MF1 background and since then it has been backcrossed partially onto C57Bl6/J/ola/HSD.

It is well known that differences in background strain can alter the phenotype of a genetic manipulation (Eisener-Dorman et al., 2009). Each strain has unique background alleles that may interact with and modify the expression of a mutation or transgene, as well as the expression of proteins that can compensate for the action of the deleted gene. Many examples of background-unique modifier genes have been shown. They may influence gene expression by suppressing or enhancing it, altering DNA transcription rates or mRNA stability, and inducing epigenetic effects, such as DNA methylation. Recently Mineur et al. (2002) and Ivanco and Greenough (2002) have described opposite effects of a null mutation in the Fmr1 gene, reporting an increase in the size of the hippocampal intra- and infrapyramidal mossy

fiber terminal field when the mutation was on an FVB background, but a decrease when the mutation was on a C57BL6/J background.

The technology for generating experimental transgenic mice of one background can lead to the insertion of unpredictable amounts of DNA from an entirely different background strain. For example, the targeting constructs used for the generation of all the *SynGAP* deletions, as is standard practice, were derived from and injected into ES cells of various 129 lines (Magin et al., 1992). Despite backcrossing onto other backgrounds it is likely that some 129 genetic material remains due to close linkage with the knock out locus, and it is possible that unlinked 129 loci also exist (reviewed in (Ridgway et al., 2007). This 'flanking gene effect' has been shown to confound phenotypic analysis where a flanking gene, rather than the ablation itself, has been found to be responsible for the observed phenotypic effect (Cool et al., ; Kanagawa et al., 2000). More generally, the expression levels of genes surrounding a transgenic locus are often found to be different to those from an undisrupted chromosome. In this flanking gene model, the flanking DNA (from ES cells) contains polymorphisms that alter gene expression relative to the genetic background of the backcrossed mice (Valor & Grant, 2007).

The effect of the deletion of SynGAP therefore may be quite different depending on the true genetic background of the experimental mice.

The knock out allele

Secondly, while an absence of SynGAP protein, using western blots probed with antibodies against the central domain, has been shown in all cases it is worth discussing that the genetic manipulation differs between the three mouse models. The point of insertion of the deletion cassette into the gene may be a factor in the variability of phenotype. Of the three genetic manipulations the model used in this thesis, the Grant mouse, has the most downstream insertion point. The Grant cassette excises the C2 domain and part of the GAP domain, whereas the Huganir cassette deletes from the middle of the more upstream PH domain, and the Kennedy deletion begins two exons upstream of the PH domain (Komiyama *et al.*, 2002; Kim *et al.*, 2003; Vazquez *et al.*, 2004). The Grant mouse deletion cassette consists of a HA epitope tag followed by stop codons, an internal ribosome entry

site, the gene for beta galactosidase and a poly adenylation signal before an MC1 neo polyA cassette. Thus a stabilised bicistronic transcript consisting of the first few *SynGAP* exons followed by the lacZ coding region exists. The Kennedy and Huganir mice rely on the removal of all translation starts sites and the frameshift effect of the deletion, given expected splicing events, to result in a premature stop codon.

It is pure conjecture to suggest that these differences might affect phenotype but there are cases where the use of cryptic start sites can lead the translation of truncated proteins of unpredictable function. In addition, it is possible that as yet unidentified isoforms of SynGAP exist and are expressed, for example, in western blots of tissue from the Huganir mouse a protein smear is detected about 10kDa lower than the position SynGAP would appear. I will discuss in Chapter Five (p187) the possible expression in our mouse of a truncated N-terminal peptide with some unique amino acid sequence, described in Chapter Three (p108) as SynGAP B-shift .

Although some differences may exist the phenotypes of the three mouse models are grossly similar in terms of deficits in synaptic plasticity and they all die postnatally .

Compensation

I mentioned above that differences in background may lead to differential compensation for the absence of an important molecule. It is notable that in yeast, central metabolic pathways appear to have more alternatives than other pathways (Maltsev et al., 2005). It has been found in an analysis of transcriptional and signal transduction networks that parallel pathways connecting a regulator to a regulated molecule are not, as is commonly perceived, rare but are actually quite common (Wagner & Wright, 2007). Paralagous genetic redundancy is often cited as a mechanism to account for lack of a knockout phenotype and there are a number of genes with high homology to *SynGAP*. For example, *SynGAP* is closely related to nGAP, DAB2IP and neurofibromin (NF1) and it is possible that these molecules could compensate for the action of SynGAP. Alternatively compensation could occur at any other point in the signalling pathway.

Overexpression of SynGAP isoforms

Overexpression of a range of SynGAP isoforms saw, as in the case of the knock out, no changes in mean protrusion length, width or density (Figure 4. 8). Also like the knock out changes in the distribution of the data were observed. There was a shift toward shorter spines irrespective of which isoform was overexpressed (Figure 4. 9). A shift toward shorter spines was also found when all SynGAP isoforms were knocked out, perhaps suggesting that the fine control exerted by endogenous SynGAP is required for normal protrusion outgrowth. However the isoforms' effects on the distribution of widths were not uniform. Given previous work on the overexpression of SynGAP alpha-1 showing a reduction of synapse strength one might expect to see a decrease in spine width. However, both SynGAPs with the alpha-1 C-terminal tail caused a change in protrusion width that involved a shift away from the thinnest and widest protrusions and an expansion of 'medium' widths. (Figure 4. 9, g) One could suggest that this pattern could reflect an impairment of the SynGAP alpha-1 expressing spine to dynamically regulate its shape. Or, if the thinnest spines bear silent synapses this change could be reflected electrophysiologically by a loss of the largest synapses. By contrast, SynGAP A-alpha-2 had no effect on protrusion widths (Figure 4. 9, e, g). The lack of effect of SynGAP A-alpha-2 acts as an internal control for this experiment, indicating that the effects of SynGAP alpha-1 are due to its function rather than a non-specific effect of overexpression. Mutation of the SynGAP alpha-1 PDZ binding domain destroyed its ability to rescue the enlarged mushroom heads (Vazquez et al., 2004) and enhanced synaptic transmission (Rumbaugh et al., 2006) of the knock out phenotype. Therefore it is not surprising that SynGAP alpha-2 (which lacks the PDZ binding domain) does not affect spine shape.

Localisation of overexpressed SynGAP isoforms

Having shown that SynGAP A-alpha-2 does not effect spine shape, while SynGAP alpha-1 does have an effect, if was important to determine if overexpressed SynGAP A-alpha-2 was in fact present in spines. We know from mass spectrometry analysis that SynGAPs A, B, alpha-1 and alpha-2 are all present in the PSD (Seth Grant, personal communication). (Mass spectrometry data regarding SynGAP C is unobtainable as it, being a truncated protein, does not have any unique peptide sequences that can be identified.) Unfortunately overexpressed proteins can be mislocalised, due to their high levels of expression trafficking and scaffolding

molecules can be saturated. Therefore it is crucial to know if all the overexpressed SynGAP isoforms used in this thesis can be localised to synapses in order to interpret experiments which involve examination of synaptic function (Chapter 5). In addition, differential localisation in itself indicates different roles for different isoforms.

The dendritic expression patterns of overexpressed SynGAP provide some noteworthy and surprising findings. The fact that SynGAP A-alpha-2 appears as competent as SynGAP A-alpha-1 in achieving punctate, apparently synaptic, expression in spines and on the dendritic shaft indicates a number of things (Figure 4. 10, a, d). First, SynGAP A-alpha-2's lack of effect on protrusion width is not due its absence in spines. Second, comparison with SynGAPs B and C-alpha-2 (Figure 4. 10, g, h, k, l) , which display almost uniform distribution patterns, suggests that the 'A' unique peptide sequence may have an independent role in determining synaptic localisation. This is the first indication of a role for an alternatively spliced N-terminal portion of SynGAP. Further evidence for a role of the N terminus in determining synaptic localisation comes from a comparison between SynGAP alpha-1s with different N termini. SynGAPs A and B –alpha-1 show high degrees of punctate expression with little diffuse dendritic stain but SynGAP C-alpha-1, although displaying some degree of punctate expression, has much more uniform expression on the dendritic shaft (Figure 4. 10, I, j). These differences imply that the localisation may be a result of the combination of N and C-termini and not entirely determined by one end or the other. One can envisage how this combinatorial schema could allow for very fine control of the positioning of SynGAP and potentially the alteration of functional outcomes.

Finally, for the overexpression experiment outlined in this chapter and those described in Chapter 5, it is essential to rule out the possibility that any differential effects of the expression of SynGAP isoforms are not due solely to differences in their relative protein expression levels. Quantification of the dendritic expression levels of SynGAP isoforms by confocal microscopy indicates that one isoform, SynGAP B-alpha-1 is expressed to a greater degree than all the other isoforms (Figure 4. 11). This should be kept in mind when interpreting experiments involving its expression. SynGAPs A and B-alpha-1 both had similar effects on spine width, despite different expression levels, which implies that the alpha-1 effect is a specific

one. SynGAP A-alpha-2 is expressed at a comparable level to SynGAP A-alpha-1, again indicating that the effect of SynGAP alpha-1 is specific.

To summarise, the previously published phenotype of enlarged dendritic spines in SynGAP $^{-/-}$ cultured neurons is not recapitulated here; some differences are apparent but they are not consistent amoung tissue types, developmental stages etc. The meaning of these changes, as well as possible causes for the lack of clear phenotype are discussed. Overexpression of different SynGAP isoforms have no effect on mean dendritic spine morphology or density despite displaying different patterns of localisation.

5 Chapter Five: Electrophysiology

5.1 Introduction

This chapter is concerned with the functional implications of altering SynGAP expression. As SynGAP is thought to regulate AMPA receptor trafficking I have examined AMPA receptor mediated currents in a range different manipulations of SynGAP expression. Namely, I have studied AMPA receptor function in *SynGAP* $^{-/-}$ neurons, wild type neurons overexpressing various SynGAP isoforms, and *SynGAP* $^{-/-}$ neurons transfected with various SynGAP isoforms. The chapter is divided into three parts to reflect these three manipulations.

The central metric used is the examination of AMPA receptor mediated miniature post synaptic currents, known as mEPSCs or colloquially 'minis'. mEPSCs are currents recorded from a neuron when all action potentials are blocked in the neural network. The lack of activity in the network ensures that all the currents recorded from the neuron are caused by spontaneous quantal neurotransmitter release from presynaptic neurons. Synaptic vesicles are released from presynaptic termini in an infrequent and stochastic fashion so each postsynaptic current is the result of one packet of neurotransmitter binding to the post synaptic receptors. mEPSCs therefore give us information about the AMPA receptor content specifically at the synapse.

Simplistically, the amplitude of an AMPA mEPSC is determined by the number of AMPA receptors at a given synapse. This truism holds up if the neurotransmitter content of synaptic vesicles is truly quantal. The concept of quantal vesicular release has been the subject of great debate in recent years with studies indicating that glutamate concentration within a synaptic vesicle may be a source of quantal size variation (Bekkers & Stevens, 1995; McAllister & Stevens, 2000; Wu *et al.*, 2007). The strength of quantal transmission is consequently determined both presynaptically, through the magnitude of neurotransmitter release, and

postsynaptically, by the number and properties of the receptors available for activation.

When single synapses are studied it is found that the median recorded size of mEPSCs is highly correlated with the current evoked by a saturating dose of glutamate (Liu *et al.*, 1999). This evidence suggests that, while we may not be able to calculate the absolute number of receptors at a synapse from mEPSC data, mEPSCs are still a useful too for comparing synaptic strength between treatments. This is especially true given the transfection conditions used in this thesis which ensure that only the post synaptic cell has been affected by overexpression.

Classically, it is considered that changes in the frequency of mPSCs reflect a modification in the probability of the presynaptic transmitter release ((Del Castillo & Katz, 1954; Malgaroli & Tsien, 1992). However, mEPSC frequency can also be determined by the number of synapses present and is influenced by the strength of synapses, which determines whether or not an mEPSC will be above the detection threshold. It is likely that the synaptic currents generated at a significant proportion of synapses may not be detectable due to the low AMPA receptor content and that these synapses may be exposed electrophysiologically when additional AMPA receptors are added (Nusser *et al.*, 1998).

Previous work on SynGAP has demonstrated that in its absence mEPSCs are increased in frequency. An increase in amplitude has been shown by one group, but another group sees no change (Vazquez *et al.*, 2004; Rumbaugh *et al.*, 2006). As one would expect, overexpression of SynGAP alpha-1 isoforms result in a decrease in mEPSC amplitude and frequency. When the PDZ binding domain of SynGAP alpha- 1 is disrupted the decrease in mEPSC frequency and amplitude are no longer apparent (Krapivinsky *et al.*, 2004; Rumbaugh *et al.*, 2006). There has been no work published on the function of other C-termini and the N-termini are never mentioned. This chapter addresses this gap in the literature.

5.2 Results

Part One Electrophysiological properties of wild type and *SynGAP* $^{-/-}$ neurons.

Part Two Electrophysiological properties of wild type neurons overexpressing various SynGAP isoforms.

Part Three Electrophysiological properties of *SynGAP* $^{-/-}$ neurons overexpressing various SynGAP isoforms.

5.2.1 Overview of Results

Part One: Electrophysiological properties of wild type and *SynGAP* $^{-/-}$ neurons.
Miniature excitatory postsynaptic currents (mEPSC) are revealed in whole cell patch clamp recordings of cultured neurons in the presence of tetrodotoxin (TTX).

There is no difference in mEPSC amplitude or frequency between wild type and *SynGAP* $^{-/-}$ neurons in high density cortical, hippocampal and low density hippocampal cells.

Whole cell NMDA and AMPA currents are unchanged in *SynGAP* $^{-/-}$ hippocampal cells but because capacitance is higher in the *SynGAP* $^{-/-}$ neurons the NMDA current density is lower. The AMPA/NMDA current density ratio remains unchanged.

Despite the difference in capacitance measurement of cell soma size in fixed cultures does not indicate a difference in soma size between wild type and *SynGAP* $^{-/-}$ neurons.

Part Two: Electrophysiological properties of wild type neurons overexpressing various SynGAP isoforms.

A large proportion of wild type neurons overexpressing SynGAP isoforms with the alpha-1 C-terminus were found to entirely lack mEPSCs. The extent of silencing was determined by which N-terminus was present. The percentage of neurons categorised as silent is as follows: GFP (10.5%), SynGAP A-alpha-1 (72.6%), SynGAP B-alpha-1 (45%) and SynGAP C-alpha-1 (44.7%).

Overexpression of SynGAP isoforms with the alpha-2 C-terminus did not cause silencing of mEPSCs. The percentage of neurons categorised as silent is as follows: GFP (10.5%), SynGAP A-alpha-2 (14.3%), SynGAP B-alpha-2 (0%) and SynGAP C-alpha-1 (5%).

In the SynGAP expressing neurons that did have mEPSCs there was no difference in their amplitude compared GFP expressing control cells.
In the minority of SynGAP A-alpha-1 cells that did have mEPSCs the frequency was lower than control cells.

When all cells (silent and non-silent) were included in analysis the mEPSC amplitude and frequency of neurons overexpressing SynGAP alpha-1 isoforms was decreased. The expression of SynGAP B-alpha-2 and C-alpha-2 caused an increase in mEPSC amplitude and frequency. SynGAP A-alpha-2 had no effect on mEPSC amplitude or frequency.

Silent cells expressing SynGAP alpha-1 did not have reduced total cell surface expression of AMPA receptors. They have synaptic AMPA receptors and are innervated by functional presynaptic termini as they respond normally to action potential mediated input.

Part Three: Electrophysiological properties of *SynGAP* $^{-/-}$ neurons overexpressing various SynGAP isoforms.

As was the case with wild type neurons a large proportion of *SynGAP* $^{-/-}$ neurons overexpressing SynGAP isoforms with the alpha-1 C-terminus were found to lack mEPSCs. The extent of silencing was determined by which N-terminus was present. The percentage of neurons categorised as silent is as follows: GFP (20%), SynGAP A-alpha-1 (80%), SynGAP B-alpha-1 (100%) and SynGAP C-alpha-1 (55%).

Again, similar to the case in wild type neurons, overexpression of SynGAP A-alpha-2 in *SynGAP* $^{-/-}$ cells did not cause silencing of mEPSCs (0% silent).

In *SynGAP* $^{-/-}$ cells there was no difference in mEPSC amplitude or, in contrast to the scenario in wild type neurons, frequency between control cells and non-silent SynGAP expressing cells.

Like the case in wild type neruons, when all cells (silent and non-silent) are included in the analysis mEPSC frequency and amplitude of SynGAP A-alpha-1 expressing

neurons is decreased, but that of SynGAP A-alpha-2 expressing neurons is unchanged.

Expression of SynGAP A-alpha-1 in *SynGAP* $^{-/-}$ cells did not rescue the increase in capacitance (or decrease in NMDA receptor current density) seen in control knock out neurons.

5.2.2 Part One: Electrophysiological properties of wild type and *SynGAP* $^{-/-}$ neurons.

5.2.3 Spontaneous miniature excitatory postsynaptic currents (mEPSCs)

Whole cell patch clamp recordings were performed on cultured neurons between DIV 9 and 14. Spontaneous currents are evident when a neuron is voltage clamped at -70mV (Figure 5. 1). The currents can be divided into two types; large currents, which are often organised into bursts, and small currents which are evident between the bursts. Application of tetrodotoxin (TTX, 1 µM) and picrotoxin (PTX, 50 µM) abolishes the large amplitude events but leaves small amplitude events known as miniature excitatory postsynaptic currents (mEPSCs). The AMPA receptor antagonist CNQX blocks all mEPSCs. Some mEPSCs of a representative neuron are shown in (Figure 5. 1). Examining mEPSCs on the most expanded time base reveals their characteristic fast risetime (~0.5 - 1 ms) and decay time constant (~ 4 - 8 ms). Events with amplitudes larger than 5 pA were analysed by measuring their peak amplitude, 10-90% risetime, decay time constant and frequency, as described in Methods (p82) 300 events were analysed per neuron.

Data produced from the analysis of the representative neuron is shown in Figure 5. 2. The mean and median mEPSC was created by aligning all the analysed events at the half maximal time point of the rising phases. As is well established in the field frequency histograms of all the analysed parameters reveal positively skewed distributions (Bekkers *et al.*, 1990; McBain & Dingledine, 1992; Wyllie *et al.*, 1994). These non Gaussian distributions are maintained when a large population of mEPSCs is examined (5783 events from 19 cells in the case of Figure 5. 3, a-d).

A concern when recording in the whole cell configuration is the effectiveness of the voltage clamp over distance, the space clamp. Miniature synaptic events that are located at great distances from the cell soma can be filtered and will appear to have longer rise times, smaller amplitudes, and longer decays (Rall, 1969). There is no

correlation between mEPSC amplitude and risetime, or amplitude and decay time constant in the population examined here (Figure 5. 3, e,f). This data suggests that the large variation in mEPSC amplitudes is not due to differential filtering of events arising at different locations on the dendritic tree.

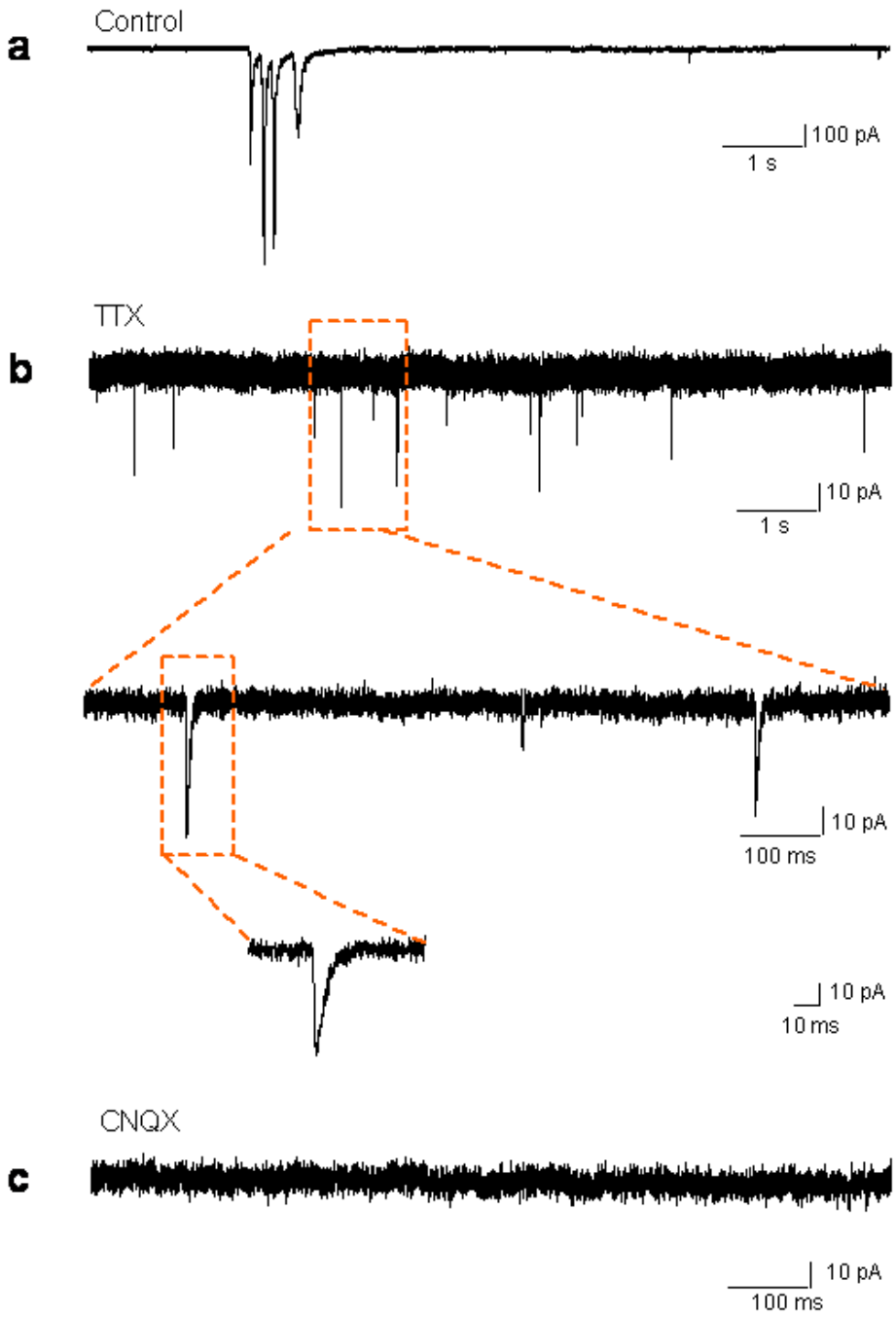

Figure 5. 1 mEPSCs are revealed in the presence of TTX and abolished by CNQX

An example voltage clamp recording of a DIV 10 cortical neuron held at the transmembrane potential of -70 mV. Large spontaneous inward currents are apparent in the absence of any drugs (a). These large currents are eliminated upon addition of 1µM TTX and reveal small amplitude spontaneous inward currents known as mEPSCs (b, mEPSCs shown with expanding time bases). mEPSCs are abolished by the addition of the AMPA receptor antagonist CNQX (5 µM) (c).

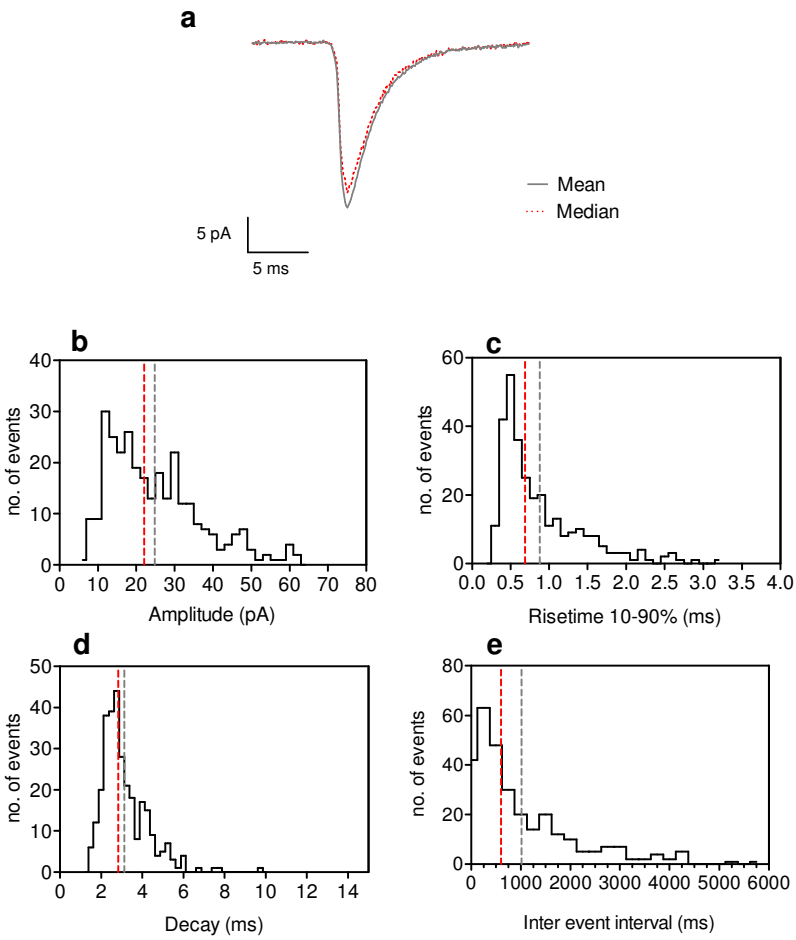

Figure 5. 2 mEPSC characteristics of an individual representative neuron.

306 mEPSC events were recorded and analysed from one hippocampal neuron at DIV 10. (a) The mean and median mEPSC waveforms are calculated by horizontally aligning all mEPSCs at their half maximal risetime. Frequency distributions for mEPSC amplitude (b, mean = 24.89 pA, median = 22.12 pA), 10 – 90 % risetime (c, mean = 0.87 ms, median = 0.69 ms), decay time constant (d, mean = 3.14 ms, median = 2.83 ms) and inter event interval (e, mean = 1014 ms, median = 605 ms) are shown with mean (grey solid line) and median (red broken line) values highlighted. The mEPSC frequency of this cell (the reciprocal of the mean inter event interval) is 0.98 Hz.

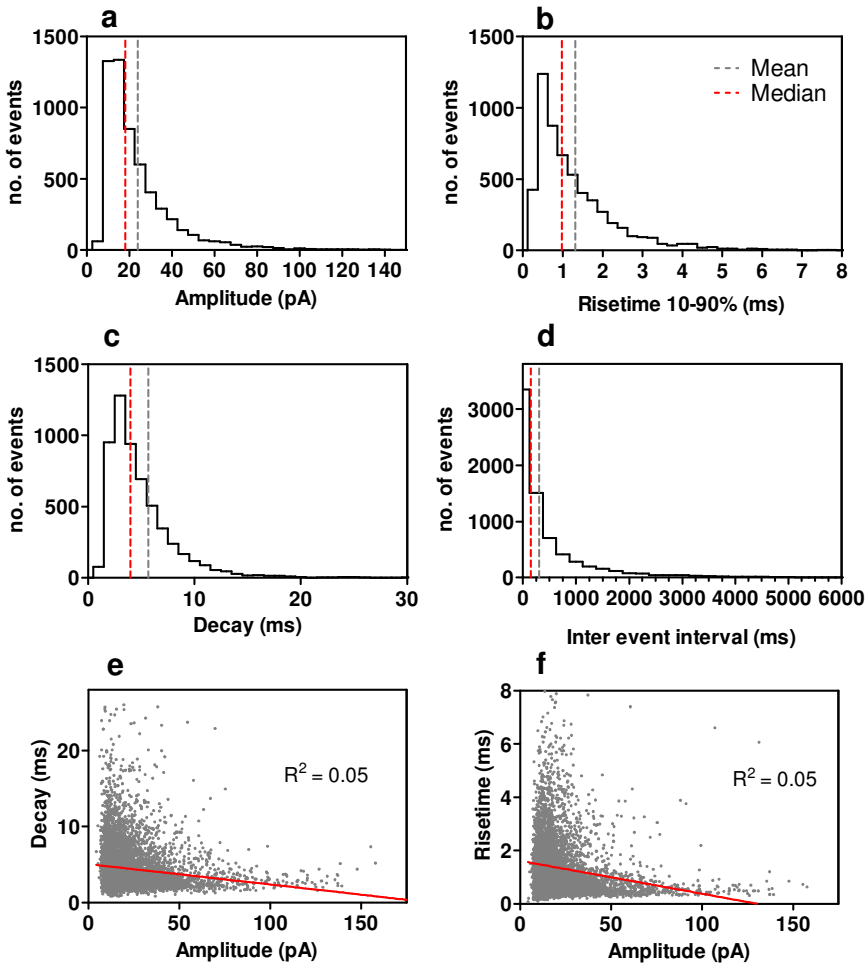

Figure 5. 3 mEPSC characteristics of a population of neurons.

At least 300 events per cell were recorded and analysed from 19 hippocampal cells. All 5783 events were pooled to create frequency distributions for mEPSC amplitude (a, mean = 23.91 pA, median = 18.04 pA), 10 – 90 % risetime (c, mean = 1.31 ms, median = 0.98 ms), decay time constant (c, mean = 5.69 ms, median = 3.99 ms) and inter event interval (d, mean = 305 ms, median = 150 ms). The mean (grey solid line) and median (red broken line) values are highlighted. There is no significant correlation between decay time constant and amplitude (e), or between the risetime and amplitude (f) in this population of mEPSCs (R^2 = 0.05 in both cases, Pearson's correlation co-efficient, shown with a linear regression fit). Data are from 3 separate cultures.

5.2.4 Mean mEPSCs in *SynGAP* $^{-/-}$ neurons

Wild type and *SynGAP* $^{-/-}$ neurons cultured from the cortex and hippocampus were examined at DIV 9 to DIV 14 (Figure 5. 4) Cells were plated at a reasonably high plating density (1500 neurons / mm^2). The mean mEPSC amplitudes of each cell were averaged to yield a population mean.

Previous work has shown an increase in mEPSC amplitude and frequency in *SynGAP* $^{-/-}$ cultures (Vazquez *et al.*, 2004; Rumbaugh *et al.*, 2006). However contrary to expectation mean mEPSC amplitudes and frequencies are unchanged in *SynGAP* $^{-/-}$ neurons under the various experimental conditions described below. Mean mEPSC amplitudes and frequencies are unchanged in *SynGAP* $^{-/-}$ cortical cells at different DIV (two way ANOVA,Figure 5. 4). Mean mEPSC amplitudes and frequencies are unchanged between wild type and *SynGAP* $^{-/-}$ hippocampal cells at different DIV (two way ANOVA, Figure 5. 5). However *SynGAP* $^{-/-}$ mEPSC frequency (+/- SEM) is increased from 4.74 +/- 0.86 Hz at DIV 9-10 to 12.53 +/- 4.16 Hz at DIV 13-14, (two way ANOVA, $p<0.05$, post hoc Bonferroni test, $p<0.05$) whereas wild type mEPSC frequency is not (Figure 5. 5,c,d)

When Vazquez et al. showed an increase in *SynGAP* $^{-/-}$ mEPSC amplitude and frequency they used neurons cultured at the sparser plating density of 200 cells/mm^2. In order to assess if plating density had an effect on the presence of the mEPSC phenotype hippocampal cells were cultured at the reduced plating density of 200 neurons/mm^2. Mean mEPSC amplitudes and frequencies are unchanged in *SynGAP* $^{-/-}$ sparsely cultured hippocampal cells at different DIV (two way ANOVA,Figure 5. 5)

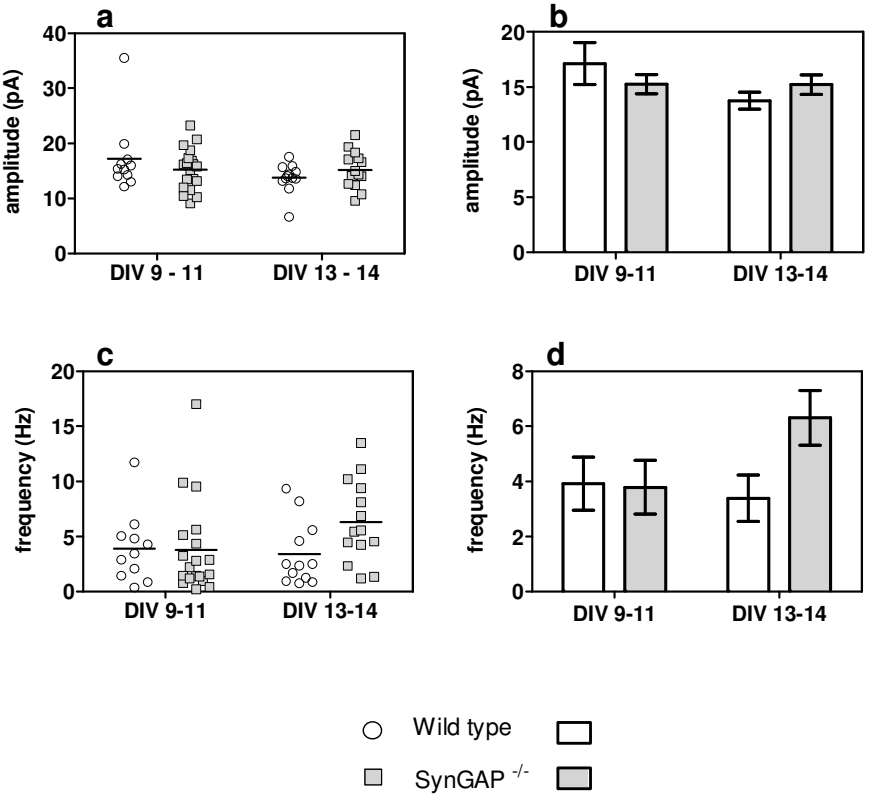

Figure 5. 4 mEPSC amplitude and frequency in wild type and *SynGAP* $^{-/-}$ cortical cells.

Mean mEPSC amplitudes and frequencies from wild type and *SynGAP* $^{-/-}$ cultured cortical cells at DIV 9-11 and DIV 13-14, (b, d, DIV 9 - 11; WT n = 11, *SynGAP* $^{-/-}$ n = 19, DIV 13 - 14; WT n = 12, *SynGAP* $^{-/-}$ = 13), and each individual cell at each time point from wild type and *SynGAP* $^{-/-}$ cells (a,c, the mean is indicated by a horizontal line). Data are from three separate cultures. Error bars represent SEM.

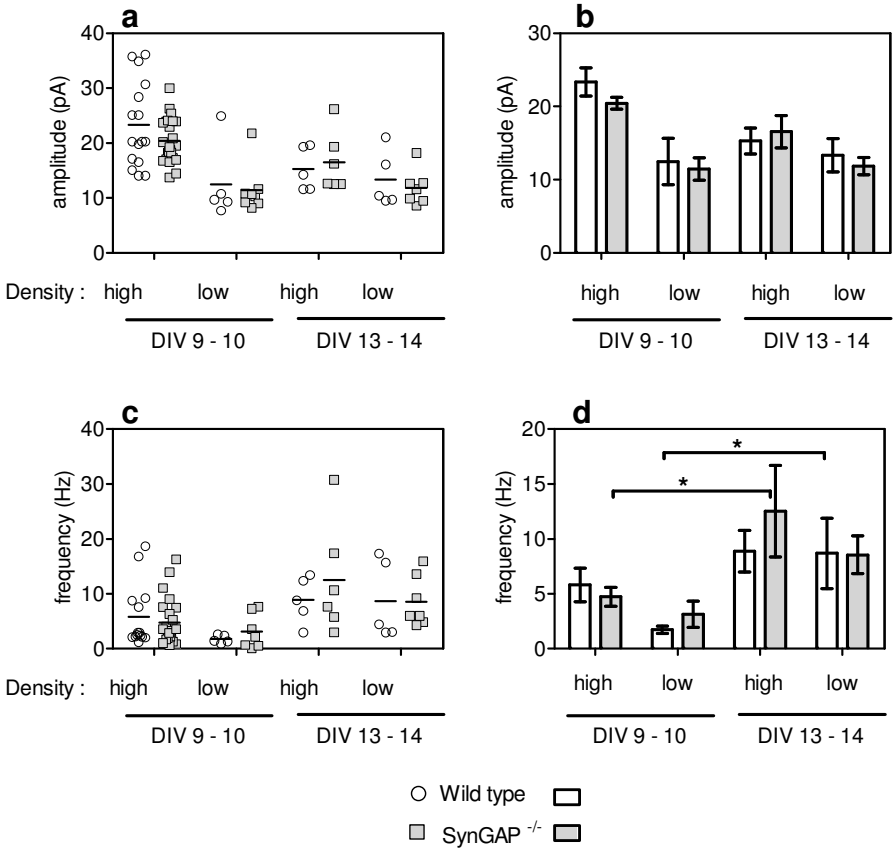

Figure 5. 5 mEPSC amplitude and frequency in wild type and *SynGAP* $^{-/-}$ hippocampal cells.

.

Mean mEPSC amplitudes and frequencies from wild type and *SynGAP* $^{-/-}$ hippocampal cells cultured at high (1500 neurons/mm^2) and low (200 neurons/mm^2) densities recorded at DIV 9 - 10 and DIV 13 - 14. The left panels (a,c) show each individual cell recorded at each time point from wild type and *SynGAP* $^{-/-}$ cells (high density; DIV 9 - 10; WT n = 16, *SynGAP* $^{-/-}$ n = 24, DIV 13 - 14; WT n = 5, *SynGAP* $^{-/-}$ = 6, low density; DIV 10; WT n = 5, *SynGAP* $^{-/-}$ n = 5, DIV 14; WT n = 8, *SynGAP* $^{-/-}$ = 7), (the mean is indicated by a horizontal line). The right panel (b,d) shows mean +/- SEM. *SynGAP* $^{-/-}$ mEPSC frequency is increased from DIV 9 - 10 (4.74 +/- 0.86 Hz) to DIV 13 - 14 (12.53 +/- 4.16 Hz) when cultured at a high density (two way ANOVA, $p<0.05$, post hoc Bonferroni test, $p < 0.05$*). However wild type mEPSC frequency is increased from DIV 9 – 10 (1.48 +/- 0.98 Hz) to DIV 13 – 14 (8.65 +/- 3.12 Hz) when cultured at a low density (two way ANOVA, $p < 0.01$, post hoc Bonferroni test, $p < 0.05$*). Data are from five separate cultures.

5.2.5 mEPSC amplitude distributions in *SynGAP* $^{-/-}$ neurons

While the mean mEPSC amplitudes of a population of cells may remain constant the distribution of the individual mEPSC amplitudes may change. For example, a positive skew in the distribution could be masked by an increase in the maximal values, or an increase or decrease in a particular subset of events. The entire pooled distribution of mEPSC amplitudes is shown as frequency distribution histograms in Figure 5. 6.

As is expected neither wild type nor *SynGAP* $^{-/-}$ mEPSCs populations display a normal distribution at any age or in any cell type (D'Agostino-Pearson normality test, all $p<0.0001$) but there is little difference between the histogram profiles of wild type and *SynGAP* $^{-/-}$ mEPSCs. The maxiumum amplitude mEPSC achieved by each individual cell was extracted to examine if this subset of the largest synapses was affected by the absence of SynGAP. However there is no difference between wild type and *SynGAP* $^{-/-}$ in the maximal amplitude mEPSCs (Figure 5. 7.

5.2.6 mEPSC amplitude and frequency covariance

To assess if amplitude and frequency co-vary, and if this relationship is the same in wild type and *SynGAP* $^{-/-}$ neurons, I plotted the mean amplitude against the frequency for each individual cell (data not shown). There is no statistically significant correlation between amplitude and frequency in cortical or high density hippocampal cells (Pearson's correlation calculation). However in hippocampal cells cultured at a low density (200 neurons/mm^2) a weak correlation is apparent in *SynGAP* $^{-/-}$ cells at DIV 10 (WT $r^2 = 0.53$, $p > 0.05$, $n = 5$, *SynGAP* $^{-/-}$ $r^2 = 0.61$, $p < 0.05$, $n = 8$) and a stronger correlation in both wild type and *SynGAP* $^{-/-}$ cells at DIV 14; (WT $r^2 = 0.92$, $p < 0.01$, $n = 8$, *SynGAP* $^{-/-}$ $r^2 = 0.76$, $p < 0.05$, $n = 7$).

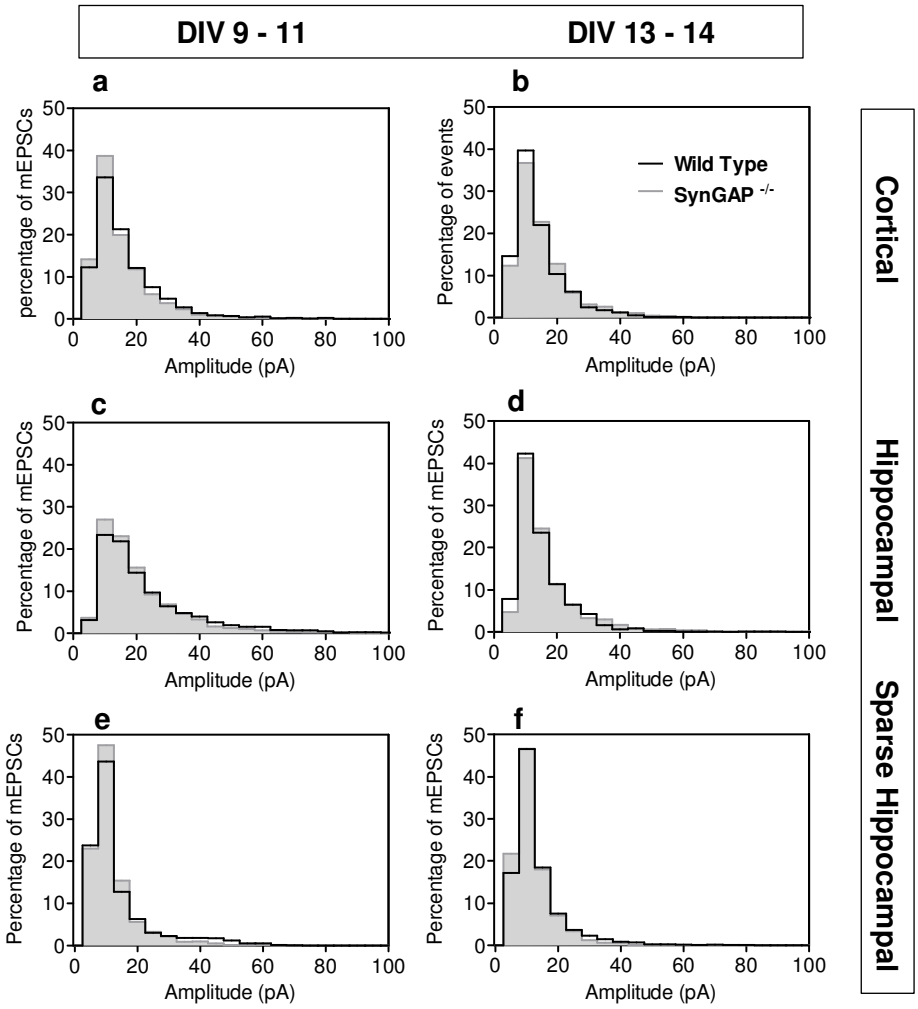

Figure 5. 6 Frequency histograms of mEPSC amplitudes from wild type and *SynGAP* $^{-/-}$ cortical, hippocampal and sparsely cultured hippocampal cells.

Frequency histograms of amplitudes of all mEPSCs recorded from cortical neurons at DIV 9-11 (a, WT n = 2718, *SynGAP* $^{-/-}$ n = 5207) and DIV 13-14 (b, WT n = 3355 , *SynGAP* $^{-/-}$ n = 3951). Frequency histograms of amplitudes of all mEPSCs recorded from hippocampal neurons at DIV 9-10 (c, WT n = 2978, *SynGAP* $^{-/-}$ n = 5126) and DIV 13-14 (d, WT n = 1468, *SynGAP* $^{-/-}$ n = 1686). Frequency histograms of amplitudes of all mEPSCs recorded from sparsely cultured hippocampal neurons at DIV 10 (e, WT n = 1061, *SynGAP* $^{-/-}$ n = 1781) and DIV 14 (f, WT n = 1531, *SynGAP* $^{-/-}$ n = 2115). Data are from three, three and two separate cultures respectively. None of the distributions follow a normal distribution (D'Agostino-Pearson normality test, all $p < 0.0001$)

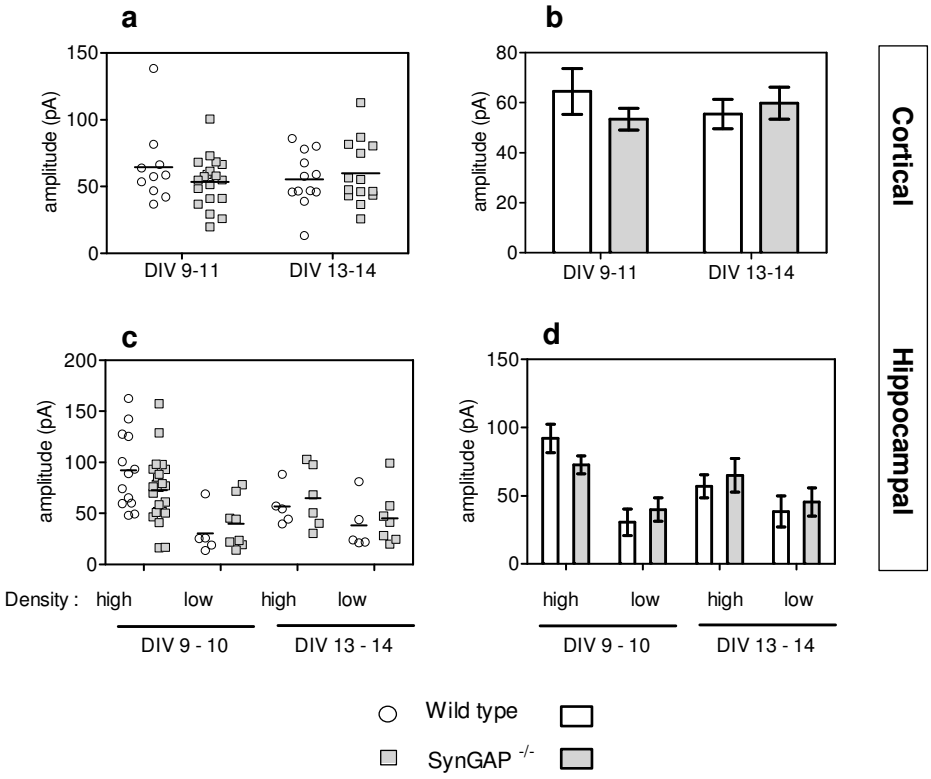

Figure 5. 7 Maximum mEPSC amplitudes per cell in wild type and *SynGAP* $^{-/-}$ cortical, hippocampal and sparsely cultured hippocampal cells.

The maximum amplitude mEPSC of each cell from wild type and *SynGAP* $^{-/-}$ cortical cells at DIV 9-11 and DIV 13-14 (a, b, DIV 9 - 11; WT n = 10, *SynGAP* $^{-/-}$ n = 19, DIV14; WT n = 12, *SynGAP* $^{-/-}$ = 14), wild type and *SynGAP* $^{-/-}$ hippocampal cells at DIV 9 - 10 and DIV 13 - 14 from high density (1500 neurons/mm^2) and low density (200 neurons/mm^2) cultures, (c,d, high density; DIV 9 - 10; WT n = 16, *SynGAP* $^{-/-}$ n = 24, DIV13 - 14; WT n = 5, *SynGAP* $^{-/-}$ = 6, low density; DIV 10; WT n = 5, *SynGAP* $^{-/-}$ n = 5, DIV14; WT n = 8, *SynGAP* $^{-/-}$ = 7). Each individual cell's maximal amplitude is displayed in the adjacent scatter plot. Data are from three, three and two separate cultures respectively and are displayed as mean +/- SEM in b,d.

5.2.7 Whole cell currents

Examining AMPA mEPSCs gives us information about AMPA receptor content at the synapse (with some caveats, to be discussed later). It appears that this aspect of cellular function is largely unchanged in *SynGAP* $^{-/-}$ neurons under the experimental conditions described here.

To obtain information about total receptor cell surface expression, synaptic and extra synaptic, saturating concentrations of AMPA (50µM) and NMDA (100 50µM) were bath applied to elicit activation of all available AMPA and NMDA receptors. An example recording is shown in Figure 5. 8 (a). The agonist is applied until the inward current reaches a plateau, then washed out before reapplication to ensure a stable response. The plateau current amplitude (pA) is normalised to the measured capacitance of the cell (pico Farads, pF) to yield a current density measurement (pA/pF). Because total membrane capacitance is directly proportional to the membrane surface area the current density measurement is independent of cell size.

Whole cell currents in SynGAP $^{-/-}$ neurons

NMDA and AMPA whole cell currents are not different between wild type and *SynGAP* $^{-/-}$ hippocampal cells (t-test, $p > 0.05$), however the mean cell capacitance (+/- SEM) is increased from -50.5 +/- 4.5 pF in wild type cells to -73 +/- 5.2 pF in *SynGAP* $^{-/-}$ neurons (t-test, $p < 0.01$) (Figure 5. 8, a,b). This suggests the *SynGAP* $^{-/-}$ neurons are larger. As a result of the difference in cell capacitance the NMDA receptor current density is decreased from -18.6 +/- 1.9 pA/pF in wild type cells to -12.8 +/- 0.8 pA/pF in *SynGAP* $^{-/-}$ neurons (t-test, $p < 0.01$) (Figure 5. 8, d). The apparent decrease in AMPA receptor current density is not statistically significant (t-test, $p = 0.083$). Once the ratio of AMPA receptor current density to NMDA receptor current density is obtained, there again is no statistically significant difference between wild type and *SynGAP* $^{-/-}$ neurons (Figure 5. 8, e).

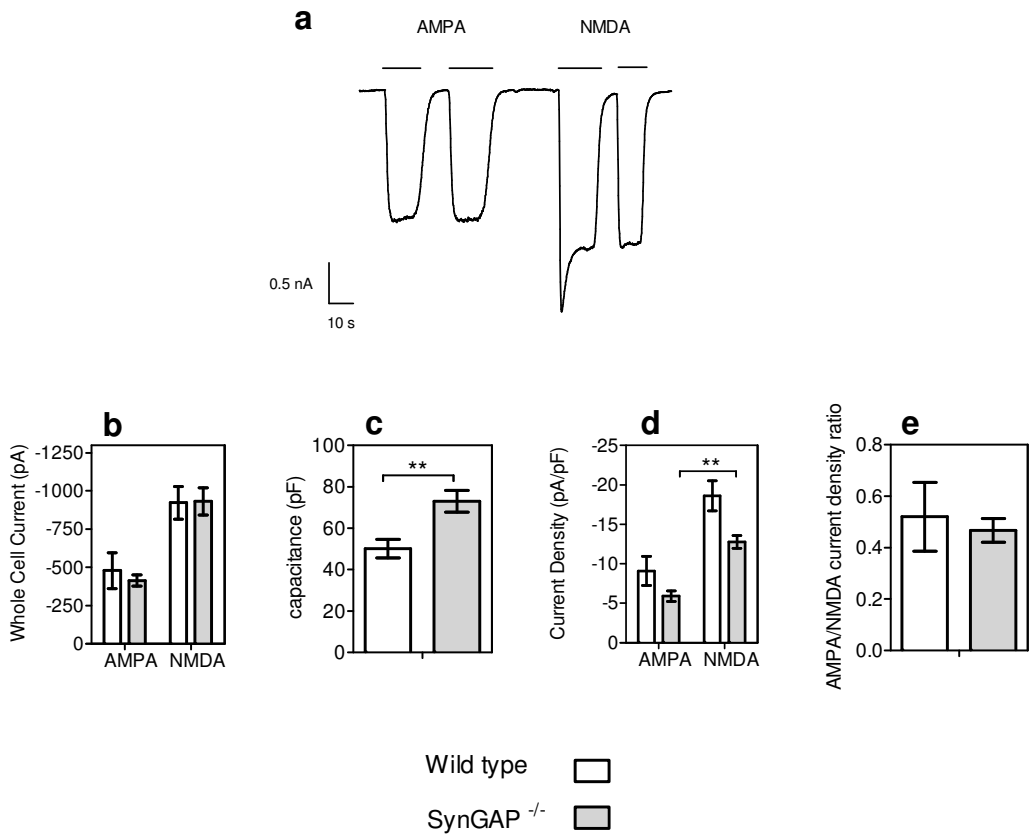

Figure 5. 8 NMDA and AMPA whole cell currents in wild type and *SynGAP* $^{-/-}$ hippocampal cells.

Representative recording of whole cell AMPA and NMDA currents from a hippocampal cell (a). Whole cell currents from wild type (n = 6) and *SynGAP* $^{-/-}$ hippocampal cells (n = 9) recorded at DIV 10 - 11 (b). Capacitance is reduced in *SynGAP* $^{-/-}$ cells (c), (WT = 50.1 +/- 4.5 pF, *SynGAP* $^{-/-}$ = 73 +/- 5.2 pF, t-test, $p < 0.01$**). NMDA and AMPA current density (pA/pF) are calculated by normalising whole cell currents (pA) to capacitance (pF) (d). (NMDA receptor current density; WT = -18.6 +/- 1.9 pA/pF, *SynGAP* $^{-/-}$ = -12.8 +/- 0.8 pA/pF, t-test, $p < 0.01$**; AMPA receptor current density; WT = -9.1 +/- 1.9 pA/pF, *SynGAP* $^{-/-}$ = -5.9 +/- 0.65 pA/pF, t-test, $p = 0.083$). The ratio of AMPA receptor current density to NMDA receptor current density (e). Data are from one culture only, and are displayed as mean +/- SEM. Statistics are one way ANOVA followed by post hoc Tukey t-test.

Soma size and neurite projection in SynGAP $^{-/-}$ neurons

To further investigate the unexpected increase in capacitance in *SynGAP* $^{-/-}$ neurons I measured the area of neuronal cell bodies in fixed GFP transfected wild type and *SynGAP* $^{-/-}$ hippocampal neurons from separate cultures (Figure 5. 9, a). This measurement showed no difference in soma area between wild type and *SynGAP* $^{-/-}$ neurons at DIV 4-5 or DIV 10. In the younger neurons I counted the number of neurites projecting from the soma (Figure 5. 9, b, c). There is no difference between wild type and *SynGAP* $^{-/-}$ neurons in the number of projecting neurites (Figure 5. 9, b).

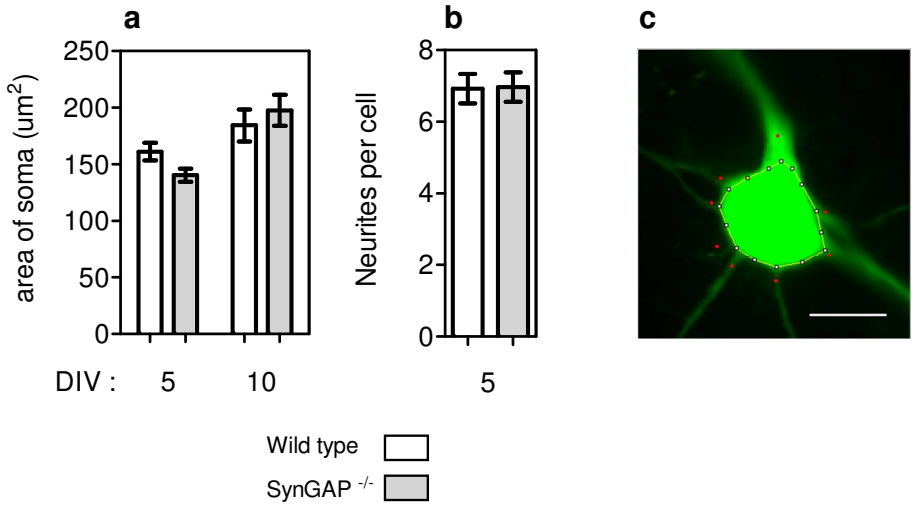

Figure 5. 9 Neuron soma size measurement in fixed GFP transfected wild type and *SynGAP* $^{-/-}$ cells.

Soma size was measured in GFP expressing wild type and *SynGAP* $^{-/-}$ hippocampal cells by outlining the cell body in a single epifluorescence image taken with a x40 objective (a). Cultures were fixed at DIV 5 and 10. The major neurites projecting from the soma were counted in DIV 5 cultures. (b). (c) Example image processed in ImageJ, red dots indicate the neurites counted, yellow outline and white dots indicate the area measured. Data are from 2 DIV 5 and two DIV 10 cultures, n = 30 neurons per condition in all cases. Scale bar is 10µm

5.2.8 Action potentials in *SynGAP* $^{-/-}$ neurons

In current clamp *SynGAP*$^{-/-}$ neurons are observed to fire action potentials in a manner that is indistinguishable from wild type controls (data not shown). They fire action potentials spontaneously and in response to stimulation of the culture with bicuculine and 4 amino-pyridine.

5.2.9 The expression of a putative truncated form of SynGAP B

During the cloning of *SynGAP* B fragments a novel form of *SynGAP* was found (see Chapter Three, p108). This *SynGAP* contains a four base pair insertion at the end of the last *SynGAP* B specific exon. These four base pairs constitute a frameshift mutation which, if translated, would lead to premature truncation. This 92 amino acid fragment includes 53 novel residues not present in full length SynGAPs and would not be recognised by any available SynGAP antibody. We do not know if this fragment, which we refer to as SynGAP B-shift, is expressed. However, the entire length of the coding region for SynGAP B-shift is 5' of the insertion site of the deletion cassette in the knock out animal used in this thesis. It is conceivable therefore that SynGAP B-shift may be expressed in the *SynGAP* $^{-/-}$ mouse.

As we do not know what effect, if any, the putative peptide may have on neurons, I assessed mEPSC amplitude and frequency in cells overexpressing SynGAP B-shift. There is no change from control levels in mEPSC amplitude or frequency when SynGAP B-shift is expressed in wild type neurons (Figure 5. 10).

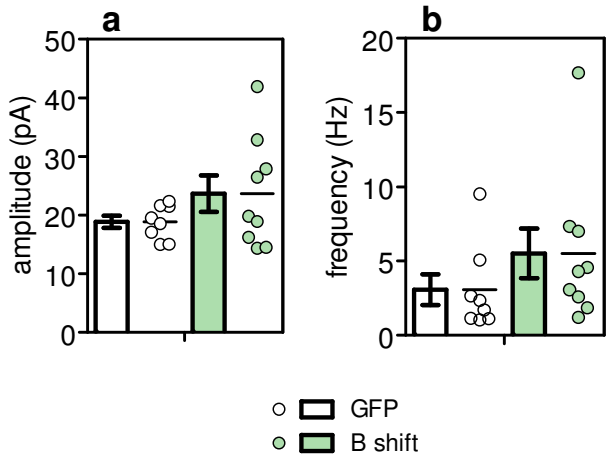

Figure 5. 10 mEPSC amplitude and frequency in wild type cells overexpressing SynGAP B-shift.

mEPSC amplitude means (a) recorded from wild type hippocampal neurons transfected with GFP only (n = 8) and SynGAP B-shift (n = 9). Mean mEPSC frequencies are shown in (b). Individual cell values (amplitude mean and frequency) are displayed in the adjacent scatter plots, horizontal lines indicate the population mean. Data were recorded at DIV 9 - 11 and are from two transfections from two cultures.

5.2.10 Part Two: Electrophysiological properties of wild type neurons overexpressing various SynGAP isoforms.

5.2.11 Expression of SynGAP isoforms

A range of SynGAP isoforms were expressed in wild type hippocampal cells to assess their effect on the electrophysiology of the neuron. Three N-termini (A, B and C) were combined with two C-termini (alpha-1 and alpha-2), resulting in six distinct isoforms; SynGAP A-alpha-1, SynGAP B-alpha-1, SynGAP C-alpha-1, SynGAP A-alpha-2, SynGAP B-alpha-2 and SynGAP C-alpha-2. SynGAP was co transfected with GFP to allow the identification of cells expressing SynGAP. See Appendix 1 for the optimisation of the co-transfection protocol and confirmation of co-expression of GFP and SynGAP. The transfection rate obtained is approximately 0.5 - 1% of neurons (Appendix Figure 7. 1 Co-expression and transfection efficiency controls). When a transfected cell is patched it is likely that only that post synaptic cell is affected by SynGAP overexpression. I have never visually observed autaptic synapses. All recordings were performed between DIV 9-11, the day after transfection (16 to 36 hrs after the transfection complexes were added to the cells).

Great difficulty was experienced in obtaining good electrophysiological recordings from transfected cells. Transfection conditions were optimised to improve the quality of recordings (Appendix 1).

5.2.12 An observation: 'Silent' cells

The primary observation I made when I began recording from neurons overexpressing SynGAP was that a large portion of the neurons transfected with isoforms ending in the C-terminal variant alpha-1 completely lacked AMPA mEPSCs. Therefore I categorised neurons depending on whether they had any mEPSCs or not. I term the neurons lacking any mEPSCs as 'silent' (Figure 5. 11)[9].

[9] Use of the term 'silent cell' should not be confused with the term 'silent synapse'. A silent synapse is defined as a synapse where an EPSC is absent at the resting membrane potential, but becomes apparent when the cell is depolarised ie silent synapses have an

A low noise recording of a minimum length of 2 minutes where no mEPSCs were apparent was required for a cell to be classified as silent. No minimum recording length was necessary to designate a cell as non-silent, the appearance of obvious mEPSCs was sufficient. Recording with high levels of noise but with mEPSCs distinguishable above the background noise were not included in this analysis.

5.2.13 Silence in SynGAP transfected cells

Neurons overexpressing SynGAP with an alpha-1 C-terminus were most likely to be silent, and within that group the extent of the silencing was determined by which N-terminus was present (Figure 5. 11)

When expressing only GFP silence was observed in 10.5% of neurons. When expressing SynGAP A-alpha-1 72.5% of neurons recorded from were silent. This figure dropped to 45 and 44.7% silence in neurons expressing SynGAP B-alpha-1 and SynGAP C-alpha-1 respectively. If we take the data for GFP only expressing neurons to represent the level of silence we would expect to see in neurons a Chi square test for expected versus observed values can be performed. All SynGAP alpha 1 isoforms are statistically significantly different from control (all $p < 0.0001$). In contrast, the expression of SynGAP alpha-2 isoforms does not increase the likelihood of a neuron being silent. When SynGAP A-alpha-2 and SynGAP C-alpha-2 were expressed 14.3% and 5% respectively of cells were silent (both $p = 0.09$, Chi square test). However, no neurons expressing SynGAP B-alpha-2 were silent, this is different to control ($p = 0.0009$, Chi square test).

NMDA receptor mediated response but no AMPA receptor mediated response (Kerchner et al., 2008; Liao et al., 1995; Isaac et al., 1995; Discussed later, 5.3.10).

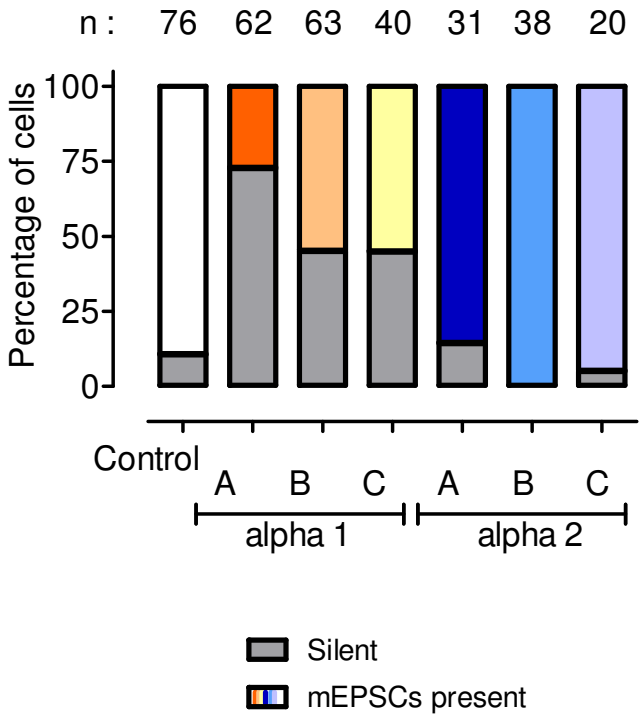

Figure 5. 11 Presence or absence of mEPSCs in wild type neurons transfected with various SynGAP isoforms.

Hippocampal neurons were categorised as either having mEPSCs (upper portion of the bar) or not (silent, lower portion of the bar). Data is displayed as a percentage of cells recorded from for each construct. The percentage of neurons categorised as silent is as follows: GFP only = 10.5%, SynGAP A-alpha-1 = 72.6%, $p < 0.0001$, SynGAP B-alpha-1 = 45%, $p < 0.0001$, SynGAP C-alpha-1 = 44.7%, $p < 0.0001$, SynGAP A-alpha-2 = 14.3%, $p = 0.09$, SynGAP B-alpha-2 = 0%, $p = 0.0009$, SynGAP C-alpha-2 = 5%, $p = 0.09$. The p value is from a Chi square test for expected v observed with GFP values are taken as the expected values. Population Chi square test, $p < 0.0001$. Data are from approximately 32 separate transfections from 16 separate cultures. The total number of cells is displayed above each bar. The C-terminal isoform alpha-1 is illustrated in the orange palette and alpha-2 is illustrated in the blue palette. The N-terminal to which they are connected is illustrated by the depth of colour; darkest colour for A, middle colour for B and lightest colour for C.

I took two approaches to examine the effect of SynGAP overexpression on mEPSCs; the first involves analysing only the cells in which mEPSCs were present; the second involves including a representative value for each silent cell to allow all cells to be included in the analyses.

5.2.14 Approach One: Exclusion of silent cells in mEPSC amplitude and frequency analysis:

mEPSC amplitudes in non-silent SynGAP transfected cells

The non-silent cells presented in the previous figure (Figure 5. 11) were analysed for mEPSC amplitude and frequency. Mean mEPSC amplitudes are shown in Figure 3.12. One-way ANOVA indicates all the data was not sampled from groups with the same mean, $p < 0.0001$. However despite the differences in silencing post-hoc Tukey t-tests indicate that there are statistically significant differences in mean mEPSC amplitudes only between alpha-1 isoforms and alpha-2 isoforms, but not between control and SynGAP transfected cells. Table (b) in Figure 5. 12 includes the p values for all the pairwise comparisons.

To reframe the experimental question to ask specifically if the expression of SynGAP alters mEPSC amplitude from control level, rather than between two SynGAPs, two additional post hoc tests were performed. The Dunnett's post hoc test compares all experimental groups to the control group only. The Bonferroni test was applied to compare each group with control. No SynGAP isoform was statistically significantly different from the GFP control in either test. A single students t-test of control against SynGAP A-alpha-1 does reach statistical significance ($p < 0.01$).

Bartlett's test for equal variances was performed on the data set and concluded that the variances differ significantly ($p = 0.015$). This variable spread of data can be seen when the mean mEPSC amplitude for each cell is displayed in a scatter plot (Figure 5. 12, a).

Using a cell's median mEPSC amplitude to calculate the population mean

If data are sampled from a Gaussian distribution then the mean and median will have very similar values, but if the distribution is skewed the values can differ a lot. I have already shown (Figure 5. 2 and Figure 5. 3) how the population of mEPSC amplitudes are not a normally distributed population. In order to asses if using a cell's median mEPSC amplitude to calculate the population mean gives a different result I repeated the above analyses. While the median mEPSC amplitudes are generally smaller than the mean the overall profile of the statistics remains very similar. The median values, results of the ANOVA, post hoc Tukey t-tests and Dunnett's tests are given in Table B of Figure 5. 12.

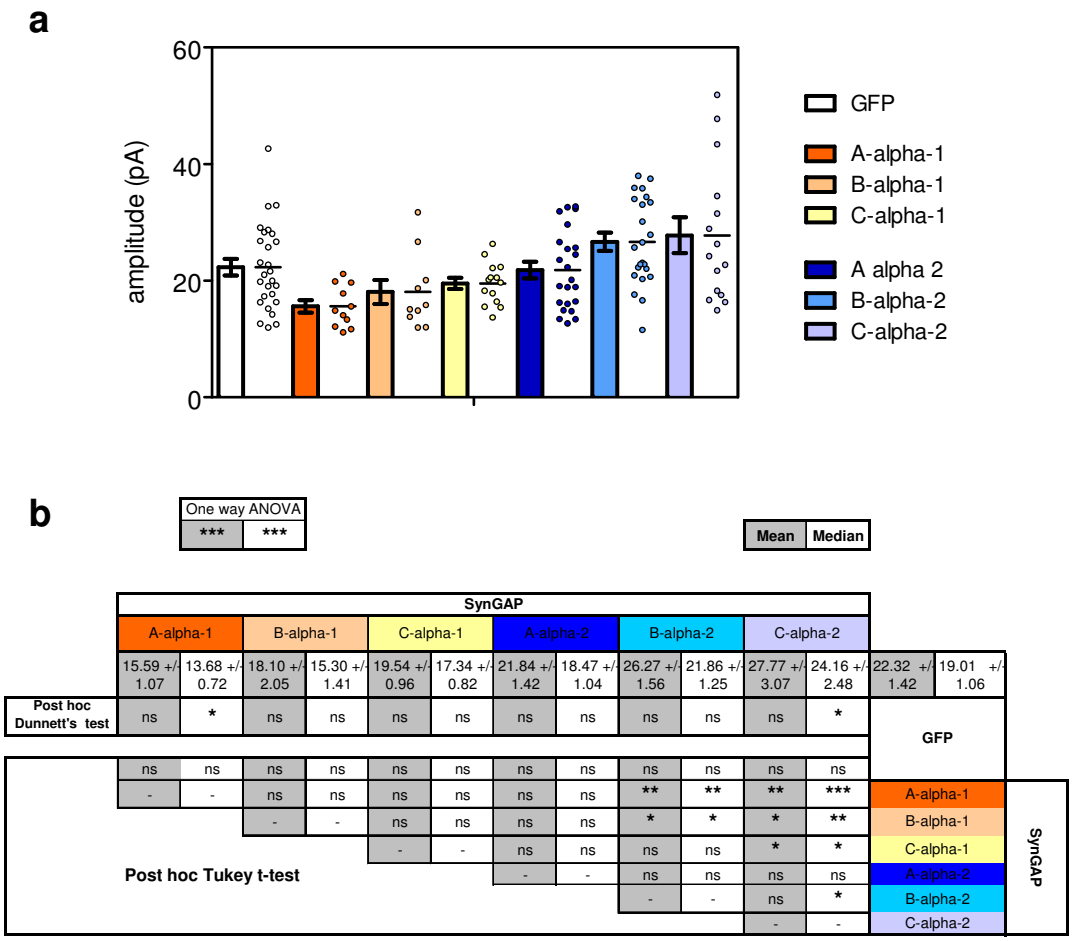

Figure 5. 12 mEPSC amplitudes from non-silent wild type neurons transfected with various SynGAP isoforms.

mEPSCs were recorded from hippocampal neurons transfected with GFP only or GFP and the SynGAP isoform indicated. (a) The mean (or the median, values shown in table (b) only) mEPSC amplitude was calculated for each cell. The mean (or the median) was then averaged to give a mean for the entire population. Cell means are shown in scatter plots next to the population mean bar. Statistical analyses yield slightly different results for the population means calculated from cell means or medians, (b).. Displayed are the p values from the post hoc Tukey and Dunnett's t-test performed on values calculated from the mean (shaded box) or median (unshaded box), $p < 0.05$*, $p < 0.01$ **, $p < 0.001$ ***. A students t-test of control vs SynGAP A-alpha-1 gives a p-value = 0.007. The n numbers are; GFP, n = 27, SynGAP A-alpha-1, n = 11, SynGAP B-alpha-1, n = 10, SynGAP C-alpha-1, n = 17, SynGAP A-alpha-2, n = 23, SynGAP B-alpha-2 n = 21, SynGAP C-alpha-2, n = 15. Data are from 13 transfections from 9 separate cultures and are shown as mean +/- SEM.

mEPSC amplitude distributions in cells transfected with SynGAP isoforms

To closer inspect the effect of SynGAP isoforms on mEPSCs I have plotted the frequency distribution of all events recorded from non-silent transfected cells (Figure 5. 13). Visual appraisal of the histograms gives rise to the impression that the SynGAP A-alpha-1 and B-alpha-1 distributions contain more small amplitude events than control, whereas SynGAP B-alpha-2 and C-alpha-2 distributions have less small amplitude events. The distributions of SynGAPs C-alpha-1 and A-alpha-2 seem to more closely match the distribution of control events.

To quantify the changes in distribution I have categorised mEPSCs amplitudes as small (5 – 12 pA), medium (13 – 17 pA), large (18 – 27 pA) and very large (28 – 260 pA) based on the quartiles of the control population (Figure 5. 14). For example small amplitude events (5 -12 pA) constitute 25% of all events recorded from control cells.

In the distribution of mEPSC amplitudes from SynGAP A-alpha-1 and B-alpha-1 expressing cells a larger proportion of events are in the smaller amplitude range of 5 – 12 pA (46% and 39% respectively). Accordingly the largest amplitude range of 28 – 260 pA contains a smaller proportion of SynGAP A-alpha-1 and B-alpha-1 events (7% and 14% respectively). The distribution of SynGAP C-alpha-1 events is shifted slightly to the medium (13 – 17 pA, 29%) and large (18 – 27 pA, 30%) ranges and away from both small (21%) and very large (21%) ranges. SynGAP A-alpha-2 follows the control distribution very closely with approximately 25% of values in each category. In contrast to SynGAP A-alpha-1 and B-alpha-1 distributions the distributions of SynGAPs B-alpha-2 and C-alpha-2 have a reduced proportion of events in the small (20% and 16% respectively) and medium (19% and 20% respectively) ranges and an increase in events in the very large category (36% and 37% respectively).

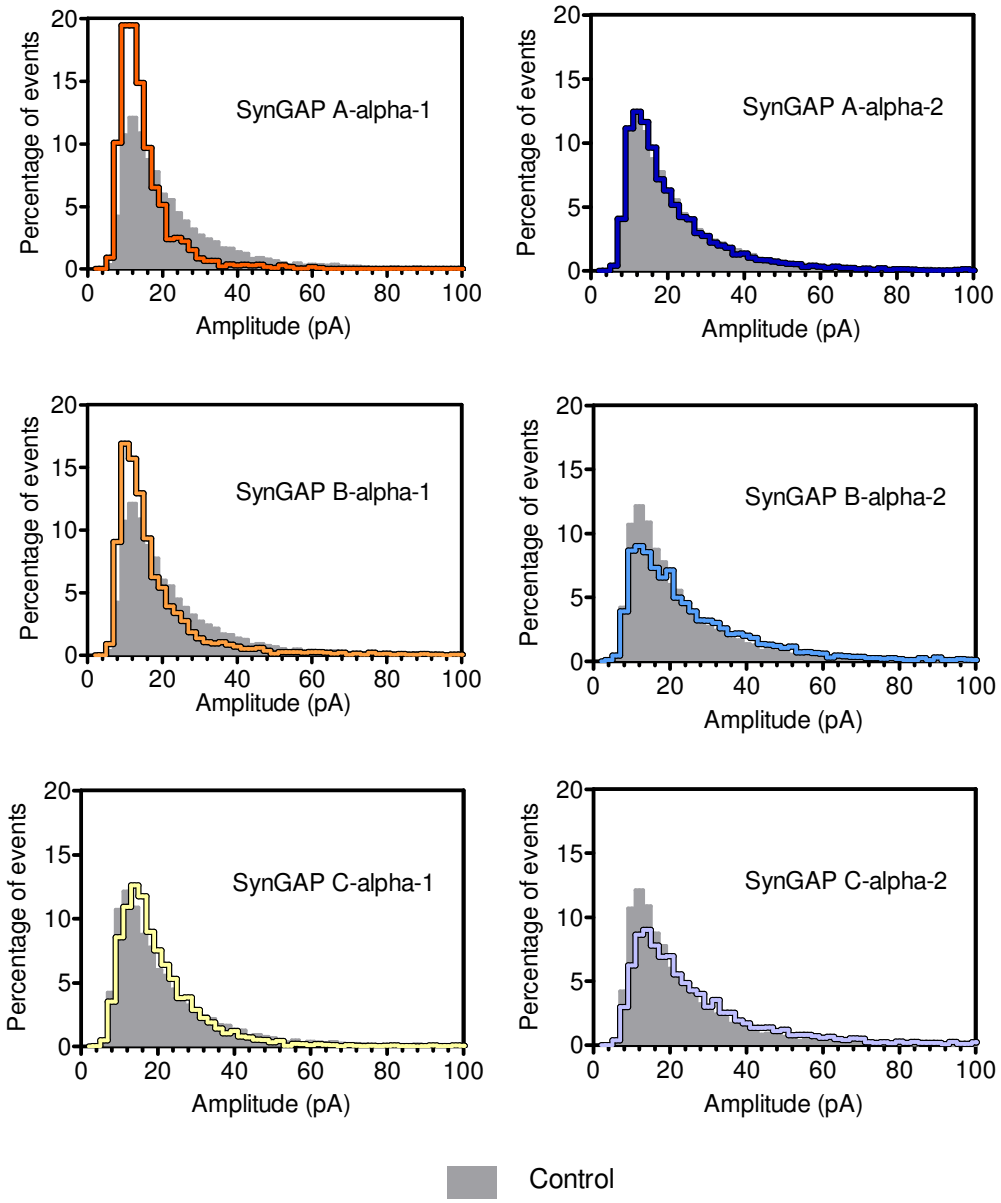

Figure 5. 13 Frequency distributions of mEPSC amplitudes recorded from wild type neurons transfected with various SynGAP isoforms.

Frequency histograms of mEPSC amplitudes recorded from hippocampal cells overexpressing SynGAP isoforms (coloured line) are overlayed on the histogram for GFP only expressing cells (filled grey area). GFP, n = 7731, SynGAP A-alpha-1, n = 2756, SynGAP B-alpha-1, n = 2664, SynGAP C-alpha-1, n = 4044, SynGAP A-alpha-2, n = 6712, SynGAP B-alpha-2 n = 6824, SynGAP C-alpha-2, n=4383. Data are from 13 transfections from 9 separate cultures.

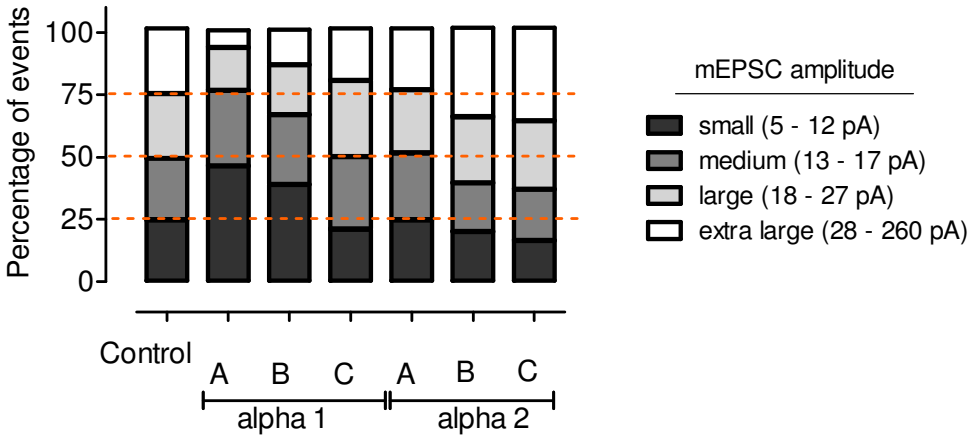

Figure 5. 14 Further analysis by classification of mEPSC amplitudes in wild type neurons transfected with various SynGAP isoforms

Classification of all mEPSCs recorded from neurons transfected with SynGAP isoforms into four amplitude categories; small (5-12 pA), medium (13 – 17 pA), large (18 – 27 pA) and extra large (28 – 260 pA). The amplitude categories are based on the quartiles of the control population of events (illustrated by the orange broken line). The n numbers are given in Figure 5. 12

Maximum amplitude mEPSCs in SynGAP transfected cells

Given the change in proportions of large amplitude events among cells transfected with different SynGAP isoforms (Figure 5. 14) I plotted the maximum amplitude mEPSC achieved by each cell to see if the very largest synapses were affected by SynGAP expression (data not shown). The spread of the data is large but is statistically significant by one way ANOVA, however only SynGAP B-alpha-2 vs A-alpha-1 ($p < 0.01$) and B-alpha-1 ($p < 0.05$) reach statistical significance by post hoc Tukey t-tests. However a single students t-test of SynGAP A-alpha-1 against control shows a statistically significant decrease in maximum amplitude mEPSC reached by SynGAP A-alpha-1 expressing cells ($p = 0.018$).

mEPSC frequency in non-silent SynGAP transfected cells

Analysis of mEPSC frequency in recordings from non-silent cells overexpressing GFP, SynGAP A, B, C-alpha-1 and A, B, C-alpha-2 are shown in Figure 5. 15. The frequency of mEPSCs is generally more variable than that of their amplitude, this is evident when each cell is plotted in a scatter plot (Figure 5. 15, a). According to a one way ANOVA is it unlikely that all of the groups are derived from populations with the same mean, $p = 0.02$. However, no pair of conditions are statistically different from each other in pairwise comparisons (post hoc Tukey and Dunnett's tests). The variances are different between the groups (Barlett's test for equal variances, $p<0.0001$) and the distributions not normal (D'Agostino and Pearson normality test, $p<0.05$ for all groups).

Transformation of mEPSC frequency data

I have transformed the data to equalise the standard deviations and make the distribution more Gaussian (Figure 5. 15, b). (Additional details regarding the data transformation are present in Methods,p86.). The log of each frequency was obtained and then normalised to the mean log frequency of the GFP control. The resulting data are normally distributed (D'Agostino and Pearson normality test, p values from 0.32 to 0.84) and no longer have unequal variances (Barlett's test for equal variances, $p = 0.56$). The data indicate the (log) fold change from control mean frequency.

When the statistical analyses are repeated on the transformed data (Figure 5. 15, b), the mEPSC frequency in neurons expressing SynGAP A-alpha-1 is decreased from that in neurons expressing GFP only (one way ANOVA, $p < 0.0001$, post hoc Tukey t-test, $p < 0.0001$). Additionally, neurons expressing SynGAP A-alpha-1 also have a slower mEPSC frequency than neurons expressing other alpha-1 isoforms (SynGAP B-alpha-1, $p < 0.05$, SynGAP C-alpha-1, $p < 0.05$) and alpha-2 isoforms (SynGAP A-alpha-2, $p < 0.05$, SynGAP B-alpha-2, $p < 0.0001$, SynGAP C-alpha-2, $p < 0.0001$). SynGAP A-alpha-2 expressing neurons have a lower mean mEPSC frequency than neurons expressing SynGAP B-alpha-2 (post hoc Tukey t-test $p < 0.001$).

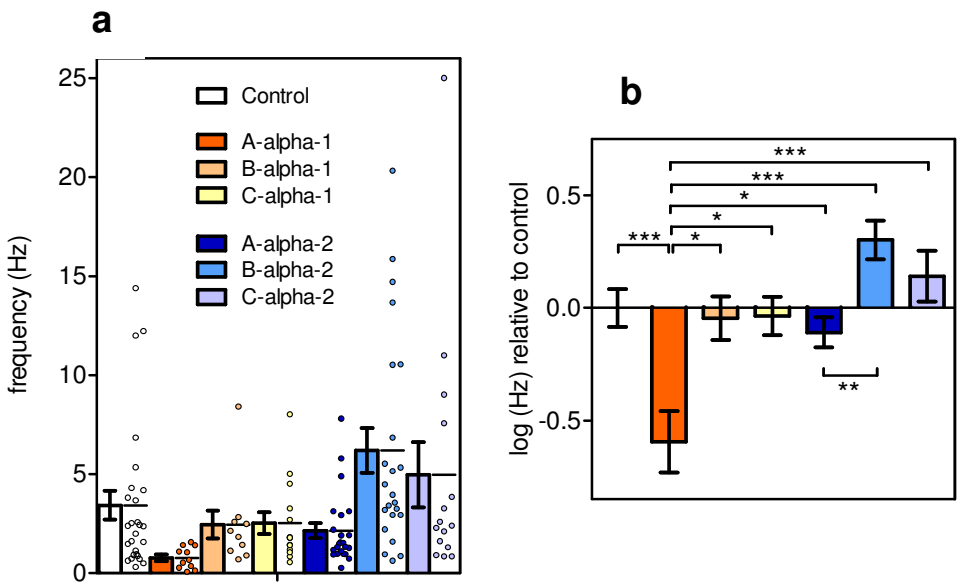

Figure 5. 15 mEPSC frequencies in non-silent wild type hippocampal neurons transfected with various SynGAP isoforms

(a) mEPSCs were recorded from neurons transfected with GFP only or GFP and the SynGAP isoform indicated. Each cell's mEPSC frequency (Hz) is displayed in the scatter plot adjacent to the population mean bar (one-way ANOVA, $p = 0.02$, Bartlett's test for equal variance, $p < 0.0001$). (b) The mEPSC frequency (Hz) is displayed as a log (Hz) transformation normalised to the mean log of the GFP control (0.325) (one-way ANOVA, $p < 0.0001$, Bartlett's test for equal variance, $p = 0.56$). Pairwise statistical significance between the following pairs was reached by post hoc Tukey t-tests; against SynGAP A-alpha-1; GFP, $p < 0.0001$***, SynGAP B-alpha-1, $p < 0.05$*, SynGAP C-alpha-1, $p < 0.05$*, SynGAP A-alpha-2, $p < 0.05$*, SynGAP B-alpha-2, $p < 0.0001$***, SynGAP C-alpha-2, $p < 0.0001$*** ;and SynGAP A-alpha-2 vs SynGAP B-alpha-2, $p < 0.001$**). The n numbers are given in Figure 5. 12. Data are from 13 transfections from 9 separate cultures and are shown as mean +/- SEM.

5.2.15 Approach Two: Inclusion of silent cells in mEPSC amplitude and frequency analysis

The second approach to examine the effect of SynGAP overexpression on mEPSCs was to include a representative value for silent cells so all cells could be included in the same analysis. As it is possible that 'silent' cells do have mEPSCs, but that they fall below the detection threshold, this value (5pA) was assigned to silent cells for population mean calculations. 'Silent' cells may also have detectable mEPSCs but they occur so infrequently that they are not seen during the recording period, therefore I assigned the slowest frequency observed (0.6 Hz) as the representative frequency value for silent cells.

Figure 5. 16 shows that, when silent cells are included in the analysis, the mEPSC amplitude (a) and frequency (b) of all SynGAP-alpha-1 expressing neurons is decreased compared to control. SynGAP A-alpha-2 expressing neurons are unchanged in both respects, in contrast to the increase in mEPSC amplitude induced by the expression of SynGAPs B-alpha-2 and C-alpha2. SynGAP B-alpha-2 also causes an increase in mEPSC frequency (Figure 5. 15, b). Statistics and means are included in the Table C of Figure 5. 15. The differences observed using this method of analysis, inclusion of silent cells, mirror those seen in the distributions of mEPSCs recorded from non-silent cells (Figure 5. 13 and Figure 5. 14).

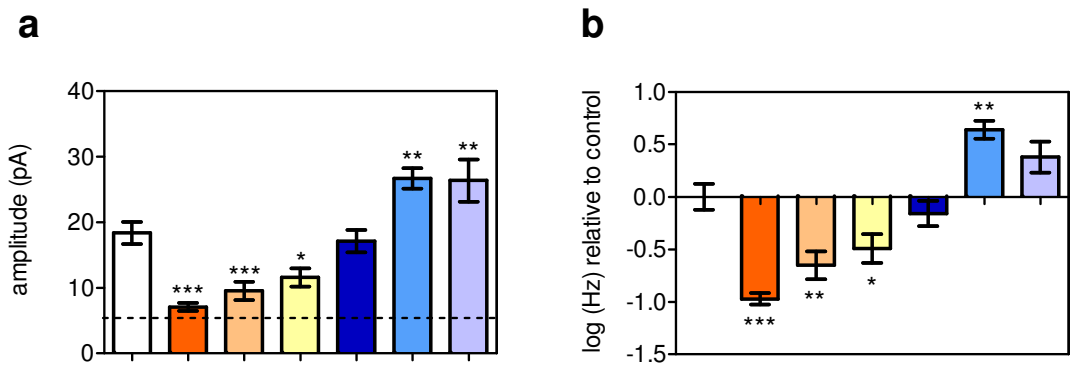

c

Amplitude (pA)		**Frequency** (log fold change)											
SynGAP													
A-alpha-1		B-alpha-1		C-alpha-1		A-alpha-2		B-alpha-2		C-alpha-2			
7.08 +/- 0.6	- 0.97 +/- 0.05	9.56 +/- 1.7	- 0.65 +/- 0.13	11.57 +/- 1.34	- 0.49 +/- 0.14	17.1 +/- 1.69	- 0.16 +/- 0.12	26.67 +/- 1.56	0.64 +/- 0.08	26.35 +/- 3.2	0.38 +/- 0.07	18.36 +/- 1.66	0 +/- 0.12
***	***	***	**	*	*	ns	ns	**	**	**	ns	**GFP**	
-	-	ns	ns	ns	*	***	*	***	***	***	***	A-alpha-1	**SynGAP**
		-	-	ns	ns	**	ns	***	***	***	***	B-alpha-1	
				-	-	ns	ns	***	***	***	***	C-alpha-1	
						-	-	***	***	**	ns	A-alpha-2	
One way ANOVA		**Post hoc Tukey t-test**						-	-	ns	ns	B-alpha-2	
***	***									-	-	C-alpha-2	

Figure 5. 16 mEPSC amplitude and frequency, including silent cells, in neurons overexpressing various SynGAP isoforms

Recordings were made from hippocampal neurons transfected with GFP only or GFP and the SynGAP isoform indicated. Neurons classified as 'silent' were assigned an amplitude of the detection threshold value (5pA, dotted line) and the frequency of the slowest cell recorded (0.06 Hz) for the purposes of calculating the population mean. The mEPSC frequency (Hz) is displayed as a log (Hz) transformation normalised to the mean log of the GFP control (0.015). Statistics are one way ANOVA, (a, amplitude and b, frequency, both $p < 0.0001$), followed by post hoc Tukey t-tests. Pairwise comparisons against control are indicated by asterisks over the bar, $p < 0.05$*, $p < 0.01$**, $p < 0.005$***. Additional pairwise comparisons are detailed in the accompanying table (c) of amplitude (shaded box) and log fold change of frequency (unshaded box) , $p < 0.05$*, $p < 0.01$**, $p < 0.005$***.

5.2.16 Whole Cell currents in SynGAP alpha-1 transfected cells

The decreases seen in mEPSCs in SynGAP-alpha-1 expressing neurons could be caused by a number of mechanisms; altered AMPA receptor surface expression, either globally or specifically at synapses (silent synapses), altered synapse number or altered neurotransmitter release. In order to investigate the possibility that global receptor surface expression was being affected by SynGAP expression I assessed whole cell AMPA and NMDA currents in wild type hippocampal cells overexpressing SynGAP isoforms (Figure 5. 17). Due to their effect in silencing mEPSCs this experiment was confined to examining SynGAP alpha-1 isoforms.

If SynGAP was regulating the synaptic content of AMPA receptors one might expect total AMPA receptor surface expression to be altered. However, apart from an increase in capacitance in neurons overexpressing SynGAP C-alpha-1 (86.12 +/- 7.61 pF) compared to that of neurons overexpressing SynGAP B-alpha-1 (62.18 +/- 4.37 pF, one way ANOVA, $p = 0.04$, post hoc Tukey t-test, $p = <0.05$, Figure 5. 15, c), there are no overall changes in AMPA or NMDA whole cell currents or current density in SynGAP-alpha-1 expressing cells (one way ANOVA, Figure 5. 15). Strikingly there is no correlation between a cell's current density and its status as silent or non-silent (Figure 5. 15, d). It would be expected that the ratio of AMPA receptor current density to NMDA receptor current density would be altered if SynGAP had a role in specifically regulating AMPA receptor trafficking to the cell surface. For example, if overexpression of SynGAP-alpha-1 isoforms led to a reduction of surface AMPA receptor, but not NMDA receptor, we would expect the AMPA/NMDA ratio to decrease. Clearly there is no change in AMPA/NMDA ratio in SynGAP alpha-1 expressing neurons (Figure 5. 15, e).

The lack of changes in AMPA and NMDA whole cell currents therefore leads me to conclude that SynGAP-alpha-1 expressing neurons have normal levels of surface expression of AMPA and NMDA receptors. This finding reduces the likelihood that the reduction in mEPSCs is due to an increase in silent synapse number (see foot note 9, (Isaac *et al.*, 1995; Liao *et al.*, 1995; Kerchner & Nicoll, 2008)) .

This result presents us with a question. If SynGAP-alpha-1 expressing neurons often lack mEPSCs, yet appear to have normal amounts of functional AMPA receptor, are they actually receiving presynaptic input?

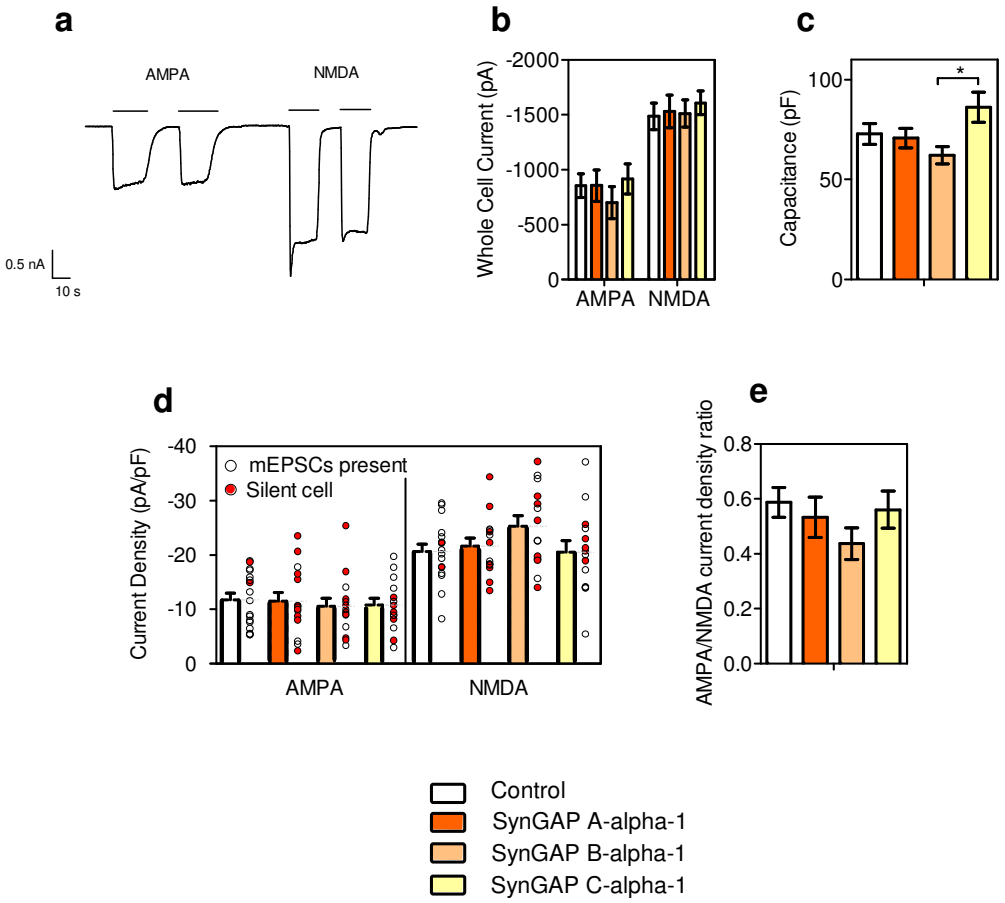

Figure 5. 17 AMPA and NMDA whole cell currents in wild type neurons transfected with SynGAP alpha-1 isoforms

Whole cell currents from wild type hippocampal cells transfected with GFP (n = 17), SynGAP A-alpha-1 (n = 14), SynGAP B-alpha-1 (n = 14) and SynGAP C-alpha-1 (n = 14), recorded at DIV 10-11 (b). An example trace is shown in (a). Capacitance (c) is lower in cells expressing SynGAP B-alpha-1 (62.18 +/- 4.372 pF) compared to those expressing SynGAP C-alpha-1 (86.12 +/- 7.61 pF, t-test, p = 0.04). NMDA and AMPA current density (pA/pF) are calculated by normalising whole cell currents (pA) to capacitance (pF) (d). The current densities of the individual cells are shown in the adjacent scatter plots, the cell's status as silent is illustrated by the colour red, the clear circles represent neurons that had mEPSCs. The ratio of AMPA receptor current density to NMDA receptor current density (e). Data are from four transfections from three separate cultures, and are displayed as mean +/- SEM. Statistics are one way ANOVA followed by post hoc Tukey t-test.

5.2.17 Spontaneous and stimulated action potential mediated activity

To address this question I removed TTX from the recording solution to allow the neurons to fire action potentials. In this situation neurotransmitter release onto the postsynaptic patched cell is no longer limited to spontaneous quantal packets but is driven by the firing of presynaptic neurons. When the cell is voltage clamped below firing threshold it cannot fire action potentials but we can monitor the flow of current into the cell caused by the firing of synapsing cells. Spontaneous neurotransmitter release can still occur but cannot be definitively distinguished from action potential driven release (Figure 5. 18, a).

After monitoring spontaneous activity I stimulated the activity of the neural network to increase the excitatory input onto the patched cell. To this end bicuculine (Bic, 50 µM), which induces waves of firing by blocking the inhibitory GABA-A receptor thus reducing the inhibitory input in the network, and 4-amino pyridine (4-AP, 250 µ M), a potassium channel blocker which increases the intrinsic excitability of all neurons, were bath applied (Figure 5. 15, b).

The spontaneous and stimulated activities of neurons expressing GFP only, SynGAP A-alpha-1, SynGAP B-alpha-1 and SynGAP C-alpha-1 were recorded. Figure 5. 15 (a) illustrates the spontaneous activity of a DIV 10 GFP transfected cell voltage clamped at -70mV. mEPSC like events are observed and occasionally larger spontaneous events are observed (not in this example, see later examples in Figure 5. 19). Bath application of Bic and 4-AP leads immediately to repeated influxes of current, which after an initial disorganised phase (10-30s) take on the form of bursts of inward current (Figure 5. 15, b). These bursts correspond to action potential bursts of the presynaptic cells. The inward currents are completely terminated by the addition of the AMPA receptor antagonist CNQX (5 µM) and are recovered when CNQX is removed (not shown). Addition of TTX also blocks the large current bursts, confirming that they are action potential dependant, and exposes non action potential dependant mEPSCs (Figure 5. 15, d).

Recordings of spontaneous (a, c) and stimulated (b, d) activity from neurons transfected with GFP and SynGAP A-alpha-1 are displayed in Figure 5. 19. All GFP

expressing neurons examined (n=10) were found to have spontaneous EPSCs (Figure 5. 15, a). 25% of neurons (n=8) expressing SynGAP A-alpha-1 (Figure 5. 15, c) and 12.5% of neurons (n=8) expressing SynGAP B-alpha-1 did not exhibit any spontaneous EPSCs. All SynGAP C-alpha-1 expressing neurons examined (n=5) were found to have spontaneous EPSCs. All neurons recorded responded to Bic/4-AP stimulation (Figure 5. 15, b, d). The nature of the response was not observed to differ depending on whether or not SynGAP was expressed or on what SynGAP isoform was expressed (data not shown). All inward currents were in every case terminated by the application of CNQX (data not shown).

The conclusion of this experiment is that SynGAP alpha-1 expressing neurons are capable of receiving excitatory input mediated by AMPA/kainate receptors. The incidence of silent cells that receive apparently normal AMAP mediated input indicates that silent cells are not dominated by silent synapses.

Current clamp recordings show that SynGAP expressing cells are capable of firing action potentials (Figure 5. 20). The traces shown are from cells stimulated with Bic/4-AP.

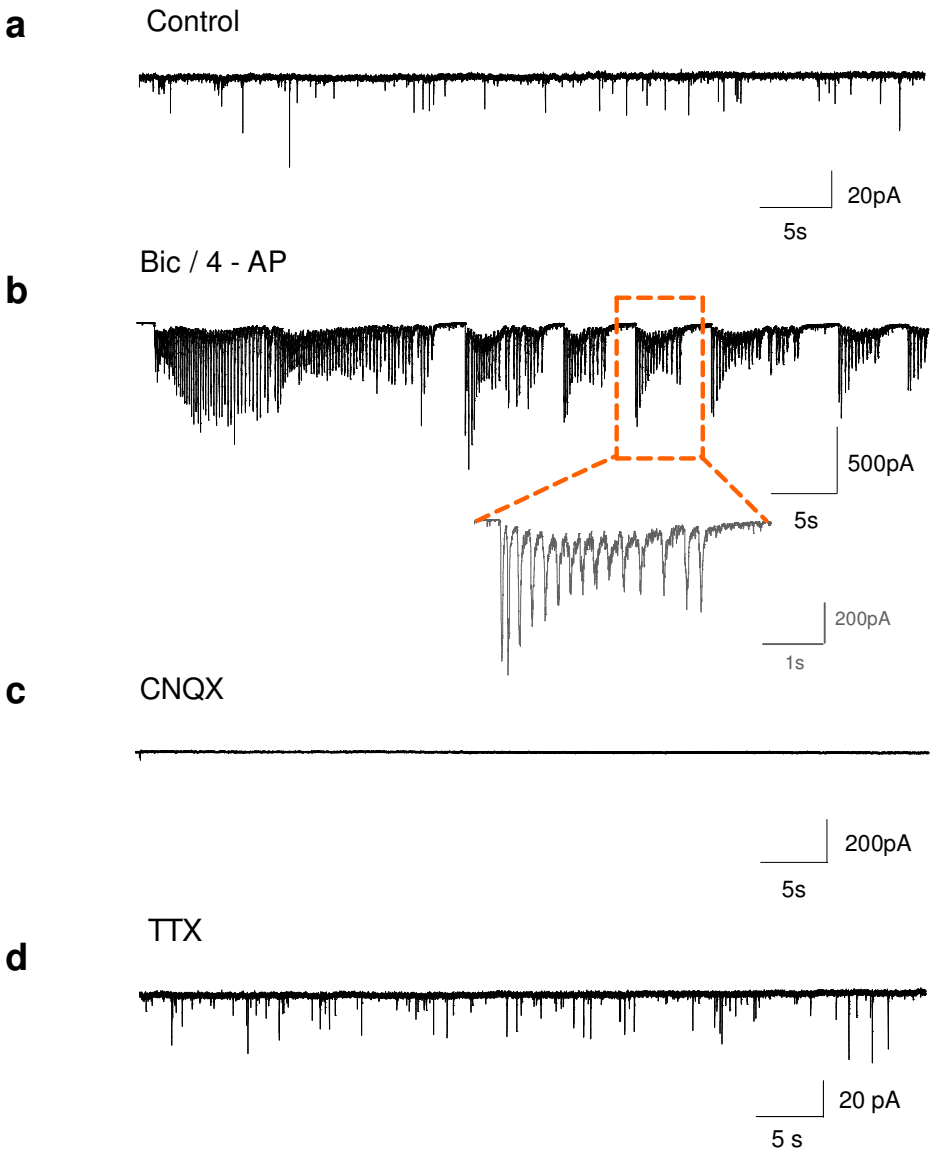

Figure 5. 18 Spontaneous and stimulated activity of a voltage clamped forebrain neuron at DIV10.

Whole cell voltage clamp (-70mV) recording from a GFP transfected forebrain neuron at DIV10. Spontaneous mEPSC like events are evident (a). Simulation by bath application of Bic and 4-AP leads to bursts of inward current (b, and inset). All currents are are terminated by the addition of CNQX (c) and return when CNQX is removed (not shown). Addition of TTX removes large current bursts but mEPSCs remain (d). Data is decimated by 10. Inset traces (grey) show a portion (indicated by an orange box) of the main trace with expanded timebase.

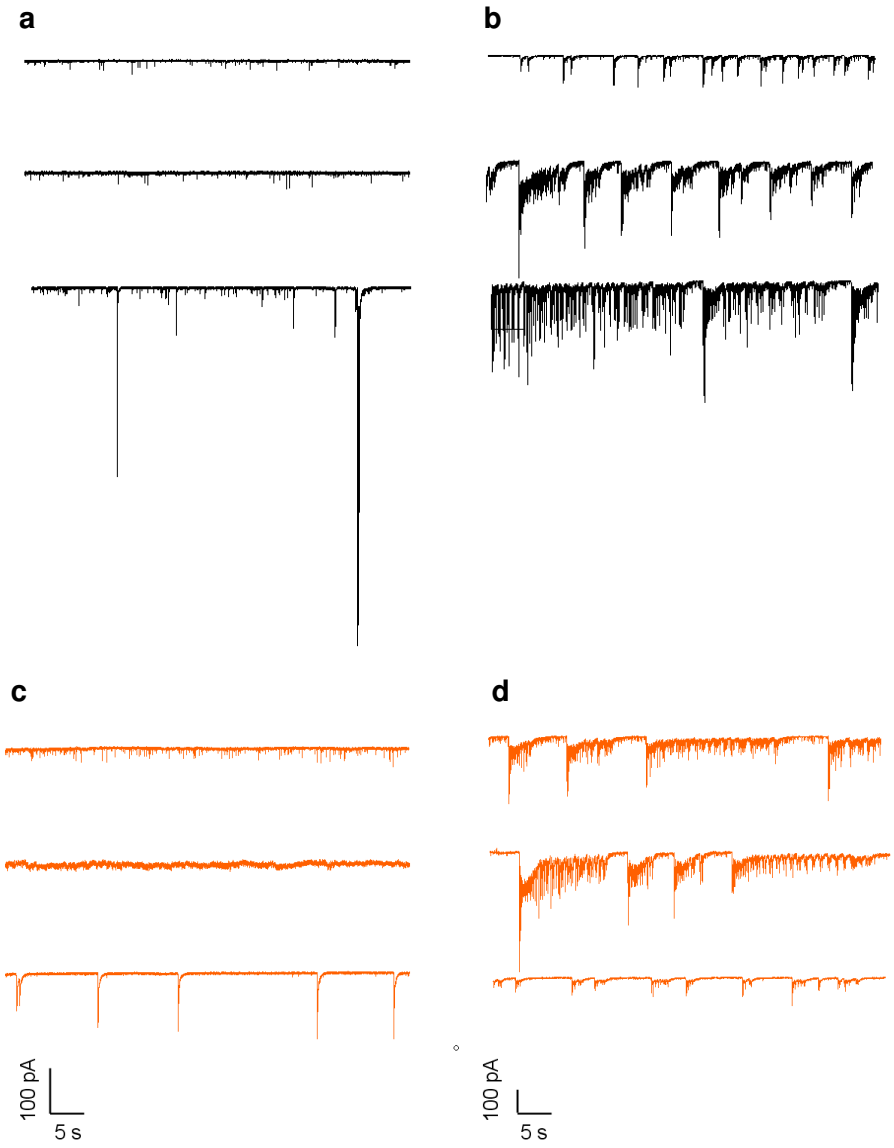

Figure 5. 19 Voltage clamp recordings of spontaneous and stimulated activity from neurons transfected with GFP and SynGAP A-alpha-1.

Representative voltage clamp (-70mV) recordings of spontaneous (left panel) and Bic and 4-AP stimulated (right panel) activity from neurons transfected with GFP only, shown in black (a, b), and SynGAP A-alpha-1, shown in orange (c, d), recorded at DIV10-11. All currents were terminated by the application of CNQX. Note that the y axis scale bar of stimulated traces (b, d) is half that of spontaneous traces (a, c). Data was gathered from four transfections of two separate cultures of forebrain neurons.

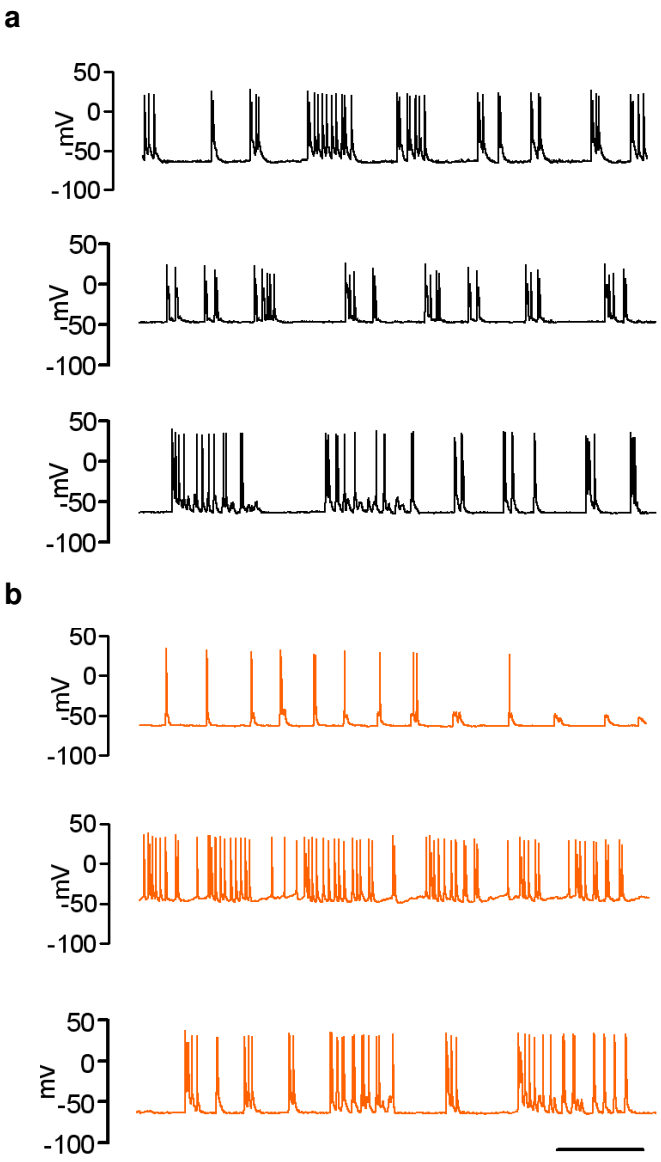

Figure 5. 20 Current clamp recordings from neurons transfected with GFP and SynGAP A-alpha-1

Representative current clamp (0 pA) recordings from neurons transfected with GFP only, shown in black (a), and SynGAP A-alpha-1, shown in orange (b), recorded at DIV10-11. These recordings are from the same cells as shown Figure 5. 19. Data was gathered from four transfections of two separate cultures of forebrain neurons.

5.2.18 NMDA mEPSCs

The conclusion that SynGAP alpha-1 expressing cells are capable of receiving input does not preclude the possibility that spontaneous quantal release from presynaptic cells may be affected. An effective way to test for the release of glutamate is to look for the effect of its receptors activation. Until now I've been looking to the AMPA receptor but presence of NMDA receptor mediated synaptic currents in the presence of TTX would serve as a control to indicate that spontaneous neurotransmitter release was occurring.

In the conditions used to examine AMPA mEPSCs the NMDA receptor is blocked. The hyperpolarised membrane potential (-70 mV) ensures that the voltage dependant Mg^{2+} block of the channel is in place. NMDA receptors do not contribute to the synaptic current under these conditions. However if the membrane potential is held at a positive voltage the Mg^{2+} block is relieved and current can flow through the receptor. Additionally positive membrane potentials are past the reversal potential for the NMDA receptor and so the NMDA current flowing will be reversed to an outward current.

Background noise becomes a problem at positive membrane potentials due to ambient glutamate activating NMDA receptors in a manner unrelated to synaptic release. In order to reduce noise and allow NMDA mEPSCs to be discerned I changed the internal pipette solution from the potassium based solution used in all previous experiments to a cesium based solution (see Methods, p81). Cesium blocks potassium channels reducing total membrane conductance and therefore noise. Using a cesium based internal solution rather than a potassium based internal does not have any effect on the shape of mEPSCs (data not shown). However, recordings made using a cesium based recording solution do have reduced background noise, particularly at positive membrane potentials.

Figure 5. 21 shows representative traces recorded from a GFP expressing neuron voltage clamped at different transmembrane potentials. AMPA mEPSCs are evident at -70 mV, but their amplitude decreases when the cell is held at - 40 mV due to the decrease in electrostatic driving force as the cell is brought closer to the reversal potential for AMPA receptors. Some of the events here may have an NMDA

component as the Mg^{2+} block may be relieved. Outward currents become apparent at positive membrane potentials. The amplitude of these events is greater at + 60 mV than at + 40 mV, again because due to the increase in electrostatic driving force. The long decay time of the events indicates that they are NMDA mediated currents. NMDA mEPSCs have a decay time constant of approximately 250 ms (Jahr and Stevens, 1990).

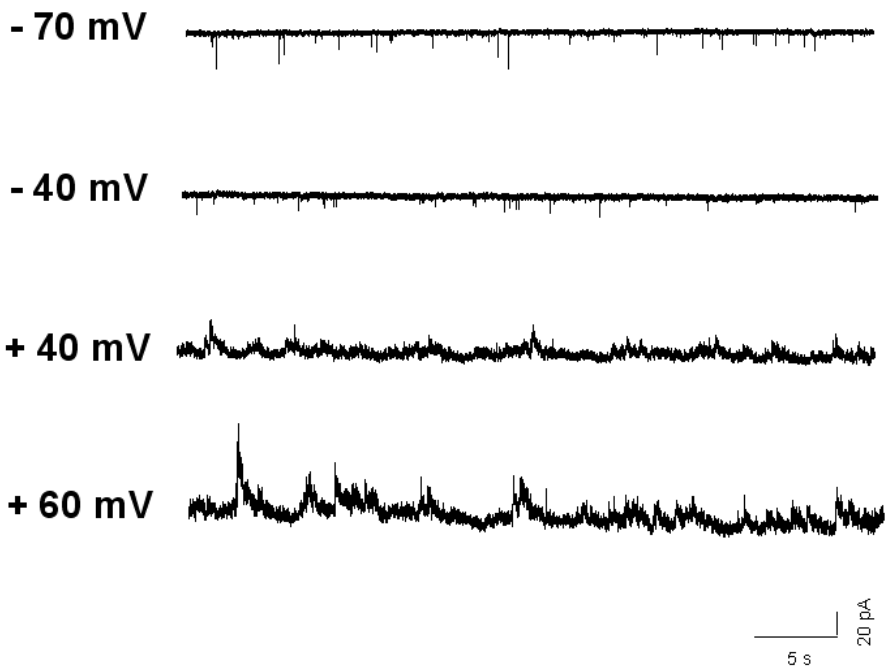

Figure 5. 21 Representative traces from a GFP transfected forebrain neuron voltage clamped at different transmembrane potentials recorded using a cesium based internal recording solution.

Representative traces from a GFP transfected neuron voltage clamped at – 70 mV, - 40 mV, + 40 mV and + 60 mV. In contrast to all previous data these traces were recorded using a cesium based internal recording solution instead of a potassium based internal recording solution. Inward AMPA mEPSCs are evident at - 70 and - 40 mV, outward currents become apparent at + 40 mV but are much clearer as NMDA mEPSCs at + 60 mV. Data is decimated by 10.

NMDA mEPSCs in cells transfected with SynGAP alpha-1

Having shown that NMDA mEPSCs are detectable in control cells with normal AMPA mEPSCs I went on to test if NMDA mEPSCs are also detectable in SynGAP A-alpha-1 expressing cells silent for AMPA mEPSCs. Shown in Figure 5. 22 are two cases of cells transfected with SynGAP A-alpha-1 in which no mEPSCs were present when the cell was voltage clamped at -70 mV. When the cells were held at + 60 mV there were obvious NMDA mEPSCs. I recorded from another two silent cells in which there were indications of NMDA mEPSCs at + 60 mV. There were two silent cells in which there were clearly no NMDA mEPSCs at + 60 mV (Figure 5. 22, lower traces). The NMDA mEPSCs were not analysed but frequency was observed to be very low.

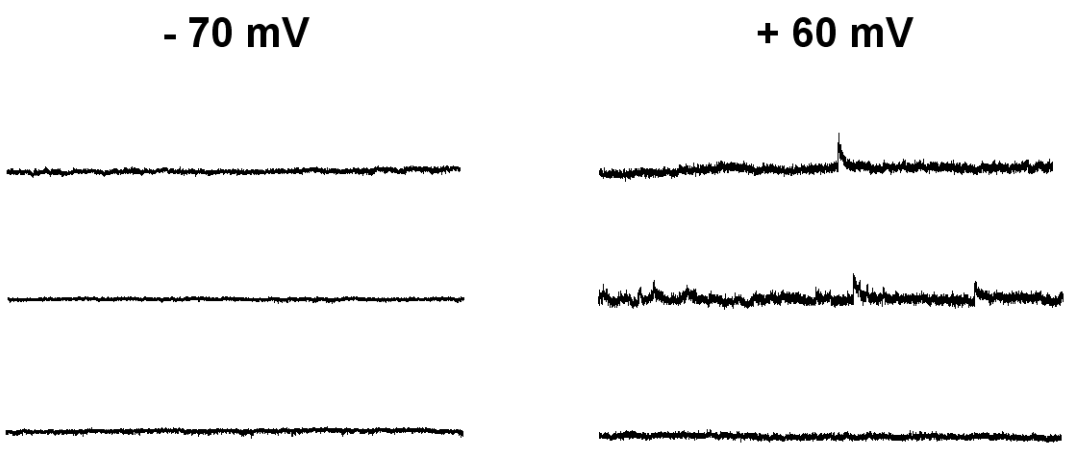

Figure 5. 22 Representative traces from three SynGAP A-alpha-1 transfected forebrain neurons recorded using a cesium based internal recording solution.

Representative traces from three SynGAP A-alpha-1 transfected neurons voltage clamped at – 70 mV (left panel) and + 60 mV (right panel) recorded using a cesium based internal recording solution.

5.2.19 Part Three:

5.2.20 Electrophysiological properties of *SynGAP* $^{-/-}$ neurons overexpressing various SynGAP isoforms.

Part Two has concentrated on the effect of individual SynGAP isoforms expressed on a wild type background. It is not known what SynGAPs are expressed *in vivo* and the presence of these endogenous SynGAPs may confound the effect of activity of the overexpressed isoform. In order to examine to effect their effect in the absence of endogenous isoforms various SynGAPs were transfected into *SynGAP* $^{-/-}$ neurons. This experiment was confined to SynGAP-alpha-1 isoforms, which had varying silencing effects in wild type neurons, and SynGAP A-alpha-2, which did not have a silencing effect.

5.2.21 Silence in SynGAP transfected *SynGAP* $^{-/-}$ cells

The levels of silence observed in cells transfected with SynGAP isoforms is comparable between wild type cells and in *SynGAP* $^{-/-}$ cells (Figure 5. 23 for *SynGAP* $^{-/-}$ data, Figure 5. 11 for wild type data). Silence was observed in 20% of neurons of control *SynGAP* $^{-/-}$ cells. When expressing SynGAP A-alpha-1 80% of neurons recorded from were silent (Figure 5. 23, a). All SynGAP B-alpha-1 cells and 55% of SynGAP C-alpha-1 were silent. No SynGAP A-alpha-2 expressing cells were silent (Chi squared test, $p<0.001$). (Note the lower n numbers for B and C alpha-1).

5.2.22 mEPSC amplitude and frequency in SynGAP transfected *SynGAP* $^{-/-}$ cells

When silent cells are excluded the amplitude and frequency of the recorded mEPSCs of SynGAP overexpressing neurons are no different from control (Figure 5. 23, b, c). However differences become apparent when representative threshold values are included for silent cells (see page , for approach two) (Figure 5. 24). Similar to the case of overexpression in wild type neurons (Figure 5. 16), both mEPSC amplitude and frequency are reduced in neurons overexpressing SynGAP A-alpha-1 (compared to control and SynGAP A-alpha-2). Again, SynGAP A-alpha-2 overexpression has no effect.

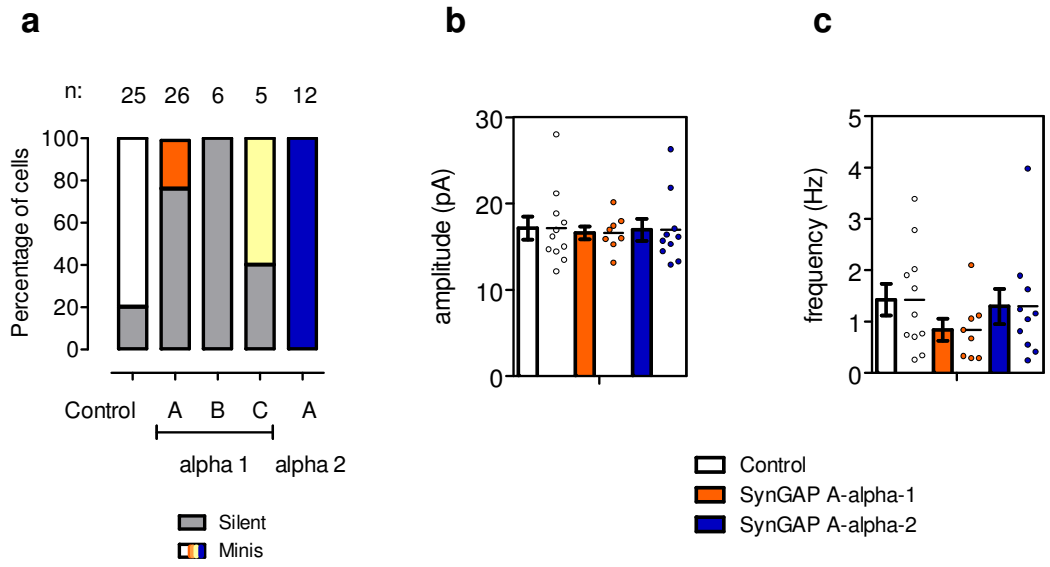

Figure 5. 23 AMPA mEPSCs in *SynGAP* $^{-/-}$ neurons transfected with various SynGAP isoforms.

SynGAP $^{-/-}$ forebrain neurons were transfected with SynGAPs A, B and C -alpha-1 and SynGAP A-alpha-2. (a) Neurons were categorised as either having mEPSCs (upper portion of the bar) or not (silent, lower part of the bar). Data is displayed as a percentage of cells recorded from for each construct. The percentage of neurons categorised as silent is as follows: GFP only = 20%, SynGAP A-alpha-1 = 80%, $p < 0.0001$, SynGAP B-alpha-1 = 100%, SynGAP C-alpha-1 = 55, SynGAP A-alpha-2 = 0%. Population Chi square test, $p < 0.0001$. The total number of cells is displayed above each bar. mEPSC amplitudes (b) and frequencies (c) from a set of non-silent cells were analysed for SynGAP A-alpha-1 (n = 8) and A-alpha-2 (n = 10) . Individual cells' mean mEPSC amplitude is displayed as a scatter plot adjacent to the population mean bar. Data are displayed as mean +/- SEM and are not statistically significantly different, one way ANOVA. Data were gathered from 5 transfections from 3 separate cultures.

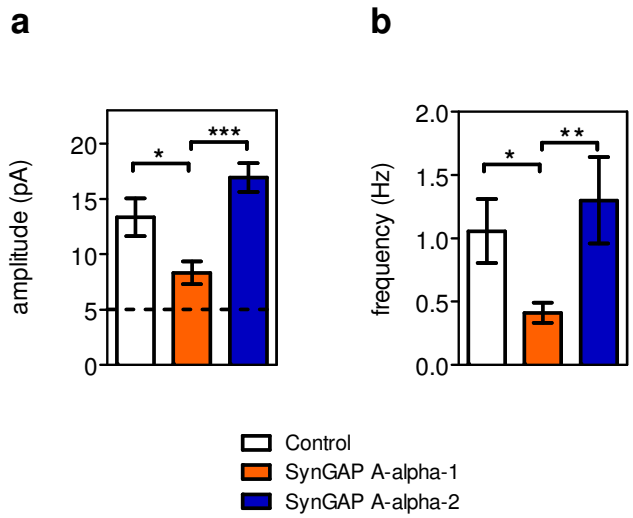

Figure 5. 24 AMPA mEPSCs amplitude and frequency, including silent cells, in *SynGAP* $^{-/-}$ neurons transfected with SynGAP A-alpha-1 and A-alpha-2

SynGAP $^{-/-}$ forebrain neurons were transfected SynGAP A-alpha-1 or A-alph-2. Neurons classified as 'silent' were assigned an amplitude of the detection threshold value (5pA, dotted line) and the frequency of the slowest cell recorded (0.24 Hz) for the purposes of calculating the population mean. a) mEPSC amplitude, one way ANOVA, $p < 0.01$, post hoc Tukey t-tests; Control (13.36 +/- 1.71 pA) Vs A-alpha-1 (20.15 +/- 1.03 pA), $p < 0.05$*; A-alpha-1 20.15 +/- 1.03 pA) Vs A-alpha-2 (16.94 +/- 1.29 pA), $p < 0.001$***. b) mEPSC frequency, one way ANOVA, $p < 0.001$, post hoc Tukey t-tests; Control (1.06 +/- 0.25 Hz) Vs A-alpha-1 (0.41 +/- 0.07 Hz), $p < 0.05$*; A-alpha-1 (0.41 +/- 0.07 Hz) Vs A-alpha-2 (1.29 +/- 0.34 Hz), $p < 0.001$***. Data are displayed as mean +/- SEM. Data were gathered from 5 transfections from 3 separate cultures

5.2.23 Whole Cell Currents in SynGAP transfected *SynGAP* $^{-/-}$ cells

Whole cell currents were recorded from *SynGAP* $^{-/-}$ cells expressing GFP only and SynGAP A-alpha-1 alongside littermate wild type cells (Fig 3.24). The wild type versus *SynGAP*$^{-/-}$ data has been presented earlier in Part One (fig 3.8) where an increase in capacitance in *SynGAP* $^{-/-}$ neurons was reported. The increase in capacitance in *SynGAP* $^{-/-}$ cells is not rescued by the expression of SynGAP A-alpha-1, and consequently neither is a decrease in NMDA receptor current density. The AMPA/NMDA current density ratio is not different between the three groups.

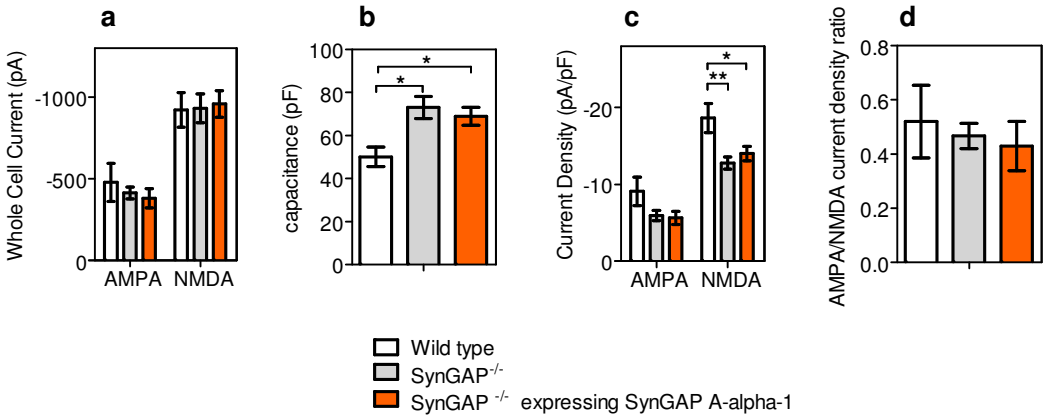

Figure 5. 25 NMDA and AMPA whole cell currents in *SynGAP* $^{-/-}$ neurons transfected with SynGAP A-alpha-1.

(a) Whole cell currents from wild type GFP (n = 6), *SynGAP* $^{-/-}$ GFP (n = 9) and *SynGAP* $^{-/-}$ transfected with SynGAP A-alpha-1 (n = 9). Capacitance is increased in *SynGAP* $^{-/-}$ cells (b), (WT GFP = 50.1 +/- 4.5 pF, *SynGAP* $^{-/-}$ GFP = 73 +/- 5.2 pF, *SynGAP* $^{-/-}$ expressing A-alpha-1 = 69 +/- 4.27 pF, one way ANOVA, p = 0.012, post hoc Tukey t-test, WT GFP vs *SynGAP* $^{-/-}$ GFP, p < 0.05*, WT GFP vs *SynGAP* $^{-/-}$ transfected with SynGAP A-alpha-1, p < 0.05*). (c) NMDA and AMPA current density (pA/pF) is calculated by normalising whole cell currents (pA) to capacitance (pF). NMDA receptor current density is reduced in *SynGAP* $^{-/-}$ cells irrespective of whether they are transfected with SynGAP A-alpha-1 or not (WT = -18.6 +/- 1.9 pA/pF, *SynGAP* $^{-/-}$ = -12.8 +/- 0.8 pA/pF; *SynGAP* $^{-/-}$ transfected with SynGAP A-

alpha-1 = -14 +/- 0.9 pA/pF, one way ANOVA, p = 0.0076, post hoc Tukey t-test, WT GFP vs *SynGAP* $^{-/-}$ GFP, p < 0.01**, WT GFP vs *SynGAP* $^{-/-}$ transfected with SynGAP A-alpha-1, p < 0.05*). (d) The ratio of AMPA receptor current density to NMDA receptor current density. Data are from one culture only, and are displayed as mean +/- SEM. The wild type and untransfected *SynGAP* $^{-/-}$ data are also presented in Figure 5. 8.

5.3 Discussion

5.3.1 Part One:

The object of the work outlined in this chapter was to establish if SynGAP isoforms have differential effects on the electrophysiological properties of neurons. The initial aim was to reproduce a previously published result showing that in the absence of SynGAP AMPA receptor mediated mEPSCs were increased in both amplitude and frequency. This result is consistent with the associated finding of increased mushroom type spines in *SynGAP* $^{-/-}$ neurons (see Chapter One. Figure 1. 3). The envisaged next step was to then express various SynGAP isoforms in *SynGAP* $^{-/-}$ neurons and assess if there was a difference in their ability to rescue the knock out phenotype.

However, in the experiments performed for this thesis, there is no difference between wild type and *SynGAP* $^{-/-}$ mEPSC amplitude or frequency (Figure 5. 4 to Figure 5. 7). Experimental protocol was altered in order to closely adhere to conditions used in the previous work (cultured hippocampal cells in FBS free growth media at 200 neurons/mm^2) but the reported phenotype was not observed. This result is constant in cultures derived from cortical and hippocampal tissue (the areas with the highest expression of SynGAP) (Kim *et al.*, 1998; Barnett *et al.*, 2006), examined at different ages and grown at different cell densities.

5.3.2 Why is there no phenotype in this *SynGAP* $^{-/-}$ mouse?

The question therefore arises, why have I found no phenotype?
Up until this thesis there was no evidence to show that different SynGAP isoforms have opposing effects on synaptic function. Given this information one could easily hypothesise that the removal of all isoforms may have no net effect, thus the lack of phenotype is consistent with the differential effect of different forms. However, other groups have shown a phenotype in the SynGAP $^{-/-}$ and this needs to be discussed.
The first thing to be addressed is to determine if the experimental system is behaving in an expected manner.

Is the neuronal culture behaving as expected?

Morphologically the cultured neurons used are healthy and similar in appearance to other preparations. The electrophysiological criteria for inclusion in experiments include a holding current and noise cut off point which eliminates unstable and compromised neurons.

Electrophysiologically the neurons appear to be normal (Figure 5. 1-Figure 5. 3). Spontaneous action potential driven activity is observed in voltage clamp, often in bursts, indicating that a neuronal network has formed. The action potential driven events are sensitive to TTX leaving small EPSCs which can now be defined as miniature EPSCs (Figure 5. 1). mEPSCs are known to be action potential independent that events arise due to the spontaneous fusion of presynaptic vesicle membranes and the subsequent release of their contents into the synaptic cleft. The mEPSCs are completely abolished by the AMPA receptor antagonist CNQX confirming that they are AMPA receptor mediated events. The mEPSCs observed have the characteristic fast decay time constant (5.7 ms) and fast rise time (1.3 ms). The distributions of mEPSC amplitude, risetime, decay time constant and inter event interval display the expected non-normal distribution with a positive skew in individual cells as well as in the pooled population (Figure 5. 2, Figure 5. 3). There is a wealth of data in the literature showing this distribution of mEPSCs (Jonas et al., 1993); (Bekkers *et al.*, 1990; McBain & Dingledine, 1992; Wyllie *et al.*, 1994)

The mean values for mEPSC amplitude correlate very well with those of other neuronal culture systems in other labs. The mean mEPSC frequency (from 3 Hz to 12 Hz) is occasionally higher than most published values which tend to range from 0.5 Hz to 5 Hz (Kato et al., 2007), (Li et al., 1998), (Rumbaugh et al., 2006) but there are reports of higher frequencies (~ 10 Hz) (Fu et al., 2007) . Indeed the control frequency published by (Vazquez et al., 2004) is exceptionally low at 0.2 Hz. All electrophysiological experiments were performed on cultures maintained without FBS and so have low levels of glial cells. One could suggest that the high variability of mEPSC frequencies observed could be due to the variability of modulation of neurotransmitter release by astrocytes (Fiacco & McCarthy, 2004; Perea & Araque, 2007).

Amplitude is observed to correlate with neither decay time constant nor risetime indicating that the large variation in mEPSC amplitudes is not due to differential filtering of events located at a range of distances from the soma.

Taken together the characteristics described above indicate that the tissue culture system is functioning as expected. Indeed the behaviour of the neurons is remarkably reflective of that *in vivo* despite the absence of cytoarchitecture and environment.

Protocol, analysis or test material?

The absence of a reported phenotype then must be due to differences in protocol, analysis or test material. In the previous chapter I also discussed possible reasons for the absence of phenotype in the *SynGAP* $^{-/-}$ mouse, these reasons remain unchanged so some repetition here is unavoidable.

Protocol

To address protocol, I have previously stated how experimental conditions were manipulated in order to replicate conditions in which a *SynGAP* $^{-/-}$ phenotype were observed. Initially cortical neurons were used, then hippocampal when no phenotype was seen, then low density when no phenotype was seen at high density. All these experiments were performed in the absence of FBS and at different DIV. Clearly variation in experimenter may also be implicated but beyond strict adherence to protocol this cannot be controlled for. If the phenotype was subtle it is plausible that slight alterations in experimental technique could perturb the outcome, however the published results indicate a 70% increase in amplitude and a 150% increase in frequency (Vazquez et al., 2004).

Analysis

Disparity in methods of analyses can lead to divergent conclusions from the same data set. How do I know that the method of analysis used here is not masking a real difference that exists in the data? To address this I went beyond merely calculating the mean mEPSC amplitude, and looked also at the distribution of the pooled event population (Figure 5. 6) and the maximum amplitude mEPSC per cell (Figure 5. 7). An alteration in these parameters would signify a change in a subset of synapses

that could be missed by looking at the mean only. Nevertheless, the resemblance of the distribution of wild type to *SynGAP* $^{-/-}$ events is striking and there is no difference in the maximum mEPSC amplitude attained by the individual cells.
The method of analysis of individual events is a manually overseen semi automated fitting of the waveforms which is performed blind. The inhouse programme is internally consistent and the rare case of a misfitting is manually corrected. Therefore I am satisfied that if a difference were present it would be exposed.

Test material : the *SynGAP* $^{-/-}$ mouse

A richer seam of conjecture lies in the existence of different mouse models of *SynGAP* $^{-/-}$. The differences between the models and the possible reasons that these might cause differences in phenotype to arise have been outlined in detail in the discussion of Chapter 4 (p160). In this Chapter I have begun to address an additional concern regarding our knock out model.

SynGAP 'B-shift' in the SynGAP $^{-/-}$ *mouse?*

As detailed in Chapter One we have cloned a novel *SynGAP* transcript that includes a 4 bp insertion at the end of the last *SynGAP* B specific exon. This insertion causes a frameshift mutation that would lead to the expression of a truncated form of SynGAP. Due to the more downstream integration point in the Grant mouse the entire coding region of this putative truncated SynGAP is present in the knockout mRNA transcript. The transcripts in the Kennedy and Huganir mice on the other hand would not contain the full coding sequence for what we have termed SynGAP B-shift.

It is conceivable, but unlikely, that SynGAP B-shift might be expressed and in some way affect the penetrance of the knock out phenotype. Quite separately, it is possible that SynGAP B-shift is expressed and does have a function but its presence in the *SynGAP* $^{-/-}$ mouse is unrelated to the lack of phenotype. It may not be expressed at all, or if expressed, it may produce a non-functional peptide.

Unfortunately, there is no antibody against epitopes of the SynGAP B-shift peptide so we cannot test for its existence. Therefore we do not know if it is present in the wild type case or in the *SynGAP* $^{-/-}$ mouse. I have attempted to address the

question of whether or not SynGAP B-shift has any function by transfecting wild type neurons with *SynGAP* B-shift and assessing the effect on AMPA mEPSCs (Figure 5. 10). The mEPSC amplitude and frequency are no different in *SynGAP* B-shift transfected cells compared to control cells. We can conclude regrettably little from this outcome, other than that SynGAP B-shift does not have a strong effect on AMPA receptor presence at synapses when overexpressed in a neuron that contains all the normally expressed SynGAPs. Ideally, the creation of a specific antibody would allow us to determine if SynGAP B-shift exists, if it exists in the knockout and therefore if this line of investigation is worth pursuing. In the absence of an antibody one could create a tagged SynGAP B-shift and assess if in cultured *SynGAP* $^{-/-}$ cells it is able to reach synapses as an indication of potential synaptic function.

At this time however discussion of a putative peptide's potential role in the non-existence of a phenotype is mere speculation.

5.3.3 Total receptor expression in *SynGAP* $^{-/-}$ neurons

It is clear that the *SynGAP* $^{-/-}$ neurons used here do not exhibit altered synaptic content of AMPA receptors. However mechanisms do exist whereby synaptic and extra-synaptic AMPA receptor content is differentially regulated (to be further discussed later in this chapter, p227). To assess the total cell surface receptor content I bath applied AMPA and NMDA in saturating quantities in order to activate all available receptors (Figure 5. 8). Previous work has shown that SynGAP effects AMPA receptor, but not NMDA receptor, trafficking and my finding of no difference between the whole cell currents elicited by NMDA application supports this view. I find no difference in the currents elicited by AMPA application, agreeing with my finding of no difference in AMPA mEPSCs. As I have discussed, my AMPA mEPSC finding is in opposition to previously published results, however total AMPA receptor surface expression has not been functionally assayed in any other *SynGAP* $^{-/-}$ mouse [10]. It would be interesting to see if, in *SynGAP* $^{-/-}$ mice with mEPSC defects,

[10] Quantification of cell surface expression of puncta of certain AMPA receptor subunits have been examined by immunocytochemistry (Kim et al., 2003) and electrophysiological assessment of AMPA receptor function has been confined to synaptic assays (Komiyama et al., 2002; Rumbaugh et al, 2006).

total cell surface AMPA receptor expression is affected or if the effect is specific to synapses.

5.3.4 Cell size

One surprising difference between wild type and *SynGAP* $^{-/-}$ neurons is that I found *SynGAP* $^{-/-}$ neurons have higher capacitance indicating that they are larger (Figure 5. 8, c). This is a highly unexpected result that has not been previously described. It has been shown that *SynGAP* $^{-/-}$ pups, while they appear similar at birth, do not grow and are often smaller than wild type littermates (Knuesel et al., 2005; Porter et al., 2005) however making a comparison between animal size and the size of a cell in a dish is no doubt fallacious.

To further investigate the result of higher capacitance in *SynGAP* $^{-/-}$ neurons I turned to GFP transfected fixed tissue which allowed the use of different techniques of cell size analysis to determine if the effect was real. Measurement of GFP expression neuron's soma area in epifluorescence microscopy images indicated there was no difference in size between wild type and *SynGAP* $^{-/-}$ neurons (Figure 5. 9). Counting the numbers of projecting neurites in young cultures (DIV 5) also suggested there was no difference in the early outgrowth of neurons. The difference in electrophysiological capacity therefore was not mirrored by morphological analysis. Additional experiments are required, the capacitance result comes from one culture only, but we could suggest that *SynGAP* $^{-/-}$ neurons respond differently to the extracellular recording solution. Perhaps they are more sensitive than wild type neurons or more prone to swelling. If this is the case the affect is not strong enough for it to influence the health of the neurons as assayed by electrophysiological criteria (holding current, noise) or morphology, as these parameters are unchanged between wild type and knock out. Kneusel et al have shown increased neuronal apoptosis in brains of *SynGAP* $^{-/-}$ mice (Kennedy) but I do not see differential rates of cell survival in culture (Figure 4. 3).

Although whole cell AMPA and NMDA currents are unchanged in *SynGAP* $^{-/-}$ neurons, because the capacitance is increased, the current density (that is the whole cell current normalised to capacitance) of the NMDA current is significantly decreased in *SynGAP* $^{-/-}$ neurons (Figure 5. 1, d). SynGAP has never been shown to affect the NMDA receptor and it should be pointed out that AMPA receptor current

density also displays a trend toward reduction (p = 0.083) and that statistical significance would likely be reached if additional experiments were performed. Despite this the ratio of NMDA to AMPA receptor current density is unchanged between wild type and *SynGAP* $^{-/-}$

From this set of experiments we can conclude that in the mouse model investigated here the absence of SynGAP does not affect synaptic or extra-synaptic expression of AMPA receptors. To reiterate, the finding of no phenotype in the case where different isoforms have opposing functions is internally consisitent and could potentially render the appearance of a phenotype more sensitive to the factors discussed above (5.3.2).

5.3.5 Part Two:

Although the initial aim of this project was to overexpress individual SynGAP isoforms in *SynGAP* $^{-/-}$ cells the absence of a knock out phenotype for a large part invalidates the rational for that experiment. Although there are clear advantages to that approach (Part Three is concerned with SynGAPs expressed in knock out cells) the difficulty in obtaining *SynGAP* $^{-/-}$ tissue lead me to perform a majority of overexpression experiments in wild type neurons.

5.3.6 Silent cells

The most striking finding is that a large portion of neurons overexpressing SynGAPs that terminated in the 'alpha-1' C-terminal tail entirely lacked AMPA mEPSCs (Figure 5. 11). While a depressing effect on mEPSCs has been demonstrated previously for SynGAP alpha-1 no one has ever looked at the effect of the N-terminus on the functionality of the C-terminus. Here I show that the extent of this mEPSC 'silencing' phenomenon is dependent on which N-terminal variant the alpha-1 was linked to. SynGAP A-alpha-1 had the strongest silencing effect and SynGAPs B and C-alpha-1 had a milder silencing affect. In stark contrast to the silencing effect of alpha-1 isoforms the alpha-2 isoforms did not increase the percentage of silent cells from control values.

Previous work examining the effect of SynGAP overexpression has been confined to only one isoform, SynGAP C-alpha-1. When Rumbaugh et al. (2006) overexpressed an N-terminally linked GFP fusion SynGAP C-alpha-1 they observed a 50% decrease in mEPSC amplitude and an 85% decrease in mEPSC frequency. No mention is made of the proportion of neurons that did or did not have mEPSCs. Mutation of the last residue of the protein (QTRV/E), part of the PDZ binding domain, removed the ability of SynGAP to decrease mEPSC amplitude and frequency. The PDZ binding domain has been shown to be crucial for SynGAP's association with the scaffolding protein PSD-95, and for its ability to rescue the knock out dendritic spine phenotype (Kim *et al*., 1998; Vazquez *et al*., 2004). Therefore my finding that the SynGAP alpha-1 isoforms have a depressing affect on mEPSCs is not surprising. Additionally, the lack of a depressing effect in the absence of a PDZ binding domain is repeated here with the PDZ binding domain lacking SynGAP alpha-2 isoforms.

What is surprising is the nature of the depressing effect. I observe a large proportion of neurons to completely lack mEPSCs, a phenomenon which has certainly not been reported in the case of SynGAP overexpression, and one which is rarely, if ever, reported in the literature. It is possible that the 'silent' cells do have mEPSCs but that they are of an amplitude that falls below the detection threshold (5pA). Indeed, in one of the rare cases in which a manipulation has lead to the absence of mEPSCs, cerebellar granule cells expressing a mutant form of the TARP stargazin, the authors designate the detection threshold level to every cell in which no mEPSCs were observed (Milstein & Nicoll, 2009). It would be illuminating to know how often 'silent' cells are encountered in the cell preparations used by other labs, and if treatments which are reported to decrease mEPSC amplitude and frequency also increase the proportion of silent cells. It would appear however that cells which lack mEPSCs are often discarded and not included in analyses.

5.3.7 Effect of SynGAP overexpression on mEPSCs

I decided to examine the data in two ways; the first of which entailed ignoring the silent cells and examining the data that was derived from the non-silent cells only (Figure 5. 9); the second approach approximated that of Chen et al. (2000) and

Milstein et al. (2009) and involved assigning a threshold value for amplitude and frequency to the silent cells to allow them to contribute to the population mean (Figure 5. 16).

Under the first approach, despite the obvious differences in silencing, mean mEPSC amplitudes do not differ between control and SynGAP expressing neurons (one way ANOVA, post hoc Tukey t-tests). The decrease in statistical power due to multiple comparisons is obvious as a single t-test indicates a statistically significant decrease in SynGAP A-alpha-1 from control values. There are however clear differences between mean mEPSC amplitudes of SynGAP alpha-1 expressing neurons compared to SynGAP alpha-2 expressing neurons again indicating differential function for the C-termini (Figure 5. 12).

Under the second approach, where a threshold value was included for silent cells, a clearer picture emerges (Figure 5. 16). Expression of any alpha-1 isoform leads to a reduction in mEPSC amplitude and frequency while the magnitude of the decrease is dependent on the N-terminus. There is a noteworthy disparity in the effect of expression of the alpha-2 isoforms; SynGAP A-alpha-2 has no effect on mEPSC amplitude or frequency, but SynGAPs B and C-alpha2 induce an increase in mEPSC amplitude, with SynGAP B-alpha-2 also increasing the mEPSC frequency.

Some may not agree with the strategy of including threshold values for cells which essentially have no value but it does allow all the recorded cells to be represented together. As long as it is clear that the means resultant from this approach do not signify absolute values, but are rather a comparative representation, I believe this method is valid.

Closer examination exposes more subtle differences between the populations of mEPSCs recorded from SynGAP expressing neurons (Figure 5. 13, Figure 5. 14). Looking at the event distribution the six SynGAP isoforms seem to fall into three categories; SynGAPs A-alpha-1 and B-alpha1 which decrease mEPSC amplitudes; SynGAPs C-alpha-1 and A-alpha-2 which have little effect on mEPSC amplitudes; SynGAPs B-alpha-2 and C-alpha-2 which increase mEPSC amplitudes. These classifications closely resemble the isoforms' effect on population mean (approach

two) adding support to the argument that using a threshold value for a silent cell is a valid approach to communicating the data.

The data outlined above are the first indication that SynGAP alpha-2 isoforms may have a distinct role at the synapse other than merely lacking the functionality of alpha-1 isoforms. It is also the first example of a role for the N-terminus of SynGAP, which has previously been entirely neglected in the literature.

We could speculate that SynGAP alpha-2 contains in its unique regions moieties that specify a function whose effect is the opposite of SynGAP alpha-1. The role of the N-termini seems to be to modulate the function determined by the C-terminus. SynGAP A-alpha-1 has the strongest effect, in terms of silencing and reduced mEPSC amplitude and frequency but SynGAP A-alpha-2 has no effect. Perhaps SynGAP A enhances the alpha-1 function but when combined with alpha-2 works to mitigate its effect. As outlined in the Introduction to this thesis SynGAP has been demonstrated to operate as a RapGAP as well as a RasGAP (Kim *et al.*, 1998; Krapivinsky *et al.*, 2004) and we hypothesise that the different termini may determine which function it performs. Sequences outside the GAP domain can be essential for the bifunctionality of Ras/RapGAPs (Kupzig et al., 2006). As Pena and co-workers (2008) demonstrated the presence of the N-terminal C2 domain is necessary for SynGAP to function as a RapGAP, while the isolated GAP domain predominantly acts as a RasGAP. Therefore there is precedent for suggesting the N-termini could have a strong effect on SynGAP function.

5.3.8 Synaptic and extra-synaptic AMPA receptors

What of the finding of no difference in whole cell AMPA elicited currents in SynGAP alpha-1 cells, a large proportion of which were ‘silent’? Should we expect that, because synaptic AMPA receptor content is altered that total cell surface expression should also have changed? Probably not, while circumstances that alter both synaptic and total receptor levels are common, so are situations that can alter either independently.

Clearly, physiological processes analogous to LTP and LTD require the rapid movement of AMPA receptors into and out of specific synapses. This redistribution

can involve, but is not limited to an interior-surface transition mediated by exocytosis and endocytosis (Passafaro et al., 2001). In addition to this mechanism lateral diffusion from extra-synaptic to synaptic sites been shown to play a major part (Ehlers *et al.*, 2007). Additionally, the process of synaptic scaling involves the strengthening or weakening of synapses without changing the relative strength of individual synapses and is accompanied by a change in total surface AMPA receptors (O'Brien *et al.*, 1998; Turrigiano *et al.*, 1998; Shepherd *et al.*, 2006)

Manipulations which alter both surface and synaptic expression have been shown by a number of groups; (Fu et al., 2007) have shown how overexpression of a constitutively active form of Rap2 leads to a decrease in mEPSC amplitude and a decrease in cell surface expression of GluR2. Similarly, the Arc/Arg3.1 knock out mouse has increased surface expression of GluR1 and increased mEPSC amplitude and frequency (Shepherd *et al.*, 2006).

The decorrelation of surface and synaptic expression can occur in a number of ways; there can be large changes in total AMPA receptor without changes becoming apparent at the synapse (overexpression of the TARP stargazin, (Schnell et al., 2002) the GluRA $^{-/-}$ mouse, (Zamanillo et al., 1999); an increase in synaptic AMPA receptors while total surface expression stays constant (overexpression of PSD-95, (Schnell et al., 2002)); or even an increase in total surface expression combined with a decrease in synaptic receptors (overexpression of the beta, but not the alpha, isoform of SAP97, (Rumbaugh et al., 2003; Waites et al., 2009)).

Evidence particularly relevant to SynGAP and our central hypothesis has come from the group that initially demonstrated Ras' involvement with AMPA receptor delivery and Rap's role in AMPA receptor removal. A recent paper has shown that the Ras/Rap controlled trafficking can be mediated by the shuttling of AMPA receptors from a peri-synaptic 'deliverable pool' into the PSD (Kielland *et al.*, 2009). This 'deliverable pool' resides near the PSD (~30–100 nm from the postsynaptic membrane) in the cytosol or on the plasma membrane.

Different mechanisms therefore can regulate surface delivery and synaptic delivery, and it seems from the evidence presented here that SynGAP may regulate the latter rather than the former. Many papers in the literature refer to SynGAP's role in

AMPA receptor trafficking but do not specify or examine the distinction between surface and synaptic trafficking. As mentioned previously all evidence showing altered AMPA receptor trafficking has been focused on synaptic responses or synaptic 'puncta'. The only study which has specifically addressed the insertion of new AMPA receptors into the plasma membrane focused its attention on GluR1 'clusters', presumptive synapses. The authors overexpressed SynGAP C-alpha-1 and found a decrease in newly inserted GluR1 cluster area, density and intensity of staining, but no change in total synapse number, as indicated by Bassoon and NR1 puncta (Rumbaugh *et al.*, 2006). Contrary to my finding, this work implies SynGAP's role is in regulating the surface insertion of AMPA receptors but is not conclusive as total and extrasynaptic expression are not addressed and only one AMPA receptor subunit is examined.

5.3.9 A presynaptic mechanism for decreased mEPSCs ?

Another potential explanation suggested for the decrease in mEPSCs is that presynaptic release sites had been affected by the postsynaptic expression of SynGAP. This scenario could arise if SynGAP was able to exert some kind of retrograde effect on the presynaptic termini. The secreted neurotrophin BDNF's effect of increasing post synaptic mEPSC frequency by modulating presynaptic release probability is a classic example of this type of mechanism (Li et al., 1998) (Stoop & Poo, 1996). While it is obvious how a secreted molecule can assert its influence on a neighbouring neuron the mechanism by which a cytosolically confined protein may accomplish this is less immediately clear. Nevertheless it may be possible that overexpression of SynGAP could influence, for example, extracellular matrix or cell adhesion molecules (CAMs) or their receptors, which in turn could cause changes in the presynaptic neuron. Cell adhesion molecules have been shown to be key players in trans-synaptic communication and can precisely coordinate presynaptic differentiation with postsynaptic specialization. At glutamatergic synapses, their retrograde signaling has been proposed to control presynaptic vesicle clustering at active zones. Several trans-synaptic adhesion systems that promote the formation and maturation of synapses have been identified including ephrin/Eph receptors, neuroligin/neurexins, SynCAMs and cadherins (Stan et al.) (Klein, 2009). For example the postsynaptic overexpression of the dominant negative form of synaptic cell adhesion molecule, SynCAM, reduces

the number of recycling synaptic vesicles (as visualised by FM dye puncta) in presynaptic neurons (Biederer et al., 2002) and overexpression of its functional form increases mEPSC frequency (Sara et al., 2005).

Intriguingly the overexpression of post synaptic scaffolding molecules, PSD-95 (El-Husseini et al., 2000), Shank (Sala *et al.*, 2001), SAP97 and SAP102 (Regalado et al., 2006) can all induce enhanced presynaptic function. The mechanisms by which they do so have not yet been fully elucidated. The molecules 'upstream' of the scaffolding molecules which constitute the reverse signalling component are likely to be CAMs. In the case of SAP 97 interference with N-cadherin, integrin, and ephrinB/EphB all effects its ability to modulate presynaptic function.
There must be molecules downstream of the scaffolding molecules which mediate signalling in the conventional direction. In the case of SAP 97 PDZ domains were shown to be essential but the downstream binding molecules which presumably mediated the effect were not identified.

Many of these adhesion molecules interact strongly with scaffolding molecules containing PDZ domains, to which SynGAP alpha-1 binds, suggesting a potential mode of action (Yamagata et al., 2003). CAM interacting PDZ proteins which have been shown to bind to SynGAP alpha-1 include PSD-95 and MAGI-1/ S-SCAM (neuron specific synaptic scaffolding molecule) which bind to neuroligins (Irie *et al.*, 1997; Hirao *et al.*, 1998) (SynGAP interaction with MAGI-1/S-SCAM, Noboru Komiyama, personal communication).

An interaction between GTPase-activating protein spine-associated RapGAP (SPAR) and the EphA4 receptor intracellular tail is required to mediate EphA4-dependent inactivation of Rap1 and Rap2 and subsequent growth cone collapse (Richter et al., 2007). In turn Rap1 (but not Rap2) inactivation is required for ephrin-A-dependent downregulation of integrin-mediated adhesion in neuronal cells. This highlights a potential mechanism of a transynaptic effect whereby post synaptic protein activity alters the surface expression of molecules involved in trans-synaptic adhesion.

The mechanism by which neuroligin binding to its presynaptic partner protein, beta neurexin, induces synapse maturation is unclear, but it is thought to trigger both

presynaptic and postsynaptic signal transduction events that activate synaptic function and specify synaptic properties. The ability of postsynaptic neuroligins to regulate presynaptic maturation has been shown to be dependent on an intact neuroligin intracellular domain (Wittenmayer et al., 2009).

Taking the above points into consideration it is perhaps not so far fetched that SynGAP alpha-1 could effect presynaptic release. However, increasing input onto a SynGAP alpha-1 overexpressing neuron by stimulating excitatory activity in the neural network shows that these neurons are in fact able to receive input from neighbouring neurons and therefore are unlikely to be subjected to greatly impaired presynaptic release (Figure 5. 19). In fact they are able to respond normally to it, as is indicated by their ability to fire normal action potentials (Figure 5. 20). It remains possible that action potential driven release is normal, while non-action potential quantal release is impaired. The observation that SynGAP A-alpha-1 expressing neurons do have NMDA mEPSCs shows that quantal release can occur onto these neurons, but still appears to not be as common as in the control case (Figure 5. 22). It is therefore possible that modulation of presynaptic release is part of the mechanism by which SynGAP alpha-1 decreases mEPSCs.

5.3.10 AMPA receptors are present at the synapses of SynGAP alpha-1 expressing neurons; silent synapses vs silent cells

The working hypothesis after finding a decrease in mEPSCs but no change in whole cell currents was that overexpression of SynGAP alpha-1 had caused the removal of AMPA receptors from synaptic to extra-synaptic sites. If a synapse lacks AMPA receptors, but contains NMDA receptors, it is defined as a silent synapse (Isaac *et al.*, 1995; Liao *et al.*, 1995; Kerchner & Nicoll, 2008) p189). However, the lack of mEPSCs in SynGAP A-alpha-1 expressing neurons is not due to an increase in silent synapses because this set of experiments (Figure 5. 19-Figure 5. 22) shows, crucially, that there are AMPA receptors at the synapses of neurons overexpressing SynGAP-alpha-1 isoforms. All inward currents recorded from these cells were entirely terminated by the application of the AMPA receptor antagonist CNQX.

Figure 5. 19 (c, middle trace) includes an example of a SynGAP A-alpha-1 neuron that would be classified as silent, but when neighbouring neurons fired was able to normally receive AMPA receptor mediated current influx (d, middle trace. (See below for a footnote an a technical aspect of this experiment,[11].) The finding that there are receptors at the synapses necessitates a refinement of the synaptic / extra synaptic argument. We can no longer argue that the effect of SynGAP-alpha-1 overexpression is to drive AMPA receptors from synaptic (a depression of mEPSCs) to extra-synaptic sites (unchanged whole cell AMPA currents) therefore we must consider a more nuanced perspective.

When we stimulate current influx are we seeing the activation of peri-or extra-synaptic AMPA receptors? Is it possible there is glutamate spillover, comparable to the case in stroke where extra-synaptic NMDA receptors become activated and lead to cell death (Hardingham et al., 2002)? Again this is doubtful as extrasynaptic AMPAR activation, unlike NMDA receptors, is probably absent or less common at most central synapses owing to their much lower glutamate affinity (Lisman & Raghavachari, 2006) and the low concentrations of extracellular glutamate (Herman & Jahr, 2007).

Subsynaptic AMPA receptor localistation

Now we have considered extrasynaptic and perisynaptic localisation we must consider subsynaptic localisation. Spontaneous neurontransmitter release and trains of action potential mediated neurotransmitter differ hugely in the amount of neurotransmitter released into the synaptic cleft. Accumulated evidence suggests that single quantal release is insufficient to saturate postsynaptic receptors and due

[11] Ideally this experiment would have been done slightly differently; I would have assessed if each neuron was 'silent' before recording spontaneous and stimulated activity. However, mEPSCs (TTX present) were not recorded at the beginning of the experiment due to the difficulty of washing out TTX and the concern that residual TTX would have impaired the bursting activity of the neurons. mEPSCs were recorded at the end of each stimulation (data not shown) but at this time the neurons had undergone extensive firing and it is possible that the quantal release likelihood had changed. If this were the case the 'silence' data would not have been directly comparable to that outlined in Figure 5. 11. The purpose of the experiment was to assess if SynGAP expressing cells were capable of receiving presynaptic input, and the conclusion that they are is unaffected by not being able to establish a relationship between mEPSC silence and spontaneous or stimulated EPSC activity.

to their relatively low affinity for glutamate only a subpopulation of AMPA receptors in the PSD are believed to be close enough to the site of vesicle fusion to respond to neurotransmitter (Liu *et al.*, 1999) (McAllister & Stevens, 2000; Raghavachari & Lisman, 2004). Therefore, in addition to the absolute number of glutamate receptors inside synapses, packing density and the subsynaptic localisation of AMPA receptors are crucial components of their signalling capacity.

Microdomains

Both EM images and single-particle tracking experiments support restricted spatial domains within the postsynaptic membrane. For example, the mobility of individual AMPA receptors is confined within subregions of the synaptic membrane and becomes more confined when the synapse is active (Ehlers *et al.*, 2007). EM studies show the presence of proteinaceous clumps and voids in isolated PSDs and the nonhomogeneous clustered distribution of AMPA receptors (Petersen et al., 2003) (Masugi-Tokita et al., 2007). It is conceivable therefore that AMPA receptors may be present in PSDs, and activatable upon bulk exocytosis of neurotransmitter, but that those not directly aligned with release sites are not exposed by spontaneous release.

Determining the impact of receptor packing density and subsynaptic confinement remains a difficult experimental problem. A recent study provides clues as to how the spatial positioning and density of glutamate receptors can be established inside the PSD (Blanpied et al., 2008). Using high-resolution optical tagging of PSD subregions, it was found that the PSD-95 behaves as a topologically stable matrix with very little internal molecular movement, although the overall structure of the matrix is plastic and flexible. By stretching or compressing the PSD-95 matrix, actin-based elasticity of the PSD might enable glutamate receptors to become locally concentrated without the need for adding or removing receptors but allowing them to align with release sites of the presynaptic active zone. This effect that could have a large influence on postsynaptic responses to released glutamate. Indeed, reducing AMPA receptor surface mobility by antibody cross-linking alters postsynaptic responses to trains of action potentials, indicating that small-scale positioning and lateral movement of AMPA receptors tune synaptic strength (Heine et al., 2008).

Discussion of the role of microdomains and packing density in relation to SynGAP is especially tempting for a number of reasons. First; total AMPA receptor number appears unchanged in SynGAP alpha-1 overexpressors despite decreases in AMPA mediated mEPSCs, therefore its mechanism of trafficking seems to be limited to surface rearrangements. Second; SynGAP alpha-1 overexpressing neurons do have AMPA receptors at the synapses but these are often not activated by quantal release indicating a very fine rearrangement of receptors. Third; overexpression of SynGAP alpha-1, despite its effect on mEPSCs, does not dramatically change dendritic spine morphology but changes in gross spine morphology would not necessarily be expected if effects were limited to within subdomains of the PSD (Figure 4. 8). Fourth; the elasticity of the PSD is based on a remodelling actin network and SynGAP alpha-1 has been shown to regulate the activity of the F-actin severing protein cofilin.

5.3.11 Part Three:

SynGAP A, B and C-alpha-1 and SynGAP A-alpha-2 were chosen to be expressed in knock out tissue in order to ascertain if their effect was the same once the potentially confounding effect of endogenous SynGAP was removed (Figure 5. 23 - Figure 5. 25). We considered this confounding effect a possibility especially in the case of SynGAP A-alpha-2, which unlike the other isoforms tested, has no influence on the proportion of silent cells or on the profiles of the mEPSCs recorded. The similarity of this data to that derived from expression in wild type tissue indicates that the endogenous expression of a range of undefined SynGAP isoforms should not be a major concern in the interpretation of the data.

5.3.12 Variability in the mEPSC data

One technical point to note is regarding variability of the data. This point applies to neurons of the transgenic *SynGAP* line (wild type and knock out) but not wild type neurons from wild type only cultures as these are of slightly different genetic background strain. The data presented in experiments when neurons were transfected with GFP (Part 3) are of lower variability than those that were not transfected with GFP (Part 1). The ability to more accurately identify cell type by morphology in GFP expressing cells could supply a possible explanation for this

phenomenon. In all experiments I try to select only neurons of a pyramidal morphology for recording. This is much more difficult when only an untransfected soma is visible in a sea of neurites compared to the entire dendritic tree being lit up with GFP. It has been shown that subsets of neurons have much higher mEPSC frequencies. El-Husseini et al. (2000) showed that GABAergic neurons have a mean frequency of 20 Hz compared to 1 Hz of pyramidal glutamatergic neurons. This question could quite easily be resolved by testing if a patched cell is GABAergic or glutamatergic by examining the profile of its action potential spiking behaviour.

To summarise, we have found no electrophysiological phenotype in SynGAP $^{-/-}$ cultured neurons, potential reasons for this are discussed above. However, an opposing effect on synaptic function was found for different SynGAP isoforms; SynGAP A-alpha-1 caused a profound silencing of mEPSCs, SynGAPs B-and C-alpha-1 had a less strong effect. SynGAP A-alpha-2 had no effect on mEPSCs presence, amplitude or frequency, while SynBAPs B- and C-alpha-2 appeared to increase synaptic strength. Surprisingly the silencing of mEPSCs was not caused by loss of synaptic AMPA receptors as these were activated when the neuronal network was stimulated, which also shows that presynaptic neurons have the ability to release neurotransmitter. The presence of NMDA mEPSCs in some SynGAP A-alpha-1 expressing silent cells shows that some spontaneous neurotransmitter release can occur occasionally. These data indicate that the mechanism by which SynGAP alpha-1 has its effect may be different to previously thought (removal of synaptic AMPA receptors) and point toward a subtle postsynaptic and presynaptic rearrangement. The specific effects of different N and C terminal isoform combinations illustrates that both ends of the molecule need to be considered together, a point which has been previously neglected.

6 Final Thoughts and Future Experiments

The initial hypothesis of this thesis was that different isoforms of SynGAP have different functions. While it was known that the C-terminal tail of SynGAP-alpha-1 was important for its function there was no data available on roles of the other isoforms. The primary finding of this thesis is the conclusion that different isoforms do result in differential functional effects of SynGAP.

The result that SynGAP alpha-1 isoforms have a striking reducing effect on AMPA mEPSCs is consistent with previous work and fits the recognised model of SynGAP operating as a RasGAP, which downregulates the ERK/MAPK signalling pathway, and ultimately results in the removal of synaptic AMPA receptors. However, the finding that the N-terminal isoform specific region of the protein can modulate SynGAP's function in a neuronal setting is novel. SynGAP A-alpha-1 has the greatest synapse weakening effect, followed by SynGAPs B-alpha-1 and C-alpha-1.

SynGAP alpha-2 may then work as a RapGAP, as SynGAPs B-alpha-2 and C-alpha-2 both increase AMPA mEPSCs, potentially via the downregulation of p38 MAPK which would result in the synaptic delivery of AMPA receptors. Again, the N termini modify this effect as, mirroring the SynGAP alpha-1 case, the SynGAP A isoform has a different effect to that of SynGAPs B and C.

Interestingly, in both C-terminal scenarios the SynGAP A isoform results in less synaptic transmission than the corresponding SynGAP B and C isoforms (summarised in Figure 6. 1). The punctate, apparently synaptic localisation of SynGAP A-alpha-2 contrasts with the more diffuse localisation pattern of the SynGAP B-alpha-2 and C-alpha-2 isoforms, suggesting that the longer SynGAP A specific region may independently mediate synaptic localisation. The differential regulation of SynGAP variants also reflects this 'A vs B/C' pattern, where *SynGAP* A is downregulated and S*ynGAPs* B and C are upregulated in response to synaptic activity. One could suggest that this downregulation of *SynGAP* A, and upregulation of *SynGAPs B* and *C* could be involved in the potentiation of the synapses induced by the waves of synaptic activity.

A caveat to this interpretation is that we do not know that this stimulation paradigm induces functional plasticity (15 minutes of Bic./4AP simulation is sufficient to induce an increase in mEPSC frequency, known as chemical LTP, (Martel *et al.*, 2009). An extended temporal regulation profile of different isoforms in response to different stimulation paradigms, for example, in neurons that exhibit functional plasticity (the induction of 'chemical LTP or LTD') would facilitate the interpretation of regulation/function correlations (Martel *et al.*, 2009).

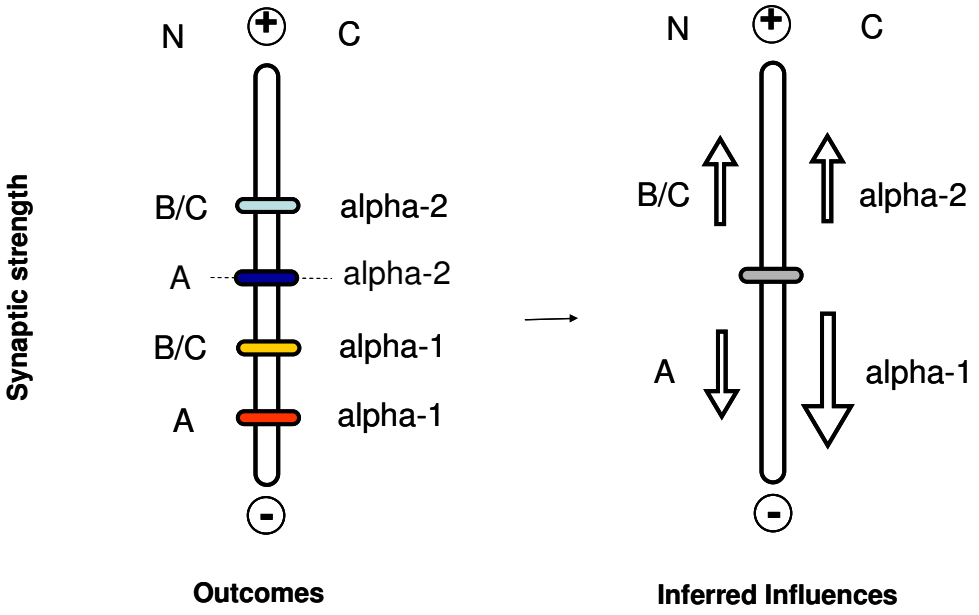

Figure 6. 1 The effect of various SynGAP isoforms on synaptic strength.

A slider scale is used to illustrate the effect of SynGAP isoforms on synaptic strength. The left panel shows the outcomes of the overexpression of individual isoforms as determined by the experiments in this thesis. The control synaptic strength is indicated with a dashed line, increased synaptic strength (+) and decreased synaptic strength (-). From this data we can infer the influences of each individual component, or terminus, illustrated in the right panel. N termini B and C are combined due to their similar, but not identical, effects. A larger arrow is used for SynGAP alpha-1 to show that its influence may be stronger than that of the other regions.

Unfortunately, such experiments would not reveal a key aspect of SynGAP structure that we now know is crucial to its function, namely which N-terminal is linked to each C-terminal. The nuanced way in which N and C-termini synergistically alter the outcome of SynGAP localisation and regulated events goes beyond SynGAP A being different to SynGAPs B and C. For example, expression of SynGAPs B-alpha-1 and C-alpha-1 cause the same percentage of silencing, but the two isoforms have different effects on the population of mEPSCs that remain and have different dendritic localisation patterns. Also, SynGAP C-alpha-2 causes an increase in mEPSC amplitude, but not frequency, while SynGAP B-alpha-2 increases both amplitude and frequency but both have grossly similar localisation patterns. (Figure 4. 10, Figure 5. 11, Figure 5. 16). It appears that the combinatorial possibilities allow for synergistic regulation of the localisation and alteration of functional outcomes.

As discussed, such N and C-terminal linkages are difficult to asses with current technologies. Development of technology generally requires an impetus and as transcriptional variation is becoming more and more apparent, hopefully it will be recognised that matching variant ends of proteins is important to their functional interpretation. Sequencing technologies like RNA paired end reads, if developed, could facilitate a comprehensive analysis of the N and C linkage of the transcriptome via large scale screening. The knowledge of which protein isoforms, of all proteins, exist would be a powerful tool in biological research.

The subtlety and complexity of the SynGAP protein may contribute to the difficulty, seen in this thesis, in exactly recapitulating the obvious knock out mEPSC and dendritic spine phenotypes previously described by other labs. The differences that are seen here, between wild tpe and *SynGAP* $^{-/-}$ data distributions rather than population means, perhaps reflect that only a subset of synapses contain SynGAPs that actively effect AMPA receptor mediated synaptic function or spine morphology. It could also indicate that the equilibrium of SynGAP regulation is finely balanced and acutely sensitive to differences in genetic strain etc. It is possible that differences in baseline neurotransmission are not greatly altered but the system may not correctly respond when perturbed, for example there may be deficits in the induction of plasticity paradigms (as is seen hippocampal slices from *SynGAP* $^{+/-}$

animals, (Komiyama *et al*., 2002)). Therefore, we should not dismiss changes as functionally insignificant just because they are small, especially since these *SynGAP* $^{-/-}$ mice have major deficits in cortical organisaiton and, like all other *SynGAP* $^{-/-}$ mice, die postnatally.

In attempting to rationalise how different SynGAP isoforms are exerting opposing effects I am invoking previous work which indicates that SynGAP can regulate the often antagonistic ERK/MAPK and p38 MAPK pathways through its action on Ras and Rap respectively (Figure 6. 2). I have no direct evidence that this is the case and gathering such evidence was not the aim of this work. Now that a differential functional effect has been determined, investigation of the mechanism is merited. The *in vitro* Ras/Rap GTPase promoting activities of different SynGAP isoforms, as well as the activation states of the proposed downstream signalling pathways, including those less studied (JNK/PI3K), are obvious avenues of further investigation. A simple experiment such as assaying the levels of activated phospho-ERK and phospho-p38 MAPK, both in neurons (to include the effects of synaptic interactions) and in a heterologous cell line, upon the expression of different isoforms would be illuminating.

The striking electrophysiological effect of SynGAP alpha-1 is not reflected in the morphological aspect of the synaptic sites but it is increasingly becoming apparent that spine dimension and synaptic responses are not always correlated (Segal). As already mentioned SynGAP is capable of regulating processes in which a decorrelation between morphology and function has been seen.

The theme of the points I have discussed up to here could have been predicted given the hypothesis of this thesis. However, when composing the hypothesis we did not explicitly consider a potential presynaptic effect of SynGAP expression, as there was no evidential basis for so doing. Given the data presented here we now need to and this is an entirely new, and unexpected, aspect of SynGAP function (see Figure 6. 2 for a speculative model). The finding that neurons whose AMPA mEPSCs have been silenced by the expression of SynGAP alpha-1 still have normal levels of surface AMPA receptors, and are able to respond to stimulated synaptic input is an intriguing one and merits further investigation.

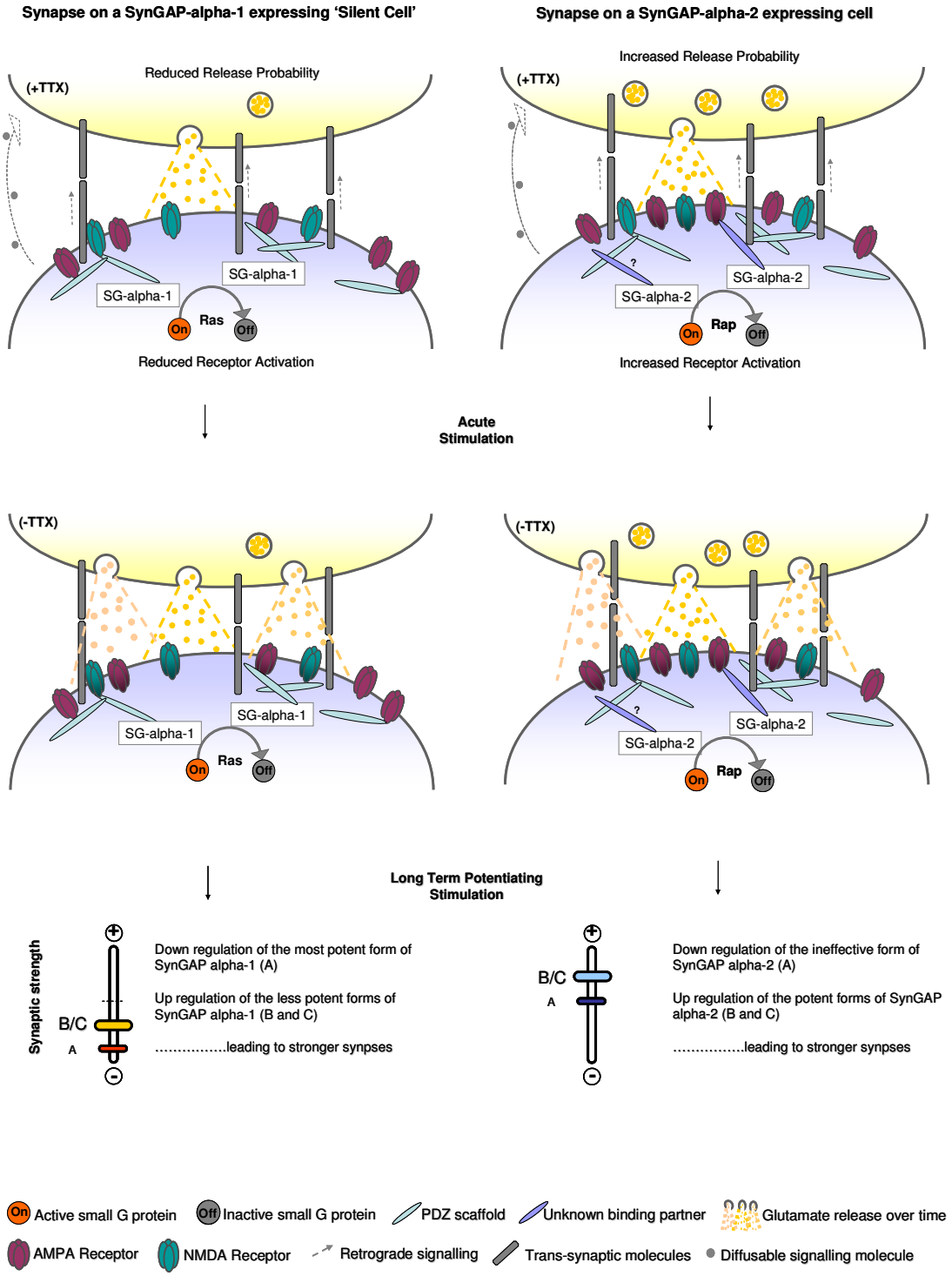

Figure 6. 2 Speculative model of SynGAP function based on data and ideas.

Legend overleaf

Figure Legend 6.2 Speculative model of SynGAP function based on data and ideas

Two speculative scenarios are shown for the purpose of illustration, on the left where SynGAP alpha-1 isoforms predominate and on the right where SynGAP alpha-2 isoforms. predominate. In the case of SynGAP alpha-1; under conditions allowing only spontaneous quantal release events (top panel, left) reduced AMPA receptor activation occurs due to less dense clustering or increased receptor mobility but AMPA receptors are present at the synapse. The probablility of synaptic vesicle fusion is reduced, possibly due to altered trans-synaptic or retrograde messenger signalling. Both presynaptic and postsynaptic effects are mediated by reduced Ras activity. Previously unactivated synaptic AMPA receptors become activated when the neural network is stimulated (middle panel, left) due to increased glutamate concentration in the synaptic cleft. When the network is undergoing long term potentiation the most potent SynGAP-alpha-1 'weakener' of synapses, SynGAP A, is down regulated and the two less potent SynGAP-alpha-1 isoforms, B and C, are upregulated in order to allow synapses to be strengthened.

In the case of SynGAP alpha-2, underconditions allowing only spontaneous quantal release (top panel, right) increased AMPA receptor activation occurs due to dense clustering, reduced receptor mobility or increased receptor insertion. The probability of release is increase due to altered trans-synaptic or retrograde messenger signalling. Both presynaptic and postsynaptic effects are mediated by reduced Rap activity. Upon stimulation (middle panel, right) the synapse receives more current input. When the network is undergoing long term potentiation the ineffective SynGAP alpha-2 variant, SynGAP A is downregulated and the two synaptic strengthening alpha- 2 variant, B and C, are upregulated allowing synapses to be strengthened.

Clearly additional work needs to be done to determine if the postsynaptic SynGAP alpha-1 cell's response to synaptic activity is completely normal, as this was not quantified in this thesis. Whether normal spontaneous neurotransmitter release onto SynGAP over expressing cells is occurring is a question that also needs to be addressed. FM dye labelling would indicate if terminals synapsing onto SynGAP overexpressing neurons are normally recycling synaptic vesicles. This functional assay would be advantageous over the labelling of presynaptic terminal by immunofluorescence due to its functional nature, and the fact that we know that presynaptic terminals are present and functional when stimulated.

If a presynaptic deficit was found we could postulate the following mechanism for a presynaptic effect of SynGAP alpha-1. Postsynaptic clustering of adhesion molecules is controlled by scaffolding proteins and overexpression of postsynaptic scaffolding proteins retrogradely enhances maturation of presynaptic terminals (El-Husseini *et al.*, 2000; Regalado *et al.*, 2006). If SynGAP alpha-1 is binding to the scaffolding proteins via its PDZ binding domain it could potentially affect presynptic function in two ways. One, that SynGAP alpha-1 has some specific signalling function that affects the retrograde signalling capacity of transynaptic molecules to which it binds via its PDZ domain, for example clustering or modulation of Ras/Rap effectors.

Two, that overexpressed SynGAP-alpha-1, by virtue of the over abundance of its PDZ binding domain is binding to these scaffolding molecules but the effect seen is non-specific and due to SynGAP outcompeting and thereby removing other PDZ binding proteins that mediate presynaptic terminal maturation. The question regarding specificity could be addressed by the overexpression of a SynGAP alpha-1 with a non-functional GAP domain. (The lack of function of SynGAP A-alpha-2 provides these experiments with an internal control for the non-physiological over-abundance of non-PDZ binding protein which is present at synapses.)

If a presynaptic deficit is not found, examination of the AMPA receptor content of SynGAP alpha-1 overexpressing synapses by electron microscopy or single particle tracking, combined with conventional surface labelling immunohistochemistry, may provide a more detailed view of microdomains and movement within the synapse. The same argument regarding the specificity of the effect of an overexpressed PDZ binding domain applies, as the scaffolding molecules crucial for the trafficking, clustering and synaptic motility of AMPA receptors are also dependent on PDZ binding domains, eg Stargazin.(Chen *et al.*, 2000; Schnell *et al.*, 2002; Milstein & Nicoll, 2009).

To conclude, SynGAP is a molecule of great complexity; at the level of gene, mRNA transcript and protein. The data presented in this thesis add to this picture of complexity and further it by demonstrating differential functional effects of various N- and C-terminal isoform combinations. This molecule illustrates the folly of believing that one protein has one function.

7 Appendices

7.1 Appendix 1 Transfection

In this appendix I outline some technical issues associated with liposome based co-transfection.

7.1.1 Co-transfection

Liposome based transfection is used throughout this thesis to make neurons express the protein products of two separate plasmids, a marker protein, eGFP, and the protein of interest, SynGAP. For the experiments to be interpretable it is crucial that neurons expressing GFP should also express SynGAP.

Co-expression of two fluorophores

To determine if two co-transfected plasmids are co-expressed and to optimise co-expression conditions I performed a co-transfection assay using varying ratios of two plasmids encoding different fluorophores, eGFP and the red fluorophore mCherry (

Appendix Figure 7. 1 , a). Fluorescing neurons were classified as expressing eGFP only, mCherry only, or both. I found that co-expression was almost ubiquitous. A small percentage (4% and 10%) of cells expressed only green at the highest eGFP:mCherry ratios (3 and 4 times eGFP DNA: mCherry DNA). No red only fluorescing cells were ever observed. It should be noted that the filter cube used to visualise red fluorescence is not optimal for the visualisation of mCherry. The filter cube used excites optimally at 515-560 nm whereas the peak excitation wavelength of mCherry is 587 nm, therefore it is likely that under these conditions the presence of mCherry is under reported. The absence of red only cells at the highest mCherry:eGFP DNA ratios also indicates that the appearance of green only cells is likely to be due to mCherry detection problems rather than true lack of expression.

Co-expression of eGFP and SynGAP isoforms

The experiment described above shows that two co-transfected fluorophore plasmids will likely co-express. For all experiments described in this thesis I chose to use a eGFP:SynGAP DNA ratio of 1:2. The most conservative interpretation of this scenario in light of the 'two fluorophores experiment' is that it is possible that there might be a few cells expressing SynGAP but not eGFP, but the reverse is very unlikely. SynGAP only expressing cells are not significant as only green fluorescing cells are recorded from.

It could be argued that the co-expression of eGFP and mCherry does not necessarily predict co-expression of eGFP and SynGAP. Evidence against this possibility comes from co-transfection of S*ynGAP* $^{-/-}$ cells with eGFP and SynGAP, followed by an immunocytochemical probe for SynGAP. I have never observed an instance where a green cell did not also stain for SynGAP, and vice versa.
Thus, I am convinced that co-transfection leads to co-expression in individual neurons.

7.1.2 Patch clamp recordings from transfected cells

Great difficulty was experienced in obtaining good quality electrophysiological recordings from eGFP expressing neurons transfected under the conditions used for the morphology experiments. Recordings from fluorescent cells transfected under these conditions were often characterised by high levels of noise and low holding currents (< -150 pA). In contrast neighbouring untransfected cells in the same well were typically in good electrophysiological condition. For transfection in a 24 well plate these conditions were; 0.6 µg total DNA composed of 0.2 µg eGFP and 0.4 µg empty vector or SynGAP and 2.33 µl Lipofectamine 2000.

To optimise transfection conditions for electrophysiology I altered DNA to Lipofectamine ratios, eGFP to empty vector DNA ratios and total DNA amounts. Lipofectamine at the lowest amounts (0.1, 0.25 µl) resulted in very low transfection efficiency (0 – 0.2%), but from 0.5 - 3 µl there was very little difference in transfection rates (0.4 – 0.6%). The inclusion of increasing amounts of empty

vector had little effect on transfection efficiency or cell fluorescence (as measured by the integrated density of the cell soma) (data not shown). Trial patch clamp recordings were made from each transfection condition and the condition which yielded the most acceptable recordings was used in all subsequent experiments. These conditions were; 0.3 µg total DNA composed of 0.1 µg eGFP and 0.2 µg empty vector or SynGAP and 1 µl Lipofectamine 2000.

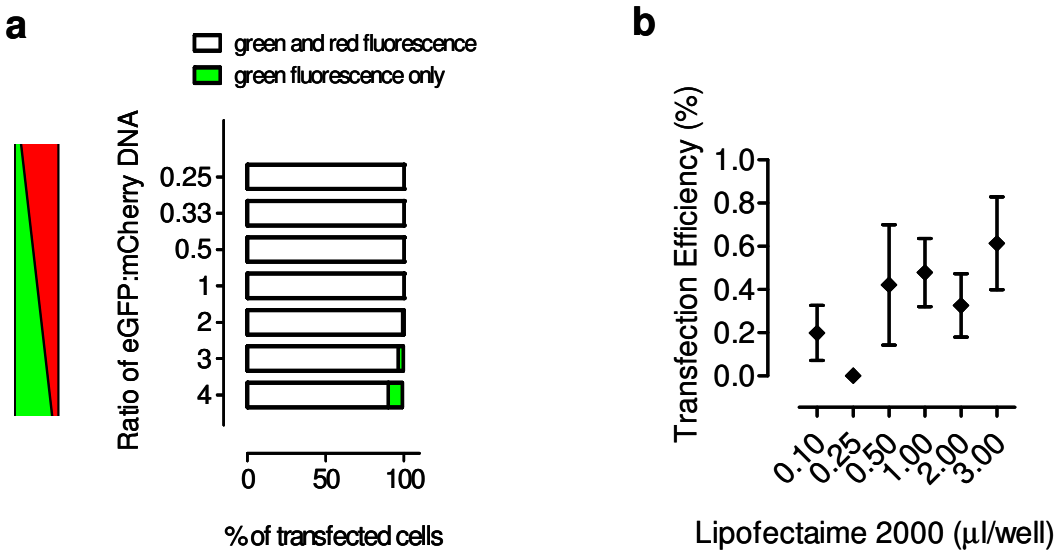

Appendix Figure 7. 1 Co-expression and transfection efficiency controls

To calculate co-transfection neurons were transfected at DIV 9 with varying ratios of eGFP to mCherry plasmid DNA, indicated schematically to the left of the Y axis (a). At DIV 10 the cells were assessed by epifluorescence microscopy to determine if they were co-expressing both fluorophores. White bars indicate the percentage of cells that were co-expressing both eGFP and mCherry. Green bars indicate the percentage of cells that were fluorescing only green. 3 coverslips were transfected per condition, and fluorescence was assessed in 5-8 fields of view per coverslip with a x 20 objective.

(b) Transfection efficiency of neurons transfected with fixed amounts of eGFP (0.1 µg) and empty vector (0.3 µg) DNA and increasing amounts of Lipofectamine 2000 is shown in.

Ras superfamily small G protein families	General cellular function	Neuronal function
Ras (Ras, Rap, Ral, Rheb, Rin and Rit)	regulate gene expression and cell proliferation	Classically associated with cell proliferation, has been co-opted in terminally differentiated non-dividing neurons to serve in activity dependent regulation of neuronal function, that is synaptic plasticity, as well as the regulation of neuronal survival (Sweatt, 2001)
Rho	regulate cytoskeletal reorganization and gene expression	Important regulators of the actin cytoskeleton and are critical for several aspects of neuronal development including the establishment of neuronal polarity, extension of axon and dendrites, neurite branching, axonal navigation and synapse formation (de Curtis, 2008).
Rab	regulate vesicle trafficking	Participates in central nervous system development, polarized neurite growth, endocytosis and axonal retrograde transport . At chemical synapses, Rabs perform specific functions in synaptic vesicle exocytosis and postsynaptic compartment dynamics of glutamate receptors (Ng and Tang, 2008).
Ran	regulate nucleocytoplasmic transport and microtubule organization.	Involved in nucleocytoplasmic transport and as such are spatial regulators of transport and signaling in distal axonal cytoplasm (Yudin and Fainzilber, 2009).
Arf	regulate vesicle trafficking	Mediates a variety of neuronal functions accompanying the structural changes of developing and mature neurons through its regulation of actin cytoskeleton reorganization and membrane traffic (Bader et al., 2004).

Appendix Table 1. 1 Neuronal functions of small G protein families

The small G protein superfamily is divided into five major families according to their homologous sequences and functional similarities. General functions are given here however, it is difficult to disentangle the separate functions of small G proteins as they often operate in sequential signalling cascades, where a member of one family can act directly on another member. Further complexity is added by extensive crosstalk between families where distinct families can regulate various cellular functions in a cooperative manner. For example the Rho and Rab families appear to co-operate in cell migration, and Rho/Rac/Cdc42 and Ras crosstalk is necessary for Ras induced cell transformation (Takai et al., 2001).

Ras family G protein	Ras	Rap
Genes (splice variants)	H-Ras, K-Ras (4A, 4B) N-Ras	Rap1 (A,B) Rap2 (A,B)
General cellular function	Central in a network controlling cell proliferation and cell survival	In lower eukaryotes predominantly controls cell adhesion, cell junction formation, cell secretion, and cell polarity . In higher eukaryotes roles are more diverse, being implicated in processes from exocytosis, phagosomal oxidation to cAMP induced neurite outgrowth. (Raaijmakers and Bos, 2009)
Subcellular localisation	Predominantly localised to the inner leaflet of the plasma membrane. Additionally individual Ras isoforms preferentially associate with different organelles and microdomains depending upon the type of membrane anchor, post-translational modification and activation state and thus, by engaging with distinct groups of effectors and activators, are capable of preferentially engaging distinct signalling pathways (Omerovic et al., 2007).	Located primarily at intracellular membranes in the perinuclear region and at endocytic and exocytic vesicles, but also at the plasma membrane (Pizon et al., 1994).
Effectors	Raf and phosphatidlylinositol 3-kinase (PI3K) were the first Ras effectors to be identified but since then at least 20 other effectors have been identified.	A range of effectors, partially overlapping with those of Ras, have been described.
Effector roles	As an effector of Ras signalling Raf remains the classic and most well studied example. It is the point of entry into a three tiered kinase cascade called the ERK/MAPK pathway (extracellular regulated kinase/mitogen activated protein kinase). MAPK signalling entails the Raf mediated phosphorylation and activation of MEK followed by the MEK mediated phosphorylation and ultimately the activation of ERK/MAPK (MEK; MAPK/ERK kinase). ERK/MAPK has over 70 substrates which include nuclear transcription factors, cytoskeletal proteins, signalling proteins and receptors (Kolch, 2005).	The Ras regulated ERK/MAPK cascade is a prototype for a family of signalling cascades that share the motif of three serially linked kinases regulating each other by sequential phosphorylation. The superfamily of MAPK signaling cascades comprises the ERKs, the JNKs and the p38 pathway and it appears that Rap1 can regulate another of these pathways, the p38 MAPK pathway, in a neuronal setting (Zhu et al., 2002). It is thought that Rap2 stimulates JNK activity in nonneuronal cells (Machida et al., 2004) and a similar role has been demonstrated in neurons (Zhu et al., 2005).
Crosstalk between pathways	Many Ras effectors are GEFs/ stimulators of other small G proteins which can regulate diverse processes such as cytoskeletal organisation, membrane trafficking and transcription, again emphasising the important of crosstalk between different G proteins.	The notion of a Rap function antagonistic to Ras came when it was observed that Ras induced transformation was inhibited by Rap1A, probably by the sequestration of its primary effector Raf (Kitayama et al., 1989). However, like Ras, Rap1 can be activated by a wide range of growth-promoting stimuli, indicating that it is not merely an antagonist to Ras signalling (Zwartkruis et al., 1998). To further complicate matters, in some cell types Rap1 has been shown to lead to the activation, rather than the inhibition, of the ERK pathway, possibly through binding different Raf isoforms (B-Raf) (Schmitt and Stork, 2000; Vossler et al., 1997).

Appendix Table 1. 2 Cellular signalling properties of Ras and Rap

References in appendix tables. (Kitayama *et al.*, 1989; Pizon *et al.*, 1994; Vossler *et al.*, 1997; Zwartkruis *et al.*, 1998; Schmitt & Stork, 2000; Sweatt, 2001; Takai *et al.*, 2001; Zhu *et al.*, 2002; Bader *et al.*, 2004; Machida *et al.*, 2004; Kolch, 2005; Zhu *et al.*, 2005; Omerovic *et al.*, 2007; de Curtis, 2008; Ng & Tang, 2008; Raaijmakers & Bos, 2009; Yudin & Fainzilber, 2009).

7.2 Acknowledgements

I'd like to thank a number of groups of people who have helped me through my PhD years.

Thanks to my supervisor Peter Kind for his support and enthusiasm, I could rely on him for getting excited about my results on my behalf. I greatly appreciate the help I've gotten from David Wyllie, who despite not being duty bound, stepped up to the electrophysiological and thesis reading bat. Thanks to Paul Skehel for his level headed comments.

The members, past and present, of the Kind lab, who actually made it a fun place to work; Lasani Wijetunge, Sally Till, Alex C-B, Aleks Domanski, Lynsey Meikle, Louise Dunn, Anne Petrie, Ruth Watson, Patrick Stoney and of course, Mark Barnett, who really is to blame for all this SynGAP carry-on. Members of greater DBuG are too numerous to mention but I count myself lucky to have worked somewhere with such a good atmosphere, and Friday morning cakes, and Firbush trips. To the first floor E-phys gang, Tim, Clare Zaltzmann, Marc-Andre, Emma Perkins, latterly Lasani, with guest appearances from Paul B; thanks for helping me cope with the electrode puller with RadioIO and Jelly Babies. The Hugh Robson Building people, all floors, who have made this a good place to be. Thanks to Darren Downing, Janet Philp, Carol Wallaston, Mark Hay, Garry and Andrew for making stuff work. Thanks especially to the Hardingham lab group, Karen Bell, Fransesc Soriano, Fred Leveille, Sofia Papadia, Paul Baxter, Clare Puddifoot, Marc Andre Martel, who have saved me with bottles of medium and technical stuff on a number of occasions. Thanks to Trudi Guillespie for confocalling.
The support, both scientific and social, has really made a difference.

Thanks to the residents of, and many visitors to, Montague St for making going home such fun; especially my friend Emma Clayton, for always being there, and Antoine Claessens, for bringing so much of Belgium into my life. It's also been great being one of the Welcomers; Aimee Deaton, Pan Filis, Judith Zilch, Antoine and I have alot to thank the Welcome Trust for, not just free peanuts and wine. Thanks to the organisers, Margarete Heck and Karen Chapman; We all know the Welcome were wrong to stop the course.
Thanks to my family for their support, especially my Mum for putting up with my PhD induced crankiness.

Finally, thank you Tim O'Leary, without whom I'm not sure I would have gotten through; electrophysiologically, nutritionally or emotionally.

No thanks to: The evil electrode puller, green cells, mice, karaoke.

References

Abraham WC, Mason SE, Demmer J, Williams JM, Richardson CL, Tate WP, Lawlor PA & Dragunow M. (1993). Correlations between immediate early gene induction and the persistence of long-term potentiation. *Neuroscience* **56,** 717-727.

Adari H, Lowy DR, Willumsen BM, Der CJ & McCormick F. (1988). Guanosine triphosphatase activating protein (GAP) interacts with the p21 ras effector binding domain. *Science (New York, NY* **240,** 518-521.

Allen NJ & Barres BA. (2005). Signaling between glia and neurons: focus on synaptic plasticity. *Current opinion in neurobiology* **15,** 542-548.

Alonso M, Medina JH & Pozzo-Miller L. (2004). ERK1/2 activation is necessary for BDNF to increase dendritic spine density in hippocampal CA1 pyramidal neurons. *Learn Mem* **11,** 172-178.

An P & Grabowski PJ. (2007). Exon silencing by UAGG motifs in response to neuronal excitation. *PLoS Biol* **5,** e36.

Artamonova, II & Gelfand MS. (2007). Comparative genomics and evolution of alternative splicing: the pessimists' science. *Chem Rev* **107,** 3407-3430.

Arvanitis DA, Vafiadaki E, Fan GC, Mitton BA, Gregory KN, Del Monte F, Kontrogianni-Konstantopoulos A, Sanoudou D & Kranias EG. (2007). Histidine-rich Ca-binding protein interacts with sarcoplasmic reticulum Ca-ATPase. *Am J Physiol Heart Circ Physiol* **293,** H1581-1589.

Ast G. (2004). How did alternative splicing evolve? *Nature reviews* **5,** 773-782.

Atkins CM, Selcher JC, Petraitis JJ, Trzaskos JM & Sweatt JD. (1998). The MAPK cascade is required for mammalian associative learning. *Nature neuroscience* **1,** 602-609.

Bader MF, Doussau F, Chasserot-Golaz S, Vitale N & Gasman S. (2004). Coupling actin and membrane dynamics during calcium-regulated exocytosis: a role for Rho and ARF GTPases. *Biochim Biophys Acta* **1742,** 37-49.

Bailey CH, Bartsch D & Kandel ER. (1996). Toward a molecular definition of long-term memory storage. *Proc Natl Acad Sci U S A* **93,** 13445-13452.

Barnett MW, Watson RF, Vitalis T, Porter K, Komiyama NH, Stoney PN, Gillingwater TH, Grant SG & Kind PC. (2006). Synaptic Ras GTPase activating protein regulates pattern formation in the trigeminal system of mice. *J Neurosci* **26,** 1355-1365.

Barron VA, Zhu H, Hinman MN, Ladd AN & Lou H. (2010). The neurofibromatosis type I pre-mRNA is a novel target of CELF protein-mediated splicing regulation. *Nucleic acids research* **38,** 253-264.

Batsche E, Yaniv M & Muchardt C. (2006). The human SWI/SNF subunit Brm is a regulator of alternative splicing. *Nat Struct Mol Biol* **13,** 22-29.

Beattie EC, Stellwagen D, Morishita W, Bresnahan JC, Ha BK, Von Zastrow M, Beattie MS & Malenka RC. (2002). Control of synaptic strength by glial TNFalpha. *Science (New York, NY* **295,** 2282-2285.

Bekkers JM, Richerson GB & Stevens CF. (1990). Origin of variability in quantal size in cultured hippocampal neurons and hippocampal slices. *Proc Natl Acad Sci U S A* **87,** 5359-5362.

Bekkers JM & Stevens CF. (1995). Quantal analysis of EPSCs recorded from small numbers of synapses in hippocampal cultures. *J Neurophysiol* **73,** 1145-1156.

Bernards A. (2003). GAPs galore! A survey of putative Ras superfamily GTPase activating proteins in man and Drosophila. *Biochim Biophys Acta* **1603,** 47-82.

Bernards A & Settleman J. (2004). GAP control: regulating the regulators of small GTPases. *Trends Cell Biol* **14,** 377-385.

Biederer T, Sara Y, Mozhayeva M, Atasoy D, Liu X, Kavalali ET & Sudhof TC. (2002). SynCAM, a synaptic adhesion molecule that drives synapse assembly. *Science (New York, NY* **297,** 1525-1531.

Black DL. (2003). Mechanisms of alternative pre-messenger RNA splicing. *Annu Rev Biochem* **72,** 291-336.

Blanpied TA, Kerr JM & Ehlers MD. (2008). Structural plasticity with preserved topology in the postsynaptic protein network. *Proc Natl Acad Sci U S A* **105,** 12587-12592.

Bliss TV & Collingridge GL. (1993). A synaptic model of memory: long-term potentiation in the hippocampus. *Nature* **361,** 31-39.

Bliss TV & Lomo T. (1973). Long-lasting potentiation of synaptic transmission in the dentate area of the anaesthetized rabbit following stimulation of the perforant path. *The Journal of physiology* **232,** 331-356.

Bonhoeffer T & Yuste R. (2002). Spine motility. Phenomenology, mechanisms, and function. *Neuron* **35,** 1019-1027.

Bos JL, Rehmann H & Wittinghofer A. (2007). GEFs and GAPs: critical elements in the control of small G proteins. *Cell* **129,** 865-877.

Boyer C, Schikorski T & Stevens CF. (1998). Comparison of hippocampal dendritic spines in culture and in brain. *J Neurosci* **18,** 5294-5300.

Brakeman PR, Lanahan AA, O'Brien R, Roche K, Barnes CA, Huganir RL & Worley PF. (1997). Homer: a protein that selectively binds metabotropic glutamate receptors. *Nature* **386,** 284-288.

Brambilla R, Gnesutta N, Minichiello L, White G, Roylance AJ, Herron CE, Ramsey M, Wolfer DP, Cestari V, Rossi-Arnaud C, Grant SG, Chapman PF, Lipp HP, Sturani E & Klein R. (1997). A role for the Ras signalling pathway in synaptic transmission and long-term memory. *Nature* **390,** 281-286.

Brown TC, Tran IC, Backos DS & Esteban JA. (2005). NMDA receptor-dependent activation of the small GTPase Rab5 drives the removal of synaptic AMPA receptors during hippocampal LTD. *Neuron* **45,** 81-94.

Butler MP, O'Connor JJ & Moynagh PN. (2004). Dissection of tumor-necrosis factor-alpha inhibition of long-term potentiation (LTP) reveals a p38 mitogen-activated protein kinase-dependent mechanism which maps to early-but not late-phase LTP. *Neuroscience* **124,** 319-326.

Cantley LC. (2002). The phosphoinositide 3-kinase pathway. *Science (New York, NY* **296,** 1655-1657.

Carlisle HJ, Manzerra P, Marcora E & Kennedy MB. (2008). SynGAP regulates steady-state and activity-dependent phosphorylation of cofilin. *J Neurosci* **28,** 13673-13683.

Chen HJ, Rojas-Soto M, Oguni A & Kennedy MB. (1998). A synaptic Ras-GTPase activating protein (p135 SynGAP) inhibited by CaM kinase II. *Neuron* **20,** 895-904.

Chen L, Chetkovich DM, Petralia RS, Sweeney NT, Kawasaki Y, Wenthold RJ, Bredt DS & Nicoll RA. (2000). Stargazin regulates synaptic targeting of AMPA receptors by two distinct mechanisms. *Nature* **408,** 936-943.

Chen M & Manley JL. (2009). Mechanisms of alternative splicing regulation: insights from molecular and genomics approaches. *Nat Rev Mol Cell Biol* **10,** 741-754.

Cheng D, Hoogenraad CC, Rush J, Ramm E, Schlager MA, Duong DM, Xu P, Wijayawardana SR, Hanfelt J, Nakagawa T, Sheng M & Peng J. (2006). Relative and absolute quantification of postsynaptic density proteome isolated from rat forebrain and cerebellum. *Mol Cell Proteomics* **5,** 1158-1170.

Chern TM, Paul N, van Nimwegen E & Zavolan M. (2008). Computational analysis of full-length cDNAs reveals frequent coupling between transcriptional and splicing programs. *DNA Res* **15,** 63-72.

Cho W & Stahelin RV. (2006). Membrane binding and subcellular targeting of C2 domains. *Biochim Biophys Acta* **1761,** 838-849.

Christopherson KS, Ullian EM, Stokes CC, Mullowney CE, Hell JW, Agah A, Lawler J, Mosher DF, Bornstein P & Barres BA. (2005). Thrombospondins are astrocyte-secreted proteins that promote CNS synaptogenesis. *Cell* **120,** 421-433.

Chung HJ, Steinberg JP, Huganir RL & Linden DJ. (2003). Requirement of AMPA receptor GluR2 phosphorylation for cerebellar long-term depression. *Science (New York, NY* **300,** 1751-1755.

Cochilla AJ, Angleson JK & Betz WJ. (1999). Monitoring secretory membrane with FM1-43 fluorescence. *Annual review of neuroscience* **22,** 1-10.

Collin C, Miyaguchi K & Segal M. (1997). Dendritic spine density and LTP induction in cultured hippocampal slices. *J Neurophysiol* **77,** 1614-1623.

Cool BH, Chan GC, Lee L, Oshima J, Martin GM & Hu Q. A flanking gene problem leads to the discovery of a Gprc5b splice variant predominantly expressed in C57Bl/6J mouse brain and in maturing neurons. *PLoS One* **5,** e10351.

Cornell-Bell AH, Finkbeiner SM, Cooper MS & Smith SJ. (1990). Glutamate induces calcium waves in cultured astrocytes: long-range glial signaling. *Science (New York, NY* **247,** 470-473.

Cruz-Martin A, Crespo M & Portera-Cailliau C. Delayed stabilization of dendritic spines in fragile X mice. *J Neurosci* **30,** 7793-7803.

Cuthbert PC, Stanford LE, Coba MP, Ainge JA, Fink AE, Opazo P, Delgado JY, Komiyama NH, O'Dell TJ & Grant SG. (2007). Synapse-associated protein 102/dlgh3 couples the NMDA receptor to specific plasticity pathways and learning strategies. *J Neurosci* **27,** 2673-2682.

Dailey ME & Smith SJ. (1996). The dynamics of dendritic structure in developing hippocampal slices. *J Neurosci* **16,** 2983-2994.

Daumke O, Weyand M, Chakrabarti PP, Vetter IR & Wittinghofer A. (2004). The GTPase-activating protein Rap1GAP uses a catalytic asparagine. *Nature* **429,** 197-201.

Davletov B, Perisic O & Williams RL. (1998). Calcium-dependent membrane penetration is a hallmark of the C2 domain of cytosolic phospholipase A2 whereas the C2A domain of synaptotagmin binds membranes electrostatically. *J Biol Chem* **273,** 19093-19096.

de Curtis I. (2008). Functions of Rac GTPases during neuronal development. *Dev Neurosci* **30,** 47-58.

de la Mata M, Alonso CR, Kadener S, Fededa JP, Blaustein M, Pelisch F, Cramer P, Bentley D & Kornblihtt AR. (2003). A slow RNA polymerase II affects alternative splicing in vivo. *Mol Cell* **12,** 525-532.

Del Castillo J & Katz B. (1954). Quantal components of the end-plate potential. *The Journal of physiology* **124,** 560-573.

Dosemeci A & Jaffe H. Regulation of phosphorylation at the postsynaptic density during different activity states of Ca2+/calmodulin-dependent protein kinase II. *Biochem Biophys Res Commun* **391,** 78-84.

Dunaevsky A, Tashiro A, Majewska A, Mason C & Yuste R. (1999). Developmental regulation of spine motility in the mammalian central nervous system. *Proc Natl Acad Sci U S A* **96,** 13438-13443.

Ehlers MD. (2000). Reinsertion or degradation of AMPA receptors determined by activity-dependent endocytic sorting. *Neuron* **28,** 511-525.

Ehlers MD, Heine M, Groc L, Lee MC & Choquet D. (2007). Diffusional trapping of GluR1 AMPA receptors by input-specific synaptic activity. *Neuron* **54,** 447-460.

Ehrlich I & Malinow R. (2004). Postsynaptic density 95 controls AMPA receptor incorporation during long-term potentiation and experience-driven synaptic plasticity. *J Neurosci* **24,** 916-927.

Eisener-Dorman AF, Lawrence DA & Bolivar VJ. (2009). Cautionary insights on knockout mouse studies: the gene or not the gene? *Brain Behav Immun* **23,** 318-324.

El-Husseini AE, Schnell E, Chetkovich DM, Nicoll RA & Bredt DS. (2000). PSD-95 involvement in maturation of excitatory synapses. *Science (New York, NY* **290,** 1364-1368.

Epshtein V & Nudler E. (2003). Cooperation between RNA polymerase molecules in transcription elongation. *Science (New York, NY* **300,** 801-805.

Erzurumlu RS & Kind PC. (2001). Neural activity: sculptor of 'barrels' in the neocortex. *Trends Neurosci* **24,** 589-595.

Evans JH, Murray D, Leslie CC & Falke JJ. (2006). Specific translocation of protein kinase Calpha to the plasma membrane requires both Ca2+ and PIP2 recognition by its C2 domain. *Mol Biol Cell* **17,** 56-66.

Evans JH, Spencer DM, Zweifach A & Leslie CC. (2001). Intracellular calcium signals regulating cytosolic phospholipase A2 translocation to internal membranes. *J Biol Chem* **276,** 30150-30160.

Fiacco TA & McCarthy KD. (2004). Intracellular astrocyte calcium waves in situ increase the frequency of spontaneous AMPA receptor currents in CA1 pyramidal neurons. *J Neurosci* **24,** 722-732.

Fiala JC, Feinberg M, Popov V & Harris KM. (1998). Synaptogenesis via dendritic filopodia in developing hippocampal area CA1. *J Neurosci* **18,** 8900-8911.

Fischer M, Kaech S, Knutti D & Matus A. (1998). Rapid actin-based plasticity in dendritic spines. *Neuron* **20,** 847-854.

Flavell SW, Kim TK, Gray JM, Harmin DA, Hemberg M, Hong EJ, Markenscoff-Papadimitriou E, Bear DM & Greenberg ME. (2008). Genome-wide analysis of MEF2 transcriptional program reveals synaptic target genes and neuronal activity-dependent polyadenylation site selection. *Neuron* **60,** 1022-1038.

Fu Z, Lee SH, Simonetta A, Hansen J, Sheng M & Pak DT. (2007). Differential roles of Rap1 and Rap2 small GTPases in neurite retraction and synapse elimination in hippocampal spiny neurons. *Journal of neurochemistry* **100,** 118-131.

Fukazawa Y, Saitoh Y, Ozawa F, Ohta Y, Mizuno K & Inokuchi K. (2003). Hippocampal LTP is accompanied by enhanced F-actin content within the dendritic spine that is essential for late LTP maintenance in vivo. *Neuron* **38,** 447-460.

Fullwood MJ, Wei CL, Liu ET & Ruan Y. (2009). Next-generation DNA sequencing of paired-end tags (PET) for transcriptome and genome analyses. *Genome research* **19,** 521-532.

Gartner U, Alpar A, Behrbohm J, Heumann R & Arendt T. (2005). Enhanced Ras activity promotes spine formation in synRas mice neocortex. *Neuroreport* **16,** 149-152.

Giese KP, Friedman E, Telliez JB, Fedorov NB, Wines M, Feig LA & Silva AJ. (2001). Hippocampus-dependent learning and memory is impaired in mice lacking the Ras-guanine-nucleotide releasing factor 1 (Ras-GRF1). *Neuropharmacology* **41,** 791-800.

Goldin M & Segal M. (2003). Protein kinase C and ERK involvement in dendritic spine plasticity in cultured rodent hippocampal neurons. *The European journal of neuroscience* **17,** 2529-2539.

Gordon GR, Baimoukhametova DV, Hewitt SA, Rajapaksha WR, Fisher TE & Bains JS. (2005). Norepinephrine triggers release of glial ATP to increase postsynaptic efficacy. *Nature neuroscience* **8,** 1078-1086.

Grewal SS, Horgan AM, York RD, Withers GS, Banker GA & Stork PJ. (2000). Neuronal calcium activates a Rap1 and B-Raf signaling pathway via the cyclic adenosine monophosphate-dependent protein kinase. *J Biol Chem* **275,** 3722-3728.

Grobler JA, Essen LO, Williams RL & Hurley JH. (1996). C2 domain conformational changes in phospholipase C-delta 1. *Nat Struct Biol* **3,** 788-795.

Grubb SC, Maddatu TP, Bult CJ & Bogue MA. (2009). Mouse phenome database. *Nucleic acids research* **37,** D720-730.

Grutzendler J, Kasthuri N & Gan WB. (2002). Long-term dendritic spine stability in the adult cortex. *Nature* **420,** 812-816.

Gu Y & Stornetta RL. (2007). Synaptic plasticity, AMPA-R trafficking, and Ras-MAPK signaling. *Acta Pharmacol Sin* **28,** 928-936.

Guo X, Hamilton PJ, Reish NJ, Sweatt JD, Miller CA & Rumbaugh G. (2009). Reduced expression of the NMDA receptor-interacting protein SynGAP causes behavioral abnormalities that model symptoms of Schizophrenia. *Neuropsychopharmacology* **34,** 1659-1672.

Hamdan FF, Gauthier J, Spiegelman D, Noreau A, Yang Y, Pellerin S, Dobrzeniecka S, Cote M, Perreau-Linck E, Carmant L, D'Anjou G, Fombonne E, Addington AM, Rapoport JL, Delisi LE, Krebs MO, Mouaffak F, Joober R, Mottron L, Drapeau P, Marineau C, Lafreniere RG, Lacaille JC, Rouleau GA & Michaud JL. (2009). Mutations in SYNGAP1 in autosomal nonsyndromic mental retardation. *N Engl J Med* **360,** 599-605.

Hardingham GE, Fukunaga Y & Bading H. (2002). Extrasynaptic NMDARs oppose synaptic NMDARs by triggering CREB shut-off and cell death pathways. *Nature neuroscience* **5,** 405-414.

Harris E & Cardelli J. (2002). RabD, a Dictyostelium Rab14-related GTPase, regulates phagocytosis and homotypic phagosome and lysosome fusion. *J Cell Sci* **115,** 3703-3713.

Harris KM & Kater SB. (1994). Dendritic spines: cellular specializations imparting both stability and flexibility to synaptic function. *Annual review of neuroscience* **17,** 341-371.

Harris KM & Stevens JK. (1988). Dendritic spines of rat cerebellar Purkinje cells: serial electron microscopy with reference to their biophysical characteristics. *J Neurosci* **8,** 4455-4469.

Hattori D, Millard SS, Wojtowicz WM & Zipursky SL. (2008). Dscam-mediated cell recognition regulates neural circuit formation. *Annu Rev Cell Dev Biol* **24,** 597-620.

Hayashi K & Shirao T. (1999). Change in the shape of dendritic spines caused by overexpression of drebrin in cultured cortical neurons. *J Neurosci* **19,** 3918-3925.

Heine M, Groc L, Frischknecht R, Beique JC, Lounis B, Rumbaugh G, Huganir RL, Cognet L & Choquet D. (2008). Surface mobility of postsynaptic AMPARs tunes synaptic transmission. *Science (New York, NY* **320,** 201-205.

Herman MA & Jahr CE. (2007). Extracellular glutamate concentration in hippocampal slice. *J Neurosci* **27,** 9736-9741.

Hirao K, Hata Y, Ide N, Takeuchi M, Irie M, Yao I, Deguchi M, Toyoda A, Sudhof TC & Takai Y. (1998). A novel multiple PDZ domain-containing molecule interacting with N-methyl-D-aspartate receptors and neuronal cell adhesion proteins. *J Biol Chem* **273,** 21105-21110.

Hofer SB, Mrsic-Flogel TD, Bonhoeffer T & Hubener M. (2009). Experience leaves a lasting structural trace in cortical circuits. *Nature* **457,** 313-317.

Holtmaat A & Svoboda K. (2009). Experience-dependent structural synaptic plasticity in the mammalian brain. *Nat Rev Neurosci* **10,** 647-658.

Hsieh H, Boehm J, Sato C, Iwatsubo T, Tomita T, Sisodia S & Malinow R. (2006). AMPAR removal underlies Abeta-induced synaptic depression and dendritic spine loss. *Neuron* **52,** 831-843.

Huang CC, You JL, Wu MY & Hsu KS. (2004). Rap1-induced p38 mitogen-activated protein kinase activation facilitates AMPA receptor trafficking via the GDI.Rab5 complex. Potential role in (S)-3,5-dihydroxyphenylglycene-induced long term depression. *J Biol Chem* **279,** 12286-12292.

Husi H, Ward MA, Choudhary JS, Blackstock WP & Grant SG. (2000). Proteomic analysis of NMDA receptor-adhesion protein signaling complexes. *Nature neuroscience* **3,** 661-669.

Irie M, Hata Y, Takeuchi M, Ichtchenko K, Toyoda A, Hirao K, Takai Y, Rosahl TW & Sudhof TC. (1997). Binding of neuroligins to PSD-95. *Science (New York, NY* **277,** 1511-1515.

Isaac JT, Nicoll RA & Malenka RC. (1995). Evidence for silent synapses: implications for the expression of LTP. *Neuron* **15,** 427-434.

Ishikawa Y, Katoh H & Negishi M. (2003). A role of Rnd1 GTPase in dendritic spine formation in hippocampal neurons. *J Neurosci* **23,** 11065-11072.

Ishikawa Y, Katoh H & Negishi M. (2006). Small GTPase Rnd1 is involved in neuronal activity-dependent dendritic development in hippocampal neurons. *Neurosci Lett* **400,** 218-223.

Ivanco TL & Greenough WT. (2002). Altered mossy fiber distributions in adult Fmr1 (FVB) knockout mice. *Hippocampus* **12,** 47-54.

Jackson WT, Giddings TH, Jr., Taylor MP, Mulinyawe S, Rabinovitch M, Kopito RR & Kirkegaard K. (2005). Subversion of cellular autophagosomal machinery by RNA viruses. *PLoS Biol* **3,** e156.

Jaffe H, Vinade L & Dosemeci A. (2004). Identification of novel phosphorylation sites on postsynaptic density proteins. *Biochem Biophys Res Commun* **321,** 210-218.

Jonas P, Major G & Sakmann B. (1993). Quantal components of unitary EPSCs at the mossy fibre synapse on CA3 pyramidal cells of rat hippocampus. *The Journal of physiology* **472,** 615-663.

Jones AL, Hulett MD & Parish CR. (2005). Histidine-rich glycoprotein: A novel adaptor protein in plasma that modulates the immune, vascular and coagulation systems. *Immunol Cell Biol* **83,** 106-118.

Kanagawa O, Xu G, Tevaarwerk A & Vaupel BA. (2000). Protection of nonobese diabetic mice from diabetes by gene(s) closely linked to IFN-gamma receptor loci. *J Immunol* **164,** 3919-3923.

Kandel ER, Schwartz, J, Jessell, T. (2000). *Principles of Neural Science*. McGraw-Hill Medical.

Kasai H, Matsuzaki M, Noguchi J, Yasumatsu N & Nakahara H. (2003). Structure-stability-function relationships of dendritic spines. *Trends Neurosci* **26,** 360-368.

Kato K, Sekino Y, Takahashi H, Yasuda H & Shirao T. (2007). Increase in AMPA receptor-mediated miniature EPSC amplitude after chronic NMDA receptor blockade in cultured hippocampal neurons. *Neurosci Lett* **418,** 4-8.

Kennedy MB, Beale HC, Carlisle HJ & Washburn LR. (2005). Integration of biochemical signalling in spines. *Nat Rev Neurosci* **6,** 423-434.

Kennedy MB, Bennett MK & Erondu NE. (1983). Biochemical and immunochemical evidence that the "major postsynaptic density protein" is a subunit of a calmodulin-dependent protein kinase. *Proc Natl Acad Sci U S A* **80,** 7357-7361.

Kerchner GA & Nicoll RA. (2008). Silent synapses and the emergence of a postsynaptic mechanism for LTP. *Nat Rev Neurosci* **9,** 813-825.

Kielland A, Bochorishvili G, Corson J, Zhang L, Rosin DL, Heggelund P & Zhu JJ. (2009). Activity patterns govern synapse-specific AMPA receptor trafficking between deliverable and synaptic pools. *Neuron* **62,** 84-101.

Kim E & Sheng M. (2004). PDZ domain proteins of synapses. *Nat Rev Neurosci* **5,** 771-781.

Kim JH, Lee HK, Takamiya K & Huganir RL. (2003). The role of synaptic GTPase-activating protein in neuronal development and synaptic plasticity. *J Neurosci* **23,** 1119-1124.

Kim JH, Liao D, Lau LF & Huganir RL. (1998). SynGAP: a synaptic RasGAP that associates with the PSD-95/SAP90 protein family. *Neuron* **20,** 683-691.

Kim MJ, Dunah AW, Wang YT & Sheng M. (2005). Differential roles of NR2A- and NR2B-containing NMDA receptors in Ras-ERK signaling and AMPA receptor trafficking. *Neuron* **46,** 745-760.

Kimura K, Wakamatsu A, Suzuki Y, Ota T, Nishikawa T, Yamashita R, Yamamoto J, Sekine M, Tsuritani K, Wakaguri H, Ishii S, Sugiyama T, Saito K, Isono Y, Irie R, Kushida N, Yoneyama T, Otsuka R, Kanda K, Yokoi T, Kondo H, Wagatsuma M, Murakawa K, Ishida S, Ishibashi T, Takahashi-Fujii A, Tanase T, Nagai K, Kikuchi H, Nakai K, Isogai T & Sugano S. (2006). Diversification of transcriptional modulation: large-scale identification and characterization of putative alternative promoters of human genes. *Genome research* **16,** 55-65.

Kitayama H, Sugimoto Y, Matsuzaki T, Ikawa Y & Noda M. (1989). A ras-related gene with transformation suppressor activity. *Cell* **56,** 77-84.

Klein R. (2009). Bidirectional modulation of synaptic functions by Eph/ephrin signaling. *Nature neuroscience* **12,** 15-20.

Knuesel I, Elliott A, Chen HJ, Mansuy IM & Kennedy MB. (2005). A role for synGAP in regulating neuronal apoptosis. *The European journal of neuroscience* **21,** 611-621.

Kolch W. (2005). Coordinating ERK/MAPK signalling through scaffolds and inhibitors. *Nat Rev Mol Cell Biol* **6,** 827-837.

Komiyama NH, Watabe AM, Carlisle HJ, Porter K, Charlesworth P, Monti J, Strathdee DJ, O'Carroll CM, Martin SJ, Morris RG, O'Dell TJ & Grant SG. (2002). SynGAP regulates ERK/MAPK signaling, synaptic plasticity, and learning in the complex with postsynaptic density 95 and NMDA receptor. *J Neurosci* **22,** 9721-9732.

Kopec CD, Real E, Kessels HW & Malinow R. (2007). GluR1 links structural and functional plasticity at excitatory synapses. *J Neurosci* **27,** 13706-13718.

Kornblihtt AR. (2005). Promoter usage and alternative splicing. *Curr Opin Cell Biol* **17,** 262-268.

Krapivinsky G, Medina I, Krapivinsky L, Gapon S & Clapham DE. (2004). SynGAP-MUPP1-CaMKII synaptic complexes regulate p38 MAP kinase activity and NMDA receptor-dependent synaptic AMPA receptor potentiation. *Neuron* **43,** 563-574.

Kriegstein AR & Dichter MA. (1983). Morphological classification of rat cortical neurons in cell culture. *J Neurosci* **3,** 1634-1647.

Kupzig S, Deaconescu D, Bouyoucef D, Walker SA, Liu Q, Polte CL, Daumke O, Ishizaki T, Lockyer PJ, Wittinghofer A & Cullen PJ. (2006). GAP1 family members constitute bifunctional Ras and Rap GTPase-activating proteins. *J Biol Chem* **281,** 9891-9900.

Lee JA, Xing Y, Nguyen D, Xie J, Lee CJ & Black DL. (2007). Depolarization and CaM kinase IV modulate NMDA receptor splicing through two essential RNA elements. *PLoS Biol* **5,** e40.

Lejeune F & Maquat LE. (2005). Mechanistic links between nonsense-mediated mRNA decay and pre-mRNA splicing in mammalian cells. *Curr Opin Cell Biol* **17,** 309-315.

Lemmon MA. (2004). Pleckstrin homology domains: not just for phosphoinositides. *Biochem Soc Trans* **32,** 707-711.

Lemmon MA. (2005). Pleckstrin homology domains: two halves make a hole? *Cell* **120,** 574-576.

Lemmon MA. (2008). Membrane recognition by phospholipid-binding domains. *Nat Rev Mol Cell Biol* **9,** 99-111.

Lendvai B, Stern EA, Chen B & Svoboda K. (2000). Experience-dependent plasticity of dendritic spines in the developing rat barrel cortex in vivo. *Nature* **404,** 876-881.

Lewis BP, Green RE & Brenner SE. (2003). Evidence for the widespread coupling of alternative splicing and nonsense-mediated mRNA decay in humans. *Proc Natl Acad Sci U S A* **100,** 189-192.

Li G & Liang Z. (2001). Phosphate-binding loop and Rab GTPase function: mutations at Ser29 and Ala30 of Rab5 lead to loss-of-function as well as gain-of-function phenotype. *Biochem J* **355,** 681-689.

Li Q, Lee JA & Black DL. (2007). Neuronal regulation of alternative pre-mRNA splicing. *Nat Rev Neurosci* **8,** 819-831.

Li W, Okano A, Tian QB, Nakayama K, Furihata T, Nawa H & Suzuki T. (2001). Characterization of a novel synGAP isoform, synGAP-beta. *J Biol Chem* **276,** 21417-21424.

Li YX, Zhang Y, Lester HA, Schuman EM & Davidson N. (1998). Enhancement of neurotransmitter release induced by brain-derived neurotrophic factor in cultured hippocampal neurons. *J Neurosci* **18,** 10231-10240.

Liao D, Hessler NA & Malinow R. (1995). Activation of postsynaptically silent synapses during pairing-induced LTP in CA1 region of hippocampal slice. *Nature* **375,** 400-404.

Lin B, Kramar EA, Bi X, Brucher FA, Gall CM & Lynch G. (2005). Theta stimulation polymerizes actin in dendritic spines of hippocampus. *J Neurosci* **25,** 2062-2069.

Lipscombe D. (2005). Neuronal proteins custom designed by alternative splicing. *Curr Opin Neurobiol* **15,** 358-363.

Lisman J & Raghavachari S. (2006). A unified model of the presynaptic and postsynaptic changes during LTP at CA1 synapses. *Sci STKE* **2006,** re11.

Lisman J, Schulman H & Cline H. (2002). The molecular basis of CaMKII function in synaptic and behavioural memory. *Nat Rev Neurosci* **3,** 175-190.

Liu G, Choi S & Tsien RW. (1999). Variability of neurotransmitter concentration and nonsaturation of postsynaptic AMPA receptors at synapses in hippocampal cultures and slices. *Neuron* **22,** 395-409.

Liu L, Wong TP, Pozza MF, Lingenhoehl K, Wang Y, Sheng M, Auberson YP & Wang YT. (2004). Role of NMDA receptor subtypes in governing the direction of hippocampal synaptic plasticity. *Science (New York, NY* **304,** 1021-1024.

Liu Q, Walker SA, Gao D, Taylor JA, Dai YF, Arkell RS, Bootman MD, Roderick HL, Cullen PJ & Lockyer PJ. (2005). CAPRI and RASAL impose different modes of information processing on Ras due to contrasting temporal filtering of Ca2+. *J Cell Biol* **170,** 183-190.

Ma Y & Hendershot LM. (2001). The unfolding tale of the unfolded protein response. *Cell* **107,** 827-830.

Machida N, Umikawa M, Takei K, Sakima N, Myagmar BE, Taira K, Uezato H, Ogawa Y & Kariya K. (2004). Mitogen-activated protein kinase kinase kinase kinase 4 as a putative effector of Rap2 to activate the c-Jun N-terminal kinase. *J Biol Chem* **279,** 15711-15714.

Magin TM, McWhir J & Melton DW. (1992). A new mouse embryonic stem cell line with good germ line contribution and gene targeting frequency. *Nucleic acids research* **20,** 3795-3796.

Malenka RC & Nicoll RA. (1999). Long-term potentiation--a decade of progress? *Science (New York, NY* **285,** 1870-1874.

Malgaroli A & Tsien RW. (1992). Glutamate-induced long-term potentiation of the frequency of miniature synaptic currents in cultured hippocampal neurons. *Nature* **357,** 134-139.

Malinow R & Malenka RC. (2002). AMPA receptor trafficking and synaptic plasticity. *Annual review of neuroscience* **25,** 103-126.

Maltsev N, Glass EM, Ovchinnikova G & Gu Z. (2005). Molecular mechanisms involved in robustness of yeast central metabolism against null mutations. *J Biochem* **137,** 177-187.

Martel MA, Wyllie DJ & Hardingham GE. (2009). In developing hippocampal neurons, NR2B-containing N-methyl-D-aspartate receptors (NMDARs) can mediate signaling to neuronal survival and synaptic potentiation, as well as neuronal death. *Neuroscience* **158,** 334-343.

Martens S, Kozlov MM & McMahon HT. (2007). How synaptotagmin promotes membrane fusion. *Science (New York, NY* **316,** 1205-1208.

Massey PV, Johnson BE, Moult PR, Auberson YP, Brown MW, Molnar E, Collingridge GL & Bashir ZI. (2004). Differential roles of NR2A and NR2B-containing NMDA receptors in cortical long-term potentiation and long-term depression. *J Neurosci* **24,** 7821-7828.

Masugi-Tokita M, Tarusawa E, Watanabe M, Molnar E, Fujimoto K & Shigemoto R. (2007). Number and density of AMPA receptors in individual synapses in the rat cerebellum as revealed by SDS-digested freeze-fracture replica labeling. *J Neurosci* **27,** 2135-2144.

Matsuda S, Launey T, Mikawa S & Hirai H. (2000). Disruption of AMPA receptor GluR2 clusters following long-term depression induction in cerebellar Purkinje neurons. *Embo J* **19,** 2765-2774.

Matsuzaki M, Ellis-Davies GC, Nemoto T, Miyashita Y, Iino M & Kasai H. (2001). Dendritic spine geometry is critical for AMPA receptor expression in hippocampal CA1 pyramidal neurons. *Nature neuroscience* **4,** 1086-1092.

Mauch DH, Nagler K, Schumacher S, Goritz C, Muller EC, Otto A & Pfrieger FW. (2001). CNS synaptogenesis promoted by glia-derived cholesterol. *Science (New York, NY* **294,** 1354-1357.

Mayer BJ. (2001). SH3 domains: complexity in moderation. *J Cell Sci* **114,** 1253-1263.

McAllister AK & Stevens CF. (2000). Nonsaturation of AMPA and NMDA receptors at hippocampal synapses. *Proc Natl Acad Sci U S A* **97,** 6173-6178.

McBain C & Dingledine R. (1992). Dual-component miniature excitatory synaptic currents in rat hippocampal CA3 pyramidal neurons. *J Neurophysiol* **68,** 16-27.

McCormack SG, Stornetta RL & Zhu JJ. (2006). Synaptic AMPA receptor exchange maintains bidirectional plasticity. *Neuron* **50,** 75-88.

McMahon HT, Kozlov MM & Martens S. Membrane curvature in synaptic vesicle fusion and beyond. *Cell* **140,** 601-605.

McPherson CE, Eipper BA & Mains RE. (2002). Genomic organization and differential expression of Kalirin isoforms. *Gene* **284,** 41-51.

McPherson CE, Eipper BA & Mains RE. (2004). Kalirin expression is regulated by multiple promoters. *J Mol Neurosci* **22,** 51-62.

Meijering E, Jacob M, Sarria JC, Steiner P, Hirling H & Unser M. (2004). Design and validation of a tool for neurite tracing and analysis in fluorescence microscopy images. *Cytometry A* **58,** 167-176.

Migaud M, Charlesworth P, Dempster M, Webster LC, Watabe AM, Makhinson M, He Y, Ramsay MF, Morris RG, Morrison JH, O'Dell TJ & Grant SG. (1998).

Enhanced long-term potentiation and impaired learning in mice with mutant postsynaptic density-95 protein. *Nature* **396,** 433-439.

Milstein AD & Nicoll RA. (2009). TARP modulation of synaptic AMPA receptor trafficking and gating depends on multiple intracellular domains. *Proc Natl Acad Sci U S A* **106,** 11348-11351.

Mineur YS, Sluyter F, de Wit S, Oostra BA & Crusio WE. (2002). Behavioral and neuroanatomical characterization of the Fmr1 knockout mouse. *Hippocampus* **12,** 39-46.

Mochizuki N, Ohba Y, Kiyokawa E, Kurata T, Murakami T, Ozaki T, Kitabatake A, Nagashima K & Matsuda M. (1999). Activation of the ERK/MAPK pathway by an isoform of rap1GAP associated with G alpha(i). *Nature* **400,** 891-894.

Moldon A, Malapeira J, Gabrielli N, Gogol M, Gomez-Escoda B, Ivanova T, Seidel C & Ayte J. (2008). Promoter-driven splicing regulation in fission yeast. *Nature* **455,** 997-1000.

Monsalve M, Wu Z, Adelmant G, Puigserver P, Fan M & Spiegelman BM. (2000). Direct coupling of transcription and mRNA processing through the thermogenic coactivator PGC-1. *Mol Cell* **6,** 307-316.

Moon IS, Sakagami H, Nakayama J & Suzuki T. (2008). Differential distribution of synGAP alpha1 and synGAP beta isoforms in rat neurons. *Brain Res* **1241,** 62-75.

Morozov A, Muzzio IA, Bourtchouladze R, Van-Strien N, Lapidus K, Yin D, Winder DG, Adams JP, Sweatt JD & Kandel ER. (2003). Rap1 couples cAMP signaling to a distinct pool of p42/44MAPK regulating excitability, synaptic plasticity, learning, and memory. *Neuron* **39,** 309-325.

Mu Y, Otsuka T, Horton AC, Scott DB & Ehlers MD. (2003). Activity-dependent mRNA splicing controls ER export and synaptic delivery of NMDA receptors. *Neuron* **40,** 581-594.

Muhia M, Feldon J, Knuesel I & Yee BK. (2009). Appetitively motivated instrumental learning in SynGAP heterozygous knockout mice. *Behav Neurosci* **123,** 1114-1128.

Muhia M, Yee BK, Feldon J, Markopoulos F & Knuesel I. (2010). Disruption of hippocampus-regulated behavioural and cognitive processes by heterozygous constitutive deletion of SynGAP. *The European journal of neuroscience* **31,** 529-543.

Murai KK, Nguyen LN, Irie F, Yamaguchi Y & Pasquale EB. (2003). Control of hippocampal dendritic spine morphology through ephrin-A3/EphA4 signaling. *Nature neuroscience* **6,** 153-160.

N. B. Standen PTAGaMJW. (1987). *Microelectrode Techniques: The Plymouth Workshop Handbook*. The Company of Biologists, Cambridge, UK.

Nagerl UV, Eberhorn N, Cambridge SB & Bonhoeffer T. (2004). Bidirectional activity-dependent morphological plasticity in hippocampal neurons. *Neuron* **44,** 759-767.

Newpher TM & Ehlers MD. (2009). Spine microdomains for postsynaptic signaling and plasticity. *Trends Cell Biol* **19,** 218-227.

Ng EL & Tang BL. (2008). Rab GTPases and their roles in brain neurons and glia. *Brain Res Rev* **58,** 236-246.

Nicoll RA, Tomita S & Bredt DS. (2006). Auxiliary subunits assist AMPA-type glutamate receptors. *Science (New York, NY* **311,** 1253-1256.

Nilsen TW & Graveley BR. Expansion of the eukaryotic proteome by alternative splicing. *Nature* **463,** 457-463.

Nimchinsky EA, Yasuda R, Oertner TG & Svoboda K. (2004). The number of glutamate receptors opened by synaptic stimulation in single hippocampal spines. *J Neurosci* **24,** 2054-2064.

Noguchi J, Matsuzaki M, Ellis-Davies GC & Kasai H. (2005). Spine-neck geometry determines NMDA receptor-dependent Ca2+ signaling in dendrites. *Neuron* **46,** 609-622.

Nurtdinov RN, Artamonova, II, Mironov AA & Gelfand MS. (2003). Low conservation of alternative splicing patterns in the human and mouse genomes. *Hum Mol Genet* **12,** 1313-1320.

Nusser Z, Lujan R, Laube G, Roberts JD, Molnar E & Somogyi P. (1998). Cell type and pathway dependence of synaptic AMPA receptor number and variability in the hippocampus. *Neuron* **21,** 545-559.

O'Brien RJ, Kamboj S, Ehlers MD, Rosen KR, Fischbach GD & Huganir RL. (1998). Activity-dependent modulation of synaptic AMPA receptor accumulation. *Neuron* **21,** 1067-1078.

O'Leary T. (2008). Homeostatic Regulation of Intrinsic Excitability in Hippocampal Neurons. University of Edinburgh

O'Leary T, van Rossum MC & Wyllie DJ. Homeostasis of intrinsic excitability in hippocampal neurones: dynamics and mechanism of the response to chronic depolarization. *The Journal of physiology* **588,** 157-170.

Oh JS, Manzerra P & Kennedy MB. (2004). Regulation of the neuron-specific Ras GTPase-activating protein, synGAP, by Ca2+/calmodulin-dependent protein kinase II. *J Biol Chem* **279,** 17980-17988.

Ohba Y, Mochizuki N, Matsuo K, Yamashita S, Nakaya M, Hashimoto Y, Hamaguchi M, Kurata T, Nagashima K & Matsuda M. (2000). Rap2 as a slowly

responding molecular switch in the Rap1 signaling cascade. *Mol Cell Biol* **20,** 6074-6083.

Okamoto K, Nagai T, Miyawaki A & Hayashi Y. (2004). Rapid and persistent modulation of actin dynamics regulates postsynaptic reorganization underlying bidirectional plasticity. *Nature neuroscience* **7,** 1104-1112.

Okazaki N, Yan J, Yuasa S, Ueno T, Kominami E, Masuho Y, Koga H & Muramatsu M. (2000). Interaction of the Unc-51-like kinase and microtubule-associated protein light chain 3 related proteins in the brain: possible role of vesicular transport in axonal elongation. *Brain Res Mol Brain Res* **85,** 1-12.

Omerovic J, Laude AJ & Prior IA. (2007). Ras proteins: paradigms for compartmentalised and isoform-specific signalling. *Cell Mol Life Sci* **64,** 2575-2589.

Pak DT, Yang S, Rudolph-Correia S, Kim E & Sheng M. (2001). Regulation of dendritic spine morphology by SPAR, a PSD-95-associated RapGAP. *Neuron* **31,** 289-303.

Pamonsinlapatham P, Hadj-Slimane R, Lepelletier Y, Allain B, Toccafondi M, Garbay C & Raynaud F. (2009). P120-Ras GTPase activating protein (RasGAP): a multi-interacting protein in downstream signaling. *Biochimie* **91,** 320-328.

Papa M, Bundman MC, Greenberger V & Segal M. (1995). Morphological analysis of dendritic spine development in primary cultures of hippocampal neurons. *J Neurosci* **15,** 1-11.

Park M, Salgado JM, Ostroff L, Helton TD, Robinson CG, Harris KM & Ehlers MD. (2006). Plasticity-induced growth of dendritic spines by exocytic trafficking from recycling endosomes. *Neuron* **52,** 817-830.

Passafaro M, Piech V & Sheng M. (2001). Subunit-specific temporal and spatial patterns of AMPA receptor exocytosis in hippocampal neurons. *Nature neuroscience* **4,** 917-926.

Patel AA & Steitz JA. (2003). Splicing double: insights from the second spliceosome. *Nat Rev Mol Cell Biol* **4,** 960-970.

Pena V, Hothorn M, Eberth A, Kaschau N, Parret A, Gremer L, Bonneau F, Ahmadian MR & Scheffzek K. (2008). The C2 domain of SynGAP is essential for stimulation of the Rap GTPase reaction. *EMBO Rep* **9,** 350-355.

Peng J, Kim MJ, Cheng D, Duong DM, Gygi SP & Sheng M. (2004). Semiquantitative proteomic analysis of rat forebrain postsynaptic density fractions by mass spectrometry. *J Biol Chem* **279,** 21003-21011.

Penzes P, Beeser A, Chernoff J, Schiller MR, Eipper BA, Mains RE & Huganir RL. (2003). Rapid induction of dendritic spine morphogenesis by trans-synaptic

ephrinB-EphB receptor activation of the Rho-GEF kalirin. *Neuron* **37,** 263-274.

Perea G & Araque A. (2007). Astrocytes potentiate transmitter release at single hippocampal synapses. *Science (New York, NY* **317,** 1083-1086.

Perea G, Navarrete M & Araque A. (2009). Tripartite synapses: astrocytes process and control synaptic information. *Trends Neurosci* **32,** 421-431.

Peters A & Kaiserman-Abramof IR. (1970). The small pyramidal neuron of the rat cerebral cortex. The perikaryon, dendrites and spines. *Am J Anat* **127,** 321-355.

Petersen JD, Chen X, Vinade L, Dosemeci A, Lisman JE & Reese TS. (2003). Distribution of postsynaptic density (PSD)-95 and Ca2+/calmodulin-dependent protein kinase II at the PSD. *J Neurosci* **23,** 11270-11278.

Pinto D, Pagnamenta AT, Klei L, Anney R, Merico D, Regan R, Conroy J, Magalhaes TR, Correia C, Abrahams BS, Almeida J, Bacchelli E, Bader GD, Bailey AJ, Baird G, Battaglia A, Berney T, Bolshakova N, Bolte S, Bolton PF, Bourgeron T, Brennan S, Brian J, Bryson SE, Carson AR, Casallo G, Casey J, Chung BH, Cochrane L, Corsello C, Crawford EL, Crossett A, Cytrynbaum C, Dawson G, de Jonge M, Delorme R, Drmic I, Duketis E, Duque F, Estes A, Farrar P, Fernandez BA, Folstein SE, Fombonne E, Freitag CM, Gilbert J, Gillberg C, Glessner JT, Goldberg J, Green A, Green J, Guter SJ, Hakonarson H, Heron EA, Hill M, Holt R, Howe JL, Hughes G, Hus V, Igliozzi R, Kim C, Klauck SM, Kolevzon A, Korvatska O, Kustanovich V, Lajonchere CM, Lamb JA, Laskawiec M, Leboyer M, Le Couteur A, Leventhal BL, Lionel AC, Liu XQ, Lord C, Lotspeich L, Lund SC, Maestrini E, Mahoney W, Mantoulan C, Marshall CR, McConachie H, McDougle CJ, McGrath J, McMahon WM, Merikangas A, Migita O, Minshew NJ, Mirza GK, Munson J, Nelson SF, Noakes C, Noor A, Nygren G, Oliveira G, Papanikolaou K, Parr JR, Parrini B, Paton T, Pickles A, Pilorge M, Piven J, Ponting CP, Posey DJ, Poustka A, Poustka F, Prasad A, Ragoussis J, Renshaw K, Rickaby J, Roberts W, Roeder K, Roge B, Rutter ML, Bierut LJ, Rice JP, Salt J, Sansom K, Sato D, Segurado R, Sequeira AF, Senman L, Shah N, Sheffield VC, Soorya L, Sousa I, Stein O, Sykes N, Stoppioni V, Strawbridge C, Tancredi R, Tansey K, Thiruvahindrapduram B, Thompson AP, Thomson S, Tryfon A, Tsiantis J, Van Engeland H, Vincent JB, Volkmar F, Wallace S, Wang K, Wang Z, Wassink TH, Webber C, Weksberg R, Wing K, Wittemeyer K, Wood S, Wu J, Yaspan BL, Zurawiecki D, Zwaigenbaum L, Buxbaum JD, Cantor RM, Cook EH, Coon H, Cuccaro ML, Devlin B, Ennis S, Gallagher L, Geschwind DH, Gill M, Haines JL, Hallmayer J, Miller J, Monaco AP, Nurnberger Jr JI, Paterson AD, Pericak-Vance MA, Schellenberg GD, Szatmari P, Vicente AM, Vieland VJ, Wijsman EM, Scherer SW, Sutcliffe JS & Betancur C. (2010). Functional impact of global rare copy number variation in autism spectrum disorders. *Nature*.

Pizon V, Desjardins M, Bucci C, Parton RG & Zerial M. (1994). Association of Rap1a and Rap1b proteins with late endocytic/phagocytic compartments and Rap2a with the Golgi complex. *J Cell Sci* **107 (Pt 6),** 1661-1670.

Porter K, Komiyama NH, Vitalis T, Kind PC & Grant SG. (2005). Differential expression of two NMDA receptor interacting proteins, PSD-95 and SynGAP during mouse development. *The European journal of neuroscience* **21,** 351-362.

Portera-Cailliau C, Pan DT & Yuste R. (2003). Activity-regulated dynamic behavior of early dendritic protrusions: evidence for different types of dendritic filopodia. *J Neurosci* **23,** 7129-7142.

Raaijmakers JH & Bos JL. (2009). Specificity in Ras and Rap signaling. *J Biol Chem* **284,** 10995-10999.

Rabenstein RL, Addy NA, Caldarone BJ, Asaka Y, Gruenbaum LM, Peters LL, Gilligan DM, Fitzsimonds RM & Picciotto MR. (2005). Impaired synaptic plasticity and learning in mice lacking beta-adducin, an actin-regulating protein. *J Neurosci* **25,** 2138-2145.

Raghavachari S & Lisman JE. (2004). Properties of quantal transmission at CA1 synapses. *J Neurophysiol* **92,** 2456-2467.

Rall W. (1969). Time constants and electrotonic length of membrane cylinders and neurons. *Biophys J* **9,** 1483-1508.

Rebecchi MJ & Scarlata S. (1998). Pleckstrin homology domains: a common fold with diverse functions. *Annu Rev Biophys Biomol Struct* **27,** 503-528.

Regalado MP, Terry-Lorenzo RT, Waites CL, Garner CC & Malenka RC. (2006). Transsynaptic signaling by postsynaptic synapse-associated protein 97. *J Neurosci* **26,** 2343-2357.

Reuther GW & Der CJ. (2000). The Ras branch of small GTPases: Ras family members don't fall far from the tree. *Curr Opin Cell Biol* **12,** 157-165.

Richter M, Murai KK, Bourgin C, Pak DT & Pasquale EB. (2007). The EphA4 receptor regulates neuronal morphology through SPAR-mediated inactivation of Rap GTPases. *J Neurosci* **27,** 14205-14215.

Ridgway WM, Healy B, Smink LJ, Rainbow D & Wicker LS. (2007). New tools for defining the 'genetic background' of inbred mouse strains. *Nat Immunol* **8,** 669-673.

Rintoul GL, Filiano AJ, Brocard JB, Kress GJ & Reynolds IJ. (2003). Glutamate decreases mitochondrial size and movement in primary forebrain neurons. *J Neurosci* **23,** 7881-7888.

Roberts RL, Barbieri MA, Ullrich J & Stahl PD. (2000). Dynamics of rab5 activation in endocytosis and phagocytosis. *J Leukoc Biol* **68,** 627-632.

Rogozin IB, Sverdlov AV, Babenko VN & Koonin EV. (2005). Analysis of evolution of exon-intron structure of eukaryotic genes. *Brief Bioinform* **6,** 118-134.

Roy BC, Kohu K, Matsuura K, Yanai H & Akiyama T. (2002). SPAL, a Rap-specific GTPase activating protein, is present in the NMDA receptor-PSD-95 complex in the hippocampus. *Genes Cells* **7,** 607-617.

Rubinfeld B, Munemitsu S, Clark R, Conroy L, Watt K, Crosier WJ, McCormick F & Polakis P. (1991). Molecular cloning of a GTPase activating protein specific for the Krev-1 protein p21rap1. *Cell* **65,** 1033-1042.

Rumbaugh G, Adams JP, Kim JH & Huganir RL. (2006). SynGAP regulates synaptic strength and mitogen-activated protein kinases in cultured neurons. *Proc Natl Acad Sci U S A* **103,** 4344-4351.

Rumbaugh G, Sia GM, Garner CC & Huganir RL. (2003). Synapse-associated protein-97 isoform-specific regulation of surface AMPA receptors and synaptic function in cultured neurons. *J Neurosci* **23,** 4567-4576.

Sala C, Cambianica I & Rossi F. (2008). Molecular mechanisms of dendritic spine development and maintenance. *Acta Neurobiol Exp (Wars)* **68,** 289-304.

Sala C, Piech V, Wilson NR, Passafaro M, Liu G & Sheng M. (2001). Regulation of dendritic spine morphology and synaptic function by Shank and Homer. *Neuron* **31,** 115-130.

Sans N, Petralia RS, Wang YX, Blahos J, 2nd, Hell JW & Wenthold RJ. (2000). A developmental change in NMDA receptor-associated proteins at hippocampal synapses. *J Neurosci* **20,** 1260-1271.

Sara Y, Biederer T, Atasoy D, Chubykin A, Mozhayeva MG, Sudhof TC & Kavalali ET. (2005). Selective capability of SynCAM and neuroligin for functional synapse assembly. *J Neurosci* **25,** 260-270.

Sasaki Y, Fukushima N, Yoshida A & Ueda H. (1998). Low-density induced apoptosis of cortical neurons is inhibited by serum factors. *Cell Mol Neurobiol* **18,** 487-496.

Schafe GE, Atkins CM, Swank MW, Bauer EP, Sweatt JD & LeDoux JE. (2000). Activation of ERK/MAP kinase in the amygdala is required for memory consolidation of pavlovian fear conditioning. *J Neurosci* **20,** 8177-8187.

Scheffzek K, Ahmadian MR, Kabsch W, Wiesmuller L, Lautwein A, Schmitz F & Wittinghofer A. (1997). The Ras-RasGAP complex: structural basis for GTPase activation and its loss in oncogenic Ras mutants. *Science (New York, NY* **277,** 333-338.

Schmitt JM & Stork PJ. (2000). beta 2-adrenergic receptor activates extracellular signal-regulated kinases (ERKs) via the small G protein rap1 and the serine/threonine kinase B-Raf. *J Biol Chem* **275,** 25342-25350.

Schmucker D, Clemens JC, Shu H, Worby CA, Xiao J, Muda M, Dixon JE & Zipursky SL. (2000). Drosophila Dscam is an axon guidance receptor exhibiting extraordinary molecular diversity. *Cell* **101,** 671-684.

Schnell E, Sizemore M, Karimzadegan S, Chen L, Bredt DS & Nicoll RA. (2002). Direct interactions between PSD-95 and stargazin control synaptic AMPA receptor number. *Proc Natl Acad Sci U S A* **99,** 13902-13907.

Scrima A, Thomas C, Deaconescu D & Wittinghofer A. (2008). The Rap-RapGAP complex: GTP hydrolysis without catalytic glutamine and arginine residues. *Embo J* **27,** 1145-1153.

Segal M. Dendritic spines, synaptic plasticity and neuronal survival: activity shapes dendritic spines to enhance neuronal viability. *The European journal of neuroscience*.

Shao X, Li C, Fernandez I, Zhang X, Sudhof TC & Rizo J. (1997). Synaptotagmin-syntaxin interaction: the C2 domain as a Ca2+-dependent electrostatic switch. *Neuron* **18,** 133-142.

Shepherd JD, Rumbaugh G, Wu J, Chowdhury S, Plath N, Kuhl D, Huganir RL & Worley PF. (2006). Arc/Arg3.1 mediates homeostatic synaptic scaling of AMPA receptors. *Neuron* **52,** 475-484.

Shi Y & Gaestel M. (2002). In the cellular garden of forking paths: how p38 MAPKs signal for downstream assistance. *Biol Chem* **383,** 1519-1536.

Silva AJ, Frankland PW, Marowitz Z, Friedman E, Laszlo GS, Cioffi D, Jacks T & Bourtchuladze R. (1997). A mouse model for the learning and memory deficits associated with neurofibromatosis type I. *Nat Genet* **15,** 281-284.

Song B, Meng F, Yan X, Guo J & Zhang G. (2003). Cerebral ischemia immediately increases serine phosphorylation of the synaptic RAS-GTPase activating protein SynGAP by calcium/calmodulin-dependent protein kinase II alpha in hippocampus of rats. *Neurosci Lett* **349,** 183-186.

Song B, Yan XB & Zhang GY. (2004). PSD-95 promotes CaMKII-catalyzed serine phosphorylation of the synaptic RAS-GTPase activating protein SynGAP after transient brain ischemia in rat hippocampus. *Brain Res* **1005,** 44-50.

Sot B, Kotting C, Deaconescu D, Suveyzdis Y, Gerwert K & Wittinghofer A. Unravelling the mechanism of dual-specificity GAPs. *Embo J* **29,** 1205-1214.

Stan A, Pielarski KN, Brigadski T, Wittenmayer N, Fedorchenko O, Gohla A, Lessmann V, Dresbach T & Gottmann K. Essential cooperation of N-cadherin and neuroligin-1 in the transsynaptic control of vesicle accumulation. *Proc Natl Acad Sci U S A* **107,** 11116-11121.

Stellwagen D & Malenka RC. (2006). Synaptic scaling mediated by glial TNF-alpha. *Nature* **440,** 1054-1059.

Stiedl O, Radulovic J, Lohmann R, Birkenfeld K, Palve M, Kammermeier J, Sananbenesi F & Spiess J. (1999). Strain and substrain differences in

context- and tone-dependent fear conditioning of inbred mice. *Behav Brain Res* **104,** 1-12.

Stoop R & Poo MM. (1996). Synaptic modulation by neurotrophic factors: differential and synergistic effects of brain-derived neurotrophic factor and ciliary neurotrophic factor. *J Neurosci* **16,** 3256-3264.

Stornetta RL & Zhu JJ. (2010). Ras and Rap Signaling in Synaptic Plasticity and Mental Disorders. *Neuroscientist*.

Sultan M, Schulz MH, Richard H, Magen A, Klingenhoff A, Scherf M, Seifert M, Borodina T, Soldatov A, Parkhomchuk D, Schmidt D, O'Keeffe S, Haas S, Vingron M, Lehrach H & Yaspo ML. (2008). A global view of gene activity and alternative splicing by deep sequencing of the human transcriptome. *Science (New York, NY* **321,** 956-960.

Sweatt JD. (2001). The neuronal MAP kinase cascade: a biochemical signal integration system subserving synaptic plasticity and memory. *Journal of neurochemistry* **76,** 1-10.

Tada T & Sheng M. (2006). Molecular mechanisms of dendritic spine morphogenesis. *Curr Opin Neurobiol* **16,** 95-101.

Takai Y, Sasaki T & Matozaki T. (2001). Small GTP-binding proteins. *Physiological reviews* **81,** 153-208.

Tall GG, Barbieri MA, Stahl PD & Horazdovsky BF. (2001). Ras-activated endocytosis is mediated by the Rab5 guanine nucleotide exchange activity of RIN1. *Dev Cell* **1,** 73-82.

Tappe A & Kuner R. (2006). Regulation of motor performance and striatal function by synaptic scaffolding proteins of the Homer1 family. *Proc Natl Acad Sci U S A* **103,** 774-779.

Thomas GM & Huganir RL. (2004). MAPK cascade signalling and synaptic plasticity. *Nat Rev Neurosci* **5,** 173-183.

Tomoda T, Bhatt RS, Kuroyanagi H, Shirasawa T & Hatten ME. (1999). A mouse serine/threonine kinase homologous to C. elegans UNC51 functions in parallel fiber formation of cerebellar granule neurons. *Neuron* **24,** 833-846.

Tomoda T, Kim JH, Zhan C & Hatten ME. (2004). Role of Unc51.1 and its binding partners in CNS axon outgrowth. *Genes Dev* **18,** 541-558.

Trachtenberg JT, Chen BE, Knott GW, Feng G, Sanes JR, Welker E & Svoboda K. (2002). Long-term in vivo imaging of experience-dependent synaptic plasticity in adult cortex. *Nature* **420,** 788-794.

Turrigiano GG, Leslie KR, Desai NS, Rutherford LC & Nelson SB. (1998). Activity-dependent scaling of quantal amplitude in neocortical neurons. *Nature* **391,** 892-896.

Ule J, Ule A, Spencer J, Williams A, Hu JS, Cline M, Wang H, Clark T, Fraser C, Ruggiu M, Zeeberg BR, Kane D, Weinstein JN, Blume J & Darnell RB. (2005). Nova regulates brain-specific splicing to shape the synapse. *Nat Genet* **37,** 844-852.

Ullian EM, Christopherson KS & Barres BA. (2004). Role for glia in synaptogenesis. *Glia* **47,** 209-216.

Underwood JG, Boutz PL, Dougherty JD, Stoilov P & Black DL. (2005). Homologues of the Caenorhabditis elegans Fox-1 protein are neuronal splicing regulators in mammals. *Mol Cell Biol* **25,** 10005-10016.

Valor LM & Grant SG. (2007). Clustered gene expression changes flank targeted gene loci in knockout mice. *PLoS One* **2,** e1303.

Varnai P & Balla T. (2006). Live cell imaging of phosphoinositide dynamics with fluorescent protein domains. *Biochim Biophys Acta* **1761,** 957-967.

Vaughn JE. (1989). Fine structure of synaptogenesis in the vertebrate central nervous system. *Synapse* **3,** 255-285.

Vazquez LE, Chen HJ, Sokolova I, Knuesel I & Kennedy MB. (2004). SynGAP regulates spine formation. *J Neurosci* **24,** 8862-8872.

Verdaguer N, Corbalan-Garcia S, Ochoa WF, Fita I & Gomez-Fernandez JC. (1999). Ca(2+) bridges the C2 membrane-binding domain of protein kinase Calpha directly to phosphatidylserine. *Embo J* **18,** 6329-6338.

Vossler MR, Yao H, York RD, Pan MG, Rim CS & Stork PJ. (1997). cAMP activates MAP kinase and Elk-1 through a B-Raf- and Rap1-dependent pathway. *Cell* **89,** 73-82.

Wagner A & Wright J. (2007). Alternative routes and mutational robustness in complex regulatory networks. *Biosystems* **88,** 163-172.

Waites CL, Specht CG, Hartel K, Leal-Ortiz S, Genoux D, Li D, Drisdel RC, Jeyifous O, Cheyne JE, Green WN, Montgomery JM & Garner CC. (2009). Synaptic SAP97 isoforms regulate AMPA receptor dynamics and access to presynaptic glutamate. *J Neurosci* **29,** 4332-4345.

Walker SA, Cullen PJ, Taylor JA & Lockyer PJ. (2003). Control of Ras cycling by Ca2+. *FEBS Lett* **546,** 6-10.

Walker SA, Kupzig S, Bouyoucef D, Davies LC, Tsuboi T, Bivona TG, Cozier GE, Lockyer PJ, Buckler A, Rutter GA, Allen MJ, Philips MR & Cullen PJ. (2004). Identification of a Ras GTPase-activating protein regulated by receptor-mediated Ca2+ oscillations. *Embo J* **23,** 1749-1760.

Wang ET, Sandberg R, Luo S, Khrebtukova I, Zhang L, Mayr C, Kingsmore SF, Schroth GP & Burge CB. (2008). Alternative isoform regulation in human tissue transcriptomes. *Nature* **456,** 470-476.

Wang XB, Yang Y & Zhou Q. (2007). Independent expression of synaptic and morphological plasticity associated with long-term depression. *J Neurosci* **27,** 12419-12429.

Wherlock M, Gampel A, Futter C & Mellor H. (2004). Farnesyltransferase inhibitors disrupt EGF receptor traffic through modulation of the RhoB GTPase. *J Cell Sci* **117,** 3221-3231.

Wilkie GS, Dickson KS & Gray NK. (2003). Regulation of mRNA translation by 5'- and 3'-UTR-binding factors. *Trends Biochem Sci* **28,** 182-188.

Wittenmayer N, Korber C, Liu H, Kremer T, Varoqueaux F, Chapman ER, Brose N, Kuner T & Dresbach T. (2009). Postsynaptic Neuroligin1 regulates presynaptic maturation. *Proc Natl Acad Sci U S A* **106,** 13564-13569.

Woolsey TA & Van der Loos H. (1970). The structural organization of layer IV in the somatosensory region (SI) of mouse cerebral cortex. The description of a cortical field composed of discrete cytoarchitectonic units. *Brain Res* **17,** 205-242.

Wu GY, Deisseroth K & Tsien RW. (2001). Spaced stimuli stabilize MAPK pathway activation and its effects on dendritic morphology. *Nature neuroscience* **4,** 151-158.

Wu JQ, Habegger L, Noisa P, Szekely A, Qiu C, Hutchison S, Raha D, Egholm M, Lin H, Weissman S, Cui W, Gerstein M & Snyder M. (2010). Dynamic transcriptomes during neural differentiation of human embryonic stem cells revealed by short, long, and paired-end sequencing. *Proc Natl Acad Sci U S A* **107,** 5254-5259.

Wu XS, Xue L, Mohan R, Paradiso K, Gillis KD & Wu LG. (2007). The origin of quantal size variation: vesicular glutamate concentration plays a significant role. *J Neurosci* **27,** 3046-3056.

Wyllie DJ, Manabe T & Nicoll RA. (1994). A rise in postsynaptic Ca2+ potentiates miniature excitatory postsynaptic currents and AMPA responses in hippocampal neurons. *Neuron* **12,** 127-138.

Xiao B, Tu JC & Worley PF. (2000). Homer: a link between neural activity and glutamate receptor function. *Curr Opin Neurobiol* **10,** 370-374.

Xie Z, Huganir RL & Penzes P. (2005). Activity-dependent dendritic spine structural plasticity is regulated by small GTPase Rap1 and its target AF-6. *Neuron* **48,** 605-618.

Xie Z, Srivastava DP, Photowala H, Kai L, Cahill ME, Woolfrey KM, Shum CY, Surmeier DJ & Penzes P. (2007). Kalirin-7 controls activity-dependent structural and functional plasticity of dendritic spines. *Neuron* **56,** 640-656.

Xin D, Hu L & Kong X. (2008). Alternative promoters influence alternative splicing at the genomic level. *PLoS One* **3,** e2377.

Yamagata M, Sanes JR & Weiner JA. (2003). Synaptic adhesion molecules. *Curr Opin Cell Biol* **15,** 621-632.

York RD, Yao H, Dillon T, Ellig CL, Eckert SP, McCleskey EW & Stork PJ. (1998). Rap1 mediates sustained MAP kinase activation induced by nerve growth factor. *Nature* **392,** 622-626.

Yoshii A & Constantine-Paton M. (2007). BDNF induces transport of PSD-95 to dendrites through PI3K-AKT signaling after NMDA receptor activation. *Nature neuroscience* **10,** 702-711.

Yudin D & Fainzilber M. (2009). Ran on tracks--cytoplasmic roles for a nuclear regulator. *J Cell Sci* **122,** 587-593.

Yuste R & Bonhoeffer T. (2001). Morphological changes in dendritic spines associated with long-term synaptic plasticity. *Annual review of neuroscience* **24,** 1071-1089.

Zamanillo D, Sprengel R, Hvalby O, Jensen V, Burnashev N, Rozov A, Kaiser KM, Koster HJ, Borchardt T, Worley P, Lubke J, Frotscher M, Kelly PH, Sommer B, Andersen P, Seeburg PH & Sakmann B. (1999). Importance of AMPA receptors for hippocampal synaptic plasticity but not for spatial learning. *Science (New York, NY* **284,** 1805-1811.

Zhang S, Charest PG & Firtel RA. (2008). Spatiotemporal regulation of Ras activity provides directional sensing. *Curr Biol* **18,** 1587-1593.

Zhang Z, Xin D, Wang P, Zhou L, Hu L, Kong X & Hurst LD. (2009). Noisy splicing, more than expression regulation, explains why some exons are subject to nonsense-mediated mRNA decay. *BMC Biol* **7,** 23.

Zhu H, Hasman RA, Barron VA, Luo G & Lou H. (2006). A nuclear function of Hu proteins as neuron-specific alternative RNA processing regulators. *Mol Biol Cell* **17,** 5105-5114.

Zhu JJ, Qin Y, Zhao M, Van Aelst L & Malinow R. (2002). Ras and Rap control AMPA receptor trafficking during synaptic plasticity. *Cell* **110,** 443-455.

Zhu Y, Pak D, Qin Y, McCormack SG, Kim MJ, Baumgart JP, Velamoor V, Auberson YP, Osten P, van Aelst L, Sheng M & Zhu JJ. (2005). Rap2-JNK removes synaptic AMPA receptors during depotentiation. *Neuron* **46,** 905-916.

Zukin RS & Bennett MV. (1995). Alternatively spliced isoforms of the NMDARI receptor subunit. *Trends Neurosci* **18,** 306-313.

Zuo Y, Lin A, Chang P & Gan WB. (2005). Development of long-term dendritic spine stability in diverse regions of cerebral cortex. *Neuron* **46,** 181-189.

Zwartkruis FJ, Wolthuis RM, Nabben NM, Franke B & Bos JL. (1998). Extracellular signal-regulated activation of Rap1 fails to interfere in Ras effector signalling. *Embo J* **17,** 5905-5912.